Universidade do Minho
Escola de Ciências

Ana Catarina Santos Leite da Silva

Valorisation of organic wastes: Assessment of compost quality

October 2022

Valorisation of organic wastes: Assessment of compost quality
Ana Catarina Santos Leite da Silva
UMinho | 2022


NORTE 2020
PROGRAMA OPERACIONAL REGIONAL DO NORTE
PORTUGAL 2020
União Europeia
Fundo Europeu de Desenvolvimento Regional
Interreg
España - Portugal
Fondo Europeo de Desarrollo Regional
Fundo Europeu de Desenvolvimento Regional
UNIÓN EUROPEA
UNIÃO EUROPEIA
RES2VALHUM

Universidade do Minho
Escola de Ciências

Ana Catarina Santos Leite da Silva

Valorisation of organic wastes: Assessment of compost quality

Doctoral Thesis in Chemistry
Doctoral Program in Chemistry
Physical and Analytical Chemistry Specialty

Work developed under the supervision of:
Professor Doctor Maria de Fátima Malveiro Bento
and
Professor Doctor Sarah Fiol López

October 2022

Acknowledgement

This thesis represents the achievement of an important stage at a professional level and, undoubtedly, an enormous challenge at a personal level. And, as with all challenges, there are always valuable contributions from various people, sometimes directly and sometimes indirectly. Therefore, I would like to express my sincere thanks to all those who in some way contributed to the realization of this thesis.

First of all, I would like to thank my supervisor, Prof. Dr. Fátima Bento and co-supervisor, Prof. Dr. Sarah Fiol, for the opportunity of the challenge, for the support, encouragement, guidance and transmission of precious knowledge.

I would also like to acknowledge to all the people in the Department of Chemistry at University of Minho for their support and advices. To all the members of the Department of Physical Chemistry and Department of Soil Science and Agricultural Chemistry at the University of Santiago de Compostela, my sincere thanks for welcoming me so well and making me feel "at home". Furthermore, whenever requested, they were available to assist me and clarify any doubts, scientific or logistical, that may arise.

A special thanks to Doctor Juan Antelo and Doctor Rocio Lopez for given me the opportunity to learn so much from their expertise and to Prof. Doctor Patricia Valderrama, who was always available to discuss with me in the area of analytical chemistry and chemometry.

An extraordinary thanks to Prof. Doctor José Paulo Pinheiro, who was always available to discuss with me about speciation and bioavailability of trace metals. Your technical support was really important.

Along these years, most of them spent in the lab, I had the pleasure to divide my workspace with excellent partners. I knew people who were truly examples of good partnership.

A very special thanks goes out to my family. Their encouragement and constant concern were an additional incentive.

I would also like to acknowledge the financial support of the Operational Programme Norte 2020 through the Project “NORTE-08-5369-FSE-000033” with a PhD grant, UMINHO/BD/40/2016.

STATEMENT OF INTEGRITY

I hereby declare having conducted this academic work with integrity. I confirm that I have not used plagiarism or any form of undue use of information or falsification of results along the process leading to its elaboration. I further declare that I have fully acknowledged the Code of Ethical Conduct of the University of Minho.

Abstract

Valorisation of organic wastes: Assessment of compost quality.

The physico-chemical and structural characterization of compost is fundamental for the valorisation of this sustainable material obtained from the aerobic decomposition of the organic solid wastes. Although the available methods and analytical parameters provide relevant information on the degree of maturation of the compost and on the content of major nutrients or contaminants, there are still some important questions that remain unanswered. In the scope of this thesis three major topics were addressed, namely, the identification of the most adequate parameters to monitor compost along the composting process and provide information on the variability of the compost features related to the feedstock and composting methods.

The first goal is relevant in view of the diversity characterization parameters obtained either directly from the compost or from its extracts. For this purpose, a total of 108 parameters, obtained using very different techniques and methodologies, were compared for the characterization of a compost at 4 composting stages. The compost used in this study was prepared by tunnel composting using the organic fraction of urban wastes obtained by selective collection. The statistical analysis of the results using a statical tool (Common Dimensions) indicated that either the solid compost or the extracts can be used interchangeably to monitor the composting process. Among the most significant parameters are the C/N molar ratio from the compost characterization, the electric conductivity from the water-soluble extract and the content of C and N in the humic-like (HA-L) and fulvic-like acid (FA-L), respectively.

The variability of the compost features was studied by means of the characterization of 7 composts of different origin, including vermicomposts and composts from industrial and domestic composting, prepared using feedstocks of different nature, such as urban wastes, sewage sludge, manure, and algae. The characterization was performed by means of physico-chemical parameters obtained from elemental, thermal and spectroscopic methods and by reactivity parameters from acid-base and metal binding titrations. Despite the stabilisation of organic matter in all composts being adequate for agricultural applications, they display distinct elemental and structural composition. The principal component analysis of the results from the direct characterization of the composts lead to samples distribution patterns that are more closely associated with the nature of the raw materials than with the composting method. Furthermore, correlation analysis suggested that the chemical structure of the constituents of the composts produced from different feedstock and composting methodologies possess important similarities. Characterization results of extracts from composts of different origins were analysed and the parameters that can better detect the changes in the composition of the extracts were identified. Within the extracts of the same nature, the higher number of correlations were found for HA-L extract with a total of 30 correlations. The HA-L extract was also the extract that exhibited a larger number of correlations with the compost characterization parameters.

Finally, the extracts of the different composts were compared with those of a non-composted fertiliser through the binding extent with Cd^{2+}. Results from the HA-L extract were the best to differentiate the composts of different origin. Using the experimental values of the metal complex concentration, $c_{ML,HA\text{-}L}$, that is related to the abundance and reactivity of the HA-L extract in the compost, a classification parameter, m_{EF}, was proposed for the first time. This parameter corresponds to the mass of fertiliser required to bind an amount of Cd (II) identical to that complexed by the HA extracts existing in 1 kg of compost. The validity of this scale was tested by comparing the reactivity parameters with growth results from a lettuce crop. The high correlation obtained demonstrates that the reactivity parameter used in the definition of the compost quality scale has a high potential to assess the bioactivity of the compost, and therefore could serve as a marker of compost bioactivity.

Keywords: Compost, Feedstock, Fertiliser, Humic-like substances, Vermicompost

Resumo

Valorização de resíduos orgânicos: Avaliação da qualidade do composto.

A caracterização físico-química e estrutural do composto é fundamental para a valorização deste material sustentável obtido a partir da decomposição aeróbica dos resíduos sólidos orgânicos. Embora os métodos e parâmetros analíticos disponíveis forneçam informação relevante sobre o grau de maturação do composto e sobre o conteúdo dos principais nutrientes ou contaminantes, existem ainda algumas questões importantes que permanecem sem resposta. No âmbito desta tese foram abordados três tópicos principais, nomeadamente, a identificação dos parâmetros mais adequados para monitorizar o composto ao longo do processo de compostagem, e fornecer informações sobre a variabilidade das características do composto relacionadas com a matéria-prima e os métodos de compostagem.

O primeiro objetivo é relevante tendo em conta a diversidade dos parâmetros de caracterização que podem ser utilizados diretamente sobre o composto e sobre os seus extratos. Para este efeito, foram comparados um total de 108 parâmetros da caracterização de um composto em quatro fases de compostagem. O composto utilizado neste estudo foi preparado por compostagem em túnel utilizando a recolha seletiva de resíduos urbanos. A análise estatística dos resultados utilizando ComDim indicou que tanto o composto sólido como os extratos podem ser utilizados de forma intermutável para monitorizar a compostagem. Entre os parâmetros mais significativos encontram-se a razão molar C/N da caracterização do composto, a condutividade elétrica do extrato solúvel em água e o conteúdo de C das substâncias tipo húmico. A variabilidade das características do composto foi estudada através da caracterização de 7 compostos de origem diferente, incluindo vermicompostos e compostos provenientes da compostagem industrial e doméstica, preparados utilizando matérias-primas de diferente natureza, tais como resíduos urbanos, lamas de esgoto, estrume e algas. A caracterização foi realizada por meio de parâmetros físico-químicos de métodos elementares, térmicos e espectroscópicos e por parâmetros de reatividade de titulações ácido-base e ligação de metais. Apesar da estabilização da matéria orgânica em todos os compostos ser adequada para aplicações agrícolas, estes apresentam uma composição elementar e estrutural distinta. A análise de componentes principais dos resultados da caracterização direta dos compostos leva a padrões de distribuição de amostras que estão mais estreitamente associados à natureza das matérias-primas do que ao método de compostagem. Além disso, a análise de correlação sugeriu que a estrutura química dos constituintes dos compostos produzidos a partir de diferentes matérias-primas e metodologias de compostagem possuem semelhanças importantes. Foram analisados os resultados da caracterização de extratos de compostos de diferentes origens e os parâmetros que melhor podem detetar melhor as alterações na composição dos extratos. Dentro dos extratos da mesma natureza, foi encontrado um total de 30 correlações para o extrato HA-L, verificando-se que foi este que apresentou um maior número de correlações com os parâmetros de caracterização do composto. Finalmente, os extratos dos diferentes compostos foram comparados com os de um fertilizante não composto através da extensão de complexação com Cd^{2+}. Os resultados do extrato HA-L foram os melhores para diferenciar os compostos de origem diferente. Utilizando os valores experimentais da concentração do metal complexado $c_{ML,HA\text{-}L}$, que está relacionado com a abundância e reatividade do extrato HA-L, foi proposto pela primeira vez um parâmetro de classificação, m_{EF}. Este parâmetro corresponde à massa de fertilizante necessária para complexar uma quantidade de Cd(II) idêntica à quantidade complexada pelos extratos de HA-L existentes num 1 kg de composto. A validade desta escala de qualidade foi verificada através da comparação dos parâmetros de reatividade com os resultados de crescimento de uma cultura de alface. A elevada correlação obtida demonstra que o parâmetro de reatividade utilizado na definição da escala do composto tem um elevado potencial para avaliar a bioatividade do composto e, portanto, servir como um marcador da bioatividade dos compostos.

Palavras-chave: Composto, Fertilizante, Matéria-prima, Substâncias tipo húmicas, Vermicomposto

Contents

List of Figures

List of Tables

List of abbreviations, variables, and acronyms

Abbreviations and acronyms

^{1}H-NMR – Proton nuclear magnetic resonance

AGNES – Absence of Gradients and Nernstian Equilibrium Stripping

ATR-FTIR – Attenuated total reflection - Fourier transform infrared

C/N - Carbon to nitrogen ratio

CA - Compost of algae

CC - Common component

CDDW - Domestic compost of domestic waste

CEC – Cation exchange capacity

CLW - Compost of livestock waste

CSS - compost of sewage sludge

$cmol_{(+)}\ kg^{-1}$ - centimoles of charge per kilogram of dry compost

ComDim – Common Dimensions

CUW - Compost of urban waste

CUW_{15} - Compost urban waste after the 1st composting cycle, t=15 days

CUW_{30} - Compost urban waste after the 2nd composting cycle, t=30 days

CVA - Vermicompost of algae

CVDW - Vermicompost of domestic waste

DOC – Dissolved organic carbon

DOM – Dissolved organic matter

DSC – Differential scanning calorimetry

DTG - Derivative Thermogravimetry

EA – Elemental Analyses

EC – Electrical conductivity

FA – Fulvic acid

FA-L – Fulvic-like acid

FLW - Fertilizer of livestock waste

GCE - glassy carbon electrode

H/C - Hydrogen to carbon ratio

HA – Humic acid

HA-L – Humic-like acid

H_i – Enthalpy

HS – Humic Substances

HS-L – Humic-like Substances

ICP-OES – Inductively coupled plasma optical emission spectrometry

IHSS – International Society for Humic Substances

IR - Infrared

m_{EF} – Equivalent mass of fertilizer

NICA – Non-ideal competitive adsorption

O/C - Oxygen to carbon ratio

OM – Organic matter

ORCHESTRA - Object Oriented Framework for Composing Chemical Speciation and Mass Transport Models

PC - Principal component

PCA – Principal component analysis

PEST - Model-Independent Parameter Estimation & Uncertainty Analysis

pKa - the negative base 10 logarithm of the acid dissociation constant, Ka

r - Coefficient of correlation

R^2 – Coefficient of determination

Res – Residue from thermogravimetric analysis

RMSE – root mean square error

rpm - Revolutions per minute

SEM - Scanning electron microscopy

TGA – Thermogravimetric analysis

TLA – total leaf area

TWL - Total weight loss

UV-vis – Ultraviolet–visible spectroscopy

UW_0 - Urban waste

v:w - volume/weight

w:w - weight/weight

WL_i – Weight loss

XRD - X-ray diffraction

Variables

$\bar{x}$ – arithmetic mean

ψ_D - homogeneous Donnan potential

$[H^+]$ – is given by the pH measure at each point

[HS] - the sample concentration in mg L^{-1}

|L| – absolute value of the loadings

$a_{D,j}$ - activity of ion j in the Donnan volume

c_{DOM} - concentration of the organic matter of DOM

C_{DOM} – carbon content of DOM

C_{DOM} – carbon content of DOM

C_{extrac}– total extractable carbon

$C_{HS\text{-}L}$ – carbon content of humic-like substances

c_L - concentration of organic matter

c_M - free metal concentration

c_{ML} - metal complex concentration

$c_{ML,DOM}$ - metal complex concentration of DOM

$c_{ML,FA\text{-}L}$ - metal complex concentration of FA-L

$C_{ML,H}$ - metal complex concentration at 0.30 µmol L^{-1}

$c_{ML,HA\text{-}L}$ - metal complex concentration of HA-L

$c_{ML,HS\text{-}L}$ - metal complex concentration of HSL

$C_{ML,L}$- metal complex concentration at 0.10 µmol L^{-1}

c_{MT} - total cadmium concentration

C_{oxi} - Oxidizable carbon

E – cell potential

E^0 – standard cell potential

F – Faraday's constant

I – the ionic strength

K – complexation ratio

K' - complexation constant

K_1 – median value of affinity distribution for proton binding by carboxyl groups

K_2 – median value of affinity distribution for proton binding by phenolic groups

K_w – the ionic product of water at the ionic strength of work

L – length

LA – leaf area

M_1 – carboxyl group content

M_2 – phenolic group content

$m_{compost}$ – mass of compost

$m_{H,1}$ – width of proton-affinity distribution of carboxyl groups

$m_{H,2}$ – width of proton-affinity distribution of phenolic groups

M_T – abundance of acid sites

$M_{T,DOM}$ – abundance of acid sites in the DOM

$M_{T,HS\text{-}L}$ – abundance of acid sites in the humic-like substances

$n_{m,1}$ – non-ideality of the ion binding by carboxyl groups

$n_{m,2}$ – non-ideality of the ion binding by phenolic groups

p_1 – intrinsic heterogeneity by carboxyl groups

p_2 – intrinsic heterogeneity by phenolic groups

Q – charge

Q_0 – charge due to occupation of the acid sites by cation

R – gas constant

s - standard deviation

T – temperature

V - volume

V_a – volume of base added at each titration point

V_D – Donnan specific volume

V_i – initial volume of the sample

W – maximum width

WL_i@air – Weight loss in air atmosphere

WL_i@N_2 – Weight loss in N_2 atmosphere

Y – yield

z_j – charge number of ion j

α – empirical coefficient

β – empirical coefficient

ε_{280} – molar absorptivity coefficient at 280 nm

Latin expressions

e.g. – exempli gratia (for example)

vs. – versus

et al. – et alii (and others)

i.e. – id est (that is).

Scientific Output

International Journals Publications

R. López, J. Antelo, **A.C. Silva,** F. Bento, S. Fiol, Factors that affect physicochemical and acid-base properties of compost and vermicompost and its potential use as a soil amendment, Journal of Environmental Management 300 (2021) 113702 https://doi.org/10.1016/j.jenvman.2021.113702

A.C. Silva, A. Teixeira, J. Antelo, P. Valderrama, R. Oliveira, A. Cunha, R. Gley, J.P. Pinheiro, S. Fiol, F. Bento, Distinctive features of composts of different origin: a thorough examination of the characterization results, Sustainability 14 (2022) 7449 https://doi.org/10.3390/su14127449

A.C. Silva, P. Rocha, J. Antelo, P. Valderrama, R. López, D. Geraldo, M.F. Proença, J.P. Pinheiro, S. Fiol, F. Bento, Comparison of a variety of physico-chemical techniques in the chronological characterization of a compost from municipal wastes, Process Safety and Environmental Protection 164 (2022) 781-793 https://doi.org/10.1016/j.psep.2022.06.057

Oral presentation:

J. Antelo, **A.C. Silva**, R. López, S. Fiol, F. Macías, F. Bento, P. Ferreira, M.C. Paiva, M.F. Proença. Influence of the feedstock material on the compost maturity, stability and reactivity. WASTES: Solutions, Treatments and Opportunities, 5th International Conference. Costa da Caparica, Portugal. Setembro 2019.

Posters in conferences:

P. Rocha, **A.C. Silva**, J. Antelo, F. Bento, P. Bettencourt, S. Fiol, D. Geraldo, R. López, F. Macías, J.P. Pinheiro, M.F. Proença, P. Ramisío. 2019. Comparison of cadmium binding by humic and fulvic acids extracted from compost samples of different feedstock. XXV Encontro Galego-Portugués de Química, Santiago de Compostela, Espanha.

A.C. Silva, P. Rocha, R. López, J. Antelo, F. Bento, S. Fiol, P. Bettencourt, P. Ferreira, D. Geraldo, F. Macías, M.C. Paiva, J.P. Pinheiro, M.F. Proença. 2019. Characterization, acid-base properties and metal complexation of humic-like substances extracted from organic matter during composting process. XXV Encontro Galego-Portugués de Química, Santiago de Compostela, Espanha.

A.C. Silva, P. Rocha, J. Antelo, F. Bento, P. Bettencourt, P. Ferreira, S. Fiol, D. Geraldo, R. López, F. Macías, M.C. Paiva, J.P. Pinheiro, M.F. Proença. 2019. Comparison of cadmium binding by humic and fulvic acids extracted from two composts of different origin. WASTES: Solutions, Treatments and Opportunities, 5th International Conference. Costa da Caparica, Portugal.

A.C. Silva, P. Rocha, J. Antelo, F. Bento, P. Bettencourt, S. Fiol, P. Ferreira, D. Geraldo, R. López, F. Macías, J.P. Pinheiro, M.F. Proença. Characterization of organic matter at different stages of a composting process, 5th international conference, Wastes: solutions, treatments and opportunities. 5th International Conference. Costa da Caparica, Portugal

Motivation and Outline of the Thesis

Motivation

The improvement of the quality of the environment and the protection of human health, depends on the efficient and rational utilization of natural resources and efficient waste management policies promoting the principles of circular economy. To accomplish these goals the European Union set 2023 as the deadline for the separate collection for biowaste with the aim of recycling by composting and digestion. Furthermore, the use of environmentally safe materials produced from bio-waste should also be increasingly encouraged by EU countries. Thus, compost production and its uses are expected to increase, as a means to fulfil the demand of clean technologies for waste management and the production of an environmentally friendly material [1,2]. The use of compost and the adoption of no-till farming practices are currently implemented by an increasing number of farmers that aim to respond to a growing demand for organic foods by the more informed consumers. These farming practices contribute to global environment protection, *e.g.* improve water retention and CO_2 fixation. Besides the numerous advantages of using compost for the soil and crops, composting is a sustainable solution for organic waste management.

The work presented in this thesis was developed in the framework of an Interreg project entitled Organic Residues Valorisation: Production of Humic Substances (Res2ValHum) which main goal was to promote composting as an instrument for the management of organic waste, with the consequent reduction of the amount of waste deposited in landfills, and the recovery of the compost produced in applications with high added value. The characterization of the composts of different origin and at different composting stages was carried out in the scope of the present PhD, in order to create more scientific and technological knowledge on composting and contribute to the valorisation of compost.

Thesis Outline

The work presented in this thesis has been organised in four chapters: Introduction, Materials and Methods, Results and Discussion, and Conclusion.

The Introduction provides an overview of waste production and treatment. Within the scope of waste treatment by composting, the critical composting methodologies and operational variables are presented. The main methods and parameters for the characterization of the compost and the humic-like substances are also reported. The properties and applications of compost and humic-like substances are described

in areas that go beyond their use as agricultural fertilisers. In Materials and Methods samples are identified and all the procedures and methods are described.

The outcome of the research conducted in the framework of this PhD is presented in the beginning of the chapter Results and Discussion. The results are presented and discussed in 5 subchapters. The selected composts for this project cover different composting methodologies and different raw materials. In this way it is pretended to recognise the impact of these operational variables in the compost quality. The compost produced from the selective collection of urban wastes by industrial composting (tunnel composting) is characterised in particular concerning the evolution of the material during the composting process and regarding the characterization of the humic-like substances following a modelling process.

In the first subchapter samples of compost produced from a variety of raw materials are characterised through a large number of data from different analytical techniques, such as spectroscopic, thermal and electroanalytical. Attempts were made to establish correlations between the molecular features of the composts, and their origin, *i.e.* raw material and composting process. Correlations between the different parameters used for the characterization of the compost were also sought with the objective of reducing the number of analyses to be carried out in the characterization of the compost.

In the second subchapter, the characterization of the reactivity of the extracts of the composts of different origin was performed by means of acid-base and cadmium complexation titrations. The reactivity of the extracts was analysed in order to establish how this property is affected by the compost origin.

In the third subchapter attempts were made to find correlations between the chemical composition and reactivity (from the third and fourth subchapters) of the extracts of the different composts. Simultaneously, the physico-chemical and reactivity parameters of the extracts were compared with the chemical composition and molecular structure of the composts. These correlations were sought in order to identify the most prominent parameters that can be used to compare composts of different origins.

In the fourth subchapter a compost produced from an organic fraction of urban wastes was investigated at four stages of composting. The analytical parameters that were more sensitive to monitor the composting process were identified through the analysis of characterization results of compost and extracts.

In the fifth subchapter, the reactivity of the extracts from CUW was made through the acid-base titrations and titrations with metallic cations (cadmium and lead) at different ionic strengths and different pH values in order to characterise these extracts at the molecular level, using the Nica-Donnan model. Due to the absence of similar data in the bibliography, the obtained results were compared with the generic parameters of organic matter of natural sources.

Finally, in the conclusion section, a general conclusion is presented based on the analysis of the results that were presented in the 5 subchapters.

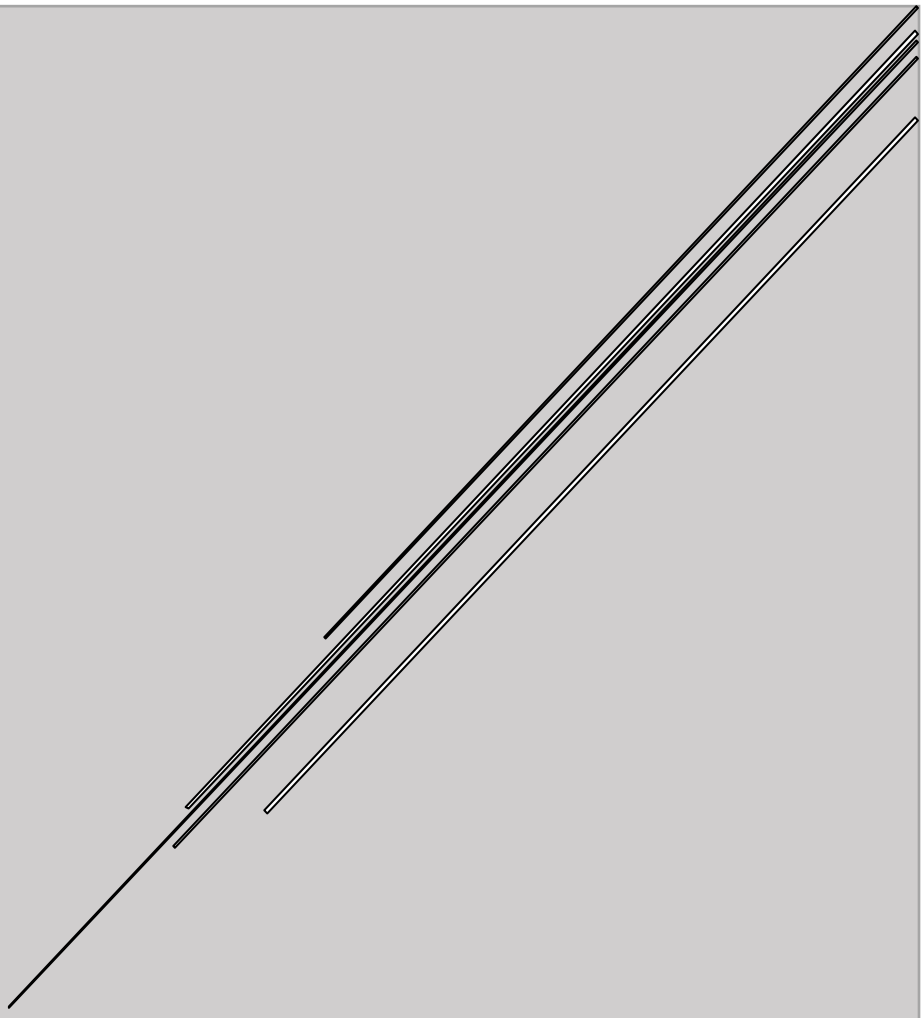

CHAPTER 1 – INTRODUCTION

1. Waste management and environmental sustainability

Environmental sustainability aims to maintain natural resources through the use of renewable energy sources and through the efficient management of raw materials, food and waste treatment to ensure that future generations have an equal, if not better, quality of life than current generations. Due to the growing number of inhabitants in cities and of the increasing consumption, urbanisation has led to detrimental effects particularly in urban communities [3,4]. The characteristics and amount of waste produced is a consequence of daily life and thus a reflection of the living conditions of the society. In the last decades the production of waste has been rising worldwide with the increase in population, both in quantity and diversity. This increase results from the demographic explosion and economic growth, as well as from the increase of purchasing power. The World Bank estimates that waste production will increase from 2.01 billion tons in 2016 to 3.40 billion tons in 2050 [5]. The inequality of global waste production is illustrated in Figure 1.1. The richest countries generate larger amounts of urban solid wastes than emerging and developing countries.

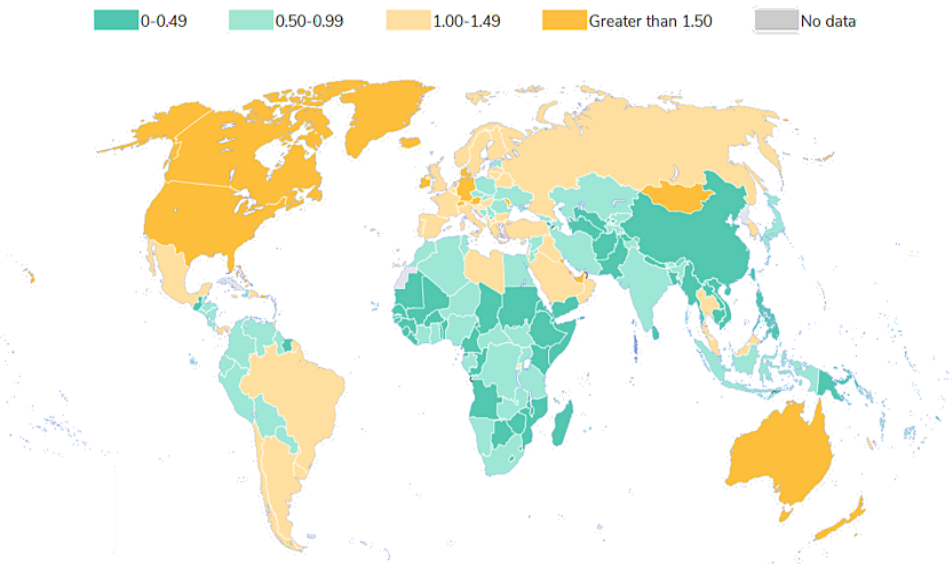

Figure 1.1: Annual urban solid waste generated per capita (kilograms/capita/day). Adapted from [5] and referred to 2018.

In Portugal about 5,28 million tons (t) of urban waste were produced just in 2020 [6]. Biowastes represent the most abundant class of urban solid waste, accounting for 36.94 % of the total urban solid wastes produced in 2021, as it is illustrated in Figure 1.2A [5,6].

Worldwide the urban waste recovery is very small (Figure 1.2B), where 19 % is achieved by recycling and composting, and 11 % by incineration [5]. Despite the increasing restrictions to the disposal of the organic waste almost 40 % is still disposed of in landfills with high negative impacts to the environment. The most

recent European directives indicate that the prevention/reduction of waste production and the waste recovery through recycling or reuse should be encouraged by Member States (*e.g.* Directive 2008/98/EC, Directive (EU) 2018/851) and set 2023 as the deadline for the implementation of separate collection of organic waste with the aim of composting and digestion.

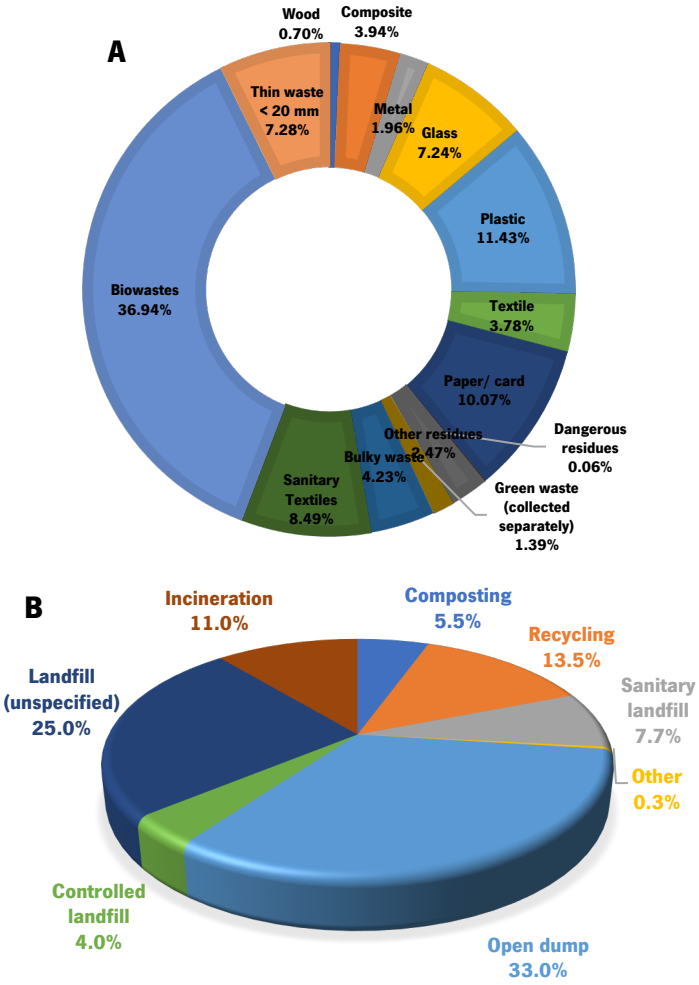

Figure 1.2: (A) Physical characterization of urban waste produced in 2020 in Portugal and (B) Treatment and disposal of urban waste worldwide. Adapted from [6,7].

Biowastes (also called organic waste) have been recognized as a valuable resource which can be converted into useful products through composting and anaerobic digestion or used for energy exploitation by incineration [8]. Incineration involves burning waste in ovens and using the heat produced to generate useful energy (in the form of electricity or heat) [9]. The main advantage of incineration compared to the other options is its capacity for removing waste, regardless of the type of residue and the volume reduction [10]. This type of treatment has important drawbacks of economic, social, and environmental nature. Waste incineration releases into the atmosphere toxic gases that are harmful to human health including metals and dioxins [11], although the quantities released of these pollutants have

decreased, due to stricter rules imposed by governments and to technological progress in this area in recent years [12].

The anaerobic digestion of biowastes is an alternative technology for energy recovery. Anaerobic digestion that is carried out by bacteria in the absence of oxygen, mainly leads to the generation of methane and carbon dioxide. The so- called biogas can be produced from different raw materials, such as biosolids, livestock manure and moist organic materials [13–15]. The process occurs in three stages: (i) decomposition of plant and animal matter by bacteria into molecules such as sugar, (ii) conversion of decomposed matter into organic acids and (iii) conversion of organic acids to methane gas. The main benefit of this process is that it prevents the release of methane into the atmosphere (as the process occurs in a closed environment), thus helping to reduce environmental pollution [16]. The anaerobic process has some disadvantages, such as long retention periods and low efficiency in removing organic compounds [17,18].

Composting is an alternative waste treatment technology of simple operation and high economic efficiency. In addition to enabling the reduction of the use of landfills and reduction of greenhouse gas emissions, composting permits the recycling of nutrients and their use in agriculture applications.

In the present context where intensive farming practices are being questioned due to its negative impacts on the soil, such as acidification, nitrification and the decrease of organic matter, leading to desertification of previously fertile areas, alternative products and techniques are demanded to comply with the Sustainable Goals [19]. The use of compost and the adoption of no-till farming practices are currently implemented by an increasing number of farmers that aim to respond to a growing demand for organic foods by the more informed consumers. Thus, an increase of the amount of biowastes that are treated by composting cannot only contribute to a more efficient waste management, with lower environmental impacts but also to the production of a natural fertiliser that can bring important benefits for agriculture and soils.

2. Composting and compost applications

Composting and vermicomposting are two complementary technologies for the treatment, recycling, and recovery of biomass of different origin, such as the organic fraction of solid urban waste and other types of wastes from agriculture, livestock, agro-industrial and forestry. Composting is the biological decomposition of organic waste in an aerobic environment. Similar to composting, vermicomposting is also used for the production of stabilised organic matter. Vermicomposting involves the interactions between earthworms and microorganisms (bacteria, fungi, actinomycetes) [2]. Among the different types

of earthworms, endogeic, anecic and epigeic, only the last one is used for vermicomposting. While endogeic and anecic are geophagous species, epigeic are detritivorous species. This species lives on the soil surface (0 to 10 cm) and feeds on organic matter in primary or intermediate stages of decomposition. They have a short life cycle, usually between 2 to 3 years, fast growth, and a rapid reproduction [20]. The most common species within the epigeic category are *Dendrodrilus rubidus, Allolobophoridella eiseni, Eudrilus eugeniae, Perionyx excavates, Eisenia andrei* and *Eisenia fetida*, although the last two are the most commonly used in vermicomposting [21].

Both composting and vermicomposting are promoted and controlled by means of different operational variables that affect the compost characteristics, including the raw material nature, the composting methodology, aeration, temperature, and humidity [22–28]. The importance of these variables in compost production is addressed in the following subsections.

2.1. Raw material

A wide variety of raw materials can be used for composting. A single type of raw material (*e.g.* fruit waste or manure) [29,30], or a mixture of wastes (*e.g.* poultry manure with wheat straw or sewage sludge with manure) [31] is possible to use. The raw materials that can be used for composting, are identified in Table 1.1, where a huge diversity of materials is possible, from animal droppings, sea waste to industrial residues. For efficient composting different materials are frequently combined to achieve a balance between the content of carbon (C) and nitrogen (N) in the feedstock. Carbon serves primarily as an energy source for the microorganisms, while a small fraction of the carbon is incorporated into the microbial cells. Nitrogen is critical for microbial population growth [32] and if it is limiting, microbial populations will remain small and decomposition rates for available carbon will be lower [33]. For this reason, the C/N ratio is an important operational variable which varies along the composting process [34,35]. The humification index (HI), *i.e.* the rate of formation of HS, depends strongly on the initial value of the C/N ratio that is typically between 20 and 30 [36].

Another important characteristic of the raw material is the particle size of the waste to be composted. The granulometric distribution of the initial feedstock material is important because it determines the gas and water exchanges and, mainly, the water retention capacity, but also has a great influence on maintaining adequate porosity for better aeration [37]. When the size of the particles is too large, since the decomposition becomes slower, and when it is too small, a compact mass can be formed, and porosity of the compost will be reduced [38]. Likewise, the moisture content is one of the most important factors for composting, as water promotes the transport of dissolved essential nutrients, for the metabolic

and physiological activities of microorganisms. The optimum moisture content is between 40 - 70 % of the weight of the compost [39,40].

Table 1.1: Suitable organic feedstock materials for composting.

Class	Examples
Animal wastes	Cattle, swine, poultry, sheep and goat manure [31,38]; waste meat and fish products [41,42].
Waste straw	Grass and cereal straw [43].
Garden (yard) waste	Grass clippings, hedge trimmings, plant remains, leaf and twig sweepings, etc. [44].
Food wastes	Mixtures of all (further processed) components from food processing above including meat, fish, vegetable, fruit and cereal-derived products, bread and baked goods, egg and egg shells, tea-leaves and coffee grounds and bags, uneaten food, spoiled food [45–52].
Fruit	Trimmings *e.g.* fruit peels (citrus, melons, apples, tomatoes), seeds (apple core, melon seeds) [53].
Vegetable trimmings	Leaves, inner tissues *e.g.* cabbage (red and green) outer leaves and cores, cauliflower leaves, sprouts, onion peelings (outer brown skin and outer fleshy layers), carrot peelings [29,30,54].
Mixed (plant and animal)	Processed food waste from all parts of processing stream, including end of line wastes, fabricated recipes containing mixtures of meat, fruit, vegetable, cereal products [55,56]
Packaging and related	Cardboard and paper from food chain and other [57,58].
Industrial waste	Textiles, carpets, etc. [59] and sewage sludge from treatment plants [55,60–64].
Wood waste	Packaging, non-treated wood waste [65,66].
Sea wastes	Seaweed of marine origin [67,68] and seafood shells [69].

2.2. Composting variables and methodologies

The composting process is divided into four stages: mesophilic phase, thermophilic phase, cooling and maturation phase [70], while the vermicomposting process has only a mesophilic and maturation phases. The mesophilic phase lasts a few days and provides the necessary conditions for the process to begin. During this stage, moderate temperatures, between 30 and 45 °C predominate and the developed colonies of mesophilic microorganisms use the soluble and rapidly degradable components of organic matter to provide a gradual increase in temperature. With this increase in temperature, mesophilic microorganisms become less competitive, giving space for the proliferation of thermophilic

microorganisms, leading to the thermophilic phase. The second phase lasts between 2 to 3 weeks, depending on the material to be composted. In this phase temperature reaches its maximum (usually larger than 55 °C) and the decomposition of organic components, reaches its maximum. For this reason, the thermophilic phase is considered an active degradation phase. The cooling phase starts when the temperature starts to decrease, when most of the organic matter has been degraded, the thermophilic microorganisms are inactivated, causing the biological activity to significantly decrease and the mesophilic microorganisms to act again. The degradation of the most resistant organic substances and where the most intense losses of moisture occur in this phase. At this moment, humification (formation humic substances) and maturation of organic matter also begins. Finally, in maturation the required amount of oxygen is lower, the temperature is close to room temperature and the mineralization of the organic matter takes place [71].

Table 1.2: Main characteristics of different composting methodologies [74,76].

Composting systems		Description
Open	Windrow composting	The outdoor composting system that strongly relies on mechanical aeration
	Aerated static composting	Piles are passively aerated via convection and diffusion
In-vessel	Rotating drums	The waste material is loaded into a horizontal slowly rotating drum with forced aeration.
	Agitated beds	Relies on a specialised windrow turner, and the use of very wide windrows with an aeration system and enclosing the entire system within a building
	Tunnels	Uses a positively aerated composting system with below-floor aeration pipes. The aeration floor and the composting pile are housed completely within a cast-in-place concrete enclosure
	Vertical flow	In this type of process, the waste material flows vertically, with or without stages, with mass flow from the top to the bottom
	Horizontal flow	This is a batch system in which the waste material is loaded with a wheel loader or transport devices into a horizontal reactor or is covered by a foil or textile material

Oxygen is an important factor that influences composting and vermicomposting [39] since these processes are directly related to microbial activity. In the first stages of rapid degradation, oxygen is rather important for the proper performance of the microorganisms. In the final stages, with the reduction of microbial activity, less oxidative conditions are preferred [40,72].

pH is another important variable for composting as it affects the microbial activity in each phase [39]. pH is an interfering factor since it favours the predominance of colonization of different microorganisms throughout these phases. At the beginning of composting, the formation of organic acids and the incorporation of organic carbon into the microbial cell protoplasm are observed, leading to a decrease of pH [73]. However, with the course of the decomposition process, organic acids are replaced with mineral acids that react with the bases released from organic matter, neutralising and transforming the compost material.

Table 1.3: Main characteristics of different vermicomposting methodologies [74,75].

Vermicomposting systems		Description
Open	Windrow	Long rows on the ground with a depth of 50 cm (organic waste is placed, and worms are introduced). Continuous flow system - Container above the ground with mesh floor. Batching system - Compiled of boxes. Wedge system - Horizontal feeding method, where at 45° angle feed is applied on the bedding.
In-vessel	Pits	Below the ground, 1-m-deep and 1.5-m-wide pits with varying lengths
	Heaps	Above the ground, heaps are made with sheets of polythene placed directly on the ground.
	Tanks	Above the ground, tanks are made with normal bricks.
	Cement rings	Cement rings made with dimensions of 90 cm diameter and 30 cm height.
	Beds or bins	Several trays on top of one another. Mostly, three trays are used with 150 mm in depth.

Composting and vermicomposting can be performed by different methodologies that enable the adequate conditions for the aforementioned processes. These can be carried out in open or in-vessel systems. In Table 1.2 and Table 1.3 are some information regarding the most common composting and vermicomposting methodologies. The methodology is selected according to the volume of materials to be composted, space and type of facilities available. Among the open systems are included windrow composting and aerated static composting while the in-vessel systems include rotating drums, agitated beds, tunnels, vertical or horizontal flow [74]. Vermicomposting can also be performed using different containers such as pits, heaps, tanks, cement rings, beds or bins. There are also open systems for

vermicomposting designated windrow [75]. Among the different composting methodologies, windrow composting is widely used, and is more adequate for treating large amounts of waste.

2.3. Compost and humic substances properties and applications

The compost has several applications, but it is more used in the field of agriculture. It can be used to complement or in substitution of chemical fertilisers and promoting higher yields of agricultural crops. Its use is also carried out in the treatment of soils, contributing to assist in reforestation efforts, restoration of wetlands and revitalization of habitats, improving contaminated, compacted and marginal soils, it can be used to remediate soils contaminated by hazardous waste, increases retention of water in soils and favours carbon sequestration [77–79].

The properties of compost are related to the presence of humic-like substances. Humic substances (HS) are formed by the natural decomposition and transformation of plant, animal and microbial residues particularly in soils, peat and leonardites. The properties of these substances are widely known. HS can modify the physical structure of the soil, causing an increase in the nutrient content and an increase of the water holding capacity, improving the soil's resistance to drought [80]. They can also stimulate plant growth, by stimulating plant enzymes, increase the natural resistance of plants against diseases and pesticides, stimulate root growth, especially vertically, allow better absorption of nutrients, increase the vitamin and mineral content of plants and increase seed germination and viability, enhance the uptake of nitrogen by plants and reduce the availability of toxic substances in soils. In addition to the direct effects on plants, HS stimulates the growth and proliferation of desirable microorganisms in the soil and helps to retain water-soluble inorganic fertilisers in root zones [80,81].

The benefits of humic substances are relatively well known in areas ranging from agriculture, industry or environment to biomedicine [82]. In agriculture, humic substances are used as additive in fertilisers in the form of calcium humate; sodium humate; ammonium humate [82–84]. They are also used bio-fertilizers that are innovative products which combine humic substances with beneficial microorganisms [83]. At an environmental level, humic substances have been characterised for the removal of metals such as lead (Pb), mercury (Hg), cadmium (Cd), chromium (Cr), copper (Cu), zinc (Zn), nickel (Ni) and aluminium (Al) [82,85,86] and been exploited as humus-based filters, for sewers purification and for removing oils and dyes from wastewater [82,87].

In the industrial area, humic substances are used in different sectors, such as in ceramics, wood, plastics, cement and concrete and in the paper industries [82,87,88]. The HS colour is used in the production of materials for painting wood, for the leather tanning process, and also for colouring plastics and ceramics

[82]. These have also been used to increase the mechanical strength of unprocessed ceramics and in clay preparation [82,89,90]. In the concrete industry HS have been also used, as they improve the physical-mechanical properties of the product. In the paper industry HS are used in the production of electrically conductive paper sheets and in paper recycling. HS are also used as expanders in lead accumulators in the battery industry [82,88,91].

The therapeutic properties of HS have also been exploited and are frequently used in traditional medicine, such as in bath salts and artificial mud-bath, for gynaecological and rheumatic treatments that are available in many SPAs [89,92]. These applications are based in the antiviral, antioxidant, anti-inflammatory, allelopathic, antigenotoxic, antimicrobial, estrogenic and anticoagulant properties of the HS [93,94]. There are also some reports on the beneficial effects of HS in varied diseases, including different tumours and cancer, where the effectiveness of the treatments has been described [95–97].

3. Composting monitoring and characterization of the compost

3.1. Composting monitoring

The chemical and biochemical reactions that occur during composting lead to important changes in the organic matter. These changes are often evaluated by elemental analysis following the variation of with total organic carbon and total nitrogen and also by means of the variation of pH, humification index (rate of the formation of HS) and the cation exchange capacity (CEC). While the pH and CEC tend to increase along the composting process, the C/N ratio and the humification index (ratio between non-humified and humified compounds) tend to decrease.

The compost, along the different composting stages, can also be monitored following the structural changes of the organic matter by other techniques, such as Fourier transform infrared spectroscopy (FTIR), thermogravimetric analysis (TGA) and differential scanning calorimetry (DSC). The analysis of the results from these techniques can be relatively straightforward, measuring the weight loss or enthalpy changes at fixed temperature ranges, or by means of aromaticity indexes that are calculated using band intensity ratios [98–100].

Typical FTIR spectra of a compost containing sludge and lignocellulosic waste at different stages of the composting process are illustrated in Figure 1.3 [99]. The FTIR spectra exhibit features that are related to the presence of functional groups that are directly involved in the humification process. To characterise the compost samples absorption intensities at characteristic wavenumbers are used, namely: the bands 2925 and 2845 cm^{-1} are attributed to asymmetric and symmetric vibrations of C-H stretching of CH_3 and CH_2 groups, a band centered around 1640–1630 cm^{-1} is attributed to aromatic C=C and C=O stretching

of amide groups and quinonic C=O and/or C=O of H-bonded conjugated ketones and a band at 1540 cm^{-1} is assigned to secondary amides. Using absorption intensity ratios at characteristic wavenumbers three empiric parameters ($I_{1630/2925}$, $I_{1630/2845}$ and $I_{1540/2925}$), designated by aromaticity indexes, may be used to follow the increase of the amount of aromatic moieties and the simultaneous decrease of aliphatic structures in the humified organic matter [101].

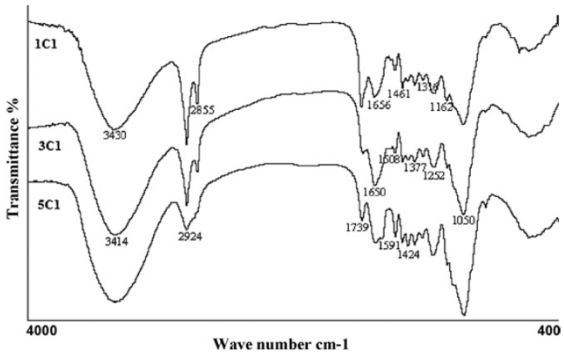

Figure 1.3: FTIR spectra during the composting process (3, 61 and 267 days, respectively) of solid olive-mill wastes [99].

Typical TGA and DTG curves of a compost from municipal solid waste at different stages of composting is shown in Figure 1.4 [102]. This technique is commonly used in the characterization of natural materials containing humified matter, providing important information on the stabilization degree of the organic matter. The TGA curves contain three main weight loss processes, WL_2 (177 - 400 °C), WL_3 (400 - 620 °C) and WL_4 (620 - 800 °C) and a secondary one at the limit of the lower temperatures, WL_1 (30 - 177 °C). The values of WL_1 are associated to dehydration and desorption processes, WL_2 is related to the easily biodegradable aromatic structures, WL_3 is related to the complex aromatic structures, such as lignin, complex aromatic structures, and humic substances and WL_4 is associated to the formation of inorganic species, such as carbonates. Through the ratio between the WL_3 and WL_2, WL_3/WL_2 at specific temperature intervals, the thermally more stable fraction of organic matter can evaluate with respect to the less stabilised one. During composting this ratio tends to increase, showing to be highly sensitive parameter to the chemical changes induced by the bio-transformation of organic materials [103,104].

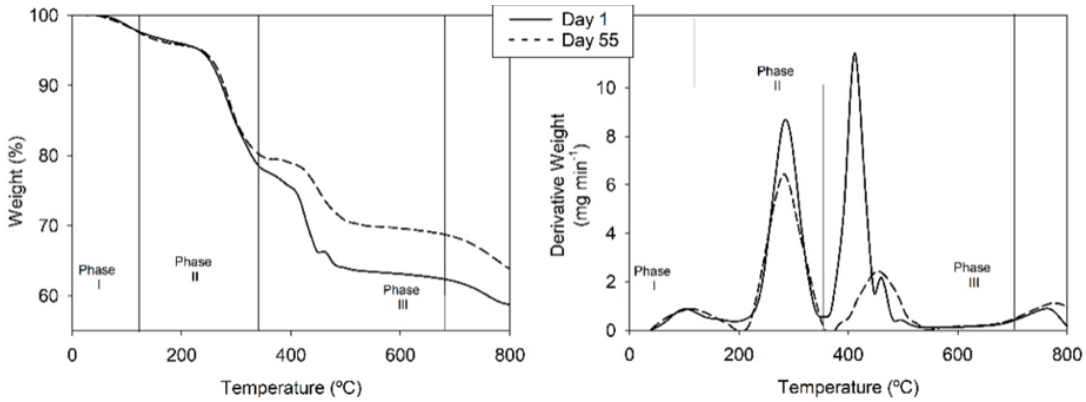

Figure 1.4: TGA and DTG (derivative weight) curves of the samples collected during the composting process of municipal solid waste [102].

In addition to thermogravimetric analysis, differential scanning calorimetry (DSC) is also used by some researchers, monitoring the thermal variations that occur simultaneously with mass variations. Figure 1.5 depicts typical DSC curve of a compost during the composting process, exhibiting endothermic or exothermic peaks. The minor endothermic process (H_1), at the lower temperature limit (close to 100 °C) is usually ascribed to dehydration reactions. The two major regions in the thermogram correspond to the overlap of exothermic processes related to the recalcitrant (H_2) and extra-recalcitrant substances (H_3), close to 320 °C and to 500 °C, respectively, are characteristic of stabilized organic matter. During the composting process the first exothermic peak tends to decrease, while the second one tends to increase [98].

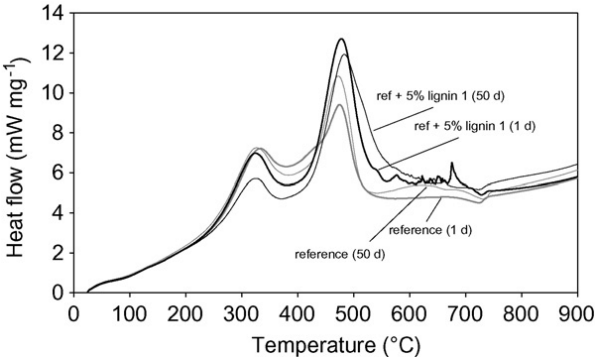

Figure 1.5: DSC curves of a compost reference and a compost mixture with 5 % lignin during the composting process [105].

Table 1.4 resumes some information regarding the main indicators used to monitor the composting process.

Table 1.4: Relevant indicators used to monitor the composting process.

Parameter	Related to	Reference
Temperature	microbial activity of thermophilic microorganisms	[106]
pH	microbial activity of mesophilic and thermophilic microorganisms	[107]
CEC	ability to retain cations, such as Ca^{2+}, Mg^{2+}, Na^{+} and K^{+}	[108]
C/N	carbon losses mainly as carbon dioxide	[101]
Humification index	amount of HS	[109]
Aromaticity indexes: $I_{1630/2925}$, $I_{1630/2845}$ and $I_{1540/2925}$	formation of aromatic (2925 and 2845 cm^{-1}) with respect to the amount of aliphatic moieties (1630 cm^{-1})	[101]
WL_3/WL_2	formation of extra-recalcitrant structures (WL_3) with respect to the recalcitrant structures (WL_2)	[103,110]
H_2	presence of recalcitrant substances	[103]
H_3	formation of extra-recalcitrant substances	[103]

3.2. Characterization of compost and its extracts

The characterization of compost can be performed directly on the solid material or by means of its aqueous extracts, obtained from simple extraction or following extraction and characterization methodologies similar to those developed for the characterization of the HS from peat [111] and soil [112]. The protocols used for the extractions may follow some laborious procedure that enable to isolate and purify the HS, as recommended by the International Humic Substances Society (IHSS) [113], or other [114]. Other extracts may be produced for characterization, simply by leaving the compost in contact with water for a certain period of time [115].

3.2.1. Compost characterization

The stability and maturity of the compost is one of its most important characteristics. The stability of the compost is related to the nature of its organic matter that does not undergo further degradation [116]. Maturity, on the other hand, is related to the degree of humification that compost has undergone [116]. These properties may be characterised by means of different approaches, using the physical, chemical and biological properties of compost [117]. Total carbon and nitrogen determined by elemental analysis, are used to obtain the C/N ratio that is used as an indicator of maturity and stability. For agriculture application the compost should have a value of this ratio lower than 15. Thermal analysis, the refractory nature of compost samples may be accessed through the ratio WL_3/WL_2 from the mass loss at 400 - 620 °C (WL_3) and at 177 - 400 °C (WL_2). In addition to these techniques, FTIR is also one of the most widely used techniques to characterize compost samples through three empiric parameters ($I_{1630/2925}$, $I_{1630/2845}$ and $I_{1540/2925}$), designated by aromaticity indexes.

In addition to the characterization of the compost stability and maturity mentioned above, the compost quality is characterised using different parameters. Table 1.5 resumes some information regarding specific parameters used to characterise the compost stability, maturity, and quality. The moisture content is a crucial indicator of compost quality whose value is typically between 40 to 60 %, although the final value depends on the type of raw material [74,118,119]. The cation exchange capacity (CEC) is also used to characterize the quality of organic matter. This quantity measures the amount of negative charges present at the surface of the solid matrix and is evaluated from the extent to which cations are exchanged. For compost application in agriculture, the minimum value recommended for CEC is 60 $cmol_{(+)}$ kg^{-1} [108]. The organic carbon content is of major importance if the compost is to be used to enhance soil organic matter content.

Table 1.5: Relevant indicators used to characterise the compost.

Characterization	Parameter	Reference value	Reference
Stability/maturity	*C/N*	<15	[101]
	WL_3/WL_2	< 1	[121]
	$I_{1630/2925}$, $I_{1630/2845}$, $I_{1540/2845}$, $I_{1540/2925}$	*	[101]
Quality	Moisture content	40 to 60 %	[74]
	CEC	> 60 $cmol_{(+)}$ kg^{-1}	[108]
	Organic carbon content	At least 15 % of dry matter	[120]
	Nutrients (N, P, K)	At least 4 % of dry matter	[120]
	Metals	<1.5 mg/kg dry matter for cadmium <2 mg/kg dry matter for chromium <1 mg/kg dry matter for mercury <50 mg/kg dry matter for nickel <120 mg/kg dry matter for lead <40 mg/kg dry matter for arsenic <300 mg/kg dry matter for copper <800 mg/kg dry matter for zinc	[120]
	Presence of pathogens	*Salmonella* (absence in 25 g) *Escherichia coli* (<1000 CFU in 1g)	[120]
	Germination index	*	[122]

* no reference value is reported

This parameter shall have a value of at least 15 % of the mass [120]. The content of essential nutrients (N, P and K) that are beneficial for the optimal growth of plants also constitutes an important quality parameter. The sum of the content of these nutrients shall be at least 4 % of the compost mass. The quality of compost is also related to the content of some undesirable compounds, such as heavy metals,

that should be low. The presence of pathogenic microorganisms is another important factor for the compost quality. The germination index (GI) which combines the measure of seed germination and root growth of seeds, is one of the most sensitive biological parameters and more reproducible used to evaluate toxicity.

3.2.2. Water soluble extracts

Water soluble extracts contain an organic fraction which is called dissolved organic matter (DOM), in addition to containing a significant inorganic fraction of salts. Where DOM is considered a heterogeneous class of water-soluble compounds with diversified chemical compositions and properties. It is described as a complex mixture of aromatic and aliphatic hydrocarbon structures that have attached amino acids, amide, carboxyl, hydroxyl, ketone, and various minor functional groups [123,124], of transphilic acids (defined as the least hydrophilic of the non-humic DOM compounds) [125] and a small fraction of fulvic acid. The inorganic fraction is commonly characterised by the quantification of the anions Cl^-, F^-, SO_4^{2-}, NO_2^-, NO_3^-, and of the major elements Si, Ca, Mg, Na, K, Fe, Al, As, Cd, Co, Cr, Cu, Mn, Ni, Pb, Zn, and also by the concentration of P, and of NH_4^+ and by electrical conductivity [99]. The organic fraction is analysed through its content of dissolved organic carbon (DOC), pH and by is coefficient of molar absorptivity (ε_{280}). However, there are other techniques that can also be used to characterise DOM such as, FTIR, fluorescence spectroscopy, inductively coupled plasma optical emission (ICP-OES), mass spectrometry (MS) and nuclear magnetic resonance (NMR) [123].

Due to its polymeric, polyfunctional, and polydispersive nature, DOM also plays an essential role in regulating the solubility and chemical speciation of trace metals, the surface properties and toxicity of nanoparticles, and the fate and transport of organic contaminants, thus influencing water quality, ecological functions, and biogeochemical processes in aquatic environments [126,127].

3.2.3. Humic-like substances

Humic-like substances (HS-L) are important constituents of the organic fraction of compost, consisting of a complex heterogeneous mixtures of carbon-based substances formed by biochemical reactions during the decay and transformation of wastes and microbial remains. HS are described as supramolecular structures of small and heterogeneous molecules, linked by hydrophobic interactions and hydrogen bonds [128]. Their molecular structures are impossible to define precisely due to the heterogeneous nature of these compounds, mainly associated with the variety of processes that can give rise to them [129].

The size, molecular weight, elemental compositions, structure, and the number and nature of functional groups of HS vary depending on their origin, method of extraction, and natural condition which prevailed

on their formation [130,131]. Individual molecules cannot be identified from humic substances, but they might be subdivided into three fractions according to their solubility in water: humic acids that are insoluble under acid conditions (pH 2) but soluble at elevated pH, fulvic acids that are the fraction of HS soluble in aqueous solutions under all pH values, and humin (Hu) that is insoluble in water at all pH values [132].

Regarding the typical elemental composition of humic substances, the carbon content generally increases from fulvic acid (FA) to humic acid (HA), whereas the oxygen content follows the reverse trend. The presence of oxygen and nitrogen in HS is an indication that certain functional groups are present. The most important functional groups that have been reported in HS include carboxyl (COOH), phenolic (Ph-OH), enolic (OH), quinone, hydroxyquinone, lactone, ether, and alcoholic (OH) [132,133].

The characterization of the main properties and functions of these substances in the environment is performed through their basic structure. HS have a wide range of molecular weights and sizes, ranging from a few hundred to as much as several hundred thousand atomic mass units (Da). The structures of FA are somewhat more aliphatic and less aromatic than HA, and FA are richer in carboxylic acid, phenolic and ketonic groups [134]. This is the main cause for the higher solubility of FA in water at all pHs. HA, being more aromatic, become insoluble when the carboxylated groups are protonated at low pH values. The HS structure allows it to have an amphiphilic behaviour, with the ability to bind both hydrophobic and hydrophilic materials.

As the HS are made up of thousands of diverse molecules it is impractical to separate out each molecule for analysis. Therefore, the characterization of such a complex mixture result in average values representing the entire mixture. In an attempt to characterise the complex properties and characteristics of HS almost every analytical technique available has been used but there is not any particular analytical method or combination of methods that may provide a complete description of the structure of HS.

The HS-L isolated from compost have been characterized by elemental analysis (EA) or by thermal (TGA and DSC) techniques [135–137] and also characterized by the spectroscopic techniques, FTIR, UV-vis, ^{1}H-NMR and ^{13}C-NMR [138,139] and by their acid-base [140] and metal binding properties.

The elemental composition provides the most fundamental information of organic compounds with a good precision. Figure 1.6 shows a typical Van Krevelen plot from humic substances extracted from a soil [141], where HA shows lower values of the O/C ratio in comparison with FA, that is a consequence of its higher content of carbon and lower content of oxygen. This result is usually attributed to the enrichment of the material in oxygenated acidic groups that lead to a larger number of acidic sites in the FA fraction. The O to C ratio (O/C) is an indicator of the degree of oxidation and carbohydrate content.

On the other side, the H/C ratio is an indicator of the extent of saturation of C atoms and/or the abundance of branched structures in the molecule, a lower H/C ratio is obtained for a higher amount of unsaturated structures. Regarding this parameter, there is not a large difference between the two extracts, as depicted in Figure 1.6.

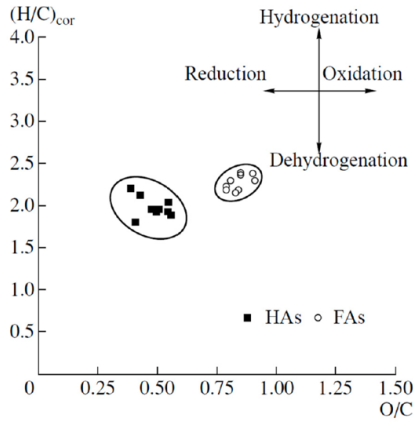

Figure 1.6: Van Krevelen plot of humic and fulvic acids extracted from a soil [141].

To obtain information on the molecular structure of HS, including the identification of functional groups, a combination of several techniques is sometimes used, including different spectroscopic methods, such as FTIR and NMR. Figure 1.7 shows a typical FTIR spectrum of HA-L isolated from the composted sludge-green waste mixture. Where the strong absorption band at 3400-3300 cm^{-1} confirmed the presence of abundant OH and amino groups, the absorption peaks that appeared near 2920 cm^{-1} are associated with aliphatic C–H stretching, at 1710 cm^{-1} are related with C=O stretching of COOH and ketonic C=O), at 1660–1600 cm^{-1} are associated with aromatic C=C and H bonded C=O, at 1460 - 1400 cm^{-1} are related with C-H deformation, at 1233-1220 cm^{-1} are associated with C–O stretching of COOR and at 1030-1020 cm^{-1} are related with C-0 stretching. This makes FTIR spectroscopy an interesting technique for the investigation of functional groups in HS.

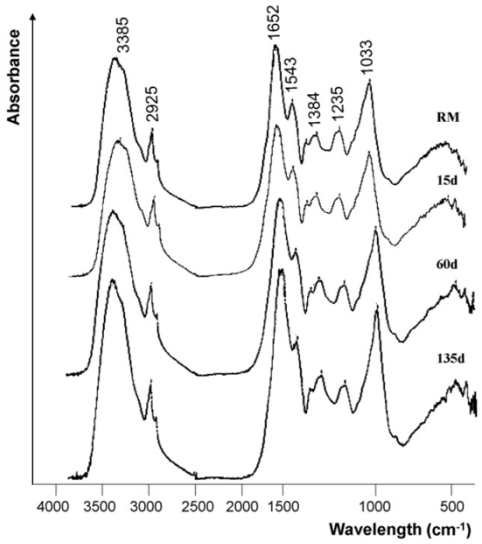

Figure 1.7: FTIR spectra of humic-like acids extracted from the composted sludge-green waste mixture at different composting stages [142].

UV-visible (UV-vis) spectroscopy provides useful information on the composition of organic matter [11–13]. Within this context, some numerical indexes were proposed in the literature. The most typical ones are the ratio E_4/E_6 between the absorbance at 465 nm and 665 nm or the coefficient of molar absorptivity, ε_{280} nm (related to the π- π* electron transitions in this region of the UV range) have proven to be useful to evaluate the degree of humification of HS extracted from organic materials of diverse origins [14–16]. NMR spectroscopy, including the ^{13}C-NMR and ^{1}H-NMR, has been widely applied in the characterization of HSs. The ^{1}H-NMR spectra illustrated in Figure 1.8 is from a HA-L extract from compost of solid mill olive wastes [143]. These proton spectra are typically divided into three main regions: (i) 0.5–3 ppm, resonance of alkyl protons and protons attached to carbon in a to aromatic ring, carboxyl and carbonyl groups (H_{ali}); (ii) 3-4.5 ppm, protons attached to carbon bearing oxygen or nitrogen; and (iii) 6–8.5 ppm, protons attached to unsaturated carbons and aromatic protons (H_{arom}).

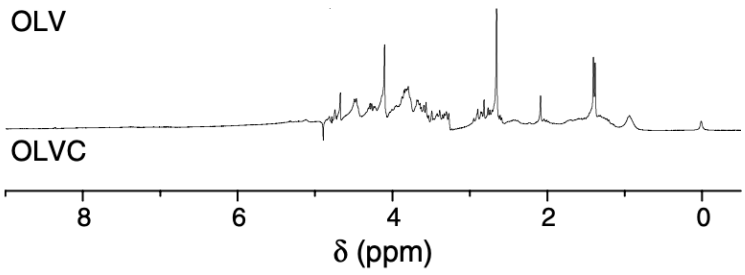

Figure 1.8: ^{1}H-NMR spectra of humic-like acid extracted from compost of solid mill olive wastes [143].

The reactivity of the extracts is usually characterized by acid-base titrations, where the deprotonated acid groups are quantified. Figure 1.9 shows experimental data of an acid-base titration of humic-like substances (HA-L and FA-L) extracted from a composted mixture of olive oil mill wastewater expressed as the negative charge as a function of proton concentration at three ionic strengths. [140]. Typically, these results depict that the increase in negative charge on HA-L and FA-L is related to the increase in pH and ionic strength and also, the HA-L exhibit smaller charge densities across the entire range of proton concentration and ionic strength than the corresponding FA-L. In these curves can also be identified two types of acid sites: carboxylic-type, at pH 3-5, and phenolic-type, at pH 8-10. Through the fitting of experimental points of the acid-base curves with the NICA-Donnan model (Equation 1.1), it is possible to have access to relevant information, such as the total acidity ($M_1 + M_2$) and the carboxyl and phenolic OH group contents (M_1 and M_2, respectively).

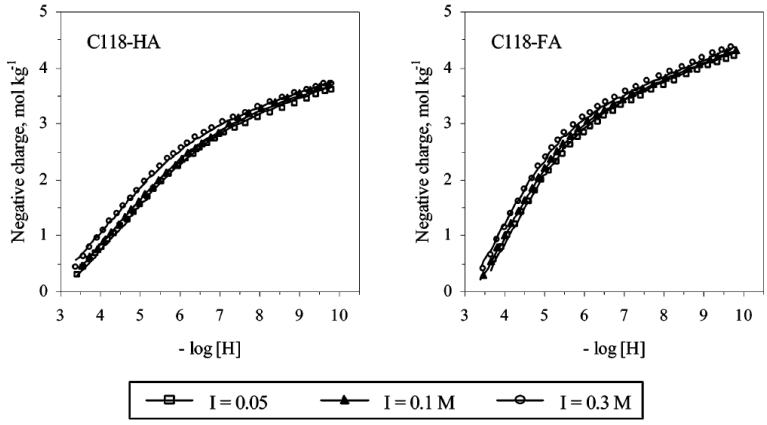

Figure 1.9: Experimental data (symbols) and fits with the NICA-Donnan model (continuous line) for proton binding by humic acids extracted from a composted mixture of olive oil mill wastewater expressed as negative charge as a function of pH at different ionic strength (KNO_3) [140].

In addition to acid-base titrations (proton binding), titrations with metallic cations, enable a more complete study. Therefore, through the simultaneous adjustment of the proton and metal titration curves with the NICA-Donnan model, meaningful data are obtained. The NICA-Donnan model is the intersection of two models: NICA model referring to intrinsic chemical heterogeneity and the Donnan model referring to the electrostatic effect [140,144,145].

$$Q_i = \frac{n_{i,1}}{n_{H,1}} \times M_1 \frac{(K_{i,1}a_i)^{n_{i,1}}}{\Sigma_i (K_{i,1}a_i)^{n_{i,1}}} \times \frac{\left[\Sigma_i (K_{i,1}a_i)^{n_{i,1}}\right]^{p_1}}{1 + \left[\Sigma_i (K_{i,1}a_i)^{n_{i,1}}\right]^{p_1}} + \frac{n_{i,2}}{n_{H,2}} \times M_2 \frac{(K_{i,2}a_i)^{n_{i,2}}}{\Sigma_i (K_{i,2}a_i)^{n_{i,2}}} \times \frac{\left[\Sigma_i (K_{i,2}a_i)^{n_{i,2}}\right]^{p_2}}{1 + \left[\Sigma_i (K_{i,2}a_i)^{n_{i,2}}\right]^{p_2}} \quad \text{(Equation 1.1)}$$

Where the parameters represent the amount bound to the HS Q_i (mol kg^{-1}), the total quantities per site M_n, median values of affinity distributions per site, $K_{i,1}$, the non-ideality factor of n_n, and the widths of the affinity distributions, which describe the intrinsic heterogeneity of the humic material, p. All these parameters are intrinsic, therefore independent of the properties of the medium such as pH, ionic strength, or concentrations of the ions in solution.

Figure 1.10 shows a typical representation of experimental data from a titration assay of lead binding to an aquatic fulvic acid at different pH values, as no data for binding with extracts from composts are yet available in the literature. Figure 1.10 displays log [Pb_{bound}] as a function of the free Pb concentration, log [Pb^{2+}], for pH values of 4.0, 4.5, and 5.0 at I=0.01 mol L^{-1}. The Pb binding is pH dependent, with more Pb bound at higher pH.

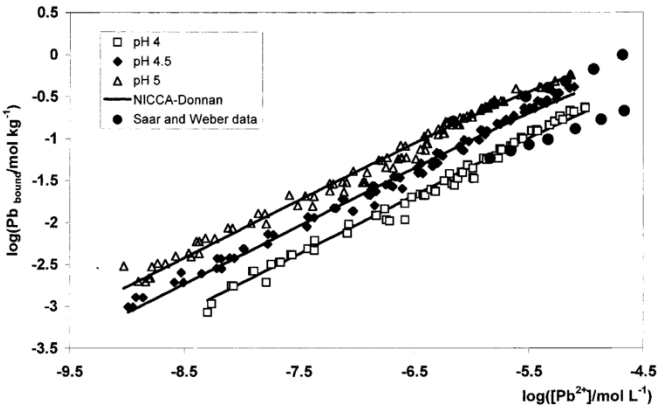

Figure 1.10: Lead binding to a soil fulvic acid in 0.01 mol L^{-1} KNO_3 at pH 4.0. 4.5 and 5.0 [146].

Table 1.6 summarises the information about the parameters used to characterise the water soluble and HS-L.

Table 1.6: Relevant indicators used to characterize the water-soluble extract (DOM) and humic-like substances from compost, with the exception of the last parameter (highlighted) only studied in HS extracted from natural organic material (*e.g.* peat, soils)

Parameter	Extract	Reference value	Information associated	Reference
DOC	DOM	> 4 g kg^{-1} of compost	content of dissolved organic carbon	[147]
EC	DOM	> 4 mS cm^{-1}	quantity of salts that dissolve in water.	[99]
NH_4^+/NO_3^-	DOM	*	inorganic N content	[148]
ε_{280}	DOM or HS-L	*	aromaticity of the extracts and allows calculating the aromaticity and molecular mass	[138,149]
O/C	HS-L	*	indicator of the degree of oxidation and carbohydrate content	[150]
H/C	HS-L	*	indicator of the extent of saturation of C atoms	[150]
E_4/E_6	HS-L	*	formation of well humified components (665 nm) with respect to the components in the first phases of humification process (465 nm)	[138]
Humification index	HS-L	*	amount of HS	[151]
b	HS-L	*	empirical parameter describing how the Donnan volume varies with ionic strength	[140]
M_1 (=$Q_{max H,1}$) and M_2 (=$Q_{max H,2}$)	HS-L	*	carboxyl group and phenolic OH group contents	[140]
K_1 and K_2	HS-L	*	median value of affinity distribution for proton binding by carboxyl and phenolic groups	[140]
m_1 and m_2	HS-L	*	width of proton-affinity distribution of carboxyl and phenolic OH groups, which describe the apparent heterogeneity of the HS	[140]
p_1 and p_2	HS-L	*	width of affinity distribution, which describes the intrinsic heterogeneity of carboxyl and phenolic OH groups of the HS	[152]

*no reference value is reported

3.3. Comparison between composts of different origins

The impact of the sort of the raw materials and composting methods have been studied in assays performed on the compost [23–26,103,153–165] and on the extracts of the compost, including humic-like substances [154,157,158,163–165] and water-soluble extracts [156,157]. The studies based on the characterization of compost may use single characterization techniques, such as elemental characterization [23,155,160] or TGA [161], or on more than one characterization techniques, combining elemental characterization information with thermogravimetric results [103,153], or with spectroscopic data [153,159], or with physico-chemical parameters [24–26,156,162], or with chemometric analyses [156,159,165], or with plant growth assays [24,26,157]. Regarding the characterization studies performed on the compost extracts, most of the works combine elemental characterization information with spectroscopic data [24,26,154,156,158,163], or with thermal analysis [163] or with acid-base titration results [154,157,158,163] or with plant growth assays [157,166,167].

Several works report different effects on the compost properties associated with the feedstock nature and composting methodologies. In a study with 3 composts and 3 vermicomposts, authors found that the C/N ratio was lower for vermicomposts [153]. By FTIR certain differences were noticed between the spectra from composts obtained from different feedstock. These differences were detected in specific

wavenumbers, depending on the nature of the feedstock [153]. By TGA it was noticed that vermicomposts showed larger residues [153]. Using a principal component analysis (PCA) result from 21 composts and 7 vermicompost were analysed. Authors identified the total N, TOC, pH and the germination index as the most relevant parameters but were not able to discriminate the samples from different composting methodologies [154]. No significant differences were found in 12 of the 17 chemical parameters analysed between the 27 samples of home composting and the 25 samples of industrial composting. However, the contents of Cu and Ni were higher in the industrial compost, while the C/N ratio was higher for the home composting samples [155].

Some trends were observed in certain characterization parameters of compost related to the nature of the feedstock. For example, the nitrogen content was reported to be higher for composts prepared from manure [26]. An association was also made between the urban biowastes and a low content of heavy metals in compost, particularly regarding to Fe, Zn, Cu, Mn and Ni [24] and between the sewage sludge and high contents of Pb, Cr and of N, P, K, S, Ca, Mg and Na [24]. The algae wastes were associated with low values of C/N ratio and high contents in Cd [23]. The presence of green wastes was shown to influence the C/N ratio of compost, although this effect is not consensual. In some studies, this type of raw material is associated to an increased values of C/N [25,26,165], whereas in another study the opposite is reported [160]. With respect to the content of heavy metals, lower amounts of Cd, Pb and Ni are associated with green wastes [25]. Regarding the essential nutrient contents, lower values of N, P, K were associated with green wastes [25], although the opposite was reported for the content of K [160]. The green waste composts were also associated to high levels of the macronutrients Na, Mg, Ca [160] and a low organic matter content [26].

The relation between plant growth and compost origin is addressed in a restricted number of papers. Whereas seed germination and plant root growth were reported to be inhibited by a compost produced from sewage sludge [24], in another study seed germination is reported to be improved by composts produced from manure and domestic wastes [157]. In a plant growth study using cucumber it was observed that the fresh weight of the fruit was increased by the use of compost containing manure [26]. The comparison between the HS-L from compost and vermicompost is addressed only in one paper [154] where higher nitrogen and higher content in aliphatic structures, and simultaneously a lower oxidation degree were found for the compost. The effect of the nature of the feedstock on the HS composition is addressed in three papers [24,158,163]. The HS-L of compost containing sewage sludge exhibited higher values of humification index ($HI = C_{extrac}\text{-}C_{HS}/C_{HS}\,\%$) and of humification rate ($HR,\ HR = 100 \times C_{HS}/TOC\ \%$) compared with those containing exclusively urban biowastes [24]. The HA-L extracts of vermicomposts

prepared from cow manure presented higher values of the HI and EC than that of sewage sludge [163]. In another study it is reported that no significant differences were found in the molecular structure and thermal characteristics of the HA-L of vermicompost containing different proportions of tomato-plant wastes and paper mill sludge, although the HA-L content was higher when the content of tomato-plant wastes was increased [158].

Plant growth assays using extracts from compost of different origin are reported in few papers [157,166,167]. While seed germination was improved by the water-soluble extract of composts of varied origins, particularly from manure and domestic wastes [157], a negative effect on seed germination was found in assays where HS-L from municipal wastes were used [167]. In a study where HS-L of green wastes were tested in a basil crop study, a noticeable positive effect was found in the plant fresh weight, in the yield, on the antibacterial properties and free radical scavengers' activity of essential oils [166].

4. References

[1]A. Cerda, A. Artola, X. Font, R. Barrena, T. Gea, A. Sánchez, Composting of food wastes: Status and challenges, Bioresource Technology. 248 (2018) 57–67. https://doi.org/10.1016/j.biortech.2017.06.133.

[2]S.L. Lim, L.H. Lee, T.Y. Wu, Sustainability of using composting and vermicomposting technologies for organic solid waste biotransformation: Recent overview, greenhouse gases emissions and economic analysis, Journal of Cleaner Production. 111 (2016) 262–278. https://doi.org/10.1016/j.jclepro.2015.08.083.

[3]A. Mesjasz-lech, Municipal waste management in context of sustainable urban development, Procedia - Social and Behavioral Sciences. 151 (2014) 244–256. https://doi.org/10.1016/j.sbspro.2014.10.023.

[4]M.D. Meena, R.K. Yadav, B. Narjary, G. Yadav, H.S. Jat, P. Sheoran, M.K. Meena, R.S. Antil, B.L. Meena, H. V Singh, V. Singh, P.K. Rai, A. Ghosh, P.C. Moharana, Municipal solid waste (MSW): Strategies to improve salt affected soil sustainability: A review, Waste Management. 84 (2019) 38–53. https://doi.org/10.1016/j.wasman.2018.11.020.

[5]S. Kaza, L. Yao, P. Bhada-Tata, F. Van Woerden, What a Waste 2.0: A Global Snapshot of Solid Waste Management to 2050, World Bank Group, 2018.

[6]A. Portuguesa do Ambiente, Relatório Anual Resíduos Urbanos, 2021. https://apambiente.pt/sites/default/files/_Residuos/Producao_Gestão_Residuos/Dados%20RU/RARU%202020_V1.pdf.

[7]S. Kaza, L. Yao, P. Bhada-Tata, F.V. Woerden, What a Waste 2.0: A Global Snapshot of Solid Waste Management to 2050, World Bank Group, 2018.

[8]L. Six, F. Velghe, S. Verstichel, Sustainability Considerations on the Valorization of Organic Waste, in: Biotransformation of Agricultural Waste and By-Products, Elsevier Inc., 2016: pp. 287–307. https://doi.org/10.1016/B978-0-12-803622-8.00011-2.

[9]J. Malinauskaite, H. Jouhara, D. Czajczyńska, P. Stanchev, E. Katsou, P. Rostkowski, R.J. Thorne, J. Colón, S. Ponsá, F. Al-Mansour, L. Anguilano, R. Krzyżyńska, I.C. López, A.Vlasopoulos, N. Spencer, Municipal solid waste management and waste-to-energy in the context of a circular economy and energy recycling in Europe, Energy. 141 (2017) 2013–2044. https://doi.org/10.1016/j.energy.2017.11.128.

[10]A. Bosmans, I. Vanderreydt, D. Geysen, L. Helsen, The crucial role of Waste-to-Energy technologies in enhanced landfill mining: A technology review, Journal of Cleaner Production. 55 (2013) 10–23. https://doi.org/10.1016/j.jclepro.2012.05.032.

[11]M. Scungio, G. Buonanno, L. Stabile, G. Ficco, Lung cancer risk assessment at receptor site of a waste-to-energy plant, Waste Management. 56 (2016) 207–215. https://doi.org/10.1016/j.wasman.2016.07.027.

[12]A. Damgaard, C. Riber, T. Fruergaard, T. Hulgaard, T.H. Christensen, Life-cycle-assessment of the historical development of air pollution control and energy recovery in waste incineration, Waste Management. 30 (2010) 1244–1250. https://doi.org/10.1016/j.wasman.2010.03.025.

[13]F. Xu, Y. Li, X. Ge, L. Yang, Y. Li, Anaerobic digestion of food waste – Challenges and opportunities, Bioresource Technology. 247 (2018) 1047–1058. https://doi.org/10.1016/j.biortech.2017.09.020.

[14]M.J. Rogoff, F. Screve, WTE technology, in: Waste-to-Energy, Elsevier, 2011: pp. 21–43. https://doi.org/10.1016/B978-1-4377-7871-7.10003-6.

[15]D.J. Batstone, B. Virdis, The role of anaerobic digestion in the emerging energy economy, Current Opinion in Biotechnology. 27 (2014) 142–149. https://doi.org/10.1016/j.copbio.2014.01.013.

[16]A.J. Ward, P.J. Hobbs, P.J. Holliman, D.L. Jones, Optimisation of the anaerobic digestion of agricultural resources, Bioresource Technology. 99 (2008) 7928–7940. https://doi.org/10.1016/j.biortech.2008.02.044.

[17]A. Khalid, M. Arshad, M. Anjum, T. Mahmood, L. Dawson, The anaerobic digestion of solid organic waste, Waste Management. 31 (2011) 1737–1744. https://doi.org/10.1016/j.wasman.2011.03.021.

[18]C. Park, C. Lee, S. Kim, Y. Chen, H.A. Chase, Upgrading of anaerobic digestion by incorporating two different hydrolysis processes, Journal of Bioscience and Bioengineering. 100 (2005) 164–167. https://doi.org/10.1263/jbb.100.164.

[19]United Nations, General Assembly Resolution A/RES/70/1. Transforming Our World, the 2030 Agenda for Sustain- able Development., FAO, n.d. http://www.un.org/ga/search/view_doc.asp?symbol=A/RES/70/1&Lang=E (accessed September 23, 2021).

[20]C.A. Edwards, N.Q. Arancon, R. Sherman, eds., Vermiculture technology: eathworms, organic wastes, and environmental management, CRC Press, Taylor & Francis Group, Boca Raton London New York, 2011.

[21]S.A. Bhat, J. Singh, A.P. Vig, Earthworms as Organic Waste Managers and Biofertilizer Producers, WASTE AND BIOMASS VALORIZATION. 9 (2018) 1073–1086. https://doi.org/10.1007/s12649-017-9899-8.

[22]L. Cai, X. Gong, X. Sun, S. Li, X. Yu, Comparison of chemical and microbiological changes during the aerobic composting and vermicomposting of green waste, PLOS ONE. 13 (2018). https://doi.org/10.1371/journal.pone.0207494.

[23]W. Han, W. Clarke, S. Pratt, Composting of waste algae: A review, Waste Management. 34 (2014) 1148–1155. https://doi.org/10.1016/j.wasman.2014.01.019.

[24]M. Jakubus, A Comparative Study of Composts Prepared from Various Organic Wastes Based on Biological and Chemical Parameters, Agronomy. 10 (2020) 869. https://doi.org/10.3390/agronomy10060869.

[25]M. Reyes-Torres, E.R. Oviedo-Ocaña, I. Dominguez, D. Komilis, A. Sánchez, A systematic review on the composting of green waste: Feedstock quality and optimization strategies, Waste Management. 77 (2018) 486–499. https://doi.org/10.1016/j.wasman.2018.04.037.

[26]S. Zmora-Nahum, Y. Hadar, Y. Chen, Physico-chemical properties of commercial composts varying in their source materials and country of origin, Soil Biology and Biochemistry. 39 (2007) 1263–1276. https://doi.org/10.1016/j.soilbio.2006.12.017.

[27]K.M. Wichuk, D. McCartney, Compost stability and maturity evaluation - a literature review, Canadian Journal of Civil Engineering. 37 (2010) 1505–1523. https://doi.org/10.1139/L10-101.

[28]A.P. Lannan, M.S. Erich, T. Ohno, Compost feedstock and maturity level affect soil response to amendment, Biology and fertility of soils. 49 (2013) 273–285. https://doi.org/10.1007/s00374-012-0715-0.

[29]E.I. Arslan, A. Ünlü, M. Topal, Determination of the Effect of Aeration Rate on Composting of Vegetable-Fruit Wastes, Clean Soil Air Water. 39 (2011) 1014–1021.

https://doi.org/10.1002/clen.201000537.

[30]M. Milinković, B. Lalević, J. Jovičić-Petrović, V. Golubović-Ćurguz, I. Kljujev, V. Raičević, Biopotential of compost and compost products derived from horticultural waste—Effect on plant growth and plant pathogens' suppression, Process Safety and Environmental Protection. 121 (2019) 299–306. https://doi.org/10.1016/j.psep.2018.09.024.

[31]I. Petric, N. Mustafić, Dynamic modeling the composting process of the mixture of poultry manure and wheat straw, Journal of Environmental Management. 161 (2015) 392–401. https://doi.org/10.1016/j.jenvman.2015.07.033.

[32]S. Gajalakshmi, S.A. Abbasi, Solid Waste Management by Composting: State of the Art, Critical Reviews in Environmental Science and Technology. 38 (2008) 311–400. https://doi.org/10.1080/10643380701413633.

[33]A. de Guardia, C. Petiot, D. Rogeau, C. Druilhe, Influence of aeration rate on nitrogen dynamics during composting, Waste Management. 28 (2008) 575–587. https://doi.org/10.1016/j.wasman.2007.02.007.

[34]B. Lv, D. Zhang, Y. Cui, F. Yin, Effects of C/N ratio and earthworms on greenhouse gas emissions during vermicomposting of sewage sludge, Bioresource technology. 268 (2018) 408–414. https://doi.org/10.1016/j.biortech.2018.08.004.

[35]J.M. Agnew, J.J. Leonard, The Physical Properties of Compost, Compost Science & Utilization. 11 (2003) 238–264. https://doi.org/10.1080/1065657X.2003.10702132.

[36]L.F. Diaz, C.G. Golueke, G.M. Savage, L.L. Eggerth, Composting and recycling municipal solid waste, 2020.

[37]L. Zhang, X. Sun, Changes in physical, chemical, and microbiological properties during the two-stage co-composting of green waste with spent mushroom compost and biochar, Bioresource Technology. 171 (2014) 274–284. https://doi.org/10.1016/j.biortech.2014.08.079.

[38]M.P. Bernal, J.A. Alburquerque, R. Moral, Composting of animal manures and chemical criteria for compost maturity assessment. A review, Bioresource Technology. 100 (2009) 5444–5453. https://doi.org/10.1016/j.biortech.2008.11.027.

[39]Z. Li, H. Lu, L. Ren, L. He, Experimental and modeling approaches for food waste composting: A review, Chemosphere. 93 (2013) 1247–1257. https://doi.org/10.1016/j.chemosphere.2013.06.064.

[40]C.O. Onwosi, V.C. Igbokwe, J.N. Odimba, I.E. Eke, M.O. Nwankwoala, I.N. Iroh, L.I. Ezeogu, Composting technology in waste stabilization: On the methods, challenges and future prospects, Journal of Environmental Management. 190 (2017) 140–157. https://doi.org/10.1016/j.jenvman.2016.12.051.

[41]F. Benlboukht, L. Lemee, S. Amir, A. Ambles, M. Hafidi, Biotransformation of organic matter during composting of solid wastes from traditional tanneries by thermochemolysis coupled with gas chromatography and mass spectrometry, Ecological engineering. 90 (2016) 87–95. https://doi.org/10.1016/j.ecoleng.2016.01.074.

[42]B.S. Valente, E.G. Xavier, H. da S. Pereira, M.V. Tabeleao Pilotto, Composting in residues management of freshwater fish, boletim do instituto de pesca. 40 (2014) 95–103.

[43]C. Zhou, Z. Liu, Z.-L. Huang, X.-L. Yu, P. Ning, A new strategy for co-composting dairy manure with rice straw: Addition of different inocula at three stages of composting, Waste management. 40 (2015) 38–43. https://doi.org/10.1016/j.wasman.2015.03.016.

[44]O. Bikovens, T. Dizhbite, G. Telysheva, Characterisation of humic substances formed during co-composting of grass and wood wastes with animal grease, Environmental Technology (United Kingdom). 33 (2012) 1427–1433. https://doi.org/10.1080/09593330.2011.632652.

[45]Z.S. Vásquez, D.P. de Carvalho Neto, G.V.M. Pereira, L.P.S. Vandenberghe, P.Z. de Oliveira, P.B. Tiburcio, H.L.G. Rogez, A. Góes Neto, C.R. Soccol, Biotechnological approaches for cocoa waste management: A review, Waste Management. 90 (2019) 72–83. https://doi.org/10.1016/j.wasman.2019.04.030.

[46]M. Raviv, Y. Oka, J. Katan, Y. Hadar, A. Yogev, S. Medina, A. Krasnovsky, H. Ziadna, High-nitrogen compost as a medium for organic container-grown crops, Bioresource Technology. 96 (2005) 419–427. https://doi.org/10.1016/j.biortech.2004.06.001.

[47]R. Kumar, D. Verma, B.L. Singh, U. Kumar, Shweta, Composting of sugar-cane waste by-products through treatment with microorganisms and subsequent vermicomposting, BIORESOURCE TECHNOLOGY. 101 (2010) 6707–6711. https://doi.org/10.1016/j.biortech.2010.03.111.

[48]C. Khatua, S. Sengupta, V.K. Balla, B. Kundu, A. Chakraborti, S. Tripathi, Dynamics of organic matter decomposition during vermicomposting of banana stem waste using Eisenia fetida, WASTE MANAGEMENT. 79 (2018) 287–295. https://doi.org/10.1016/j.wasman.2018.07.043.

[49]O. Muter, A. Pogulis, M. Grube, M. Gavare, A. Berzins, S. Strikauska, U. Hansons, A. Hansons, Potato pulp as a composting substrate, Zemdirbyste-agriculture. 101 (2014) 57–66. https://doi.org/10.13080/z-a.2014.101.008.

[50]B. Eshetu, K.-U. Eckhardt, P. Leinweber, Soil organic matter alterations by short-term composted coffee pulp waste: evidence from pyrolysis-field ionisation mass spectrometry, Landbauforschung. 63 (2013) 191–199. https://doi.org/10.3220/LBF_2013_191-200.

[51]S.H. Chang, Bio-oil derived from palm empty fruit bunches: Fast pyrolysis, liquefaction and future prospects, Biomass & bioenergy. 119 (2018) 263–276. https://doi.org/10.1016/j.biombioe.2018.09.033.

[52]R. Parillo, V. Ventorino, O. Pepe, P. Cornejo Rivas, A. Testa, Use of Compost from Chestnut Lignocellulosic Residues as Substrate for Tomato Growth, Waste and Biomass Valorization. 8 (2017) 2711–2720. https://doi.org/10.1007/s12649-016-9761-4.

[53]A. Isibika, B. Vinnerås, O. Kibazohi, C. Zurbrügg, C. Lalander, Co-composting of banana peel and orange peel waste with fish waste to improve conversion by black soldier fly (Hermetia illucens (L.), Diptera: Stratiomyidae) larvae, Journal of Cleaner Production. 318 (2021) 128570. https://doi.org/10.1016/j.jclepro.2021.128570.

[54]A. Chorolque, G. Pellejero, M.C. Sosa, J. Palacios, G. Aschkar, C. García-Delgado, R. Jiménez-Ballesta, Biological control of soil-borne phytopathogenic fungi through onion waste composting: implications for circular economy perspective, Int. J. Environ. Sci. Technol. (2021). https://doi.org/10.1007/s13762-021-03561-2.

[55]Z. Majbar, K. Lahlou, M. Ben Abbou, E. Ammar, A. Triki, W. Abid, M. Nawdali, H. Bouka, M. Taleb, M. El Haji, Z. Rais, Co-composting of Olive Mill Waste and Wine-Processing Waste: An Application of Compost as Soil Amendment, Journal of chemistry. (2018). https://doi.org/10.1155/2018/7918583.

[56]A. Torres-Climent, P. Gomis, J. Martin-Mata, M.A. Bustamante, F.C. Marhuenda-Egea, M.D. Perez-Murcia, A. Perez-Espinosa, C. Paredes, R. Moral, Chemical, Thermal and Spectroscopic Methods to Assess Biodegradation of Winery-Distillery Wastes during Composting, PLOS ONE. 10 (2015). https://doi.org/10.1371/journal.pone.0138925.

[57]G.K. Evanylo, W.L. Daniels, Paper mill sludge composting and compost utilization, Compost Science and Utilization. 7 (1999) 30–39. https://doi.org/10.1080/1065657X.1999.10701961.

[58]V. Oliveira, M. Reis, Valorisation of pulp and paper industry residues through composting, in: 12th International Multidisciplinary Scientific Geoconference, SGEM 2012, Vol. IV, 2012: pp. 813–820.

[59]S. Biyada, M. Merzouki, K. Elkarrach, M. Benlemlih, Spectroscopic characterization of organic matter transformation during composting of textile solid waste using UV–Visible spectroscopy, Infrared spectroscopy and X-ray diffraction (XRD), Microchemical Journal. 159 (2020) 105314. https://doi.org/10.1016/j.microc.2020.105314.

[60]N. Asses, A. Farhat, S. Cherif, M. Hamdi, H. Bouallagui, Comparative study of sewage sludge co-composting with olive mill wastes or green residues: Process monitoring and agriculture value of the resulting composts, Process safety and environmental protection. 114 (2018) 25–35. https://doi.org/10.1016/j.psep.2017.12.006.

[61]A. Viel, F. Stellin, M. Carlot, C. Nadai, G. Concheri, P. Stevanato, A. Squartini, V. Corich, A. Giacomini, Characteristics of Compost Obtained from Winemaking Byproducts, WASTE AND BIOMASS VALORIZATION. 9 (2018) 2021–2029. https://doi.org/10.1007/s12649-017-0160-2.

[62]A.I. Nunes Leite, R.C. Alves, F.D. Soares, M.H. Otenie, V.R. de Paula, Characterization of solid waste generated by the dairy industry, Journal of Candido Tostes Dairy Institute. 73 (2018) 73–81. https://doi.org/10.14295/2238-6416.v73i2.672.

[63]G.W. Price, J. Zeng, P. Arnold, Influence of agricultural wastes and a finished compost on the decomposition of slaughterhouse waste composts, Journal of environmental management. 130 (2013) 248–254. https://doi.org/10.1016/j.jenvman.2013.08.050.

[64]K. Thomas, P. Rahman, Brewery wastes. Strategies for sustainability. A review., Aspects of Applied Biology. (2006) 1–12.

[65]A. Jouraiphy, S. Amir, M. El Gharous, J.C. Revel, M. Hafidi, Chemical and spectroscopic analysis of organic matter transformation during composting of sewage sludge and green plant waste, International Biodeterioration and Biodegradation. 56 (2005) 101–108. https://doi.org/10.1016/j.ibiod.2005.06.002.

[66]O. Bikovens, T. Dizhbite, G. Telysheva, Characterisation of humic substances formed during co-composting of grass and wood wastes with animal grease, Environmental technology. 33 (2012) 1427–1433. https://doi.org/10.1080/09593330.2011.632652.

[67]M. Illera-Vives, S. Seoane Labandeira, M.E. López-Mosquera, Production of compost from marine waste: Evaluation of the product for use in ecological agriculture, Journal of Applied Phycology. 25 (2013) 1395–1403. https://doi.org/10.1007/s10811-013-9997-3.

[68]P.E. Gibilisco, J.L. Lancelotti, V.L. Negrin, Y.L. Idaszkin, Composting of seaweed waste: Evaluation on the growth of Sarcocornia perennis, Journal of Environmental Management. 274 (2020) 111193. https://doi.org/10.1016/j.jenvman.2020.111193.

[69]A.M. Martin, Composting of seafood wastes, in: Maximising the Value of Marine By-Products, Elsevier, 2007: pp. 486–515. https://doi.org/10.1533/9781845692087.3.486.

[70]M. Tuomela, Biodegradation of lignin in a compost environment: a review, Bioresource Technology. 72 (2000) 169–183. https://doi.org/10.1016/S0960-8524(99)00104-2.

[71]E. Rudnik, Composting methods and legislation, in: Compostable Polymer Materials, Elsevier, 2019: pp. 127–161. https://doi.org/10.1016/B978-0-08-099438-3.00005-7.

[72]V.K. Sharma, M. Canditelli, F. Fortuna, G. Cornacchia, Processing of urban and agro-industrial residues by aerobic composting: Review, Energy Conversion and Management. 38 (1997) 453–478. https://doi.org/10.1016/S0196-8904(96)00068-4.

[73]L.F. Diaz, G.M. Savage, Factors that affect the process, Waste Management Series. 8 (2007) 49–65. https://doi.org/10.1016/S1478-7482(07)80007-8.

[74]R.T. Haug, The Practical Handbook of Compost Engineering, 1st ed., Routledge, 1993. https://doi.org/10.1201/9780203736234.

[75]U. Ali, N. Sajid, A. Khalid, L. Riaz, M.M. Rabbani, J.H. Syed, R.N. Malik, A review on vermicomposting of organic wastes, Environmental progress & sustainable energy. 34 (2015) 1050–1062. https://doi.org/10.1002/ep.12100.

[76]H.-J. Jördening, J. Winter, eds., Environmental biotechnology: concepts and applications, Wiley-VCH, Weinheim, 2005.

[77]J.D. Flores-Félix, E. Menéndez, R. Rivas, M. de la E. Velázquez, Future Perspective in Organic Farming Fertilization, in: Organic Farming, Elsevier, 2019: pp. 269–315. https://doi.org/10.1016/B978-0-12-813272-2.00010-0.

[78]S. Ahmad, R. Khalid, S. Abbas, R. Hayat, I. Ahmed, Potential of compost for sustainable crop production and soil health, in: Recent Advancement in Microbial Biotechnology, Elsevier, 2021: pp. 123–170. https://doi.org/10.1016/B978-0-12-822098-6.00005-7.

[79]J.R. Reeve, L.A. Hoagland, J.J. Villalba, P.M. Carr, A. Atucha, C. Cambardella, D.R. Davis, K. Delate, Organic Farming, Soil Health, and Food Quality: Considering Possible Links, in: Advances in Agronomy, Elsevier, 2016: pp. 319–367. https://doi.org/10.1016/bs.agron.2015.12.003.

[80]X. Guo, H. Liu, S. Wu, Humic substances developed during organic waste composting: Formation mechanisms, structural properties, and agronomic functions, Science of the Total Environment. 662 (2019) 501–510. https://doi.org/10.1016/j.scitotenv.2019.01.137.

[81]M.H.B. Hayes, R.S. Swift, Vindication of humic substances as a key component of organic matter in soil and water, in: Advances in Agronomy, Elsevier, 2020: pp. 1–37. https://doi.org/10.1016/bs.agron.2020.05.001.

[82]M.E. Peña-méndez, J. Havel, J. Patočka, Humic substances – compounds of still unknown structure: applications in agriculture , industry , environment , and biomedicine, J. Appl. Biomed. 3 (2005) 13–24. https://assets.motherearthlabs.com/resources/4.humic_.substances.compnds.of_.unkwn_.structure2005.pdf.

[83]L.P. Canellas, F.L. Olivares, N.O. Aguiar, D.L. Jones, A. Nebbioso, P. Mazzei, A. Piccolo, Humic and fulvic acids as biostimulants in horticulture, Scientia Horticulturae. 196 (2015) 15–27. https://doi.org/10.1016/j.scienta.2015.09.013.

[84]F. Meng, Q. Huang, G. Yuan, Y. Cai, F.X. Han, The beneficial applications of humic substances in agriculture and soil environments, in: New Trends in Removal of Heavy Metals from Industrial Wastewater, Elsevier, 2021: pp. 131–160. https://doi.org/10.1016/B978-0-12-822965-1.00007-6.

[85]S. Trevisan, O. Francioso, S. Quaggiotti, S. Nardi, Humic substances biological activity at the plant-soil interface: from environmental aspects to molecular factors., Plant Signaling & Behavior. 5 (2010) 635–43. https://doi.org/10.4161/psb.5.6.11211.

[86]K. (NSW D. Billingham, Humic products – potential or presumption for agriculture? Can humic products improve my soil?, in: Proceedings of the 27th Annual Conference of e Grassland Society of NSW,

2012: pp. 43–50. https://doi.org/ISBN 978 174256 257 5.

[87]Humintech®, Applications: Wastewater treatment, (n.d.). https://www.humintech.com/industry/applications/wastewater-treatment.html (accessed January 31, 2018).

[88]Humintech®, Applications: Cement & Concrete, (n.d.). https://www.humintech.com/industry/applications/cement-concrete.html (accessed January 31, 2018).

[89]K.H. Tan, Humic Matter in Soil and the Environment: Principles and Controversies, 2003.

[90]M.E. Essington, Organic Matter in Soil, in: Soil and Water Chemistry: An Integrative Approach, 2004: pp. 129–180. https://doi.org/10.1017/CBO9781107415324.004.

[91]Humintech®, Applications: Other applications, (n.d.). https://www.humintech.com/industry/applications/other-applications.html (accessed January 31, 2018).

[92]Kim H. Tan, Organic Soil Constituents, in: Environmental Soil Science, 2000: pp. 80–145.

[93]M. Verrillo, M. Salzano, D. Savy, V. Di Meo, M. Valentini, V. Cozzolino, A. Piccolo, Antibacterial and antioxidant properties of humic substances from composted agricultural biomasses, Chem. Biol. Technol. Agric. 9 (2022) 28. https://doi.org/10.1186/s40538-022-00291-6.

[94]U. Wollina, Peat: A natural source for dermatocosmetics and dermatotherapeutics, J Cutan Aesthet Surg. 2 (2009) 17. https://doi.org/10.4103/0974-2077.53094.

[95]R. Klöcking, B. Helbig, Medical Aspects and Applications of Humic Substances, Biopolymers for Medical and Pharmaceutical Application. (2005) 3–16.

[96]B. Alice, G. De Melo, F.L. Motta, M. Helena, A. Santana, Humic acids: Structural properties and multiple functionalities for novel technological developments, Materials Science & Engineering C. 62 (2016) 967–974. https://doi.org/10.1016/j.msec.2015.12.001.

[97]C.E.J. van Rensburg, The Antiinflammatory Properties of Humic Substances: A Mini Review, Phytotherapy Research. 795 (2015) 791–795. https://doi.org/10.1002/ptr.5319.

[98]J.M. Fernández, C. Plaza, A. Polo, A.F. Plante, Use of thermal analysis techniques (TG-DSC) for the characterization of diverse organic municipal waste streams to predict biological stability prior to land application, Waste Management. 32 (2012) 158–164. https://doi.org/10.1016/j.wasman.2011.08.011.

[99]Z. Droussi, V. D'orazio, M.R. Provenzano, M. Hafidi, A. Ouatmane, Study of the biodegradation and transformation of olive-mill residues during composting using FTIR spectroscopy and differential scanning calorimetry, Journal of Hazardous Materials. 164 (2009) 1281–1285. https://doi.org/10.1016/j.jhazmat.2008.09.081.

[100]W. Abid, I.B. Mahmoud, S. Masmoudi, M.A. Triki, S. Mounier, E. Ammar, Physico-chemical and spectroscopic quality assessment of compost from date palm (Phoenix dactylifera L.) waste valorization, Journal of Environmental Management. 264 (2020) 110492–110492. https://doi.org/10.1016/j.jenvman.2020.110492.

[101]Y. Inbar, Y. Chen, Y. Hadar, Solid-state carbon-13 nuclear magnetic resonance and infrared spectroscopy of composted organic matter, Soil Science Society of America Journal. 53 (1989) 1695–1701. https://doi.org/10.2136/sssaj1989.03615995005300060014x.

[102]A. Palma, V.M. Doña-Grimaldi, M. Ruiz-Montoya, I. Giráldez, J.C. García, J.M. Loaiza, F. López, M.J. Díaz, MSW Compost Valorization by Pyrolysis: Influence of Composting Process Parameters, ACS Omega. 5 (2020) 20810–20816. https://doi.org/10.1021/acsomega.0c01866.

[103]M.T. Dell'Abate, S. Canali, A. Trinchera, A. Benedetti, P. Sequi, Thermal analysis in the evaluation of compost stability: A comparison with humification parameters, Nutrient Cycling in Agroecosystems. 51 (1998) 217–224. https://doi.org/10.1023/A:1009734816502.

[104]C. Mondini, M.T. Dell'Abate, L. Leita, A. Benedetti, An Integrated Chemical, Thermal, and Microbiological Approach to Compost Stability Evaluation, J. Environ. Qual. 32 (2003) 2379–2386. https://doi.org/10.2134/jeq2003.2379.

[105]E. Smidt, K. Meissl, M. Schmutzer, B. Hinterstoisser, Co-composting of lignin to build up humic substances—Strategies in waste management to improve compost quality, Industrial Crops and Products. 27 (2008) 196–201. https://doi.org/10.1016/j.indcrop.2007.07.007.

[106]M. De Nobili, F. Petrussi, Humification index (HI) as evaluation of the stabilization degree during composting, Journal of Fermentation Technology. 66 (1988) 577–583. https://doi.org/10.1016/0385-6380(88)90091-X.

[107]E. Iglesias Jiménez, V. Pérez García, Composting of domestic refuse and sewage sludge. I. Evolution of temperature, pH, C/N ratio and cation-exchange capacity, Resources, Conservation and Recycling. 6 (1991) 45–60. https://doi.org/10.1016/0921-3449(91)90005-9.

[108]Y. Harada, A. Inoko, Relationship between cation-exchange capacity and degree of maturity of city refuse composts, Soil Science and Plant Nutrition. 26 (1980) 353–362. https://doi.org/10.1080/00380768.1980.10431220.

[109]N. Senesi, Composted materials as organic fertilizers, Science of the Total Environment, The. 81–82 (1989) 521–542. https://doi.org/10.1016/0048-9697(89)90161-7.

[110]M.T. Dell'Abate, A. Benedetti, P. Sequi, Thermal methods of organic matter maturation monitoring during a composting process, Journal of Thermal Analysis and Calorimetry. 61 (2000) 389–396. https://doi.org/10.1023/A:1010157115211.

[111]A. Piccolo, A. Mirabella, Molecular weight distribution of peat humic substances extracted with different inorganic and organic solutions, Science of the Total Environment. 62 (1987) 39–46. https://doi.org/10.1016/0048-9697(87)90479-7.

[112]A. Piccolo, P. Zaccheo, P.G. Genevini, Chemical characterization of humic substances extracted from organic-waste-amended soils, Bioresource Technology. 40 (1992) 275–282. https://doi.org/10.1016/0960-8524(92)90154-P.

[113]R.S. Swift, Organic Matter Characterization, in: D.L. Sparks, A.L. Page, P.A. Helmke, R.H. Loeppert, R.S. Swift (Eds.), Methods of Soil Analysis Part 3—Chemical Methods, Soil Science Society of America, American Society of Agronomy, 1996: pp. 1011–1069. https://doi.org/10.2136/sssabookser5.3.c35.

[114]J. Cegarra, D. Garcia, A. Navarro, M.P. Bernal, Effects of heat on the alkali extraction of humic substances from peat, Communications in Soil Science and Plant Analysis. 25 (1994) 2685–2695. https://doi.org/10.1080/00103629409369218.

[115]G. Gigliotti, K. Kaiser, G. Guggenberger, L. Haumaier, Differences in the chemical composition of dissolved organic matter from waste material of different sources, Biology and Fertility of Soils. 36 (2002) 321–329. https://doi.org/10.1007/s00374-002-0551-8.

[116]S. Mahapatra, Md.H. Ali, K. Samal, Assessment of compost maturity-stability indices and recent

development of composting bin, Energy Nexus. 6 (2022) 100062. https://doi.org/10.1016/j.nexus.2022.100062.

[117]M.P. Bernal, S.G. Sommer, D. Chadwick, C. Qing, L. Guoxue, F.C. Michel, Current Approaches and Future Trends in Compost Quality Criteria for Agronomic, Environmental, and Human Health Benefits, in: D. Sparks (Ed.), Advances in Agronomy, 2017: pp. 143–233. https://doi.org/10.1016/bs.agron.2017.03.002.

[118]C. Liang, K.C. Das, R.W. McClendon, The influence of temperature and moisture contents regimes on the aerobic microbial activity of a biosolids composting blend, Bioresource Technology. 86 (2003) 131–137. https://doi.org/10.1016/S0960-8524(02)00153-0.

[119]N.N. Gurusamy, N. Puffer, C. de Jongh, C. Rodriguez Gil, T.J. Aspray, Effect of initial moisture content and sample storage duration on compost stability using the ORG0020 dynamic respiration test, Waste Management. 125 (2021) 215–219. https://doi.org/10.1016/j.wasman.2021.02.048.

[120]European Commission, Regulation (EC) No 2019/1009, 2019. https://eur-lex.europa.eu/legal-content/EN/TXT/PDF/?uri=OJ:L:2019:170:FULL&from=NL.

[121]M.J. Díaz, M. Ruiz-Montoya, A. Palma, M.-V. de-Paz, Thermogravimetry Applicability in Compost and Composting Research: A Review, Applied Sciences. 11 (2021) 1692. https://doi.org/10.3390/app11041692.

[122]F. Zucconi, A. Monaco, M. Forte, Phytotoxins during the stabilization of organic matter, in: Composting of Agricultural and Other Wastes, Elsevier Applied Science Publication, 1985: pp. 73–86.

[123]E.C. Minor, M.M. Swenson, B.M. Mattson, A.R. Oyler, Structural characterization of dissolved organic matter: a review of current techniques for isolation and analysis, Environ. Sci.: Processes Impacts. 16 (2014) 2064–2079. https://doi.org/10.1039/C4EM00062E.

[124]J.A. Leenheer, J.-P. Croué, Peer Reviewed: Characterizing Aquatic Dissolved Organic Matter, Environ. Sci. Technol. 37 (2003) 18A-26A. https://doi.org/10.1021/es032333c.

[125]B. Smreczak, A. Ukalska-Jaruga, Dissolved organic matter in agricultural soils, Soil Sci. Ann. (2021). https://doi.org/10.37501/soilsa/132234.

[126]A. Nebbioso, A. Piccolo, Molecular characterization of dissolved organic matter (DOM): a critical review, Anal Bioanal Chem. 405 (2013) 109–124. https://doi.org/10.1007/s00216-012-6363-2.

[127]D.L. Baun, T.H. Christensen, Speciation of Heavy Metals in Landfill Leachate: A Review, Waste Manag Res. 22 (2004) 3–23. https://doi.org/10.1177/0734242X04042146.

[128]A. Piccolo, The supramolecular structure of humic substances: A novel understanding of humus chemistry and implications in soil science, Advances in Agronomy. 75 (2002) 57–134. https://doi.org/10.1016/S0065-2113(02)75003-7.

[129]J. Lag, A. Hadas, R.W. Fairbridge, J.C.N. Muñoz, X.P. Pombal, A.M. Cortizas, G. Almendros, Humic Substances, in: W. Chesworth (Ed.), Encyclopedia of Soil Science, Springer Netherlands, Dordrecht, 2008: pp. 315–323. https://doi.org/10.1007/978-1-4020-3995-9_273.

[130]E. Balnois, K.J. Wilkinson, J.R. Lead, J. Buffle, Atomic Force Microscopy of Humic Substances: Effects of pH and Ionic Strength, Environ. Sci. Technol. 33 (1999) 3911–3917. https://doi.org/10.1021/es990365n.

[131]M.H.B Hayes, Humic Substances: Progress Towards More Realistic Concepts of Structures, in: Humic Substances: Structures, Properties And Uses, 1998: pp. 1–30.

[132]F.J. Stevenson, Organic Matter in Soils: Pools, Distribution, Transformations, and Function, in: Humus Chemistry: Genesis, Composition, Reactions, 1994: pp. 1–10.

[133]J.C.M. de Wit, W.H. van Riemsdijk, L.K. Koopal, Proton binding to humic substances. 1. Electrostatic effects, Environ. Sci. Technol. 27 (1993) 2005–2014. https://doi.org/10.1021/es00047a004.

[134]M. Bernoux, C.E.P. Cerri, Geochemistry - Soil, Organic Components, in: Encyclopedia of Analytical Science, Elsevier, 2005: pp. 203–208. https://doi.org/10.1016/B0-12-369397-7/00245-4.

[135]J.H. Hsu, S.L. Lo, Chemical and spectroscopic analysis of organic matter transformations during composting of pig manure, Environmental Pollution. 104 (1999) 189–196. https://doi.org/10.1016/S0269-7491(98)00193-6.

[136]Y. Inbar, Y. Hadar, Y. Chen, Characterization of humic substances formed during the composting of solid wastes from wineries, Science of The Total Environment. 113 (1992) 35–48. https://doi.org/10.1016/0048-9697(92)90015-K.

[137]P. Melis, P. Castaldi, Thermal analysis for the evaluation of the organic matter evolution during municipal solid waste aerobic composting process, Thermochimica Acta. 413 (2004) 209–214. https://doi.org/10.1016/j.tca.2003.09.026.

[138]Y.-P. Chin, G. Aiken, E. O'Loughlin, Molecular weight, polydispersity, and spectroscopic properties of aquatic humic substances, Environmental Science & Technology. 28 (1994) 1853–1858. https://doi.org/10.1021/es00060a015.

[139]G. Gigliotti, A. Macchioni, C. Zuccaccia, P.L. Giusquiani, D. Businelli, A spectroscopic study of soil fulvic acid composition after six-year applications of urban waste compost, Agronomie. 23 (2003) 719–724. https://doi.org/10.1051/agro:2003048.

[140]C. Plaza, N. Senesi, A. Polo, G. Brunetti, Acid-base properties of humic and fulvic acids formed during composting, Environmental Science & Technology. 39 (2005) 7141–7146. https://doi.org/10.1021/es050613h.

[141]E. Lodygin, E. Abakumov, The Impact of Agricultural Use of Retisols on the Molecular Structure of Humic Substances, Agronomy. 12 (2022) 144. https://doi.org/10.3390/agronomy12010144.

[142]S. Amir, A. Jouraiphy, A. Meddich, M. El Gharous, P. Winterton, M. Hafidi, Structural study of humic acids during composting of activated sludge-green waste: Elemental analysis, FTIR and 13C NMR, Journal of Hazardous Materials. 177 (2010) 524–529. https://doi.org/10.1016/j.jhazmat.2009.12.064.

[143]M. Fuentes, R. Baigorri, G. González-Gaitano, J.M. García-Mina, The complementary use of ^{1}H NMR, ^{13}C NMR, FTIR and size exclusion chromatography to investigate the principal structural changes associated with composting of organic materials with diverse origin, Organic Geochemistry. 38 (2007) 2012–2023. https://doi.org/10.1016/j.orggeochem.2007.08.007.

[144]A.H. Rosa, J.P. Pinheiro, A.S.C. Monteiro, N. Janot, B.J. Groenenberg, Especiação termodinâmica de metais traço com substâncias húmicas: o modelo Nica-Donnan, Química Nova. 40 (2017) 1191–1203. https://doi.org/10.21577/0100-4042.20170107.

[145]J.M. Fernández, C. Plaza, N. Senesi, A. Polo, Acid-base properties of humic substances from composted and thermally-dried sewage sludges and amended soils as determined by potentiometric titration and the NICA-Donnan model, Chemosphere. 69 (2007) 630–635. https://doi.org/10.1016/j.chemosphere.2007.02.063.

[146]J.P. Pinheiro, A.M. Mota, M.F. Benedetti, Lead and calcium binding to fulvic acids: Salt effect and competition, Environmental Science and Technology. 33 (1999) 3398–3404.

https://doi.org/10.1021/es990210f.

[147]S. Zmora-Nahum, O. Markovitch, J. Tarchitzky, Y. Chen, Dissolved organic carbon (DOC) as a parameter of compost maturity, Soil Biology and Biochemistry. 37 (2005) 2109–2116. https://doi.org/10.1016/j.soilbio.2005.03.013.

[148]M.P.P. Bernal, C. Paredes, M.A.A. Sánchez-Monedero, J. Cegarra, Maturity and stability parameters of composts prepared with a wide range of organic wastes, Bioresource Technology. 63 (1998) 91–99. https://doi.org/10.1016/S0960-8524(97)00084-9.

[149]S. Glatzel, K. Kalbitz, M. Dalva, T. Moore, Dissolved organic matter properties and their relationship to carbon dioxide efflux from restored peat bogs, Geoderma. 113 (2003) 397–411. https://doi.org/10.1016/S0016-7061(02)00372-5.

[150]F.J. Stevenson, Humus Chemistry: Genesis, Composition, Reactions, Second Edition, Division of Chemical Education, 1994. https://doi.org/10.1021/ed072pA93.6.

[151]R. Zbytniewski, B. Buszewski, Characterization of natural organic matter (NOM) derived from sewage sludge compost. Part 1: Chemical and spectroscopic properties, Bioresource Technology. 96 (2005) 471–478. https://doi.org/10.1016/j.biortech.2004.05.018.

[152]D.G. Kinniburgh, C.J. Milne, M.F. Benedetti, J.P. Pinheiro, J. Filius, L.K. Koopal, W.H. Van Riemsdijk, Metal Ion Binding by Humic Acid: Application of the NICA-Donnan Model, Environ. Sci. Technol. 30 (1996) 1687–1698. https://doi.org/10.1021/es950695h.

[153]N. Soobhany, S. Gunasee, Y.P. Rago, H. Joyram, P. Raghoo, R. Mohee, V.K. Garg, Spectroscopic, thermogravimetric and structural characterization analyses for comparing Municipal Solid Waste composts and vermicomposts stability and maturity, Bioresource Technology. 236 (2017) 11–19. https://doi.org/10.1016/j.biortech.2017.03.161.

[154]P. Campitelli, S. Ceppi, Effects of composting technologies on the chemical and physicochemical properties of humic acids, Geoderma. 144 (2008) 325–333. https://doi.org/10.1016/j.geoderma.2007.12.003.

[155]R. Barrena, X. Font, X. Gabarrell, A. Sánchez, Home composting versus industrial composting: Influence of composting system on compost quality with focus on compost stability, Waste Management. 34 (2014) 1109–1116. https://doi.org/10.1016/j.wasman.2014.02.008.

[156]P. Campitelli, S. Ceppi, Chemical, physical and biological compost and vermicompost characterization: A chemometric study, Chemometrics and Intelligent Laboratory Systems. 90 (2008) 64–71. https://doi.org/10.1016/j.chemolab.2007.08.001.

[157]R. López, J. Antelo, A.C. Silva, F. Bento, S. Fiol, Factors that affect physicochemical and acid-base properties of compost and vermicompost and its potential use as a soil amendment, Journal of Environmental Management. 300 (2021) 113702. https://doi.org/10.1016/j.jenvman.2021.113702.

[158]M.J. Fernández-Gómez, R. Nogales, A. Plante, C. Plaza, J.M. Fernández, Application of a set of complementary techniques to understand how varying the proportion of two wastes affects humic acids produced by vermicomposting, Waste Management. 35 (2015) 81–88. https://doi.org/10.1016/j.wasman.2014.09.022.

[159]M.E.F. Silva, L.T. de Lemos, O.C. Nunes, A.C. Cunha-Queda, Influence of the composition of the initial mixtures on the chemical composition, physicochemical properties and humic-like substances content of composts, Waste management. 34 (2014) 21–27. https://doi.org/10.1016/j.wasman.2013.09.011.

[160]A. Muscolo, T. Papalia, G. Settineri, C. Mallamaci, A. Jeske-Kaczanowska, Are raw materials or composting conditions and time that most influence the maturity and/or quality of composts? Comparison of obtained composts on soil properties, Journal of Cleaner Production. 195 (2018) 93–101. https://doi.org/10.1016/j.jclepro.2018.05.204.

[161]V. Dhyani, M. Kumar Awasthi, Q. Wang, J. Kumar, X. Ren, J. Zhao, H. Chen, M. Wang, T. Bhaskar, Z. Zhang, Effect of composting on the thermal decomposition behavior and kinetic parameters of pig manure-derived solid waste, Bioresource Technology. 252 (2018) 59–65. https://doi.org/10.1016/j.biortech.2017.12.083.

[162]D.B. Dresbøll, K. Thorup-Kristensen, Structural differences in wheat (Triticum aestivum), hemp (Cannabis sativa) and Miscanthus (Miscanthus ogiformis) affect the quality and stability of plant based compost, Scientia Horticulturae. 107 (2005) 81–89. https://doi.org/10.1016/j.scienta.2005.06.006.

[163]X. Li, M. Xing, J. Yang, Z. Huang, Compositional and functional features of humic acid-like fractions from vermicomposting of sewage sludge and cow dung, JOURNAL OF HAZARDOUS MATERIALS. 185 (2011) 740–748. https://doi.org/10.1016/j.jhazmat.2010.09.081.

[164]M. Fuentes, G. González-Gaitano, J.M. García-Mina, The usefulness of UV-visible and fluorescence spectroscopies to study the chemical nature of humic substances from soils and composts, Organic Geochemistry. 37 (2006) 1949–1959. https://doi.org/10.1016/j.orggeochem.2006.07.024.

[165]E. Smidt, J. Tintner, Application of differential scanning calorimetry (DSC) to evaluate the quality of compost organic matter, Thermochimica Acta. 459 (2007) 87–93. https://doi.org/10.1016/j.tca.2007.04.011.

[166]M. Verrillo, V. Cozzolino, R. Spaccini, A. Piccolo, Humic substances from green compost increase bioactivity and antibacterial properties of essential oils in Basil leaves, Chem. Biol. Technol. Agric. 8 (2021) 28. https://doi.org/10.1186/s40538-021-00226-7.

[167]M. Ayuso, C. Garcia, T. Hernandez, Effect of Humic Fractions from Urban Wastes and Other More Evolved Organic Materials on Seed Germination, Journal of the Science of Food and Agriculture. 72 (1996) 461–468. https://doi.org/10.1002/(SICI)1097-0010(199612)72:4<461::AID-JSFA680>3.0.CO;2-%23.

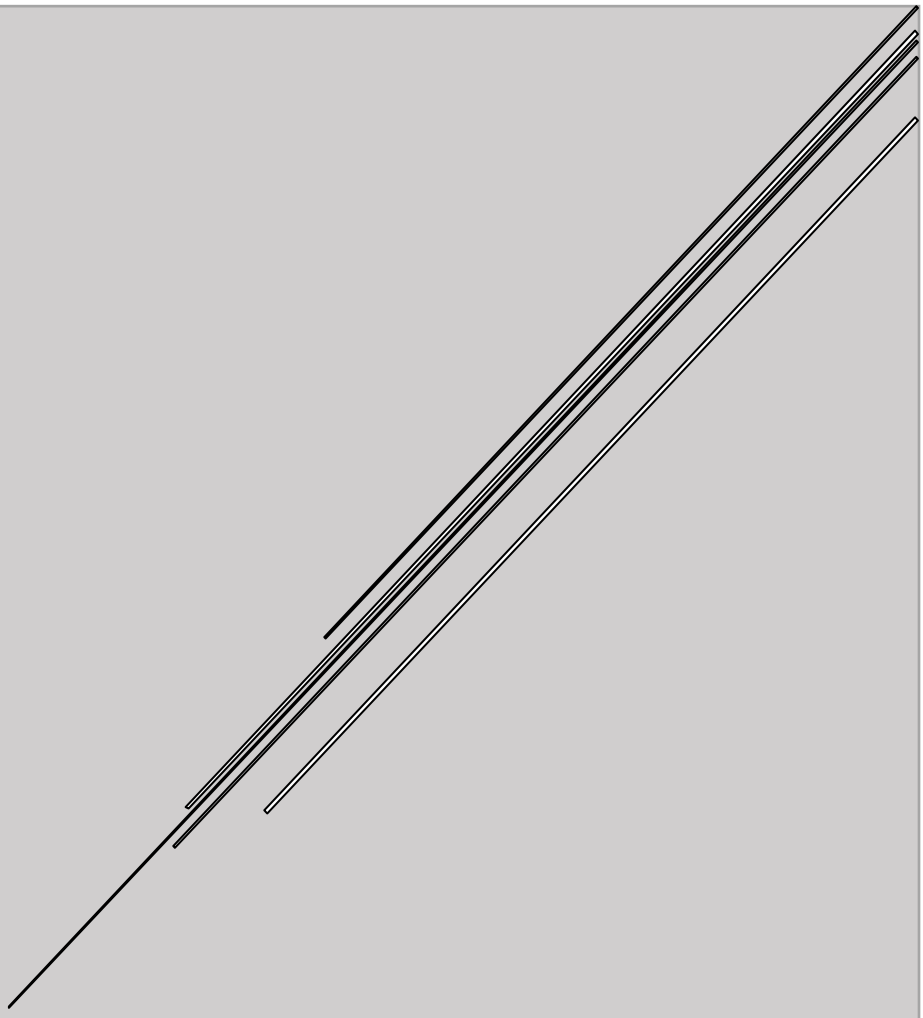

CHAPTER 2 – MATERIAL AND METHODS

1. Samples

1.1. Identification of the samples

The compost samples analysed in this thesis are identified in Table 2.1. Each sample is listed by a name and an acronym. The composting process used in its production and the feedstock are also identified. Samples are divided in two groups, according to the nature of the study where they were used. In the first group are presented samples obtained from different stages of the composting process. The samples assigned by UW_0, CUW_{15}, CUW_{30}, CUW correspond to raw material, compost produced after 15 days of composting, after 30 days of composting and the final product that was further subjected to a maturation process, respectively. In the second group are included the compost samples, that were produced using different composting methodologies: by industrial composting (CUW, CLW, CSS, CA), domestic composting (CDDW) and by earthworms (CVDW, CVA). The feedstock used consisted predominantly of vegetables (CVDW, CDDW, CUW), also incorporated manure (CVA, CLW, CSS) sludge from urban wastewater treatment (CSS) and algae (CVA, CA). Additionally, an organic fertilizer (100 % animal waste, not composted) presented in the last row, was characterized by the same methods used for compost samples and was used for comparison purposes, considering that both types of materials (composted and not composted) are used quite indiscriminately in agriculture.

1.2. Preparation of the extracts from compost samples

Three different extracts were prepared from each sample. Humic-like acids (HA-L) and fulvic-like acids (FA-L) extracts and the equilibrium solutions (containing the dissolved organic matter (DOM)). The first two extracts belong to the group of humic-like substances (HS-L) that consist in heterogeneous, and complex mixtures [1]. HA-L are soluble in alkaline solutions, but insoluble in acidic solutions, while FA-L are soluble at any pH. The DOM is defined as the soluble organic matter fraction.

1.2.1. Humic-like substances

The extraction and purification of the humic-like substances (HS-L), namely fulvic-like acid (FA-L) and humic-like acid (HA-L) were carried out following the method recommended by the International Society for Humic Substances (IHSS) [2]. The IHSS recommends this extraction procedure with the aim of normalizing the isolation and fractionation of HS from soils. According to this procedure, the compost sample (previously dried) was mixed with 0.1 mol L^{-1} HCl (Panreac) at an extractant to compost ratio of 10:1 (v:w) and kept at low agitation (100 rpm) for approximately 7 days.

Table 2.1: Description of the samples analysed.

Group	Sample	Type of composting	Description
1	Urban waste (UW_0)	**Tunnel composting**	**Initial mixture that enters the composting tunnel.** Mixture made of food wastes (40 %) with green wastes (60 %) that are obtained from the selective collection. Food wastes are from households, restaurants, canteens, markets and other events such as fairs, festivities, pilgrimages, whereas green wastes are from cemeteries (flowers) and households (grass and pruning).
	Compost urban waste (CUW_{15}) after the 1st composting cycle, t=15 days		**Sample collected at the end of the 1st composting phase.** In the 1st composting cycle, the feedstock is heated up to 60 °C during 48 hours. Then the temperature is set at 50 °C for a period of 15 days.
	Compost urban waste (CUW_{30}) after the 2nd composting cycle, t=30 days		**Sample collected at the end of the 2nd composting phase.** After the 1st cycle of composting, the mixture is sieved with a 60 mm sieve. After this step, the mixture is replaced in the tunnel for a 2nd cycle, identical to the 1st one.
	Compost of urban waste (CUW)		**Sample collected at the end of the maturation phase.** After the 2nd composting cycle, the maturation phase takes between 4 to 6 weeks
2	Vermicompost of algae (CVA)	**Vermicomposting**	Compost made from a mixture of 60 % manure and 40 % vegetable remains (fruits and algae), which is digested by *Eisenia foetida* earthworms.
	Vermicompost of domestic waste (CVDW)		Compost made from a mixture of green wastes (flowers, leaves, grass, fruit peels) and brown wastes (straw, dry leaves, dry grass), which is digested by *Eisenia foetida* or *Lumbricus rubellus* earthworms.
	Compost of livestock waste (CLW)		Compost made from a mixture of 100 % from animal waste (a mixture of 5 % sheep manure without straw, 25 % chicken manure and 70 % pig manure).
	Compost of algae (CA)	**Pile composting**	Compost made from a mixture of 60 % manure and 40 % vegetable remains (fruits and algae).
	Compost of sewage sludge (CSS)		Compost made from a mixture of forestry waste, sludge from urban wastewater treatment and sludge from local effluent treatment.
	Domestic compost of domestic waste (CDDW)	**Domestic Composting**	Compost made from a mixture of green residues (flowers, leaves, grass, fruit peels) and brown residues (straw, dry leaves, dry grass).
	Fertiliser of livestock waste (FLW)		Fertiliser made from a mixture of 100 % animal waste (chicken manure). Mixture subjected to a high temperature to eliminate pathogens.

During this process, there was a progressive change in the colour of the solution from colourless to dark yellow, characteristic of the fulvic acids that have passed into the solution. The solution was then left to rest for three days and then centrifuged. The supernatant was again centrifuged to eliminate all suspended particles. This supernatant, where the first FA-L extract is found, passes through a column containing a resin XAD-8 (Supelite) (a hydrophobic, macroporous resin containing a methyl methacrylate ester, previously prepared by the Leenheer method [3]) until it saturates with FA-L. After the resin was saturated with FA-L, distilled water was passed through the column to remove chlorides and finally the FA-L were eluted with 0.1 mol L^{-1} NaOH (Merck). Then this FA-L solution passed through a new column with H^+-saturated cation exchange resin (Amberlite IR 120) to convert it in its protonated form.

In order to separate the humic-like fractions (HA-L and FA-L) existing in the solid from the remaining substances present in the sample (inorganic matter and the humin), a strong basic treatment with a mixture of 0.1 mol L^{-1} and 1 mol L^{-1} NaOH (pH ≈ 13) under N_2 atmosphere at an extractant to compost ratio of 10:1 (v:w) was carried out. The suspension was kept under constant agitation for three days, then it is left to stand for one day and then centrifuged to collect the supernatant, in which the HA-L and the second FA-L extract are dissolved. To separate these two fractions, the solution is acidified with 6 mol L^{-1} HCl until a pH ≈ 1, for the HA-L precipitation. The suspension was left to rest for 12 to 16 hours and was subsequently centrifuged to separate the humic fraction (precipitate) from the fulvic fraction (supernatant). The second FA-L extract was subjected to the same treatment of the first FA-L extract (indicated above). The precipitate (HA-L) was redissolved in 0.1 mol L^{-1} KOH (Merck) in a N_2 atmosphere, and KCl (Merck) was added. This solution containing the HA-L extract was centrifuged to eliminate all suspended solids and re-acidified with 6 mol L^{-1} HCl until a pH ≈ 1 to precipitate the HA-L. After allowing the suspension to stand for 12 to 16 hours, it was centrifuged to discard the supernatant and the solid was suspended in a solution of 0.1 mol L^{-1} HCl/0.3 mol L^{-1} HF keeping the suspension under stirring for 12 hours. This operation is intended to eliminate mineral impurities and therefore the process was repeated until the ashes in the final extract do not exceed 1 %. After the suspension was centrifuged, the solid was transferred to a dialysis membrane (Spectra/Por® MWCO 1 kD) that was submerged in distilled water bath, which was renewed until complete removal of Cl^-. The solutions containing the FA-L extracts (resulting from the mixture of the 1st and the 2nd fractions) and the HA-L extracts were firstly frozen and then were lyophilized to obtain the final solid extracts. The scheme of the procedure is presented in Figure 2.1.

1.2.2. Water-soluble extracts

The water-soluble extracts containing the dissolved organic matter (DOM) and water-soluble inorganic components, that are also called equilibrium solutions, were extracted using a less aggressive procedure. Succinctly, 7.50 g of the compost were placed in 150 mL of ultra-pure water at natural pH for 5 days in an open system. After 5 days (equilibration time), the supernatants were centrifuged (6000 rpm for 20 minutes) and isolated for characterization.

2. Characterization methods

2.1. Elemental characterization

Elemental characterization is of key importance in the characterization of this type of natural sample providing information on the absolute amount of the major constituents. The C, H, N and S contents of the compost samples and of their extracts (FA-L and HA-L) were characterised following the standard methodologies for this type of materials using an element analyser (TruSpec CHN-1000, LecoSC-144DR). The sample was completely and instantly oxidized (1000 - 1100 °C), thus transforming all organic and inorganic matter into combustion products. The resulting gases pass through a reduction furnace (500 - 600 °C) and are conducted by a stream of helium to a chromatographic column, in which they are separated and, later, they were analysed by a thermal conductivity detector.

The ash content, of FA-L and HA-L, was determined gravimetrically by combustion at 650 °C and the oxygen content was determined as O = 100 – (C + N + H + S + ash).

Oxidizable C content of the compost samples was determined by Sauerlandt's method [4] and the dissolved organic carbon content of equilibrium solutions was determined using a total organic carbon analyser (TOC-L CSN Shimadzu). The concentration of P was determined in the compost samples and in the equilibrium solutions by the molybdenum blue method, in the case of the solid samples, after acid digestion with *aqua regia* [5].

2.2. Cation Exchange Capacity

The cation exchange capacity (CEC) of the compost samples was carried out to evaluate the amount of negative charges in the solid matrix [6] and characterise the ability of compost to retain cations, such as Ca^{2+}, Mg^{2+}, Na^{+} and K^{+}.

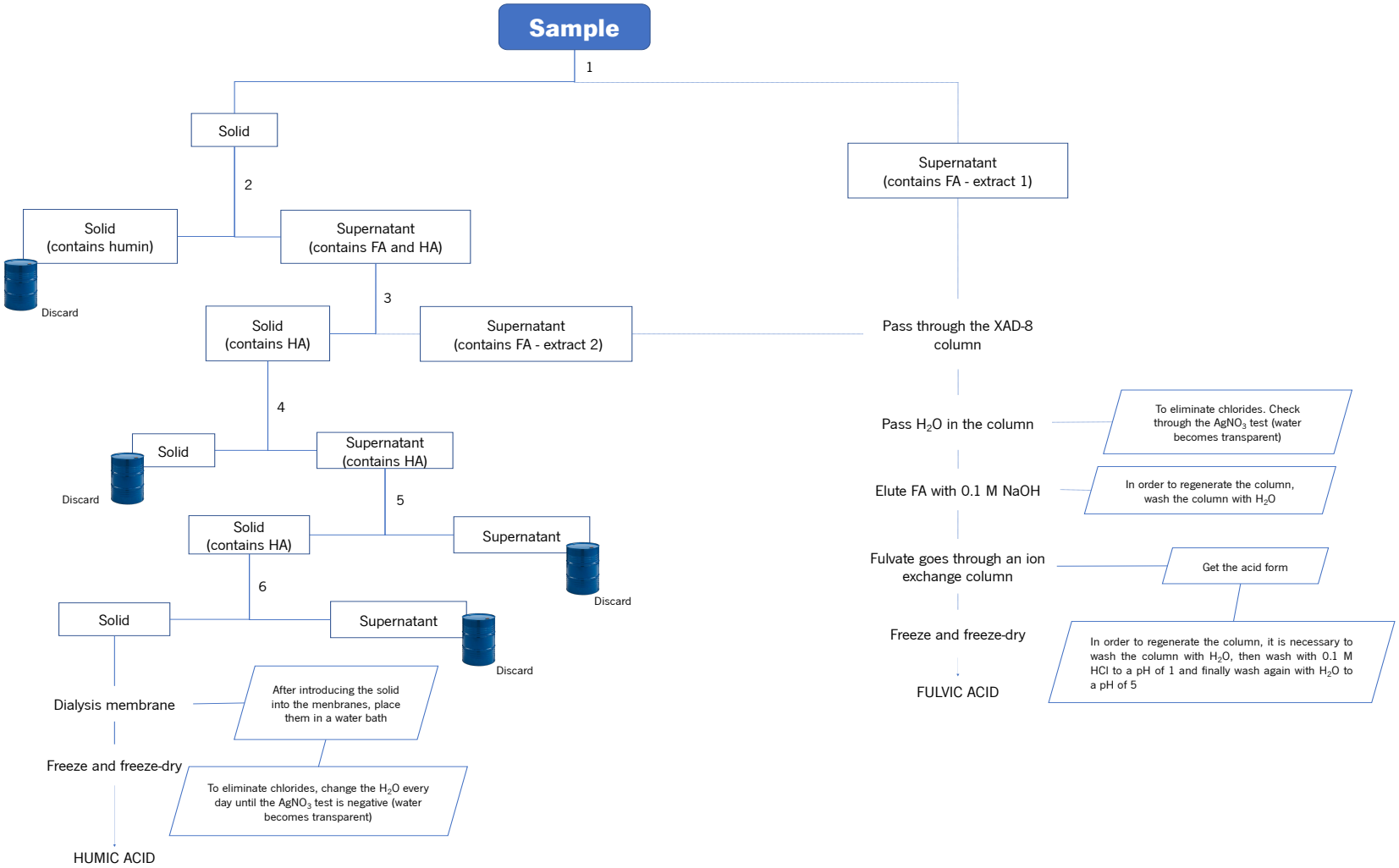

Figure 2.1: Scheme of the extraction process of humic-like substances.

*1 - Add 0.1 M HCl - 10:1 ratio (extractant/solid). Keep stirring for 7 days. Stand for 2 to 3 days, decant and centrifuge.
2 - Add 0.1 M NaOH - 10:1 ratio (extractant - solid), pH 13. Keep stirring for 3 days. Stand for 1 day, decant and centrifuge.
3 - Add 6 M HCl (until pH = 1). Stand for 12 to 16 hours and centrifuge.
4 - Redissolve with 0.1 M KOH in N_2 atmosphere. Add KCl to get $[K^+]$ = 0.3 M. Centrifuge.
5 - Add 6 M HCl (until pH = 1). Stand for 12 to 16 hours and centrifuge.
6 - Add 0.1 M HCl/0.3 M HF. Shake for 12 hours and centrifuge. Repeat the process if the ash content is greater than 1%.

The cation exchange capacity (CEC) of compost samples was determined by the summation of the exchangeable cations (Ca^{2+}, Mg^{2+}, Na^{+} and K^{+}) and expressed in units of charge per weight of compost ($cmol_{(+)}\ kg^{-1}$ - centimoles of charge per kilogram of dry compost). The exchangeable cations were obtained by ICP-OES.

2.3. Ion Chromatography

Ion chromatography is an analytical technique for the determination of the common cations and anions. It is applied mainly to the determination of anions such as Cl^{-}, F^{-}, SO_4^{2-}, NO_2^{-}, NO_3^{-}. The anion's concentration was determined in equilibrium solutions extract and was carried out using a Dionex 4500i. The chromatographic conditions were flow rate of 2 mL min^{-1}, a pressure of 2000 psi and a 9 mM Na_2CO_3 was used as an eluent for anionic chromatography.

2.4. Spectroscopic techniques

2.4.1. ICP – OES

Inductively coupled plasma optical emission spectrometry (ICP-OES) was used to evaluate the concentrations of the major elements in the compost samples (Ca, Mg, Na, K, Fe, Al, As, Cd, Co, Cr, Cu, Mn, Ni, Pb, Zn) and in the equilibrium solutions (Si, Ca, Mg, Na, K, Fe, Al, As, Cd, Co, Cr, Cu, Mn, Ni, Pb, Zn). This technique is based on the fact that atoms and ions absorb distinct energies to promote electrons from the ground state to an excited state, the source of that energy is heat from an argon plasma that operates at 10.000 K. The ICP-OES principle relies on those excited atoms releasing light at specific wavelengths as they transition to a lower energy level.

The compost samples (solid sample) were introduced in the ICP-OES after an acid digestion with *aqua regia*, whereas the equilibrium solutions (DOM extract) were introduced directly into the plasma. The concentrations of the major elements were measured using an ICP-OES with a Perkin-Elmer Optima 3300DV.

2.4.2. UV–visible

The UV-vis spectroscopy was used to characterize the FA-L, HA-L and DOM extracts of all compost samples. The presence of aromatic structures in these extracts as well as carbonyl and carboxyl groups are responsible for their absorption in the UV region. The absorption spectra is affected by structural characteristics such as the degree of condensation of the aromatic rings, the total carbon content, the molecular weight or the ratio between aromatic and aliphatic carbon [1,7]. The presence of other groups, called auxochromes, such as R-OH and $R\text{-}NH_2$ can also affect the absorption spectra [1,8]. Moreover, the

structural aspects of the molecule, the UV-visible spectra is also affected by the solution pH. The absorptivity of the chromophore groups can be changed due to conformational changes in their molecular structure associated to the variations of the degree of dissociation or protonation of the carboxylic and phenolic groups. Although the spectra from the UV region do not provide any structural information, the absorption intensities in the maximum of absorption bands are often used for quantitative information.

The solutions of the extracts were prepared in 10 mmol L^{-1} $C_2H_3NaO_2$ and the pH adjusted to 7.0 with CH_3COOH. The absorbance of the solutions was measured at a fixed wavelength (280 nm) using a Jasco V-530 spectrophotometer. The coefficient of molar absorptivity at 280 nm (ε_{280}) was calculated from measurements performed in solutions of different concentrations (10 - 0.06 g L^{-1}). The obtained values of ε_{280} were used to obtain a measurement of the aromaticity by means of a semi-empirical relationship (% aromaticity = 0.05 x ε_{280} + 6.74) and with the molar mass (molar mass = 3.99 x ε_{280} + 490) [9].

2.4.3.ATR - FTIR spectroscopy

Compost samples and the FA-L and HA-L extracts were characterized by ATR-FTIR spectroscopy. The spectroscopy in the IR region provides information about the nature and distribution of chemical bonds. This technique is based on the fact that particular vibration modes (*e.g.* stretching, deformation) of chemical bonds of certain groups (of atoms occur at given frequencies) giving rise to an absorption band of the spectrum. Spectroscopic analysis of IR spectroscopy allows the identification of functional groups or structural entities in a sample from the intensity and position of a given absorption band. Despite the difficulty in interpreting the IR spectra due to the complexity of their structure, these spectra present a series of characteristic bands that have been assigned quite clearly to the different functional groups commonly identified in this type of substances (Table 2.2).

The width of the bands is the result of the overlapping of absorptions that come from functional groups of the same type but with a different chemical environment, which makes their interpretation difficult. The fact that these samples have similar spectra does not imply that they have the same structure, but rather that the content of functional groups and structural entities may be similar.

The FTIR spectra were recorded in the transmission mode using a Jasco FTIR - 4100 Spectrometer with an ATR Specac Golden Gate, in the wavenumber range 600–3800 cm^{-1} and corrected against ambient air as background.

Table 2.2: The main absorbance bands, of compost and HA-L and FA-L samples, in FTIR spectra and their assignments.

Compost			
Wavenumber (cm^{-1})	**Vibration**		**Reference**
3600-3000	O–H C–H N–H	stretching stretching stretching	[10]
2925	C–H	asymmetric stretching	[11]
2845	C–H	symmetric stretching	[11]
1640 - 1630	C=O C=C	stretching stretching	[10]
1540	N–H	stretching	[12]
1440 - 1420	O–H C–O COO^- C–H	deformation stretching stretching deformation	[13]
1020	Si–O–Si Si–O C–O	 stretching stretching	[14]
870	C–O		[10]
Humic-like substances			
Wavenumber (cm^{-1})	**Vibration**		**Reference**
3600-3000	O–H N–H	stretching stretching	[15]
2925	C–H	asymmetric stretching	[15]
2845	C–H	symmetric stretching	[15]
1700	C=O	stretching	[16]
1640 - 1630	C=O C=C	stretching stretching	[17]
1530 - 1520	C=N C=C N – H	stretching stretching bending	[18]
1450 - 1410	C – H	deformation	[19]
1220	C – O C – O O – H	stretching bending bending	[19]
1020	C – O	stretching	[18]

Each spectrum is the result of 64 scans with a resolution of 1 cm^{-1}. Samples of each compost were obtained from a portion of a sample (1 – 5 g) that was homogenized by manually grinding in an agate mortar. The spectra were corrected with the baseline and submitted to a deconvolution process (Figure 2.2) using the Origin 2019b software. In the deconvolution process, the compensation of the intrinsic linewidths is made to solve overlapping bands.

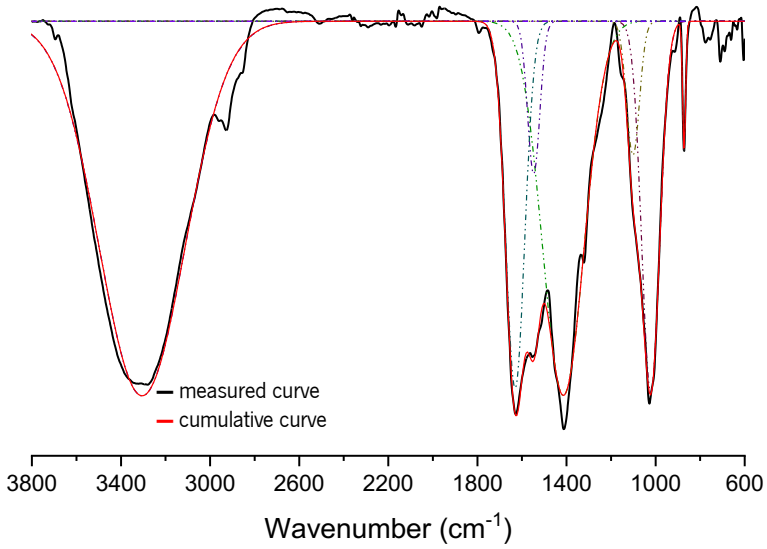

Figure 2.2: Deconvolution of FTIR spectra from the compost CUW.

2.4.4.[1] H-NMR spectroscopy[1]

The ^{1}H-NMR spectroscopy was used to characterize the FA-L and HA-L extracts of compost samples. This technique has been used for the characterization of HS [20], since it allows a semi-quantitative analysis. Using this technique, it is possible to calculate the proportions of different functional groups or structural entities. ^{1}H-NMR was carried out using a 400 MHz Bruker Avance II spectrometer NMR. Chemical shifts (δ) are given in parts per million (ppm), downfield from tetramethylsilane (TMS), and coupling constants (J) in hertz (Hz). The HS-L solutions were obtained by dissolving 5 mg of the sample in 800 µL of deuterated water (Merck) and the pH was adjusted to 12 with 40 % NaOD (Sigma-Aldrich) [21]. The proton spectra are shown in Figures A1 and A2 (in Annexes).

2.5. Characterization by SEM and X-ray diffraction analysis[2]

The surface morphology of CA and CVA samples were studied by scanning electron microscope (SEM) using a SEM Leica Cambridge S360 apparatus. The mineralogical composition of these two samples was determined by X-ray diffraction using a Bruker D8 Discover diffractometer with an X-ray tube using Cu Kα1 radiation (λ=1.54060 Å) operated at 40 kV and 40 mA. X-ray diffraction patterns were recorded on powder samples using a LynxEye detector, under ambient conditions and within a range of 2.5° to 65° 2θ, with 0.035° 2θ step size, and a 3 s counting time per step at 20 rpm.

[1] as part of a collaboration with Prof. Doctor Fernanda Proença
[2] as part of a collaboration with Prof. Doctor José Paulo Pinheiro.

2.6. Thermal techniques

The thermogravimetric analysis (TGA) and differential scanning calorimetry (DSC) are two powerful techniques that are frequently used to characterize the thermal degradability of organic matter, to evaluate its stabilization, as well as the amount of recalcitrant C in compost samples [22].

In this thesis compost samples and the FA-L and HA-L extracts were characterized by DSC and TGA. The analyses in the compost samples were performed in N_2 and in air atmospheres, whereas in the FA-L and HA-L extracts only in air atmosphere. The thermal analysis was carried out in the Thermal Analysis Instruments TGA500 for the N_2 atmosphere and in the Perkin Elmer Simultaneous Thermal Analyzer STA 6000 for the air atmosphere at the temperature range from 30 °C to 800 °C with a heating rate of 10 °C min^{-1}. The analyses were performed on a dry basis using aluminium and ceramic crucibles (60 µL) in N_2 and in air atmospheres, respectively. The baseline correction of the curves was performed using an empty pan. Samples (30-50 mg) of each sample were obtained from a portion of a sample of 1 to 5 g that was homogenized by manual grinding in an agate mortar.

The evaluation of the weight loss in each temperature range was carried out after a careful analysis of the derivative thermogravimetric (DTG) curve. The enthalpies were calculated by integrating the area below the DSC curve in each temperature range, between 30 and 800 °C, drawing a horizontal baseline (heat flow 0), with the aid of Origin 2019b software.

In the TGA curves four main weight loss processes were identified (Table 2.3): WL_1 (30 - 177 °C), WL_2 (177 - 400 °C), WL_3 (400 - 620 °C) and WL_4 (620 - 800 °C). The DSC curves exhibit a minor endothermic process, in the 1st temperature range identified in the TGA curves, and two major regions, corresponding to the overlap of exothermic processes, in the 2nd, in the 3rd and in some cases in the 4th temperature ranges of the TGA curves (Table 2.3).

For the calorimetric measurements, the relative standard uncertainty of the heat values at each temperature range (H_1, H_2, H_3) were estimated from the analysis of duplicates of 10 samples for a total number of degrees of freedom of 10 (N = 20 - 10). The uncertainties associated with results from TGA were estimated from triplicates measurements performed to 10 compost samples. in a total of 20 degrees of freedom, N = 30-10. The estimated values of relative standard uncertainties are presented in Table 2.4. The replicates of DSC and TGA are shown in Figures A3 and A4 (in Annexes).

Table 2.3: Identification of the decomposition processes related to the weight loss (TGA) and enthalpies (DSC) in the different temperature ranges.

Temperature ranges (°C)	Regions	Information
30 – 177 *(WL_1/ H_1)*	Decomposition of labile substances	Dehydration and desorption processes [23–26]
177 - 400 *(WL_2/ H_2)*	Decomposition of recalcitrant substances	Degradation of the easily biodegradable aromatic structures (carbohydrates moieties and aliphatic compounds) [24,25,27–29]
400 - 620 *(WL_3/ H_3)*	Decomposition of extra-recalcitrant substances	Degradation of complex aromatic structures, such as lignin and humic substances [24,27–30]
620 - 800 *(WL_4)*	Formation of inorganic species	Formation of carbonates [31,32]

The estimated relative standard uncertainties from this replicate analysis have two main contributions, the heterogeneity of the samples and the uncertainty of the measurements. However, as the compost samples are quite heterogeneous, the uncertainties reflect predominantly the sampling variability [33,34].

Table 2.4: Relative standard uncertainties calculated using data from TGA and DSC from 10 samples of compost, analysed in triplicate for TGA and in duplicate for DSC.

Technique	WL_1	WL_2	WL_3	WL_4	*TWL*	*Res*
TGA	26 %	7.8 %	8.8 %	30 %	3.0 %	6.5 %
DSC	23 %	13 %	4.7 %	-	-	-

As this factor is identical for both assays, in air and N_2, the values of the relative standard uncertainties calculated from data obtained in the air atmosphere were used as a meaningful estimation of the uncertainty of the results obtained in the N_2 atmosphere. These uncertainties obtained from compost were also considered for the HS-L although the heterogeneity of the extracts is lower.

2.7. Electrochemical techniques

2.7.1. *Electrical conductivity and potentiometric determination of pH and NH_4^+*

The electrical conductivity (*EC*) of the equilibrium solution was measured using a conductivity meter Crison GLP 32, equipped with a conductivity cell (52-92 model) after the calibration according to the instrument instructions. The pH of the equilibrium solution was measured with a combined glass

electrode (Crison, pH 0-14) and the concentration of NH_4^+ was measured with a selective electrode (Elit electrode Nico 2000). To perform the electrode calibration, standard solutions were prepared by serial dilution (0.5, 1, 10, 20, 50, 100, 200 and 1000 ppm) of a concentrated standard (1000 ppm). The measurements were taken right after the extraction procedure was completed.

2.7.2. Acid-base titrations[3]

Acid-base titrations of the extracts (HA-L, FA-L and DOM) of the compost samples were performed in order to get information about the binding mechanism and obtain parameters from a model of ion binding under different conditions. The charging behaviour was characterized by charge-pH curves in the presence of different concentrations of a salt. Due to the large variety of functional groups present in the HS and DOM, these are considered heterogeneous ligands, containing several acidic groups that are chemically non-identical but have similar ionization constants, in such a way that prevent the appearance of separate titration end points. Other complicating factors are the polydispersity of HS, their polyelectrolyte behaviour, conformational changes, and electrostatic effects make the interpretation of the titrations curves difficult in terms of determining individual pKa values of each type of functional group [35–37].

The acid-base titrations were performed following the protocol proposed by López et al. (2003) [38]. Fully automated acid-base titrations were performed using a Crison microBU 2031 burette and a Crison 2002 pH meter connected to a computer using a home-made software, Vpalia. The scheme of experimental setup used in the acid-base titrations of DOM solutions and both the HA-L and FA-L extracts is shown in Figure 2.3.

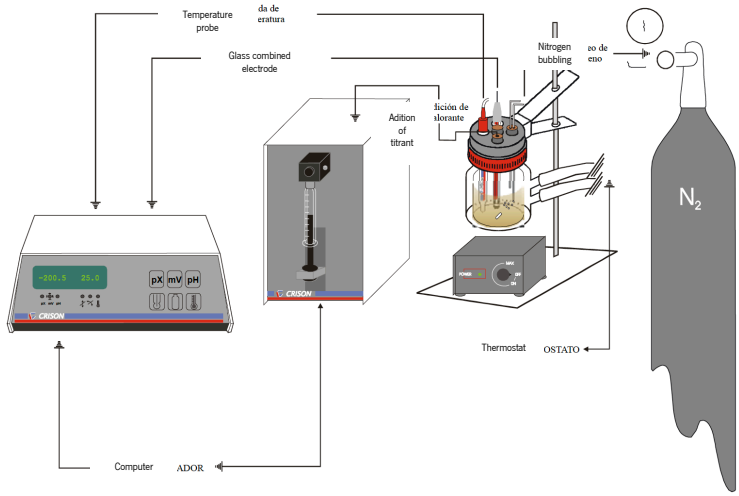

Figure 2.3: Scheme of the experimental setup used in DOM and HS-L acid-base titrations.

[3]Data kindly provided by Doctor Rocio López

The software that controls the experiments is subjected to restrictions to ensure reproducibility and to avoid stabilization problems or the drift of the response of glass combined electrode (Radiometer GH 2401 C, Ag/AgCl as reference). Once the titrant is added, the process is paused for 10 s (to allow the sample homogenization). The measurement of potential starts after this homogenization time. To ensure reproducibility of the glass combined electrode the potential value is read every 3 s until a set of six consecutive values that agree by less than 0.2 mV are obtained. The actual value is calculated as the average of the set of values obtained (with a standard error that does not exceed 0.2 mV). Sample volumes of 50 mL were placed in a thermostated cell at 24.8 ± 0.1 °C and titrated by adding small aliquots (0.01 mL) of 0.02 mol L^{-1} KOH CO_2-free solution. Water saturated nitrogen gas was bubbled through the solution to maintain a CO_2-free atmosphere. In all cases, titrations were performed at least three times to ensure reproducibility. Prior to each titration a calibration curve for the H^+ ion concentration at the working ionic strength was constructed by titrating a strong acid (HCl) with a strong base (KOH).

The titrations of the DOM present in the supernatant of each equilibrium solution were conducted after adjusting their concentration by means of adequate dilutions (obtaining a range of concentrations from 5 to 20 g L^{-1} of compost). The concentration adjustments were made using a colour intensity criterion based on visual perception. The titration of the HA-L and FA-L extracts were performed to solutions with concentrations close to 0.1 g L^{-1} of HS-L.

Due to the relatively high pH values of the equilibrium solutions, two aliquots were taken from each sample to characterize the protonation (titration with 0.1 mol L^{-1} HCl (Panreac)) and deprotonation processes (titration with 0.1 mol L^{-1} KOH (Merck)).

The different solutions of FA-L and HA-L were prepared from a 0.1 g_{HS} L^{-1} stock solution, which in the case of FA-L was prepared directly by dissolving the necessary amount of solid in double distilled water, while for HA-L it was necessary to dissolve the solid in alkaline medium. To do this, a known number of moles of KOH was added to the solid to reach a basic pH and the solution obtained was kept under constant stirring for 2 hours, the time necessary for it to completely dissolve and bubbling N_2 to avoid carbonation of the solution. Once the humic-loke acid was dissolved, a stoichiometric amount of HCl was added to neutralize the moles of KOH initially added, in such a way that the final pH of the humic acid solution was the natural one. The titration of the DOM was conducted at 0.1 mol L^{-1} ionic strength in KNO_3 (Merck) while titrations of the HA-L and FA-L extracts were conducted at 0.01 mol $L^{-1}$and 0.1 mol L^{-1}.

Theory/calculation

Data processing: the charge curves

Before carrying out the potentiometric titrations of the HA-L, FA-L and DOM extracts, it was necessary to calibrate the glass electrode to the ionic strength at which the work was carried out to verify the linear response of the electrode in acidic and basic medium. By means of this relationship, the parameter E^0 can be calculated from Equation 2.1. With these parameters, the measured potential values can be transformed into pH values into the potentiometric titrations of HS-L for each titration point.

$$E = E^0 + 2.303\frac{RT}{F}log(H^+) \qquad \text{(Equation 2.1)}$$

Along the titration curve, as the pH increases by adding the base, the concentration of ionized acid groups and with it the charge on the molecules in the samples increases. This charge generated is a way to quantify the concentration of ionized positions for each pH value.

The magnitude of the charge of the HS-L generated in solution can be calculated from the titration data (pH and base volume) through a charge balance (Equation 2.2) that is applied at each titration point and considers all ions present in solution (except inert electrolyte):

$$Q\ (mmoles) = V_a[KOH] + (V_i + V_a)[H^+] - (V_i + V_a)\frac{K_w}{[H^+]} \qquad \text{(Equation 2.2)}$$

Where V_a and V_i (in mL) refer to the volume of base added at each titration point and the initial volume of the sample (50 mL) respectively, the [K^+] calculated from the concentration of KOH added at each point, [H^+] is given by the pH measure at each point and [OH^-] calculated from [H^+] and the value of K_w, the ionic product of water at the ionic strength of work, obtained from the electrode calibration. Finally, to obtain the charge in C g^{-1}, Equation 2.3 is used, where F is Faraday's constant (96485 C mol^{-1}) and [HS] is the sample concentration in mg L^{-1}. The concentration of the sample in solution is corrected considering the ash content calculated from the elemental composition.

$$Q\ (C\ g^{-1}) = \frac{Q\ (mmoles)F}{0.001V_i[HS]} \qquad \text{(Equation 2.3)}$$

The proton is the only component for which the binding experiments can be carried out without competition from other cations. Thus, the NICA equation can be simplified to a double Langmuir-Freundlich (Equation 2.4):

$$Q = M_1 \frac{(K_1 a_H)^{m_1}}{1 + (K_1 a_H)^{m_1}} + M_2 \frac{(K_2 a_H)^{m_2}}{1 + (K_2 a_H)^{m_2}} \qquad \text{(Equation 2.4)}$$

The proton binding parameters are M_1 (carboxyl group content), M_2 (phenolic group content), K_1 (median value of affinity distribution for proton binding by carboxyl groups), K_2 (median value of affinity distribution for proton binding by phenolic groups), $m_{H,1}$ (width of proton-affinity distribution of carboxyl groups) and $m_{H,2}$ (width of proton-affinity distribution of phenolic groups). Since with one component system it is impossible to discriminate n (non-ideality factor) and p (intrinsic heterogeneity parameter), $m_{H,1}$ and $m_{H,2}$ are the 'apparent heterogeneities' and are equal to $n_{i,1}.p_1$ and $n_{i,2}.p_2$, respectively. .

2.7.3. Binding capacity determination of the compost extracts by AGNES

The quantification of the capacity of the compost extracts to bind metal cations was carried out using Cd(II) as a probe. Cadmium is used as a probe, because it exists in nature in residual concentrations [39] therefore its quantification does not suffer external interference, and also because the electroanalytical technique used can detect extremely low concentrations of the metal (at the nmol L^{-1} level) in solution [40].

Absence of Gradients and Nernstian Equilibrium Stripping (AGNES) is an electroanalytical technique more adequate for this kind of measurement as quantifies the free metal in equilibrium with metal bound to the compost extracts (HS-L or DOM) [40]. Besides the comparison of the reactivity of all extracts that was performed by means of the cadmium complexation, the CUW extracts were also characterized using lead. For all samples the titrations with cadmium were conducted at pH 7.0, in order to optimize resources. This value was chosen within the range of pH values that naturally arise in the environment (between 5.0 and 8.0). For the CUW extracts further titrations were performed at pH 6.0, 7.0 and 8.0. The titration of the CUW extracts with lead were carried out at pH 5.0, 5.5, 6.0 and 7.0. All assays were performed in duplicate in presence of a fixed amount of the corresponding extract and with successive additions of known aliquots of a standard cadmium or lead solution.

An Autolab PGSTAT30 potentiostat connected to a Metrohm 663 VA Stands controlled by means of the GPES 4.9 software (EcoChemie) was used to carry out the electroanalytical measurements. The electrochemical cell containing a working glassy carbon rotating disk electrode (Metrohm, 6.1204.300)

modified by a thin mercury film, an auxiliary carbon rod electrode (Metrohm, 6.1248.040) and an Ag/AgCl reference electrode (World Precision Instruments, Driref-5). The thin mercury film electrode was prepared following the published procedure [41]. Briefly, the glassy carbon electrode (GCE) surface was polished with an alumina slurry (grain size 0.05 µm, Metrohm) and sonicated in pure-ultra water for 60 s, to a mirror-like finish. Then, an electrochemical pre-treatment was carried out with a multicycle voltammetric scanning (50×) between -0.8 and +0.8 V at 0.1 V s^{-1}, in a solution of 1.0 mol L^{-1} ammonium acetate (PanReac Applichem) prepared in 0.50 mol L^{-1} hydrochloric acid 37 % (VWR Chemicals). The mercury thin film was then *ex situ* prepared at constant potential, -1.2 V for 240 s and a rotation rate of 1000 rpm in a 0.48 mmol L^{-1} mercury (II) nitrate, (pH 1.9), adjusted with a 1.0 mol L^{-1} nitric acid (VWR Chemicals), prepared from a 0.05 mol L^{-1} mercury (II) nitrate titripur standard solution (Merck) solution. At the end of the experiments, the film of mercury was evaluated by square wave voltammetry (initial potential: -1.2 V; end potential: -0.2 V; step potential: 0.0051 V; amplitude: 0.02505 V). The pH measurements were performed using a glass combined electrode (HI11311, Hanna instruments) connected to a pH meter (Thermo Scientific, Model CyberScan pH 510).

AGNES was used to quantify free cadmium ions in presence of the different FA, HA and DOM extracts. The methodology includes two steps: first a calibration step carried out at pH 4.0 and 12 mmol L^{-1} ionic strength were the blank and four aliquots of cadmium ions were measured. The second step consists of the cadmium/OM titrations. At the end of the calibration a fixed amount (between 0.68 and 13.6 mg L^{-1}) of the OM extract is added to the electrochemical cell and the pH is set to 7.0 by NaOH 0.1 mol L^{-1} addition. The total concentration of cadmium of the first titration point is the same as the last calibration point corrected by the dilution effect. The titration proceeds by several additions of known aliquots of a standard cadmium solution (10^{-5} or 10^{-6} mol L^{-1}) so that the total cadmium range is between 10^{-8} and 10^{-6} mol L^{-1}. All AGNES measurements were carried out in triplicate. The concentration of metal bound to the HS-L was obtained from the difference between the concentration of added metal and the concentration of free metal.

The lead (II) and cadmium (II) stock solutions were prepared from dilution of lead and cadmium standard solutions (1000 mg L^{-1} Merck) in 0.5 mol L^{-1} HNO_3 (Merck), respectively. The electrolyte solutions were prepared by dilution of $NaNO_3$ (Merck) and HNO_3 (PanReac Applichem). In the complexation experiments, the ionic strength of the solutions was adjusted to 12 mmol L^{-1} using 1.0 mol L^{-1} HNO_3 (PanReac Applichem) and 1.0 mol L^{-1} $NaNO_3$ (Merck). The pH of the cell solutions was adjusted using 0.1 mol L^{-1} NaOH (Merck) or 0.1 mol L^{-1} HNO_3. The solutions (400 mg L^{-1}) of the (i) FA-L and (ii) HA-L were prepared by placing 20 mg of the corresponding extract in 50 mL of ultra-pure water at (i) natural pH or (ii) at pH

9.0 and with an argon purge (in order to avoid carbonation) and stirring for about 12 hours. The equilibrium solutions (containing the DOM) were diluted before the electrochemical assay, according to the respective values of dissolved organic carbon (DOC).

Theory/calculation

NICA-Donnan model

The NICA-Donnan model is a combination of the non-ideal competitive adsorption (NICA) model, which describes competitive binding of protons and metal cations to HS considering ion-specific non-ideality and a Donnan equilibrium model that describes non-specific electrostatic adsorption.

This model accounts for binding site heterogeneity by distinguishing two different groups of binding sites, generally associated with carboxylic and phenolic or minor functional groups. For a component *i* with solution activities a_i (mol L^{-1}), its amount bound to the HS Q_i (mol kg^{-1}) is given by the NICA-Donnan Equation 2.5 [42]:

$$Q_i = \frac{n_{i,1}}{n_{H,1}} \times M_1 \frac{(K_{i,1}a_i)^{n_{i,1}}}{\Sigma_i (K_{i,1}a_i)^{n_{i,1}}} \times \frac{\left[\Sigma_i (K_{i,1}a_i)^{n_{i,1}}\right]^{p_1}}{1 + \left[\Sigma_i (K_{i,1}a_i)^{n_{i,1}}\right]^{p_1}} + \frac{n_{i,2}}{n_{H,2}} \times M_2 \frac{(K_{i,2}a_i)^{n_{i,2}}}{\Sigma_i (K_{i,2}a_i)^{n_{i,2}}} \times \frac{\left[\Sigma_i (K_{i,2}a_i)^{n_{i,2}}\right]^{p_2}}{1 + \left[\Sigma_i (K_{i,2}a_i)^{n_{i,2}}\right]^{p_2}} \quad \text{(Equation 2.5)}$$

Four parameters are characteristic of the HS: M_1 and M_2 are the total number of available proton binding site within each distribution; p_1 and p_2 are a measure of the widths of the affinity distributions, which describe the intrinsic heterogeneity of the humic material. Four parameters are specific for each considered component i and describe the median affinities ($K_{i,1}K_{i,2}$) and non-idealities ($n_{i,1}$, $n_{i,2}$) of the ion binding to both distributions.

According to the Donnan electrostatic model the charge inside the volume of the humic particle Q (mol kg^{-1}) needs to be compensated by the accumulation of counter-ions and the exclusion of co-ions within a Donnan gel, resulting in the following charge balance (Equation 2.6) [43]:

$$Q + V_D\left(\Sigma z_j a_{D,j}\right) = 0 \quad \text{(Equation 2.6)}$$

with V_D (L kg^{-1}) being the Donnan specific volume, z_j the charge number of ion *j* and $a_{D,j}$ (mol L^{-1}) the activity of ion *j* in the Donnan volume. The activity of an ion *j* in the Donnan volume ($a_{D,j}$) is related to its concentration in the bulk solution $a_{0,j}$ (mol L^{-1}) according to Equation 2.7:

$$a_{D,j} = a_{0,j} exp\left(-\frac{z_j F \psi_D}{RT}\right) \quad \text{(Equation 2.7)}$$

with ψ_D (V) being the homogeneous Donnan potential, and *F, R* and *T* the Faraday constant, gas constant and absolute temperature respectively. Benedetti et al. (1996) showed that the dependence of the Donnan volume on ionic strength for several HA and FA could be described well using the empirical Equation 2.8 [43]:

$$logV_D = \alpha + \beta log I \quad \text{(Equation 2.8)}$$

where I (mol L^{-1}) is the ionic strength and α and β are empirical coefficients (different for HA and FA). Kinniburgh et al. (1999) simplified this equation assuming that for all HS the Donnan volumes converge to a constant value of 0.1 L kg^{-1} at I=10 M, resulting in the following Equation 2.9 [44]:

$$logV_D = b(1 - log\ I) - 1 \quad \text{(Equation 2.9)}$$

where *b* is an empirical constant (positive) which varies amongst HS.

2.8. PEST-ORCHESTRA tool

In this work the PEST-ORCHESTRA tool was used to obtain the best NICA-Donnan parameters of the humic- (HA-L) and fulvic-like (FA-L) from CUW using data from the binding of proton, Cd(II) and Pb(II) following the method described by Janot *et al.* (2017) [45].

2.9. Statistical analysis[4]

The relative dispersion of data was evaluated by means of the coefficient of variation ($s/\bar{x}$) where $\bar{x}$ is the arithmetic mean and *s* the standard deviation [46]. For quantities where results from different samples showed high dispersion, the median was used as a reference value.

The chemometric methods provide a way to visualize variation within large multivariate datasets. Principal component analysis (PCA) is probably one of the most used methods for exploratory data analysis. However, it may not be always effective when there are multiple influential factors therefore an extension of PCA, multi-block analysis, was designed to find the underlying relationships between several sets of possibly related data with the emphasis to reveal the "common trend" between these data.

[4] as part of a collaboration with Prof. Doctor Patrícia Valderrama

2.9.1.Multi-block data analysis

Common Dimensions (ComDim) belongs to the family of multiblock components analyses, being attractive due to the possibility of integrating and evaluating multiple information describing the same samples, highlighting, in an exploratory way, interesting features of multiple data blocks [47,48]. The ComDim-based method calculates a weighted sum of the sample variance-covariance matrix of each block, followed by the extraction of the first principal component standardized and named Common Component (CC). Then, the global and local components are extracted from multiple blocks of data sequentially and iteratively calculate the weight or salience of each block for the calculated CC. After calculating the first CC, each original data block matrix is deflated, and the procedure is repeated for calculating the second CC, and so on. In summary, the salience indicates the importance of each block in the construction of the CC, each CC is the first PC of a weighted sum of the sample variance-covariance of deflated matrices, and the importance of each block and its inter-block relationships is graphically shown through saliences plot [47–50]. In other words, this unsupervised multiblock analysis determines a common space for all different data blocks, in which each data block has a specific contribution ("salience") to the determination of each dimension of this common space. For this purpose, it is extracting, in a sequential way, global and local (block) components that recover the maximum of the total variance in the set of data blocks [47]. Besides improving the results interpretability [48], with the salience result it is possible to verify the relationship between different analysis types and/or blocks [47–49,51–53]. Another important result from the ComDim analysis are the informative graphs showing similarities and differences between the samples through scores, and which variables are responsible for the similarities and differences observed in the samples through loadings. In this way, clustering of samples reveals similarities between the samples, while no clustering shows differences. On the other hand, the clustering of variables indicates inter-variable relationships [48,51,53].

ComDim analysis was implemented through the Matlab software R2007b and is mathematically step by step described in detail elsewhere [49,51].

2.9.2.Principal component analysis

The chemometric evaluation was performed by unsupervised pattern recognition through principal component analysis (PCA). PCA is one of the most powerful and common techniques used for reducing the dimensionality of large data sets without information loss. PCA implies a mathematical procedure that transforms the overall set of original variables (X matrix) into two matrices (scores and loadings matrices) by principal components, (PCs) [54–56]. The scores and loadings can be visualized by informative plots,

where the scores matrix brings information regarding sample similarities, while loadings show how variables are responsible for the pattern observed in the scores clusters. PCA was applied by using the Matlab software version R2007b (The Mathworks Inc., MA, EUA), with autoscale preprocess (since the variables present different magnitudes and units).

2.9.3. Correlation heatmap analysis

Correlation heatmap is graphical representation of a correlation matrix representing association between different variables. Two heatmaps were built using correlation analysis results from quantitative data and properties related to structural features of the different samples [57]. The maximum value of the correlation coefficient (r=1) is represented by the more intense red colour, whereas the minimum value (r=0) is represented by white and the antagonistic correlations between variables with a maximum value (r= -1) are represented by intense blue. The correlation analysis was performed using the Matlab software version R2007b.

2.10. Plant field experiment[5]

To identify eventual biological effects, three different compost samples were tested on a relevant crop species at the field level. The organic fertilizer was also tested for comparative purposes.

2.10.1. Biological material

Lettuce (*Lactuca sativa* L.) rooted plantlets of the variety Maravilha das 4 Estações were acquired from Casa Comercial Bragro (Braga, Portugal) and planted in the same day. Similar plants, of about 15 cm height and 4-6 leaves, were chosen.

2.10.2. Experimental design and sampling

On a plot of 25 m^2 located at organic community gardens of the University of Minho, 15 beds were prepared for plantation. The composts CUW, CVA, CA and the fertilizer FLW were applied to topsoil and mixed coarsely following technical recommendations (Table 2.5). Control beds just with native soil were also used. Treatments and controls were randomly assigned to beds with three beds per condition as replicates. In each bed 7 lettuce plantlets were planted 0.3 m away from each other (21 plants per condition). Plants were watered regularly whenever necessary. After 5 weeks of growth, 2 to 3 plants were collected from the inner region of all bed-replicates to prevent border effects (totalizing 6-9 replicates

[5] Data kindly provided by Prof. Doctor Ana Cunha and Prof. Doctor Rui Oliveira

per condition), and the plant total leaf area was determined. For this, the length (L) and maximum width (W) of all leaves were measured and the leaf area (LA) of each leaf was calculated from the equation: LA = 0.7764 L*W – 0.9761 (R^2=0.98).

Table 2.5: Recommended doses from the producers (technical sheets) and amount applied considering a bed area of 0.54 m^2 (1.8 m long x 0.3 m wide).

Compost	Recommended doses (kg/m^2)	Applied amount per bed (kg)
CUW	0.15 - 0.35	0.079 and 0.18
CVA	1.53	0.8
CA	2.55	1.34
Fertilizer	**Recommended doses (kg/m^2)**	**Applied amount per bed (kg)**
FLW	0.3 - 0.5	0.16 and 0.26

This equation was previously obtained after L and W measurements and estimations of the respective leaf area of more than 70 leaves of different sizes. Here the leaf area of each leaf was estimated by the method of leaf silhouette on paper (relating the weight of the paper with the known area). Plant growth results are displayed as $\bar{x} \pm s$ ($4 \leq n \leq 8$).

One-way ANOVA followed by Tukey's multiple comparisons test was performed using GraphPad Prism version 7.0c for MAC OS X (GraphPad Software, La Jolla, CA, USA, www.graphpad.com). Significant differences ($p \leq 0.05$) between samples are indicated with different letters (*a*, *b* and *c*).

3. References

[1]F.J. Stevenson, Humus Chemistry: Genesis, Composition, Reactions, Second Edition, Division of Chemical Education, 1994. https://doi.org/10.1021/ed072pA93.6.

[2]R.S. Swift, Organic Matter Characterization, in: D.L. Sparks, A.L. Page, P.A. Helmke, R.H. Loeppert, R.S. Swift (Eds.), Methods of Soil Analysis Part 3—Chemical Methods, Soil Science Society of America, American Society of Agronomy, 1996: pp. 1011–1069. https://doi.org/10.2136/sssabookser5.3.c35.

[3]J.A. Leenheer, Comprehensive approach to preparative isolation and fractionation of dissolved organic carbon from natural waters and wastewaters, Environmental Science & Technology. 15 (1981) 578–587. https://doi.org/10.1021/es00087a010.

[4]A. Walkley, A critical examination of a rapid method for determining organic carbon in soils – effect of variations in digestion conditions and of inorganic soil constituents, Soil Science. 63 (1947) 251–264. https://doi.org/10.1097/00010694-194704000-00001.

[5]J. Murphy, J.P. Riley, A modified single solution method for the determination of phosphate in natural waters, Analytica Chimica Acta. 27 (1962) 31–36. https://doi.org/10.1016/S0003-2670(00)88444-5.

[6]K.M. Wichuk, D. McCartney, Compost stability and maturity evaluation - a literature review, Canadian Journal of Civil Engineering. 37 (2010) 1505–1523. https://doi.org/10.1139/L10-101.

[7]P.R. Bloom, J.A. Leenheer, Vibrational, electronic and high–energy spectroscopic methods for characterizing humic substances, in: M.H.B. Hayes, P. MacCarthy, R.L. Malcolm, R.S. Swift (Eds.), Humic Substances. 2: In Search of Structure / Ed. by Michael H. B. Hayes, Wiley, Chichester, 1989: pp. 409–448.

[8]M. Schnitzer, S.U. Khan, Humic substances: chemistry and reactions, in: Soil Organic Matter, 1978: pp. 1–58.

[9]Y.-P. Chin, G. Aiken, E. O'Loughlin, Molecular weight, polydispersity, and spectroscopic properties of aquatic humic substances, Environmental Science & Technology. 28 (1994) 1853–1858. https://doi.org/10.1021/es00060a015.

[10]T. Carballo, M.V. Gil, X. Gómez, F. González-Andrés, A. Morán, Characterization of different compost extracts using Fourier-transform infrared spectroscopy (FTIR) and thermal analysis, Biodegradation. 19 (2008) 815–830. https://doi.org/10.1007/s10532-008-9184-4.

[11]M. Kaiser, R.H. Ellerbrock, Functional characterization of soil organic matter fractions different in solubility originating from a long-term field experiment, Geoderma. 127 (2005) 196–206. https://doi.org/10.1016/j.geoderma.2004.12.002.

[12]A. Jouraiphy, S. Amir, M. El Gharous, J.C. Revel, M. Hafidi, Chemical and spectroscopic analysis of organic matter transformation during composting of sewage sludge and green plant waste, International Biodeterioration and Biodegradation. 56 (2005) 101–108. https://doi.org/10.1016/j.ibiod.2005.06.002.

[13]M. Fuentes, R. Baigorri, G. González-Gaitano, J.M. García-Mina, The complementary use of ^{1}H NMR, ^{13}C NMR, FTIR and size exclusion chromatography to investigate the principal structural changes associated with composting of organic materials with diverse origin, Organic Geochemistry. 38 (2007) 2012–2023. https://doi.org/10.1016/j.orggeochem.2007.08.007.

[14]G.A. Baddi, J.A. Alburquerque, J. Gonzálvez, J. Cegarra, M. Hafidi, Chemical and spectroscopic

analyses of organic matter transformations during composting of olive mill wastes, International Biodeterioration and Biodegradation. 54 (2004) 39–44. https://doi.org/10.1016/j.ibiod.2003.12.004.

[15]G.A. Baddi, M. Hafidi, J. Cegarra, J.A. Alburquerque, J. Gonzálvez, V. Gilard, J.C. Revel, Characterization of fulvic acids by elemental and spectroscopic (FTIR and ^{13}C-NMR) analyses during composting of olive mill wastes plus straw, Bioresource Technology. 93 (2004) 285–290. https://doi.org/10.1016/j.biortech.2003.10.026.

[16]M. González Pérez, L. Martin-Neto, S.C. Saab, E.H. Novotny, D.M.B.P. Milori, V.S. Bagnato, L.A. Colnago, W.J. Melo, H. Knicker, Characterization of humic acids from a Brazilian Oxisol under different tillage systems by EPR, ^{13}C NMR, FTIR and fluorescence spectroscopy, Geoderma. 118 (2004) 181–190. https://doi.org/10.1016/S0016-7061(03)00192-7.

[17]M.E.F. Silva, L.T. Lemos, M.M.S.M. Bastos, O.C. Nunes, A.C. Cunha-Queda, Recovery of humic-like substances from low quality composts, Bioresource Technology. 128 (2013) 624–632. https://doi.org/10.1016/j.biortech.2012.11.013.

[18]R. Spaccini, A. Piccolo, Molecular characteristics of humic acids extracted from compost at increasing maturity stages, Soil Biology and Biochemistry. 41 (2009) 1164–1172. https://doi.org/10.1016/j.soilbio.2009.02.026.

[19]A. Hanc, V. Enev, T. Hrebeckova, M. Klucakova, M. Pekar, Characterization of humic acids in a continuous-feeding vermicomposting system with horse manure, Waste Management. 99 (2019) 1–11. https://doi.org/10.1016/j.wasman.2019.08.032.

[20]J. Mao, N. Chen, X. Cao, Characterization of humic substances by advanced solid state NMR spectroscopy: Demonstration of a systematic approach, Organic Geochemistry. 42 (2011) 891–902. https://doi.org/10.1016/j.orggeochem.2011.03.023.

[21]A. Rodrigues, A. Brito, P. Janknecht, M.F. Proença, R. Nogueira, Quantification of humic acids in surface water: effects of divalent cations, pH, and filtration, J. Environ. Monit. 11 (2009) 377–382. https://doi.org/10.1039/B811942B.

[22]M.J. Díaz, M. Ruiz-Montoya, A. Palma, M.-V. de-Paz, Thermogravimetry Applicability in Compost and Composting Research: A Review, Applied Sciences. 11 (2021) 1692. https://doi.org/10.3390/app11041692.

[23]M. Giovanela, E. Parlanti, E.J. Soriano-Sierra, M.S. Soldi, M.M.D. Sierra, Elemental compositions, FT-IR spectral and thermal behavior of sedimentary fulvic and humic acids from aquatic and terrestrial environments, Geochemical Journal. 38 (2004) 255–264. https://doi.org/10.2343/geochemj.38.255.

[24]Y. Zhang, J. Du, F. Zhang, Y. Yu, J. Zhang, Chemical characterization of humic substances isolated from mangrove swamp sediments: The Qinglan area of Hainan Island, China, Estuarine, Coastal and Shelf Science. 93 (2011) 220–227. https://doi.org/10.1016/j.ecss.2010.12.025.

[25]G.M. de Moraes, F.A. da S. Xavier, E. de S. Mendonça, J.A. de Araújo Filho, T.S. de Oliveira, Chemical and structural characterization of soil humic substances under agroforestry and conventional systems, Revista Brasileira de Ciência Do Solo. 35 (2011) 1597–1608. https://doi.org/10.1590/s0100-06832011000500014.

[26]M.R. Provenzano, N. Senesi, M. V., Characterization of Composts and Humic Acids from Pulp and Paper Mill Biosludges by DSC in Association with FT-IR Spectroscopy, Journal of Thermal Analysis. 52 (1998) 1037–1046.

[27]P. Boguta, Z. Sokołowska, K. Skic, Use of thermal analysis coupled with differential scanning calorimetry, quadrupole mass spectrometry and infrared spectroscopy (TG-DSC-QMS-FTIR) to monitor

chemical properties and thermal stability of fulvic and humic acids, PLoS ONE. 12 (2017) 1–18. https://doi.org/10.1371/journal.pone.0189653.

[28]J.M. Fernández, W.C. Hockaday, C. Plaza, A. Polo, P.G. Hatcher, Effects of long-term soil amendment with sewage sludges on soil humic acid thermal and molecular properties, Chemosphere. 73 (2008) 1838–1844. https://doi.org/10.1016/j.chemosphere.2008.08.001.

[29]J. Kučerík, J. Kovář, M. Pekař, Thermoanalytical investigation of lignite humic acids fractions, Journal of Thermal Analysis and Calorimetry. 76 (2004) 55–65. https://doi.org/10.1023/B:JTAN.0000027803.24266.48.

[30]F.Z. El Ouaqoudi, L. El Fels, P. Winterton, L. Lemée, A. Amblès, M. Hafidi, Study of Humic Acids during Composting of Ligno-Cellulose Waste by Infra-Red Spectroscopic and Thermogravimetric/Thermal Differential Analysis, Compost Science & Utilization. 22 (2014) 188–198. https://doi.org/10.1080/1065657X.2014.910148.

[31]P. Melis, P. Castaldi, Thermal analysis for the evaluation of the organic matter evolution during municipal solid waste aerobic composting process, Thermochimica Acta. 413 (2004) 209–214. https://doi.org/10.1016/j.tca.2003.09.026.

[32]M.P. Som, L. Lemée, A. Amblès, Stability and maturity of a green waste and biowaste compost assessed on the basis of a molecular study using spectroscopy, thermal analysis, thermodesorption and thermochemolysis, Bioresource Technology. 100 (2009) 4404–4416. https://doi.org/10.1016/j.biortech.2009.04.019.

[33]C. Gron, J.B. Hansen, B. Magnusson, A. Nordbotten, M. Krysell, K.J. Andersen, U. Lund, Uncertainty from sampling – A Nordtest handbook for sampling planners on sampling quality assurance and uncertainty estimation, 2007.

[34]Eurachem, EUROLAB, CITAC, Nordtest, R.A.M. Committee, Measurement uncertainty arising from sampling: a guide to methods and approaches, 2007.

[35]M.J. Avena, L.K. Koopal, W.H. van Riemsdijk, Proton Binding to Humic Acids: Electrostatic and Intrinsic Interactions, Journal of Colloid and Interface Science. 217 (1999) 37–48. https://doi.org/10.1006/jcis.1999.6317.

[36]C. Plaza, G. Brunetti, N. Senesi, A. Polo, Proton Binding to Humic Acids from Organic Amendments and Amended Soils by the NICA-Donnan Model, Environ. Sci. Technol. 39 (2005) 6692–6697. https://doi.org/10.1021/es0503377.

[37]I. Christl, R. Kretzschmar, Relating Ion Binding by Fulvic and Humic Acids to Chemical Composition and Molecular Size. 1. Proton Binding, Environmental Science & Technology. 35 (2001) 2505–2511. https://doi.org/10.1021/es0002518.

[38]R. López, S. Fiol, J.M. Antelo, F. Arce, Analysis of the effect of concentration on the acid-base properties of soil fulvic acid. Conformational changes, Colloids and Surfaces A: Physicochemical and Engineering Aspects. 226 (2003) 1–8. https://doi.org/10.1016/S0927-7757(03)00358-3.

[39]E. Smolders, J. Mertens, Cadmium, in: B.J. Alloway (Ed.), Heavy Metals in Soils: Trace Metals and Metalloids in Soils and Their Bioavailability, Springer Netherlands, Dordrecht, 2013: pp. 283–311. https://doi.org/10.1007/978-94-007-4470-7_10.

[40]J. Galceran, E. Companys, J. Puy, J. Cecilia, J.L. Garces, AGNES: A new electroanalytical technique for measuring free metal ion concentration, Journal of Electroanalytical Chemistry. 566 (2004) 95–109. https://doi.org/10.1016/j.jelechem.2003.11.017.

[41]L.S. Rocha, E. Companys, J. Galceran, H.M. Carapuça, J.P. Pinheiro, Evaluation of thin mercury film rotating disk electrode to perform absence of gradients and Nernstian equilibrium stripping (AGNES) measurements, Talanta. 80 (2010) 1881–1887. https://doi.org/10.1016/j.talanta.2009.10.038.

[42]D.G. Kinniburgh, C.J. Milne, M.F. Benedetti, J.P. Pinheiro, J. Filius, L.K. Koopal, W.H. Van Riemsdijk, Metal Ion Binding by Humic Acid: Application of the NICA-Donnan Model, Environ. Sci. Technol. 30 (1996) 1687–1698. https://doi.org/10.1021/es950695h.

[43]M.F. Benedetti, W.H. Van Riemsdijk, L.K. Koopal, Humic substances considered as a heterogeneous Donnan gel phase, Environmental Science and Technology. 30 (1996) 1805–1813. https://doi.org/10.1021/es950012y.

[44]D.G. Kinniburgh, W.H. Van Riemsdijk, L.K. Koopal, M. Borkovec, M.F. Benedetti, M.J. Avena, Ion binding to natural organic matter: competition, heterogeneity, stoichiometry and thermodynamic consistency, Colloids and Surfaces A: Physicochemical and Engineering Aspects. 151 (1999) 147–166.

[45]N. Janot, J.P. Pinheiro, W.G. Botero, J.C.L. Meeussen, J.E. Groenenberg, PEST-ORCHESTRA, a tool for optimising advanced ion-binding model parameters: derivation of NICA-Donnan model parameters for humic substances reactivity, Environ. Chem. 14 (2017) 31. https://doi.org/10.1071/EN16039.

[46]P. Lovie, Coefficient of Variation, in: B.S. Everitt, D.C. Howell (Eds.), Encyclopedia of Statistics in Behavioral Science, John Wiley & Sons, Ltd, Chichester, UK, 2005: p. bsa107. https://doi.org/10.1002/0470013192.bsa107.

[47]V. Cariou, D.J.-R. Bouveresse, E.M. Qannari, D.N. Rutledge, ComDim methods for the analysis of multiblock data in a data fusion perspective, in: Data Handling in Science and Technology, Elsevier, 2019: pp. 179–204. https://doi.org/10.1016/B978-0-444-63984-4.00007-7.

[48]M. Rocha Baqueta, A. Coqueiro, P. Henrique Março, M. Mandrone, F. Poli, P. Valderrama, Integrated 1H NMR fingerprint with NIR spectroscopy, sensory properties, and quality parameters in a multi-block data analysis using ComDim to evaluate coffee blends, Food Chemistry. (2021) 129618. https://doi.org/10.1016/j.foodchem.2021.129618.

[49]D.J.-R. Bouveresse, R.C. Pinto, L.M. Schmidtke, N. Locquet, D.N. Rutledge, Identification of significant factors by an extension of ANOVA–PCA based on multi-block analysis, Chemometrics and Intelligent Laboratory Systems. 106 (2011) 173–182. https://doi.org/10.1016/j.chemolab.2010.05.005.

[50]E.M. Qannari, I. Wakeling, P. Courcoux, H.J.H. MacFie, Defining the underlying sensory dimensions, Food Quality and Preference. 11 (2000) 151–154. https://doi.org/10.1016/S0950-3293(99)00069-5.

[51]A. El Ghaziri, V. Cariou, D.N. Rutledge, E.M. Qannari, Analysis of multiblock datasets using ComDim: Overview and extension to the analysis of (K + 1) datasets: ComDim analysis: overview and extension, J. Chemometrics. 30 (2016) 420–429. https://doi.org/10.1002/cem.2810.

[52]L.M. Leme, H. Rocha Montenegro, L. da Rocha dos Santos, M.J. Sereia, P. Valderrama, P.H. Março, Relation Between Near-Infrared Spectroscopy and Physicochemical Parameters for Discrimination of Honey Samples from Jatai weyrauchi and Jatai angustula Bees, Food Anal. Methods. 11 (2018) 1944–1950. https://doi.org/10.1007/s12161-018-1148-7.

[53]L.N. Rosa, L.C. de Figueiredo, E.G. Bonafé, A. Coqueiro, J.V. Visentainer, P.H. Março, D.N. Rutledge, P. Valderrama, Multi-block data analysis using ComDim for the evaluation of complex samples: Characterization of edible oils, Analytica Chimica Acta. 961 (2017) 42–48. https://doi.org/10.1016/j.aca.2017.01.019.

[54]N. Kettaneh, A. Berglund, S. Wold, PCA and PLS with very large data sets, Computational Statistics

and Data Analysis. 48 (2005) 69–85. https://doi.org/10.1016/j.csda.2003.11.027.

[55]R. Zbytniewski, B. Buszewski, Characterization of natural organic matter (NOM) derived from sewage sludge compost. Part 2: Multivariate techniques in the study of compost maturation, Bioresource Technology. 96 (2005) 479–484. https://doi.org/10.1016/j.biortech.2004.05.019.

[56]A. Vergnoux, M. Guiliano, Y. Le Dréau, J. Kister, N. Dupuy, P. Doumenq, Monitoring of the evolution of an industrial compost and prediction of some compost properties by NIR spectroscopy, Science of the Total Environment. 407 (2009) 2390–2403. https://doi.org/10.1016/j.scitotenv.2008.12.033.

[57]S. Zhao, Y. Guo, Q. Sheng, Y. Shyr, Advanced Heat Map and Clustering Analysis Using Heatmap3, BioMed Research International. 2014 (2014) 1–6. https://doi.org/10.1155/2014/986048.

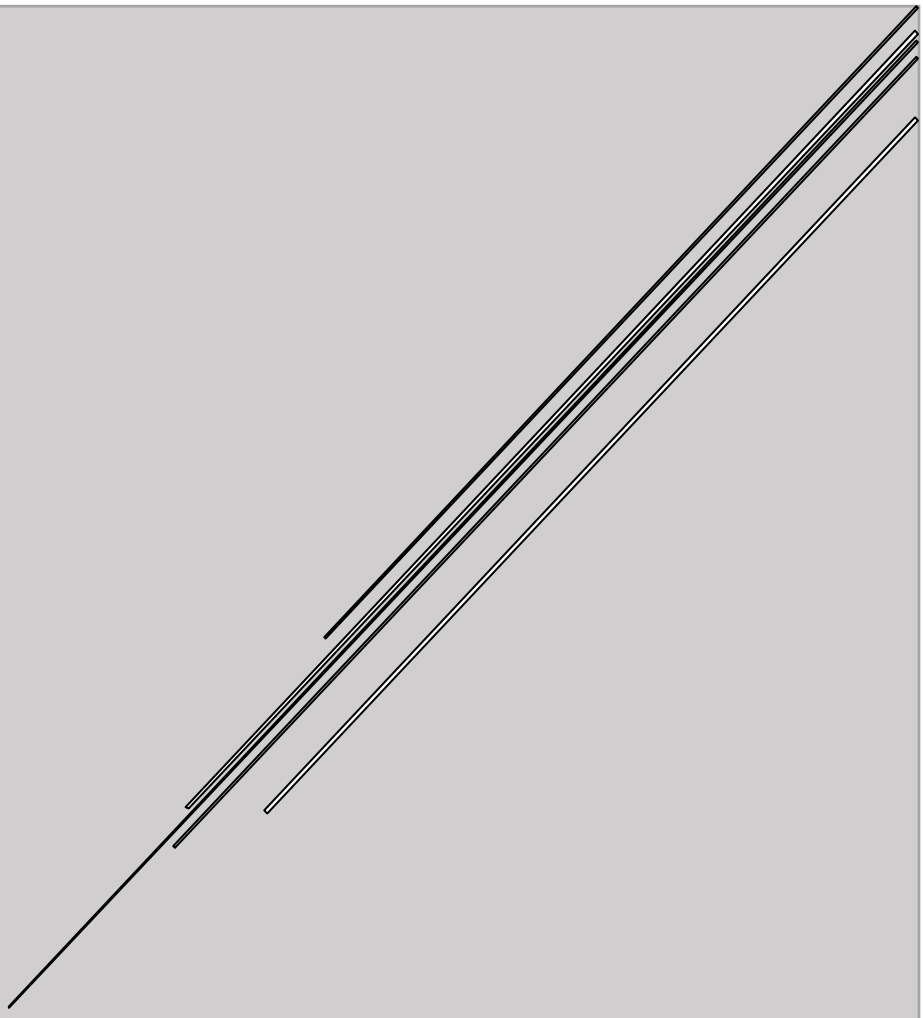

CHAPTER 3 – RESULTS AND DISCUSSION

Chapter 3.1 – Distinctive features of composts of different origin: a thorough examination of the characterization results

This chapter was intended to ascertain the capability of discriminating the origin of different composts based on the characterization parameters obtained from the direct analysis of the compost, that is the most common information provided to users from composition labelling. Seven compost samples produced from distinct feedstock and by different composting methodologies are compared among them and with an organic non-composted fertiliser (Table 2.1). The compost diversity is evaluated from the comparison between results of each analytical technique and also from two chemometric analyses, regarding the elemental composition (using 21 variables) and the structural features (from 14 variables). A field experiment using lettuce as a crop model was carried out with some of the representative samples to showcase how the compost origin may enhance some compost properties that may be suitable for specific crops.

1. Elemental characterization and CEC

The total content of carbon (C) and of the macronutrients nitrogen (N), phosphorus (P), potassium (K), calcium (Ca), magnesium (Mg) and sulphur (S), that are essential for plant and microbial growth in soils are presented in Table 3.1. The content of the micronutrients iron (Fe), zinc (Zn), manganese (Mn), copper (Cu), niquel (Ni) and cobalt (Co), are also presented in Table 3.1. together with the content of sodium (Na), arsenic (As), chromium (Cr) and lead (Pb).

Table 3.1: Data from elemental composition and from CEC of the compost samples and the organic fertiliser (highlighted).

Parameter	CVA	CVDW	CLW	CSS	CDDW	CUW	CA	FLW
C (%)	29.7	43.9	22.8	31.3	23.3	34.0	6.0	22.5
C_{ox}(%)	27.5	33.1	17.8	30.6	18.8	29.3	5.7	15.4
N (%)	2.4	4.8	1.8	3.6	2.3	2.7	0.6	1.7
S (%)	0.4	0.4	0.7	1.1	0.2	0.2	0.23	0.1
C/N	12.5	9.2	12.8	8.6	10.3	12.6	9.97	13.2
C_{ox}/C	92.5	75.4	77.8	97.8	81.0	86.1	94.6	68.2
P (g kg^{-1})	4.15	5.51	13.51	9.86	2.51	5.00	3.20	11.31
Ca (g kg^{-1})	13.10	9.63	78.04	19.88	16.10	77.47	11.82	212.1
Mg (g kg^{-1})	4.52	4.43	18.23	5.20	3.62	3.74	3.13	6.18
Na (g kg^{-1})	1.75	1.09	10.48	2.15	0.62	4.83	1.54	3.03
K (g kg^{-1})	10.25	14.58	30.19	4.27	7.60	12.24	4.70	18.28
Fe (g kg^{-1})	3.47	0.88	6.46	23.11	13.00	4.02	4.40	1.70
Al (g kg^{-1})	3.11	1.28	8.26	24.72	19.92	5.71	6.11	2.40
As (g kg^{-1})	0.003	< DL	0.009	0.008	0.004	0.006	< DL	0.003
Co (g kg^{-1})	< DL	< DL	0.003	0.005	0.003	0.003	< DL	< DL
Cr (g kg^{-1})	0.00	0.03	0.03	0.08	0.02	0.01	0.01	0.01
Cu (g kg^{-1})	0.05	0.05	0.18	0.25	0.07	0.04	0.03	0.07
Mn (g kg^{-1})	0.44	0.07	0.35	0.25	0.18	0.13	0.15	0.29
Ni (g kg^{-1})	< DL	< DL	< DL	< DL	< DL	< DL	< DL	< DL
Pb (g kg^{-1})	< DL	0.09	n.d.	0.06	0.04	0.02	0.01	< DL
Zn (g kg^{-1})	0.15	0.04	1.05	0.63	0.15	0.12	0.09	0.24
CEC ($cmol_{(+)}$ kg^{-1})	137	98.9	150	51.6	95.3	167	46	101

Note: < DL (lower than the detection limit) and – (not measured).

The compost samples present varied amounts of C and N these elements are shown by the relatively high values of $s/\bar{x}$ for C (43 %) and for N (51 %). The compost samples with the highest and lowest content of C and N are CVDW and CA, respectively. The highest values of the macronutrients, P, K, Ca, Mg and S, are obtained for CLW whereas CSS exhibits the highest amounts of micronutrients, with the

exception of Mn that is higher for CVA. Regarding the *C/N* ratio, which is an important indicator of the compost maturity [1], the characterised compost samples exhibit values ranging from 8.6 (CSS) to 12.8 (CLW) with a $s/\bar{x}$ of 16 %. As all the values of the *C/N* ratios are lower than 15, that is the maximum value of this parameter recommended for agronomic application, it can be concluded that all compost samples have a maturity degree compatible to this application. It is noteworthy to remark that the organic fertiliser (FLW) exhibits a value of 13.2, which is higher than all compost samples. The values obtained from the CEC characterization vary over a wide range of values, from 46 to 167 $cmol_{(+)}\ kg^{-1}$, with $s/\bar{x}$ of 44 %, where the highest value is from CUW and the lowest from CSS and CA (Table 3.1). The values from these last two compost samples are lower than 60 $cmol_{(+)}\ kg^{-1}$, which is the minimum value expected for a fully matured compost [2].

2. ATR-FTIR characterization

The ATR-FTIR results are shown in Figure 3.1. The spectra of all samples show the characteristic peaks of humified organic matter, namely: a band at 3320 cm^{-1}, that is ascribed to C-H bonds and to O-H of

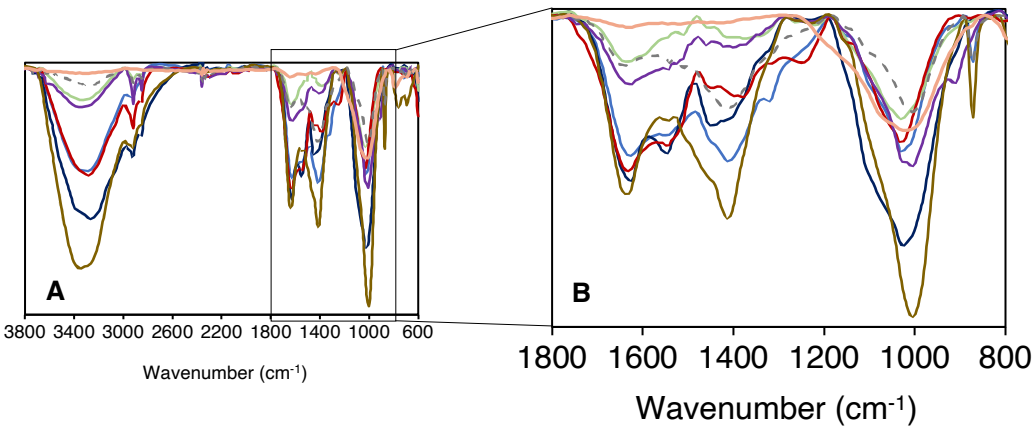

Figure 3.1: ATR-FTIR spectra of the different compost samples in (A) a wide range and in (B) a short-range frequency. CDDW (purple), CVDW (red), CVA (green), CA (orange), CUW (blue), CSS (dark blue), CLW (brown) and FLW (grey). The ATR-FTIR spectra of the analysed samples are in the same scale.

alcohols, phenols or O-H carboxyl and also to N-H vibrations in amide functions [3]; two bands at 2925 and 2845 cm^{-1}, attributed to symmetric and asymmetric vibrations of C-H stretching of CH_3 and CH_2 groups [4]; a band centred around 1640–1630 cm^{-1}, attributed to aromatic C=C and C=O stretching of amide groups and quinonic C=O and/or C=O of H-bonded conjugated ketones [3]; a band at 1540 cm^{-1}, assigned to secondary amides [3]; two other bands between 1440 and 1420 cm^{-1}, associated with the O-H deformation and C-O stretching of carboxylic group, C-H deformations of CH_3 and CH_2 groups and asymmetric stretching of COO^- groups [5]; a band around 1020 cm^{-1}, that was attributed to the

combination of C-O stretching of polysaccharides, in addition to Si-O-Si bonds of silica and to the group Si-O-C [3] and a band at 870 cm^{-1} assigned to carbonates [6].

To characterise the humified organic matter regarding the relative amount of aromatic structures with respect to the aliphatic structures, empiric parameters, designated by aromaticity indexes are calculated using the absorption intensities at characteristic frequencies, namely 1540, 1630, 2845 and 2945 cm^{-1} [7]. According to the values obtained for the four aromaticity indexes $I_{1630/2925}$, $I_{1630/2845}$, $I_{1540/2845}$, $I_{1540/2925}$, samples can be arranged in three groups: CDDW and CSS with the lowest values, CLW, CUW, CVDW and CVA with intermediate values and CA with the highest values (Table 3.2).

Table 3.2: Data from ATR-FTIR of the compost samples and the organic fertiliser (highlighted).

Parameter	CVA	CVDW	CLW	CSS	CDDW	CUW	CA	FLW
$I_{1630/12925}$	3.0	2.8	4.9	1.5	0.32	3.4	9.9	3.0
$I_{1630/12845}$	5.0	5.0	7.7	1.8	0.51	3.3	13	4.4
$I_{1540/2925}$	4.9	1.3	3.5	0.91	0.29	2.3	6.2	1.1
$I_{1540/2845}$	8.1	2.4	5.5	1.2	0.46	2.3	8.2	1.6

3. DSC and TGA characterization

Differential scanning calorimetry (DSC) and thermogravimetric analysis (TGA) provide important information on the thermal resilience and the stabilisation degree of the organic matter and are frequently used for the characterization of materials containing humified organic matter [8].

In the DSC curves that are shown in Figure 3.2A, it can be noticed that the DSC curves exhibit marked changes in shape and height, despite having some common features, such as a minor endothermic band at the lower temperature limit (around 100 °C), usually ascribed to dehydration reactions, and two exothermic bands (around 320 °C and 500 °C), characteristic of stabilised organic matter and attributed to the decomposition of recalcitrant and extra-recalcitrant organic components [9–11]. The enthalpy values obtained by the integration of the DSC bands at the three temperature ranges 30-177 °C, 177-400 °C and 400-620 °C, designated by H_1, H_2 and H_3 respectively, are shown in Table 3.3.

The DSC curves of the samples CA, CSS and CVDW show distinctive features with respect to the remaining four samples (CVA, CLW, CDDW and CUW). Although the shape of the DSC curve of CA is similar to that of the most representative curves, the values of H_2 (-0.24 kJ g^{-1}) and H_3 (-0.35 kJ g^{-1}) are abnormally lower than the median values (-1.55 and -2.98 kJ g^{-1}, respectively) despite the ratio H_3/H_2 (1.46) being close to the median value (1.92).

Table 3.3: Data from TGA and DSC of the compost samples and the organic fertiliser (highlighted).

Parameter	CVA	CVDW	CLW	CSS	CDDW	CUW	CA	FLW
WL_1@air (%)	7.6 ± 2.0	12.5 ± 3.2	9.3 ± 2.4	13 ± 3.4	8.6 ± 2.2	9.3 ± 2.4	2.0 ± 0.5	7.0 ± 1.8
WL_2@air (%)	31 ± 2.4	35 ± 2.7	20.5 ± 1.6	31.9 ± 2.5	23 ± 1.8	28 ± 2.2	6.1 ± 0.47	21 ± 1.6
WL_3@air (%)	23 ± 2.0	27 ± 2.4	19 ± 1.7	18.7 ± 1.6	22 ± 1.9	27 ± 2.4	5.0 ± 0.68	17 ± 2.3
WL_4@air (%)	0.4 ± 0.1	17.2 ± 5.2	1.8 ± 0.5	0.2 ± 0.1	1.1 ± 0.3	7.4 ± 2.2	0.2 ± 0.06	14 ± 4.2
Res@air (%)	37 ± 2.4	7.9 ± 0.5	48.9 ± 3.2	36.8 ± 2.4	46.3 ± 3.0	27.9 ± 1.8	88 ± 5.8	41 ± 2.7
WL_3@air/WL_2@air	0.74 ± 0.09	0.78 ± 0.09	0.94 ± 0.11	0.58 ± 0.07	0.96 ± 0.11	0.96 ± 0.11	0.82 ± 0.10	0.79 ± 0.09
WL_1@N_2 (%)	7.3 ± 1.9	2.6 ± 0.7	0.3 ± 0.1	9.5 ± 2.5	8.1 ± 2.1	4.9 ± 1.3	0.12 ± 0.03	-
WL_2@N_2 (%)	43 ± 3.4	45.1 ± 3.5	23.1 ± 1.8	29.8 ± 2.3	23.4 ± 1.8	19.9 ± 1.5	7.7 ± 0.6	-
WL_3@N_2 (%)	8.7 ± 0.8	12.5 ± 1.1	5.6 ± 0.5	7.0 ± 0.6	13.0 ± 1.1	26.7 ± 2.3	2.1 ± 0.3	-
WL_4@N_2 (%)	4.6 ± 1.4	n.d.	12.0 ± 3.6	5.4 ± 1.6	4.2 ± 1.3	10.2 ± 3.1	1.9 ± 0.6	-
Res@N_2 (%)	36 ± 2.4	39.7 ± 2.6	59 ± 3.9	48 ± 3.2	51 ± 3.3	38 ± 2.5	88 ± 5 .76	-
WL_3@N_2/WL_2@N_2	0.20 ± 0.02	0.28 ± 0.03	0.24 ± 0.03	0.23 ± 0.03	0.56 ± 0.07	1.34 ± 0.16	0.27 ± 0.03	-
WL_3@N_2/WL_3@air	0.38 ± 0.05	0.46 ± 0.06	0.29 ± 0.04	0.37 ± 0.05	0.59 ± 0.07	0.99 ± 0.12	0.42 ± 0.05	-
H_1 (kJ g^{-1})	0.25 ± 0.06	0.38 ± 0.09	0.28 ± 0.06	0.31 ± 0.07	0.31 ± 0.07	0.16 ± 0.04	0.08 ± 0.02	0.26 ± 0.06
H_2(kJ g^{-1})	-1.74 ± 0.22	-0.73 ± 0.09	-1.48 ± 0.19	-2.89 ± 0.37	-1.55 ± 0.20	-2.08 ± 0.27	-0.24 ± 0.03	-0.81 ± 0.10
H_3(kJ g^{-1})	-3.77 ± 0.18	-5.96 ± 0.28	-2.23 ± 0.10	-2.74 ± 0.13	-2.98 ± 0.14	-4.65 ± 0.22	-0.35 ± 0.02	-2.63 ± 0.12
H_3/H_2	2.17 ± 0.30	8.18 ± 1.12	1.50 ± 0.21	0.95 ± 0.13	1.92 ± 0.26	2.23 ± 0.30	1.46 ± 0.20	3.24 ± 0.44

Note: n.d. (not detected) and – (not measured).

The DSC curve of CSS stands out because it does not show a clear distinction between the two exothermic processes displaying a value of H_2 (-2.89 kJ g^{-1}) that is above the median value and consequently a ratio H_3/H_2 (0.95) is significantly lower than the median value. The shape of the DSC curve of CVDW shows an abnormally wide second exothermic process that extends to 780 °C and exhibits an abnormally low value of H_2 (-0.73 kJ g^{-1}) and a rather high value of H_3 (-5.93 kJ g^{-1}), leading to a value of the ratio H_3/H_2 (8.18) that is four times larger than the median.

The TGA curves and the corresponding DTG curves of the compost samples recorded in air and N_2 are shown in Figure 3.2B and Figure 3.2C, respectively. The values of weight loss in air and in N_2 atmospheres are shown in Table 3.3. Although the air atmosphere is more frequently used for the characterization of samples, such as compost and soil, the TGA in N_2 can provide interesting information, particularly if results from both atmospheres are compared [12]. The shape of the TGA curves in air, regarding the two first peaks, is similar. A third and for some samples a fourth peak are also visible. The differences between the shapes and the position of the peaks can be observed through the corresponding DTG curves (dotted lines in Figure 3.2B). Although all the DTG peaks are rather asymmetrical the third peak is particularly uneven, indicating that this peak results from the overlay of multiple single processes. From the DTG curves four temperature ranges were defined and related to four main processes: dehydration and desorption processes (WL_1, 30 - 177 °C) [13,14], decomposition of the easily biodegradable aromatic structures (carbohydrates moieties and aliphatic compounds) (WL_2, 177 - 400 °C) [13,14],

decomposition of the most stabilised organic matter (WL_3, 400 - 620 °C) [13] and decomposition of inorganic carbonates (WL_4, 620 - 800 °C) [13].

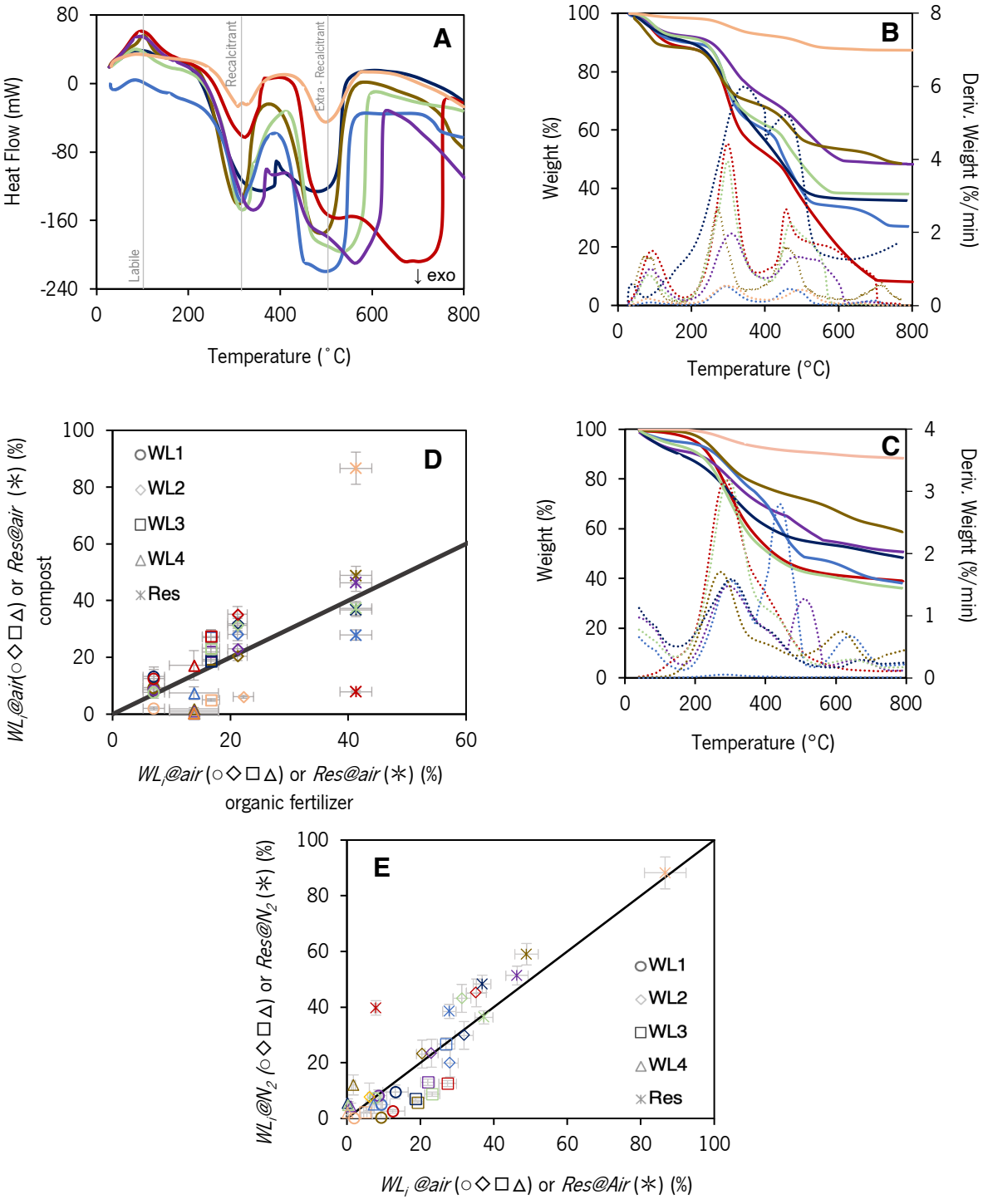

Figure 3.2: Thermogravimetric characterization of composts: (A) DSC curves; TGA and DTG curves obtained in (B) air and in (C) N_2 atmospheres; (D) comparison of TGA data obtained under the atmosphere of air with an organic fertilizer (FLW) and (E) comparison of TGA data obtained under the two atmospheres. CDDW (purple), CVDW (red), CVA (green), CA (orange), CUW (blue), CSS (dark blue) and CLW (brown). The straight line corresponds to the equivalence line y=x.

According to the temperature range of each process an association can be established between the decomposition processes and enthalpies, namely WL_1 can be associated with H_1 (related to dehydration and desorption processes); WL_2 with H_2 (corresponding to decomposition of the recalcitrant substances) and WL_3+ WL_4 with H_3 (associated to decomposition of the extra-recalcitrant substances and carbonates). The values of the total weight loss (*TWL*) of the compost samples in air show important differences. The samples CLW, CDDW, CVA, CSS and CUW display values that are close to the median value of all samples (62.7 %), while CVDW exhibits the highest value (92.3 %) and CA the lowest value (13.3 %). Despite the observed differences in the weight loss values, the ratio WL_3/WL_2, which is used as an indicator of the compost maturation degree [15] varies within a relative narrow range, is between 0.58 and 0.96 for CSS and CUW, respectively. Using this parameter, samples can be divided into three groups, where CLW, CUW and CDDW display the highest values; CA, CVA and CVDW the intermediate values and CSS the lowest value.

The comparison of TGA results of the compost samples with an organic fertiliser, FLW, is shown in Figure 3.13D. From the analysis of the plot, it is possible to conclude that while the residue of the compost samples was evenly distributed above and below the $y = x$ line, the weight loss values of the four parameters showed a clear tendency to be either above (WL_1, WL_2 and WL_3) or below (WL_4) this line, excluding CA, whose values were abnormally low and always lower than the corresponding ones of FLW. Values above the line indicate that the composts have larger amounts of recalcitrant and extra-recalcitrant substances than FLW and also that these substances have higher ability to bind water and other low molecular weight molecules that are oxidized in the 1st temperature range. With respect to the values of WL_4 it seems that FLW is richer in inorganic substances, such as inorganic carbonates or other species that are decompose at temperatures lower than 620 to 800 °C. Another interesting feature of FLW is that its residue is comparable (11 % higher) to the estimated value based on the ICP-OES results. This result validates the estimation procedure and reinforces the hypothesis of the presence of silica, in different amounts, in the residues of the compost samples.

The results of TGA (weight loss and residue) obtained in the N_2 atmosphere are compared with those obtained in air (Figure 3.13E). Most of the data from the residue (star symbol) are located close to the equivalence line 1:1, but above it, indicating that the residues tend to be larger in the N_2 atmosphere. CVDW is the only compost that shows a marked deviation from the equivalence line. With respect to the weight loss in the different temperature ranges, the values of WL_2 and WL_4 are positioned along and in both sides of the equivalence line, suggesting that the thermal decomposition occurs in similar extension by oxidation and pyrolysis. In opposition, the values of WL_1 and WL_3 are positioned under the equivalence

line indicating that the weight loss extent is larger in oxidative conditions. The outcome of WL_1 suggests that oxidation reactions are likely to occur besides the dehydration and desorption processes commonly assigned to this temperature range. With respect to WL_3, significantly higher values were obtained for all samples in the presence of oxygen, except for CUW, whose point is located over the equivalence line. The average value of difference between the extent of weight loss in the two atmospheres (for samples located below the equivalence line) is about 58 %, which is a considerable difference considering the magnitude of these values. A detailed analysis of this difference is carried out in section 4.

4. Correlations between physico-chemical parameters

Results from the different physico-chemical parameters were used in two correlation analyses. The first uses the quantitative data from elemental characterization, TGA residue and *CEC* (Figure 3.3A), whereas the second uses values from intensive properties, such as the reaction enthalpies (H_1, H_2, H_3), intrinsic parameters associated to the maturity of compost (*e.g.* $I_{1630/2925}$, WL_3*@air/*WL_2*@air*), and normalised quantities, *e.g.* WL_1*@air/TWL@air*, *CEC/C* (Figure 3.3B).

In Figure 3.14A the most prominent positive correlations ($r > 0.7$) are among: i) *C*, C_{oxi}, *N* and *Pb*; ii) *P*, *Mg*, *Na*, *K* and *Zn* and iii) *Fe*, *Al*, *Co*, *Cr*, *Cu*, *Ni* and *S*. Simultaneously, negative correlations with $|r| > 0.7$ are observed for *C,* C_{oxi} and *N* with *Res@air*. Even though some of these correlations were not anticipated, particularly those in group iii), the correlations of group ii) can be due to the simultaneous occurrence of these elements in vegetables products [16]. The positive correlations in group i) and the negative correlations with the *Res@air* can be explained considering that an increase in the residue must be followed by a decrease in the elements that constitute the organic fraction of compost.

In Figure 3.3B, the most prominent positive correlations found ($r > 0.7$) are among the following variables: i) $I_{1630/2925}$, H_3 and *CEC/C*; and ii) WL_1*@air/TWL@air*, WL_2*@air/TWL@air* and WL_3*@air/TWL@air*. At the same time, negative correlations ($|r| < 0.7$) are found for: i) $I_{1630/2925}$ and *CEC/C* with H_1; ii) WL_4*@air/TWL@air* and $H_2$with C_{oxi}/C; and iii) WL_1*@air/TWL@air* and WL_2*@air/TWL@air* with *CEC/C*. The positive correlations in the first group indicate that there is a strong association between the relative amount of aromatic moieties ($I_{1630/2925}$), the stabilisation degree of the organic matter (higher values of H_3) and the ability to exchange cations *per* carbon content (*CEC/C*). The correlations found in the second group are less obvious and are ruled by the amount of residue, *i.e.* the larger amounts of residue are associated with the lower values of weight loss in all temperature ranges. With respect to the first group of negative correlations, the relationships indicate suggests that the samples that strongly adsorb low molecular weight molecules (H_1) are those with lower relative abundance of aromatic moieties ($I_{1630/2925}$)

and lower ability to exchange cations *per* carbon content (*CEC/C*). The correlations between *WL_4@air/TWL@air* with C_{oxi}/C in the second group may be associated to the fact that *WL_4@air/TWL@air* is linked to the inorganic fraction of *C* while C_{oxi}/C is related to the organic fraction. The negative correlation between H_2 and C_{oxi}/C indicates that the decomposition of recalcitrant structures releases lower amounts of energy when the ratio C_{oxi}/C increases, suggesting that the carbon that is not readily oxidizable can contribute significantly to H_2.

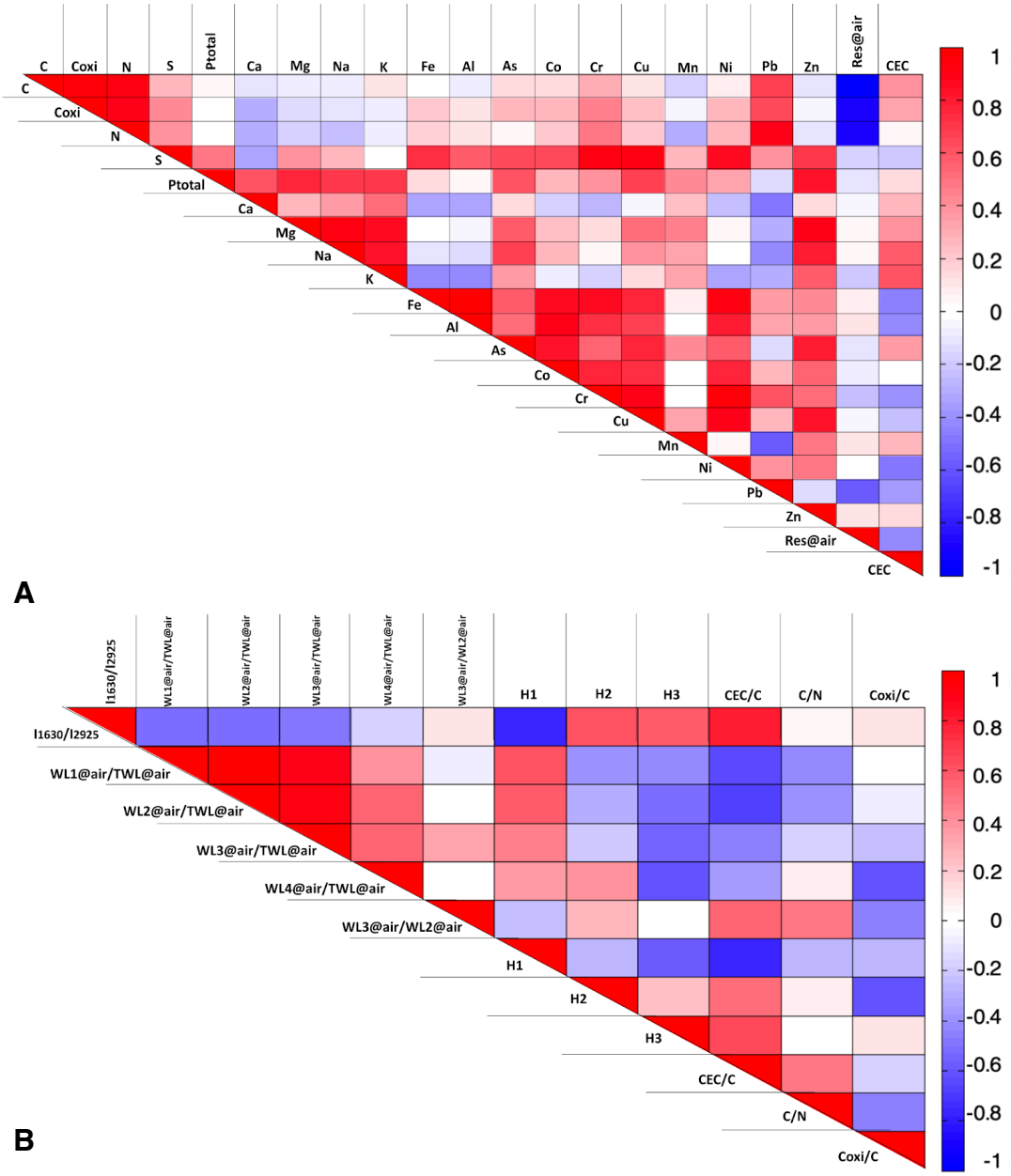

Figure 3.3: Triangular heat map showing the pairwise Pearson correlation coefficients (*r*) of the parameters related to (A) elemental characterization data and (B) data related to molecular structure.

In these correlation analyses only the aromaticity index $I_{1630/2925}$ was used, despite the previous allusion to four ratios calculated from the four independent absorption intensities. This decision was based on the result of the comparison between these aromaticity indexes (Figure 3.4A), which showed that the four parameters are correlated.

The correlation between $I_{1630/2925}$ and $I_{1540/2925}$ and between $I_{1630/2845}$ and $I_{1540/2845}$ suggests that the chemical structures of the constituents in each compost sample have important similarities regarding a constant proportion between the amount of secondary amides (related to $I_{1540/2925}$ and $I_{1540/2845}$) with respect to the moieties containing C=C and C=O (related to $I_{1630/2845}$ and $I_{1630/2925}$). The observed deviation of results of CVA points out that the molecular structures in this compost may differ significantly from the remaining ones.

The correlation between total weight loss in air (*TWL@air*) and total carbon content shown in Figure 3.4B was suggested by the negative correlation found between *Res@air* and C (Figure 3.3A). The slope of this correlation line corresponds to a stoichiometric proportion between the mass loss released by the combustion and the mass of carbon. This slope is similar for all compost samples and corresponds to about 2.1 g *per* gram of carbon (25.2 g *per* mol C). This value depends on the C:O:H molar ratio of the substances that are converted into CO_2 and can vary from 44 g *per* mol C (for carbonates) to 14 g *per* mol C (for alkanes). The fact that all compost samples fit the same straight line suggests that the chemical structure of the fraction of compost that is decomposed by combustion has important similarities. A relevant outcome of the observed correlation is the possibility of estimating the carbon content of compost from a TGA analysis.

In order to explain the difference between the weight loss values in the two atmospheres (N_2 and air) in the range 400 - 620 °C, values of ΔWL_3 ($= WL_3@air - WL_3@N_2$) were calculated and were plotted against different quantities, attempting to correlate these values with elemental or structural data. The most significant correlation relates this quantity with the inorganic carbon through the representation of $\Delta WL_3 + WL_4$ as a function of $C\text{-}C_{oxi}$ (Figure 3.4B), where WL_4 accounts for the amount of carbonates and ΔWL_3 may represent inorganic carbon in the form of carbon nanostructures. The presence of carbon nanostructures, such as graphenes or carbon-based dots, previously found in natural occurring humic substances using ^{13}C-NMR [17], Raman, Transmission Electron Microscopy (TEM) and Atomic Force Microscope (AFM) [18], can explain the observed differences in weight loss in the range 400 – 620 °C as these types of structures are not decomposed in inert atmosphere but are oxidised in this temperature range [12].

If we consider that the formation of these nanostructures occurs during the maturation of compost alongside the formation of the humic-like substances it is expectable that the relative amount of these

nanostructures may be related with the degree of aromaticity of the composts. In fact, there is a good correlation between $\Delta WL_3/TWL@air$ and $I_{1630/2925}$ (r=0.81) for five of the seven compost samples (represented as full symbols in Figure 3.4C). The fact that CUW and CA did not follow the general trend suggests that the maturation of these two samples did not favour the formation of these nanostructures to the same extent of the remaining five samples.

To interpret and possibly justify the origin of the larger differences between the values of the TGA residues in air atmosphere (Figure 3.2B), these values were compared with the amount of metal oxides estimated using the ICP-OES results and considering the formation of the higher oxides of each metal (Figure 3.4D).

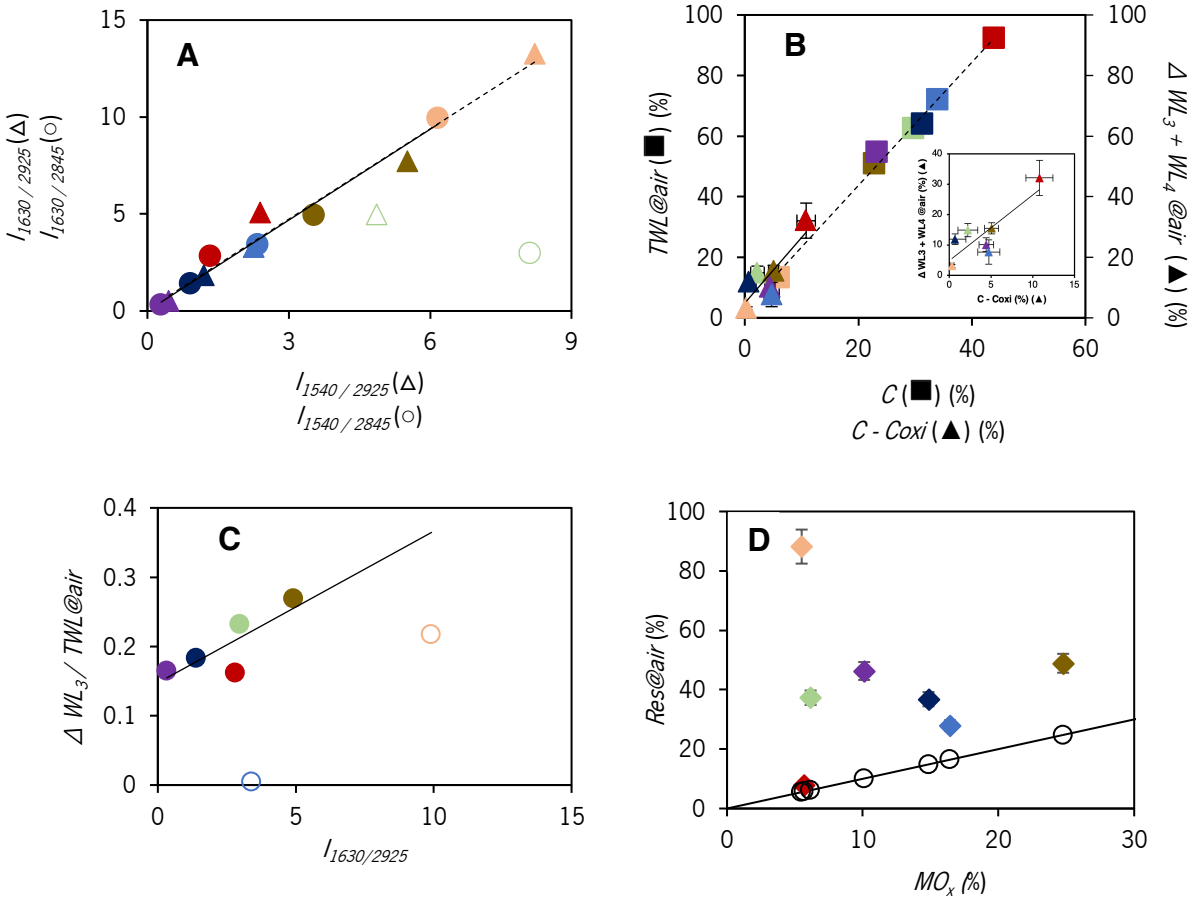

Figure 3.4: Correlations between characterization data from ATR-FTIR, TGA, EA and ICP-OES of the compost samples CDDW (purple), CVDW (red), CVA (green), CA (orange), CUW (blue), CSS (dark blue) and CLW (brown): (A) (▲) $I_{1630/2925}$ *vs.* $I_{1540/2925}$ and (●) $I_{1630/2845}$ *vs.* $I_{1540/2845}$ where a full line represents the linear fitting (r=0.99). Data from CVA (open symbols) were not included in the fitting; (B) (■) *TWL@air vs.* total carbon content, *C* and the dotted line represents the linear fitting (r=0.99), (▲) $\Delta WL_3 + WL_4@air$ *vs.* non-oxidizable carbon content ($C\text{-}C_{oxi}$) and the full line represents the linear fitting (r=0.84); (C) (●) $\Delta WL_3/TWL@air$ *vs.* $I_{1630/2925}$ where data from CUW and CVA (open symbols) were not included in the fitting and the full line was obtained by linear fitting (r=0.81); and (D) (◆) *Res@air vs.* MO_x, where open symbols are estimates of the total metal oxides mass and the line represents $y = x$.

Although *Res@air* of all composts exceeded the calculated values considering exclusively the presence of metal oxides, the values from CVDW, CUW, CSS and CLW were the most closed to the performed estimate. In the case of CDDW, produced by domestic composting, the large deviation observed to the calculated residue may be due to the addition of soil to the composting mixture, which is a common practice in this composting technique. For CA and CVA the large difference can be due to the presence of micro and nanometric silica residues from the algae collected from shore environments.

Though the raw material of CVA and CA is apparently identical (60 % manure and 40 % vegetable remains including algae) the difference observed between the CA residue obtained in the TGA analysis and predicted exclusively from the metal oxides is 2.65 times higher than that of CVA, which must certainly be due to the heterogeneity of the feedstock. The SEM images of these two composts confirm the observed differences (Figure 3.5). The CVA images display packed fluffy and floc-like structures of organic matter while CA images exhibit larger amounts of scattered structures. The amplified image of CA shows that the most abundant structures resemble silicate structures besides the presence of diatoms (in small amounts).

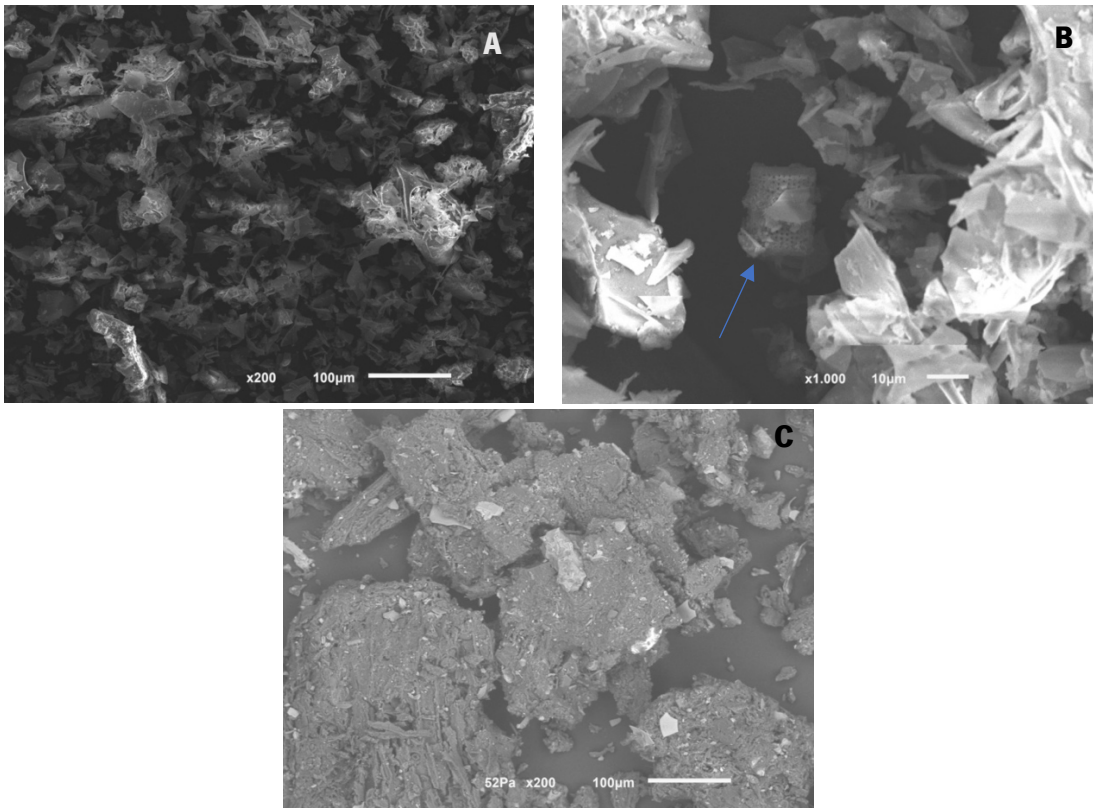

Figure 3.5: Scanning electron images of (A) CA with a 200X magnification, (B) CA with a 1000X magnification and (C) CVA with a 200X magnification.

The XRD analysis (Figure 3.6) of CA identified large amounts of silicates in the forms of quartz, phyllosilicates (predominantly muscovite) and feldspars, whereas CVA shows a larger amount of amorphous material (most likely organic matter) and the predominance of quartz, with smaller amounts of phyllosilicates (muscovite), gypsum and traces of calcite.

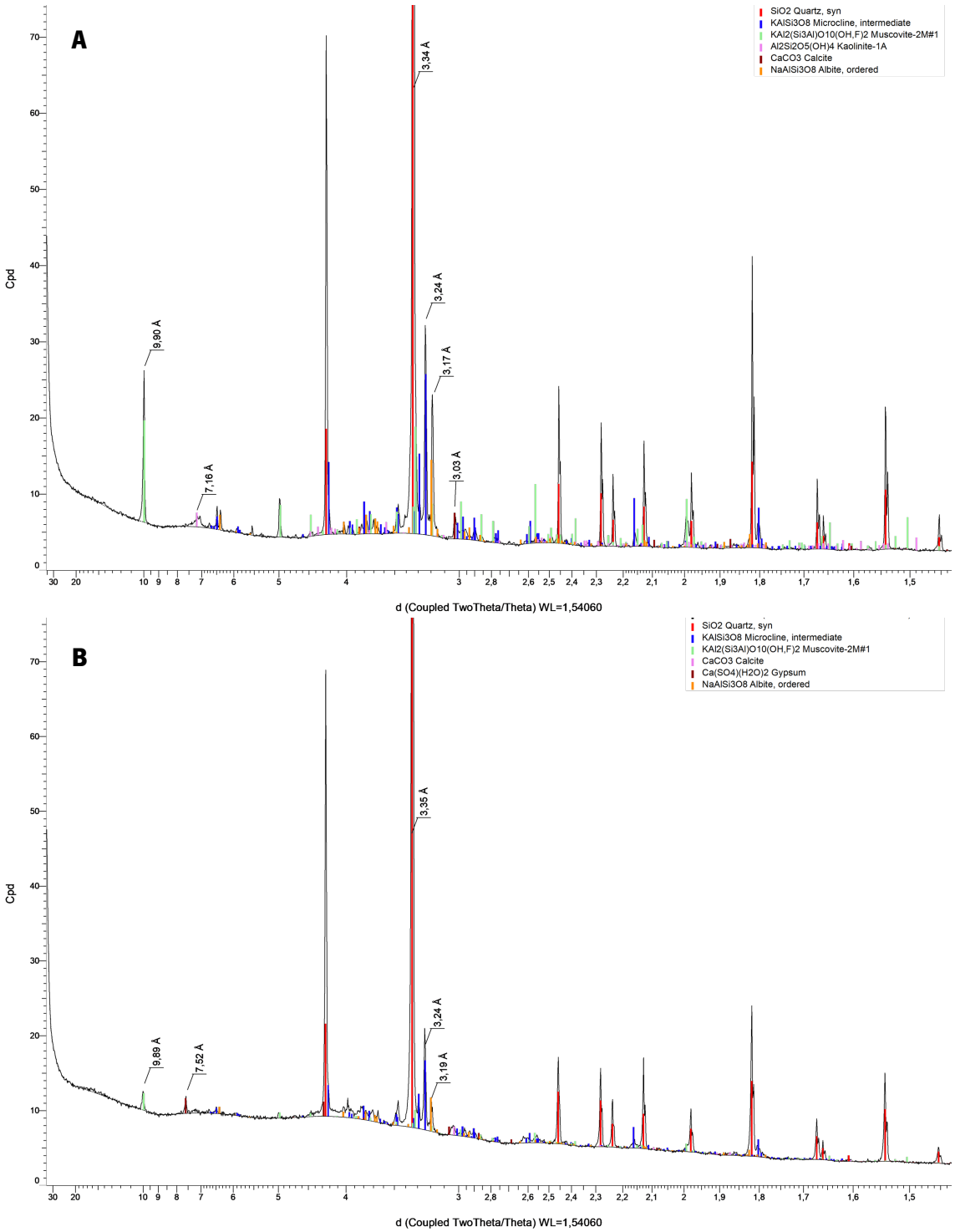

Figure 3.6: X-ray diffraction (XRD) profiles of (A) CA and (B) CVA.

5. PCA analysis

The physico-chemical parameters characterised and analysed throughout this study were organised in two PCA. The first PCA (PCA1) aims to search for pattern in samples using quantitative data and from the parameters previously considered in the correlation analysis of Figure 3.3A, while the second PCA (PCA2) is built using parameters related to the structural properties of the samples previously analysed in Figure 3.3B.

The three first principal components in PCA1 explained 83.85 % of the total variance. Figure 3.7A shows the simultaneous representation of the loadings and scores on PC2 against PC3. The biplot of PC2 and PC3 was considered the most adequate to portray the differences between the samples, despite the explained variance of PC2 and PC3 being moderate (27.13 % and 19.38 %, respectively). In previous studies it was shown that sometimes the main information of a dataset is not present in the PC with the highest explained variance [19,20]. In the biplot of PCA1 two samples are isolated and the remainder can be aggregated in two groups, despite the distance between some of the samples, which in some cases is considerably large. The samples FLW and CLW (both derived exclusively from animal wastes) can be grouped on the PC2 and PC3 positive side. The distinction is associated mainly with higher values of the macronutrients P, K, Ca and Mg and of *CEC*. The CUW, CVA, CSS and CDDW may be grouped on the PC2 negative side. This group stands out for the values of the macronutrient S and of the micronutrients Cr, Cu, Fe, Al, and Ni, wherein CSS displays the highest values. The compost samples CA and CVDW, that show up isolated, are separated from the other groups, CVDW on the negative side of PC2 and on the positive side of PC3 and CA on the negative values of PC2 and PC3. Although CVDW stands out for the highest values of N, C, C_{oxi} and Pb, CA is highlighted for the highest values of residue (*Res@air*).

Regarding PCA2, the two first principal components explained 67.65% of the total variance. Although this biplot samples are well spread, an organisation based on three groups and one isolated sample can be arranged (Figure 3.7B). The compost CSS is isolated on the positive side of PC1 and negative side of PC2, distinctly characterised for the highest value of C_{oxi}/C. The CLW and the fertiliser FLW appear close to each other on the positive side of PC2 and on the negative side of PC1 and are characterised by high values of the parameters H_2, *C/N* and WL_3*@air/*WL_2*@air,* where the latter two are common indicators of the stability of organic matter. The compost samples CVDW and CUW are grouped with CDDW despite the distance observed between them, as they are separated from the others on the positive sides of PC1 and PC2. These samples are characterised for displaying the higher values of H_1, WL_1*@air/TWL@air,* WL_2*@air/TWL@air,* WL_3*@air/TWL@air* and particularly of WL_4*@air/TWL@air*. Composts in this group are

from urban biowastes, which seems to be the main factor for the relative proximity of the three composts. In contrast, the composting methods, that are different for three samples (*i.e.* vermicomposting, industrial and domestic composting), did not play a significant role on the thermal stability of the compost. Similarly, the two algae-based compost samples CA and CVA arise on the negative side of PC1 and PC2.

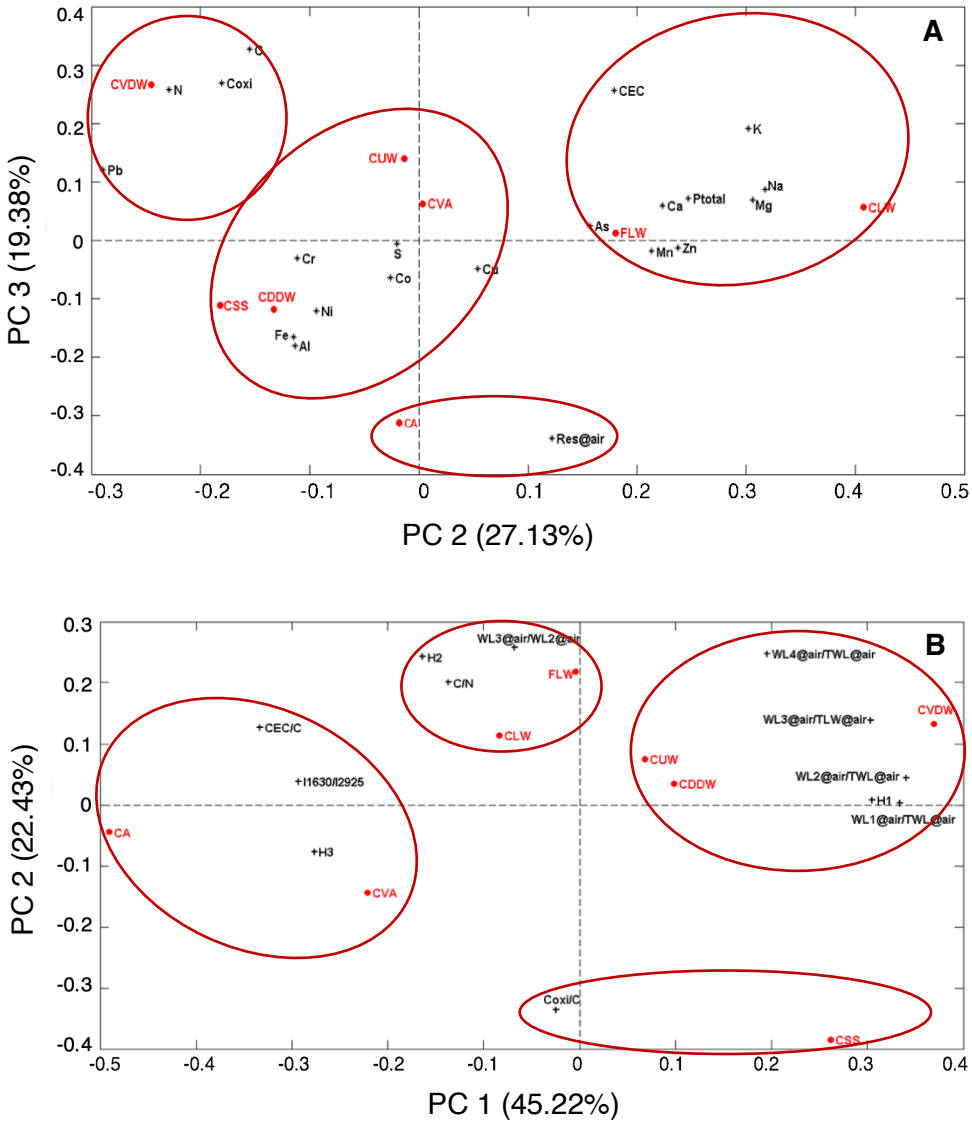

Figure 3.7: Principal Component Analysis (PCA) as biplot representation with loadings and scores in the coordinates (A) PCA1 using elemental characterization data and (B) PCA2 using data related to molecular structure of the compost samples (CDDW, CVDW, CVA, CA, CUW, CSS and CLW) and the organic fertiliser (FLW).

Despite the distance between the two samples in the plot, both are highlighted by the same parameters ($I_{1630/2925}$ and H_3 and CEC/C) that are characteristic of the presence of aromatic molecular structures with high stability and the presence of functional groups capable of complexing metallic cations. From the analysis of PCA1 and PCA2 it is possible to conclude that the distribution pattern of samples in the

representation plots follows a trend that is more closely associated with the nature of the raw materials than with the composting method.

6. Impacts of different composts and fertiliser on lettuce leaf area

A crop field experiment was designed to investigate the potential effect of the compost origin at the plant level, using lettuce. The samples CUW, CA and CVA were selected for this study based on the nature of the feedstock and composting process. In this study, FLW (100 % animal waste, not composted) was used as a reference organic fertiliser.

Results of this study, Figure 3.8A, display the total leaf area obtained for the composts and organic fertilizer applications and for the control with native soil. Fertile soil may be used as control to evaluate the effect of compost application [21,22]. Despite the tested samples being fitted for agricultural purposes, only the compost CA (assigned with c) and the organic fertiliser FLW (assigned with b) at the highest dose promoted a significant increase in the total leaf area (*TLA*) in relation to the control (Figure 3.8A). The results that cannot be differentiated from the control are assigned with a. Results from CUW (0.35), CVA (1.53) and FLW (0.30) are assigned with a, b because they cannot be statistically differentiated either from the control or FLW (0.50). Regarding the compost dosage effect, no significant differences were detected on *TLA* for CUW and FLW when comparing the minimum and maximal doses recommended by producers, suggesting that the lower dose was sufficient to maximise the vegetative growth for this productivity variable and for this plant crop species.

The amounts of N, P and K effectively applied *per bed* (Figure 3.8B) were calculated to compare results given the used doses (based on the suppliers' indications). The larger amounts of N and K were provided to the soil by CVA, which are about 58 % and 23 % higher than those for CA, respectively. The largest amount of P was provided by CA (23 % higher than the provided by CVA). Nevertheless, the observed impact of CA application is hardly explained by the value of P, as the variation of this nutrient with respect to CVA is lower than the observed for the dosage effect (using CUW and FLW).

The differential growth of lettuce where sample CA stood out was not explained by the relative amounts of N, P and K, considering the results from parameters related to structural properties. In PCA2, CA is associated with CVA whose results from the lettuce grow experiments were not significantly different from the control. Although CA is isolated in the PCA1, this placing is related to the higher amount of residue. It is not expected that this fraction of material can be responsible for the increased growth of lettuce as the residue is essentially composed of inert substances, mainly silicates. Furthermore, despite the differences in the composition of CVA and CUW (as the two samples are in two different groups in PCA2)

the impact of these two samples in lettuce growth is indistinguishable. Although the characterization data of the technical sheet that accompanies the compost refer to the characterization of the solid, it was not possible to find among these parameters one that could justify the effects observed in the growth of lettuce. Thus, we are led to think that other properties, namely those related to the reactivity of its components present in the different extracts, may be at the origin of these results. The characterization of extracts of these composts will be presented in the chapters 3.2 and 3.3.

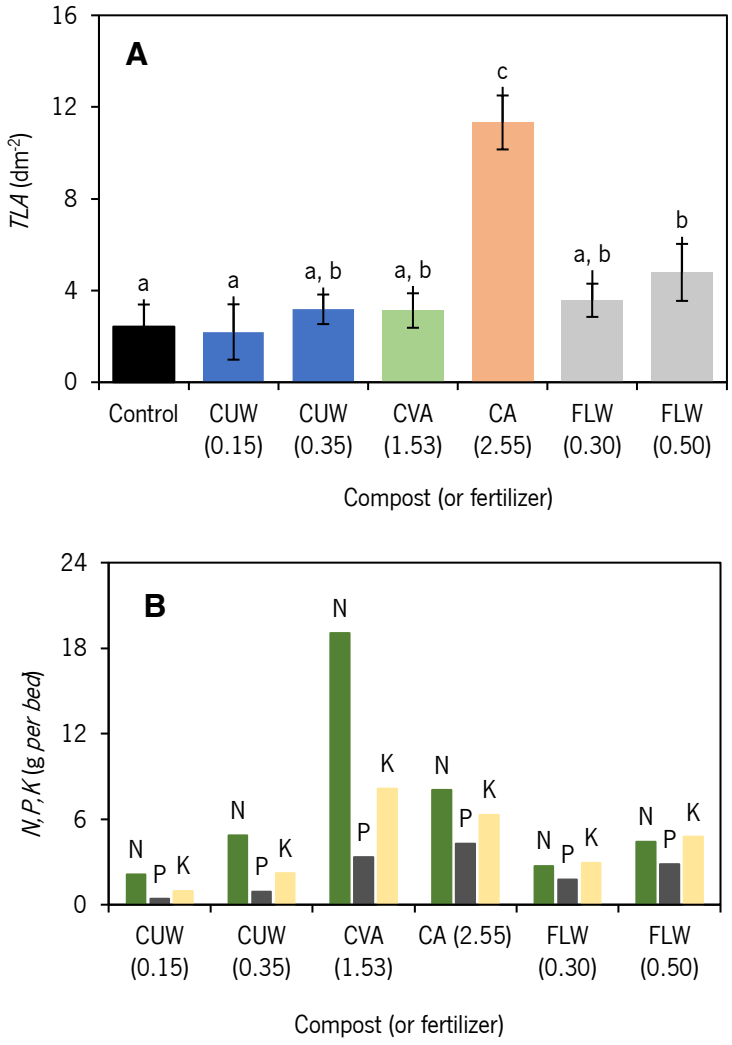

Figure 3.8: (A) Impact of the application of CUW, FLW, CVA and CA at the tested doses on total leaf area of lettuce plants after 5 weeks of culture in a field plot. Error bars represent the standard deviation and mean values topped by different letters (a, b and c) are significantly different ($p \leq 0.05$); (B) The applied amount of N, P and K *per bed*. The number in each abbreviation refers to the applied dose in kg m^{-2}.

7. References

[1] N. Soobhany, S. Gunasee, Y.P. Rago, H. Joyram, P. Raghoo, R. Mohee, V.K. Garg, Spectroscopic, thermogravimetric and structural characterization analyses for comparing Municipal Solid Waste composts and vermicomposts stability and maturity, Bioresource Technology. 236 (2017) 11–19. https://doi.org/10.1016/j.biortech.2017.03.161.

[2] Y. Harada, A. Inoko, Relationship between cation-exchange capacity and degree of maturity of city refuse composts, Soil Science and Plant Nutrition. 26 (1980) 353–362. https://doi.org/10.1080/00380768.1980.10431220.

[3] G.A. Baddi, J.A. Alburquerque, J. Gonzálvez, J. Cegarra, M. Hafidi, Chemical and spectroscopic analyses of organic matter transformations during composting of olive mill wastes, International Biodeterioration and Biodegradation. 54 (2004) 39–44. https://doi.org/10.1016/j.ibiod.2003.12.004.

[4] M. Kaiser, R.H. Ellerbrock, Functional characterization of soil organic matter fractions different in solubility originating from a long-term field experiment, Geoderma. 127 (2005) 196–206. https://doi.org/10.1016/j.geoderma.2004.12.002.

[5] M. Fuentes, R. Baigorri, G. González-Gaitano, J.M. García-Mina, The complementary use of ^{1}H NMR, ^{13}C NMR, FTIR and size exclusion chromatography to investigate the principal structural changes associated with composting of organic materials with diverse origin, Organic Geochemistry. 38 (2007) 2012–2023. https://doi.org/10.1016/j.orggeochem.2007.08.007.

[6] E. Smidt, K. Meissl, M. Schwanninger, P. Lechner, Classification of waste materials using Fourier transform infrared spectroscopy and soft independent modeling of class analogy, Waste Management. 28 (2008) 1699–1710. https://doi.org/10.1016/j.wasman.2007.08.003.

[7] Y. Inbar, Y. Chen, Y. Hadar, Solid-state carbon-13 nuclear magnetic resonance and infrared spectroscopy of composted organic matter, Soil Science Society of America Journal. 53 (1989) 1695–1701. https://doi.org/10.2136/sssaj1989.03615995005300060014x.

[8] A.F. Plante, J.M. Fernández, J. Leifeld, Application of thermal analysis techniques in soil science, Geoderma. 153 (2009) 1–10. https://doi.org/10.1016/j.geoderma.2009.08.016.

[9] J.M. Fernández, C. Plaza, A. Polo, A.F. Plante, Use of thermal analysis techniques (TG-DSC) for the characterization of diverse organic municipal waste streams to predict biological stability prior to land application, Waste Management. 32 (2012) 158–164. https://doi.org/10.1016/j.wasman.2011.08.011.

[10] M.T. Dell'Abate, A. Benedetti, A. Trinchera, C. Dazzi, Humic substances along the profile of two Typic Haploxerert, Geoderma. 107 (2002) 281–296. https://doi.org/10.1016/S0016-7061(01)00153-7.

[11] A. Merino, M.T. Fonturbel, C. Fernández, B. Chávez-Vergara, F. García-Oliva, J.A. Vega, Inferring changes in soil organic matter in post-wildfire soil burn severity levels in a temperate climate, Science of the Total Environment. 627 (2018) 622–632. https://doi.org/10.1016/j.scitotenv.2018.01.189.

[12] S.G. King, L. McCafferty, V. Stolojan, S.R.P. Silva, Highly aligned arrays of super resilient carbon nanotubes by steam purification, Carbon. 84 (2015) 130–137. https://doi.org/10.1016/j.carbon.2014.11.061.

[13] M.P. Som, L. Lemée, A. Amblès, Stability and maturity of a green waste and biowaste compost assessed on the basis of a molecular study using spectroscopy, thermal analysis, thermodesorption and

thermochemolysis, Bioresource Technology. 100 (2009) 4404–4416. https://doi.org/10.1016/j.biortech.2009.04.019.

[14] S.L. Lim, T.Y. Wu, Determination of maturity in the vermicompost produced from palm oil mill effluent using spectroscopy, structural characterization and thermogravimetric analysis, Ecological Engineering. 84 (2015) 515–519. https://doi.org/10.1016/j.ecoleng.2015.09.050.

[15] M.T. Dell'Abate, S. Canali, A. Trinchera, A. Benedetti, P. Sequi, Thermal analysis in the evaluation of compost stability: A comparison with humification parameters, Nutrient Cycling in Agroecosystems. 51 (1998) 217–224. https://doi.org/10.1023/A:1009734816502.

[16] M. Reyes-Torres, E.R. Oviedo-Ocaña, I. Dominguez, D. Komilis, A. Sánchez, A systematic review on the composting of green waste: Feedstock quality and optimization strategies, Waste Management. 77 (2018) 486–499. https://doi.org/10.1016/j.wasman.2018.04.037.

[17] L. Haumaier, W. Zech, Black carbon—possible source of highly aromatic components of soil humic acids, Organic Geochemistry. 23 (1995) 191–196. https://doi.org/10.1016/0146-6380(95)00003-W.

[18] Y. Dong, L. Wan, J. Cai, Q. Fang, Y. Chi, G. Chen, Natural carbon-based dots from humic substances, Scientific Reports. 5 (2015) 10037–10037. https://doi.org/10.1038/srep10037.

[19] M.M.C. de de Almeida, C.R.L. Francisco, A. de Oliveira, S.S. de Campos, A.P. Bilck, R.H.B. Fuchs, O.H. Gonçalves, P. Valderrama, A.K. Genena, F.V. Leimann, Textural, Color, Hygroscopic, Lipid Oxidation, and Sensory Properties of Cookies Containing Free and Microencapsulated Chia Oil, Food Bioprocess Technol. 11 (2018) 926–939. https://doi.org/10.1007/s11947-018-2057-x.

[20] I. Moreira, I.S. Scarminio, Chemometric discrimination of genetically modified Coffea arabica cultivars using spectroscopic and chromatographic fingerprints, Talanta. 107 (2013) 416–422. https://doi.org/10.1016/j.talanta.2013.01.053.

[21] G.C. Pavlou, C.D. Ehaliotis, V.A. Kavvadias, Effect of organic and inorganic fertilizers applied during successive crop seasons on growth and nitrate accumulation in lettuce, Scientia Horticulturae. 111 (2007) 319–325. https://doi.org/10.1016/j.scienta.2006.11.003.

[22] F.T. Santos, P. Goufo, C. Santos, D. Botelho, J. Fonseca, A. Queiros, M.S.S.M. Costa, H. Trindade, Comparison of five agro-industrial waste-based composts as growing media for lettuce: Effect on yield, phenolic compounds and vitamin C, Food Chemistry. 209 (2016) 293–301. https://doi.org/10.1016/j.foodchem.2016.04.087.

Chapter 3.2 – Characterization of composts of different origin by means of the reactivity of their extracts

The reactivity of the humic and fulvic-like extracts (HA-L and FA-L) and of the water- soluble extract (obtained from equilibrium solutions), denominated by dissolved organic matter (DOM), isolated from compost samples of different origins is assessed by means of the extent of proton and cadmium binding.

1. Reactivity of the HA-L, FA-L and water-soluble extracts

The characterization of the extracts, FA-L, HA-L and DOM was performed by means of acid-base and cadmium complexation titrations. The titration curves were fitted using the NICA-Donnan model to obtain parameters such as the content of carboxylic and phenolic-type of groups, the medium value of the affinity distributions, the width of the proton distributions and the heterogeneity of the samples.

Results from the different composts, obtained from all the previously characterised composts, produced from different feedstock and composting processes, are compared with the results of an uncomposted organic fertiliser.

1.1. Acid-base titrations of humic-like substances (FA-L and HA-L) and water-soluble extract

The acid-base behaviour of the organic matter in the humic-like extracts FA-L and HA-L and of the DOM from CUW were characterized by means of titrations. The titration curves that were obtained as pH *vs*. volume of KOH were transformed into their corresponding charge *vs.* pH curves (Q-pH) [1] (Figure 3.9A). To allow the comparison with DOM, *Q* is expressed in mmol *per* gram of carbon, using the carbon content of each sample presented in Table 3.6 (in section 1.3).

The proton affinity distributions (Figure 3.9B) were obtained from the first derivative of the Q-pH curves. These curves enable the identification of the most representative groups of acid functions. While the titrations of FA-L and HA-L started at pH 4.0, the titrations of DOM started at a lower pH (pH 2.0) due to the presence of stronger carboxylic acid sites. Thus, both the charge curves and the proton affinity distributions of DOM exhibit a quite different profile. The charge represented in the charge curves is expressed in mmol *per* gram of carbon (instead of gram of the sample) to allow the comparison of results from HS-L with DOM (for whose the mass of the extract were not quantified).

In the proton affinity distribution curves of the HA-L and FA-L extracts two types of acid sites were identified: carboxylic-type, at pH 3.0-5.0, and phenolic-type, at pH 8.0-10.0, while for DOM three types of sites are found: carboxylic groups in amino acids, at pH 3.0-4.0, carboxylic groups in organic acids, at pH 5.5-7.5 and phenolic hydroxyl groups, hydroxyl in carbohydrate units and amino groups from amino acids, at pH 9.0-11.0 [2]. The organic species present in the DOM may include some FA-L, HA-L in minor quantities and other organic soluble species that may be similar

to the transphilic species. These last species which were identified in natural occurring organic matter [3,4] are the least hydrophilic of non-humic DOM compounds.

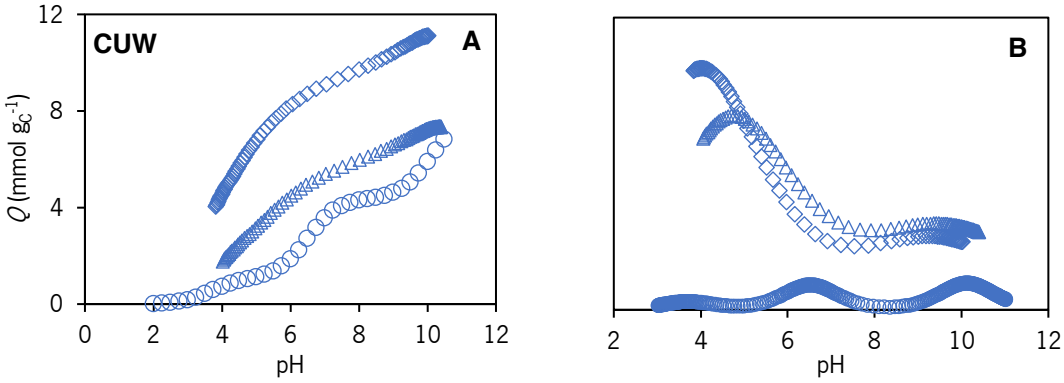

Figure 3.9: (A) Charge curves as a function of pH and (B) proton affinity distributions obtained for the FA-L (◊), HA-L (Δ) and DOM (o) from CUW.

The charge curves from all the remaining composts and non-composted fertiliser are depicted in Figure 3.10. The proton distribution curves of all samples are not provided as they are similar to those of CUW that was discussed earlier. The shapes of the charge curves of the humic-like substances FA-L and HA-L extracted from all composts and fertiliser reveal distinctive features as compared to DOM. The FA-L extracts display higher values of charge than HA-L for all samples. However, the position of the curve of DOM is located in different positions, indicating that the content of acid sites of this extract can vary substantially and independently of the humic-like substances. For CUW, CLW and FLW it is located below the curve of HA-L for the whole pH interval. For CVA a different situation is observed, as the curve of DOM is located above that of FA-L. For CVDW, the DOM displays similar values of charge as compared to HA-L in the entire pH range. For CA and CSS the DOM shows similar values of charge to HA-L at pH<6.0, *i.e.* indicating a similar amount of carboxylic acid sites to HA-L, whereas the DOM from CDDW displayed similar amount of carboxylic acid sites to FA-L, within the same pH range.

The charge curves were analysed using bimodal distributions for FA-L and HA-L extracts and by trimodal distributions for DOM. The fitted parameters are displayed in Table 3.4 and Table 3.5 [5]. Albeit approximated, since it ignores the charge contribution in the binding, the NICA-Donnan model provides a first order approximation to the protonation constant, K_n, and the abundance, M_n, (mmol g^{-1}) of functional groups [5]. The obtained parameters from the fitting to the experimental charge curves of the humic-like extracts revealed clear differences between FA-L and HA-L, showing that the total number of acid sites (M_T, mmol g^{-1}) is larger for FA-L than for HA-L.

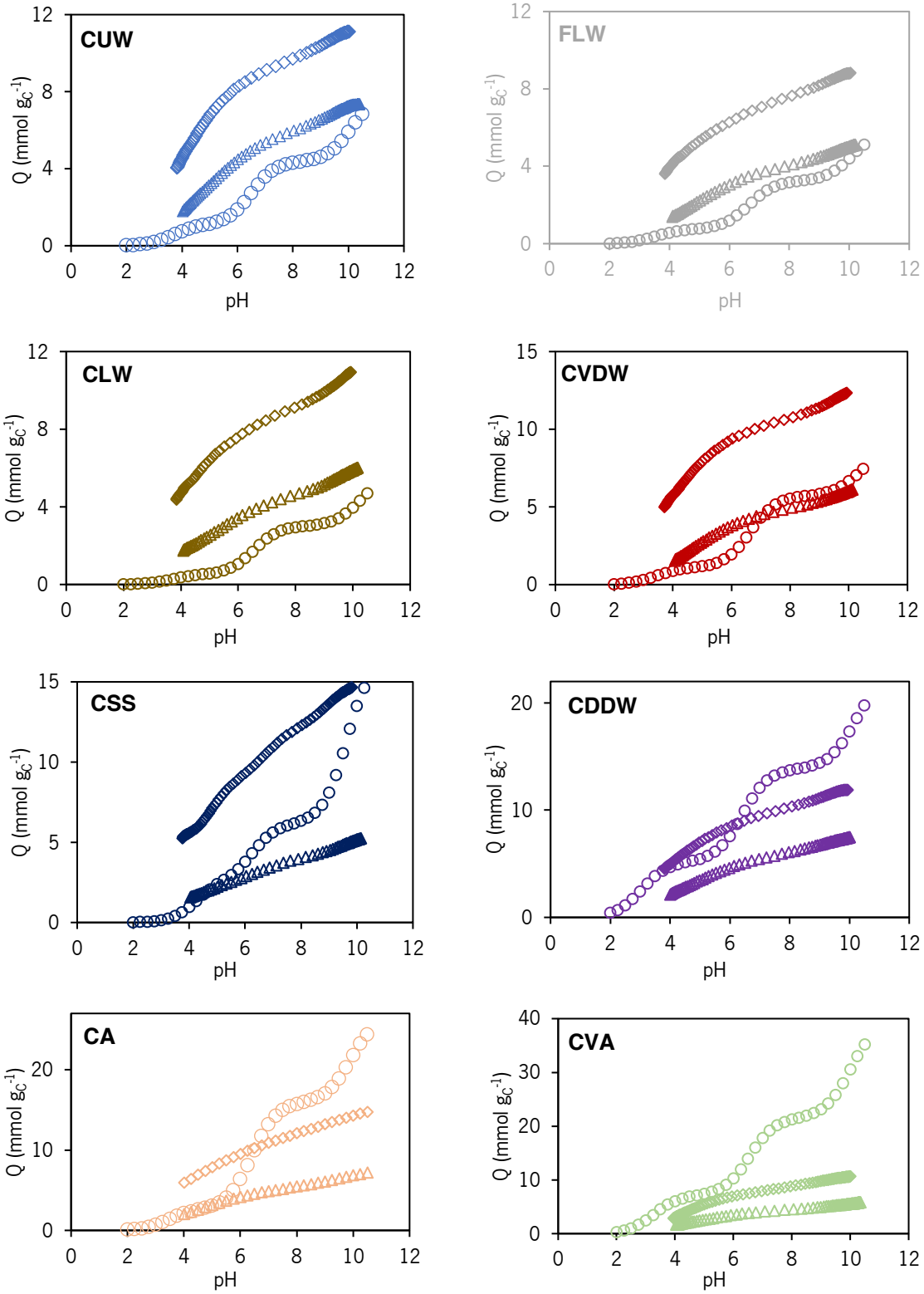

Figure 3.10: Charge curves as a function of pH of the FA-L (◇), HA-L (Δ) and DOM (o) extracted from the samples, CDDW (purple), CVDW (red), CVA (green), CA (orange), CUW (blue), CSS (dark blue), CLW (brown) and FLW (grey), at 0.1 mol L^{-1} KNO_3.

The composts whose FA-L extracts have higher amounts of acid sites (*i.e.* higher values of M_1) are CA and CSS, while the lowest amounts of acid sites were obtained for CLW that has an abundance close to that of the organic fertilizer (FLW). For the HA-L extracts, the composts can be

divided into two groups, CA, CUW and CDDW with higher amounts of acid sites and CVDW, CVA, CLW and CSS with the lower amounts.

Table 3.4: Acid-base parameters of FA-L and HA-L extracts from the composts and organic fertiliser (highlighted) obtained in 0.1 mol L^{-1} KNO_3 by fitting Equation 3.1 to the experimental data. The uncertainties associated to each parameter are included.

Sample		log K_1	M_1(mmol/g_{ms-L})	$m_{H,1}$	log K_2	M_2(mmol/g_{ms-L})	$M_{H,2}$	R^2	*RMSE*	$^*M_T$ (mmol/g_{ms})	Reference
CLW	FA-L	3.84±0.03	3.11±0.05	0.36±0.01	9.84±0.12	1.47±0.16	0.42±0.04	0.9997	0.0144	4.58	[5]
CUW		3.99±0.02	3.65±0.05	0.47±0.01	9.38±0.15	1.46±0.17	0.35±0.04	0.9999	0.0094	5.11	[5]
CDDW		3.82±0.03	4.01±0.09	0.41±0.01	9.48±0.29	1.24±0.29	0.35±0.08	0.9998	0.015	5.25	[5]
CSS		4.57±0.05	5.0±0.13	0.37±0.01	9.7±0.18	2.57±0.41	0.4±0.06	0.9998	0.0231	7.57	[5]
CVA		4.36±0.01	3.2±0.09	0.6±0.01	9.1±0.1	2.42±0.23	0.31±0.03	0.9999	0.014	5.63	[5]
CVDW		3.81±0.01	4.19±0.02	0.4±0.01	9.87±0.04	1.42±0.05	0.48±0.02	0.9999	0.0088	5.61	[5]
CA		4.0±0.18	5.38±0.45	0.28±0.02	9.59±0.25	2.24±0.88	0.31±0.1	0.9998	0.0104	7.62	
FLW		3.61±0.06	2.31±0.21	0.45±0.03	9.24±0.36	1.59±0.54	0.25±0.09	0.9997	0.0144	3.9	
CLW	HA-L	4.92±0.04	2.74±0.03	0.32±0.01	10.06±0.13	1.2±0.15	0.57±0.05	0.999	0.0075	3.95	[5]
CUW		4.7±0.06	2.92±0.18	0.46±0.02	9.65±0.24	1.82±0.47	0.32±0.08	0.9996	0.0231	4.74	[5]
CDDW		4.44±0.06	3.05±0.1	0.38±0.01	9.72±0.28	1.37±0.33	0.38±0.08	0.9998	0.015	4.42	[5]
CSS		5.17±0.08	2.71±0.06	0.25±0.01	10.11±0.22	0.99±0.22	0.56±0.09	0.9999	0.0077	3.7	[5]
CVA		4.75±0.03	2.57±0.03	0.35±0.01	10.04±0.11	0.99±0.11	0.58±0.06	0.9998	0.0104	3.56	[5]
CVDW		4.76±0.02	2.56±0.02	0.45±0.01	9.91±0.15	1.2±0.14	0.52±0.05	0.9999	0.0085	3.75	[5]
CA		4.6±0.03	2.89±0.04	0.36±0.01	9.89±0.1	1.52±0.14	0.44±0.03	0.9999	0.0077	4.42	
FLW		4.83±0.01	2.36±0.01	0.39±0.01	9.67±0.04	0.91±0.04	0.56±0.02	0.999	0.0075	3.27	

$^*R^2$, coefficient of determination; *RMSE*, root-mean-square error after optimization; M_1, carboxyl group content (mmol g^{-1} on moisture- and ash-free basis); K_1, median value of affinity distribution for proton binding by carboxyl groups; $m_{H,1}$, width of proton-affinity distribution of carboxyl groups; M_2, phenolic OH group content (mmol g^{-1} on moisture- and ash-free basis); K_2, median value of affinity distribution for proton binding by phenolic OH groups; $m_{H,2}$, width of proton-affinity distribution of phenolic OH groups; $M_T = M_1 + M_2$ corresponds to the total abundance of acid positions.

With respect to the DOM in the equilibrium solution, CSS has the highest abundance of acid sites (M_T) while CA has the lower amount (Table 3.5). The most acidic sites (carboxylic acids) for all samples were found in the DOM whose log K values are lower than the corresponding carboxylic acids from the FA-L extract (*i.e.* log K_1 (DOM) < log K_1 (FA-L)) and the log K values of the weakest acidic sites are lower for the FA-L extract compared to the DOM, *i.e.* log K_2 (FA-L)< log K_3 (DOM). The presence of these carboxylic acid groups in DOM that are stronger than those found in FA-L and HA-L have been identified in a group of water-soluble organic substances, denominated transphilic acids that are characterized by not being retained in XAD-8 columns (used in the extraction process) [3,4]. Though these substances were identified in natural environments, they are more likely to be present in materials where the organic matter is stabilized, such as compost or organic fertilisers.

Table 3.5: Acid-base parameters of DOM from the equilibrium solutions of composts and organic fertiliser (highlighted) obtained in 0.1 mol L^{-1} KNO_3 by fitting Equation 3.2 to the experimental data. The uncertainties associated to each parameter are included.

Sample	log K_1	M_1 (mmol/$g_{compost}$)	log K_2	M_2 (mmol/$g_{compost}$)	log K_3	M_3 (mmol/$g_{compost}$)	Q_o (mmol/$g_{compost}$)	R^2	*RMSE*	$^*M_T$ (mmol/$g_{compost}$)	Reference
CLW	3.67± 0.02	0.09±0.01	6.56±0.01	0.43±0.01	10.25± 0.01	0.45±0.01	-0.48±0.01	*0.9997*	*0.0055*	0.96	[5]
CUW	3.69±0.03	0.06± 0.01	6.51±0.01	0.18± 0.01	10.11±0.01	0.19± 0.01	-0.23±0.01	*0.9997*	*0.0024*	0.44	[5]
CDDW	3.06±0.03	0.06± 0.01	6.42±0.01	0.1± 0.01	10.17±0.01	0.1± 0.01	-0.14± 0.01	*0.9999*	*0.0009*	0.25	[5]
CSS	4.24±0.02	0.18± 0.01	6.27±0.01	0.25± 0.01	9.65± 0.01	0.74±0.01	-0.4± 0.01	*0.9998*	*0.0062*	1.17	[5]
CVA	3.27±0.07	0.04± 0.01	6.55±0.01	0.08± 0.01	10±0.01	0.1± 0.01	-0.1± 0.01	*0.9996*	*0.0013*	0.22	[5]
CVDW	3.45±0.02	0.08± 0.01	6.65±0.01	0.33± 0.01	10.33±0.01	0.21± 0.01	-0.36± 0.01	*0.9993*	*0.0052*	0.62	[5]
CA	3.44±0.04	0.01± 0.01	6.41± 0.01	0.05± 0.01	9.91± 0.01	0.04± 0.01	-0.06± 0.01	*0.9996*	*0.0013*	0.1	
FLW	3.53±0.04	0.14± 0.01	6.66±0.01	0.46± 0.01	10.12±0.01	0.49± 0.01	-0.59± 0.01	*0.9997*	*0.0024*	1.09	

*R^2, coefficient of determination; *RMSE*, root-mean-square error after optimization; M_1, carboxylic groups in amino acids content (mmol g^{-1} on moisture- and ash-free basis); K_1, median value of affinity distribution for proton binding by carboxylic groups in amino acids; M_2, carboxylic groups in organic acids content (mmol g^{-1} on moisture- and ash-free basis); K_2, median value of affinity distribution for proton binding by carboxylic groups in organic acids; M_3, phenolic OH groups content (mmol g^{-1} on moisture- and ash-free basis); K_3, median value of affinity distribution for proton binding by phenolic OH groups; $M_T = M_1 + M_2 + M_3$ corresponds to the total abundance of acid positions.

1.2. Study of the reactivity of the extracts by cadmium complexation

The ability of HS-L to bind metal cations is used to evaluate the reactivity of these substances since the extent of this process is strongly associated with the nature of the functional groups present and with the structure of the molecular aggregates formed by humic substances [6]. Besides, the binding ability of the DOM is undoubtedly relevant for understanding the fate of environmental pollutants in soils [7]. The fraction of the organic substances present in these extracts is the most mobile and therefore may impact the trace metal transport, speciation and nutrient bioavailability in the environment.

The results obtained for cadmium binding by FA-L, HA-L and DOM from each compost and by the non-composted fertiliser are shown in Figure 3.11. In each plot the complexation ratio, K (expressed in $(\mu mol/L)^{-1}$) is represented as a function of the total cadmium concentration, c_{MT}, (expressed in $\mu mol\ L^{-1}$) and the K values were calculated as the ratio $c_{ML}/(c_M \times c_L)$. Where c_{ML}, c_M, c_L are the complex metal, the free metal, and the organic ligand concentrations, respectively and were normalised by the abundance of deprotonated groups at pH 7.0, $Q_{pH\ 7}$ calculated from the acid-base titrations. The data points in the plots of Figure 3.11 show a variation that define a negative exponential type of function which is typical of heterogeneous materials, where the binding capacity is strongly dependent on the metal to ligand ratio and the binding by the strongest groups (carboxylic groups) occurs for lower concentrations of Cd^{2+}[9]. The decrease of the average value of K occurs progressively with the increasing involvement of the weaker binding groups due to the occupation of the stronger sites.

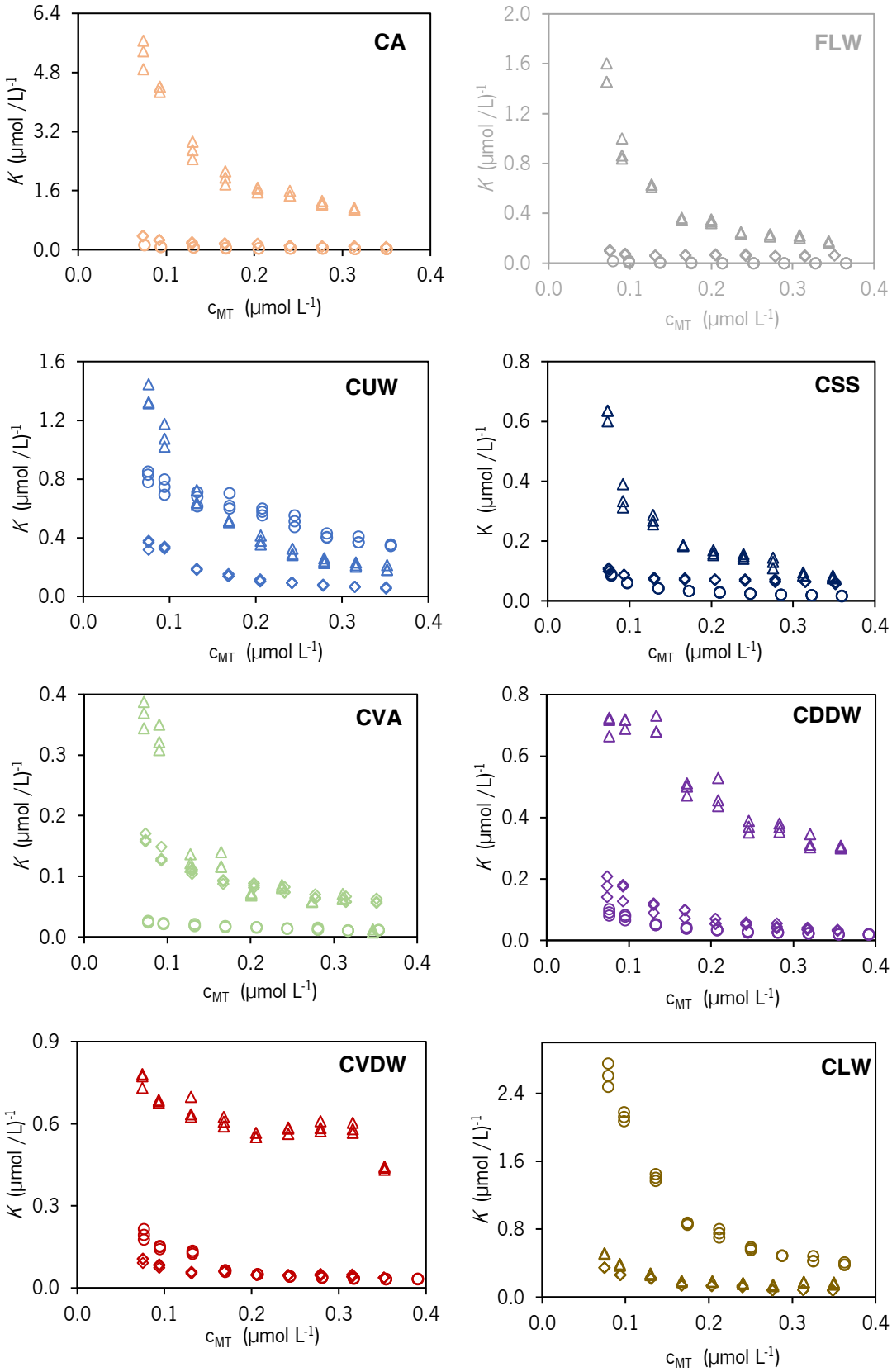

Figure 3.11: Experimental data expressed as complexation ratio, *K*, as a function of the total cadmium concentration, c_{MT} at pH 7.0 and ionic strength 12 mmol L^{-1} in $NaNO_3$ and HNO_3 for FA-L (◇), HA-L (Δ) and DOM (o) extracted from: CDDW (purple), CVDW (red), CVA (green), CA (orange), CUW (blue), CSS (dark blue), CLW (brown) and FLW (grey).

As depicted from Figure 3.11, the majority of HA-L extracts have a higher binding capacity than the corresponding FA-L extract, which in turn have higher complexing ability than DOM. The only samples that do not follow this general trend are CUW and CLW. For CUW the *K* values of DOM are higher than those of FA-L. Moreover, the weakest binding groups of DOM exhibit higher values of *K* than HA-L. For CLW, the binding capacity of FA-L is comparable to that of HA-L and both are lower than that of DOM.

The comparison between the binding curves from the extracts of the same nature is illustrated in Figure 3.12, where in each plot are represented results from the different composts and one fertiliser. From the absolute variation of the *K* values it is possible to make a qualitative appraisal of the heterogeneity of the structures present in each extract. The HA-L extracts for CA displays the largest heterogeneity, as *K* values vary from 5.9 $(\mu mol/L)^{-1}$ to 0.63 $(\mu mol/L)^{-1}$, whereas CVDW, CVA, CLW and FLW exhibit the lowest heterogeneities (*e.g.* for CVDW the *K* values vary from 0.77 $(\mu mol/L)^{-1}$ to 0.43 $(\mu mol/L)^{-1}$). The heterogeneity of the FA-L extracts is lower than the observed for the HA-L extracts. The FA-L extracts from CUW, CA and CLW have higher heterogeneity as they show a higher absolute variation in *K* values, approximately between 0.38 $(\mu mol/L)^{-1}$ to 0.06 $(\mu mol/L)^{-1}$ comparable to less heterogeneous HA-L extracts. Regarding heterogeneity of the DOM extracts, CLW display the larger heterogeneity with *K* values that vary between 2.75 $(\mu mol/L)^{-1}$ to 0.41 $(\mu mol/L)^{-1}$, in opposition to CVA which is the least heterogeneous sample with a variation of *K* values between 0.03 $(\mu mol/L)^{-1}$ and 0.01 $(\mu mol/L)^{-1}$.

The relative position of the experimental data for each sample on the plots of Figure 3.12 provide information on the relative reactivity of each type of extract. For the FA-L extracts the data points of the different samples are very close to each other, indicating that the reactivity of these extracts does not vary significantly among this set of materials (Figure 3.12A). Regarding the HA-L extracts, CA stands out with the highest values of *K*. The remaining samples can also be differentiated although the relative *K* values of the samples change across the range of c_{MT} values. Concerning results from the DOM extracts, CLW displayed the highest values followed by CUW. The curves from the remaining composts appear very close to each other.

1.3. Evaluation of the extent of cadmium binding by the different extracts

Although the reactivity of the extracts is important for the sake of their characterization, the operational relevance of this parameter is limited as the extent of the interaction is also associated with the HA-L, FA-L or DOM content.

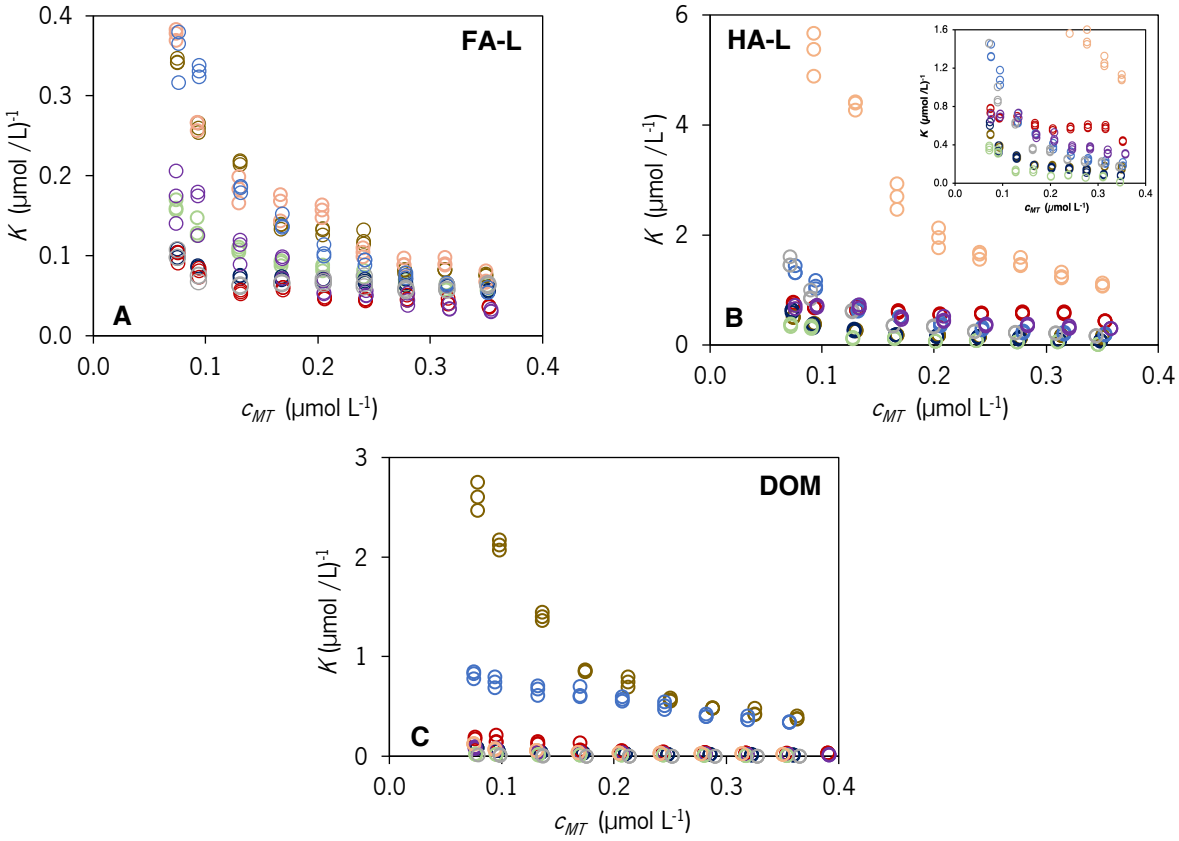

Figure 3.12: Experimental data expressed as complexation ratio, *K*, as a function of the total cadmium concentration, c_{MT} at pH 7.0 and ionic strength 12 mmol L^{-1} in $NaNO_3$ and HNO_3 for (A) FA-L, (B) HA-L and (C) DOM extracted from: CDDW (purple), CVDW (red), CVA (green), CA (orange), CUW (blue), CSS (dark blue), CLW (brown) and from the fertiliser FLW (grey).

This is relevant for compost applications such as in agriculture, where the dose of compost is a key factor to obtain the desired effects. The recommended dose to be applied depends on the compost and also of species-specific needs and is provided in technical sheets.

The carbon content of each extract C_{HS} *and* C_{DOM} expressed in terms of g_C $kg_{compost}^{-1}$ is presented in Table 3.6. These values were calculated using Equations 3.1 and 3.2, for the HS-L (HA-L and FA-L) and DOM, respectively:

$$C_{HS} = \frac{C}{100} \times Y \qquad \text{(Equation 3.1)}$$

$$C_{DOM} = \frac{DOC}{\frac{m_{compost}}{V}} \qquad \text{(Equation 3.2)}$$

where, *C* is the carbon content of the HS-L (% w/w), *Y* is the yield of the extractions (w/w, g_{HS} $kg_{compost}^{-1}$), *DOC* is the concentration of dissolved organic carbon (mg L^{-1}) and $m_{compost}/V$ is the mass of compost *per* volume of solution used to prepare the equilibrium solution (50 $g_{compost}$ L^{-1}).

Table 3.6: Carbon content of the extracts HA-L, FA-L and DOM and yield (Y) of the HA-L and FA-L extractions.

	HA-L			FA-L			DOM	
Sample	*C* (%)	*Y* (g kg^{-1})	C_{HA-L} (g_C $kg_{compost}^{-1}$)	*C* (%)	*Y* (g kg^{-1})	C_{FA-L} (g_C $kg_{compost}^{-1}$)	*DOC* (mg L^{-1})	C_{DOM} (g_C $kg_{compost}^{-1}$)
CVA	53.5	33.4	17.9	49.7	2.27	1.14	111	2.22
CVDW	52.7	19.0	13.9	39.8	4.73	1.87	717	14.3
CA	53.3	19.9	10.6	45.8	2.67	1.22	75.2	1.5
CLW	55.2	34.9	19.3	35.4	7.00	2.48	861	17.2
CUW	54.5	21.1	11.5	40.8	3.33	1.35	548	11
CDDW	50.6	26.4	9.62	38.4	4.20	1.61	115	2.31
CSS	58.5	23.8	13.9	40.9	4.84	1.97	698	14
FLW	57.5	53.6	30.9	36.9	10.9	4.02	921	18.4

The carbon content of the HA-L and FA-L extracts of each sample is compared with that of the DOM in Figure 3.13A. For composts CVA, CA and CDDW the HA-L extracts contain about 4 to 8 times more carbon than the respective DOM, whereas for the remaining composts and the fertiliser the amount of carbon of the DOM is comparable to that of HA-L ($C_{HA-L}/C_{DOM}\sim1$). With regard to FA-L, it contains less carbon than DOM as the ratio C_{FA-L}/C_{DOM} is lower than 1 for all composts, with an average value of 0.35.

The abundance of DOM sites is plotted against those of HA-L and FA-L in Figure 3.13B where good correlation between results of FA-L and DOM is observed (r=0.90). This correlation line has a slope of 0.022, indicating that the abundance of acid sites in the DOM is extremely high in face of FA-L. The existence of a correlation can be explained by the common origin of FA-L and DOM, in addition to the fact that FA-L may constitute a fraction of the DOM, albeit small one. The large difference between the values of M_T of the two extracts can be partially attributed to significative losses in the purification process of the FA-L extracts, and also to the presence of divalent (Ca, Mg) and trivalent cations (Al and Fe) in the DOM, with values ranging from 28.6 mg kg^{-1} (CA) to 171.1 mg kg^{-1} (CSS) whose hydrolysis may contribute to the overestimation of the acid sites in this extract.

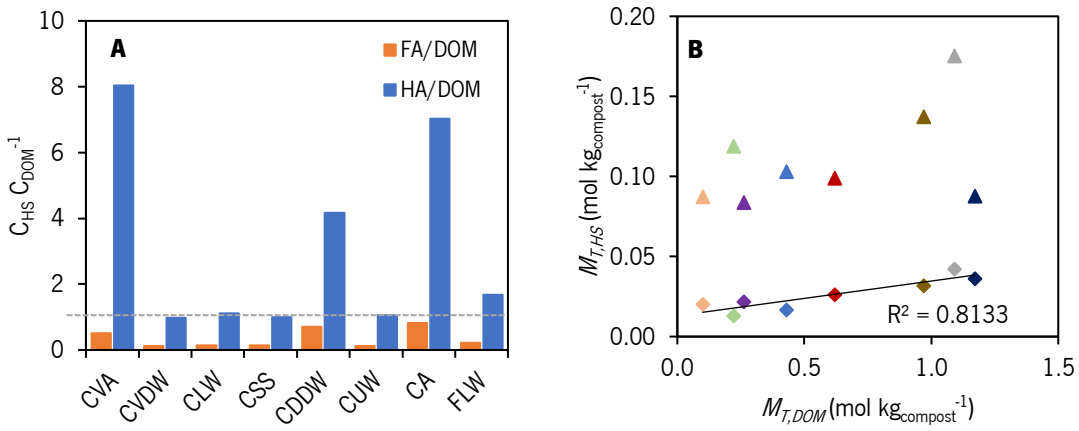

Figure 3.13: (A) Ratio between the carbon content in the humic extracts (FA-L and HA-L) with respect to the carbon present in the DOM (C_{HS}/C_{DOM}) and (B) correlation between the abundance of acid sites of FA-L (◊) and HA-L (Δ) with the DOM of the composts: CDDW (purple), CVDW (red), CVA (green), CA (orange), CUW (blue), CSS (dark blue), CLW (brown) and the fertiliser FLW (grey). The horizontal line is settled for C_{HS}/C_{DOM}=1

The presence of non-humified organic matter, designated transphilic acids [3,4] may be the most abundant fraction of the organic material present in the DOM. Regarding HA-L, the abundance of acid sites is on average 5 times lower than that of the DOM. Once again, the disparity between the carbon content in the two extracts results from the sequential purification steps that the HA-L extract is submitted to. Nevertheless, results suggest that the DOM may have an important role on the acid-base properties of the soils where the compost is applied, as the amount of charge released is significant. This is particularly relevant in the context of using composts directly in farmlands instead of HS-L solutions (requiring technical expertise to prepare) allowing a more practical, sustainable and profitable crop treatment for the growers.

The abundance of the acid sites, $M_{T,HS}$, $M_{T,DOM}$ (expressed in mol $kg_{compost}^{-1}$) were calculated attending to the values of M_T from each extract (expressed in mmol g_c^{-1}) and to C_{HS} *or* C_{DOM} (expressed in g_c $kg_{compost}^{-1}$), using Equations 3.3 and 3.4.

$$M_{T,HS} = M_T \times C_{\mathrm{HS}} \qquad \text{(Equation 3.3)}$$

$$M_{T,DOM} = M_T \times C_{DOM} \qquad \text{(Equation 3.4)}$$

The extent of the Cd^{2+} binding by the different extracts was calculated from complexation data at pH 7.0 and at different concentrations of Cd^{2+}, $c_{ML,HS}$ and $c_{ML,DOM}$ (expressed in mmol $kg_{compost}^{-1}$), using Equations 3.5 and 3.6 for the humic-like and water-soluble extracts, respectively:

$$c_{ML,HS} = \left(\frac{c_{ML}}{c_{HS}}\right) \times Y \qquad \text{(Equation 3.5)}$$

$$c_{ML,DOM} = \frac{c_{ML}}{F_d \times 50} \times 10^6 \qquad \text{(Equation 3.6)}$$

where c_{ML} is the metal complex concentration (expressed in mol L^{-1}), c_{HS} is the concentration of organic matter (of the HA-L and FA-L) (expressed in kg_{HS} L^{-1}), Y is the yield of the extractions (expressed in g_{HS} $kg_{compost}^{-1}$), F_d is the dilution factor (= V_{DOM}/ V_{Total}) and 50 corresponds to the amount of compost *per* litre used to prepare the equilibrium solution ($g_{compost}$ L^{-1}).

Figures 3.14A and 3.14B compare the extent of the binding by HA-L and FA-L, respectively, with that of DOM for all samples of compost. The extent of the binding by FA-L extracts tends to be comparable to thar of DOM for the samples CA, CSS, CVA and CDDW (whose points are above or along the line y=x) or lower than that of the DOM for CVDW, CUW and CLW (whose points are below the line y=x). The extent of the Cd^{2+} binding is comparable in the two extracts for four of the compost samples, despite the carbon content and of the abundance of acid sites are much larger for DOM.

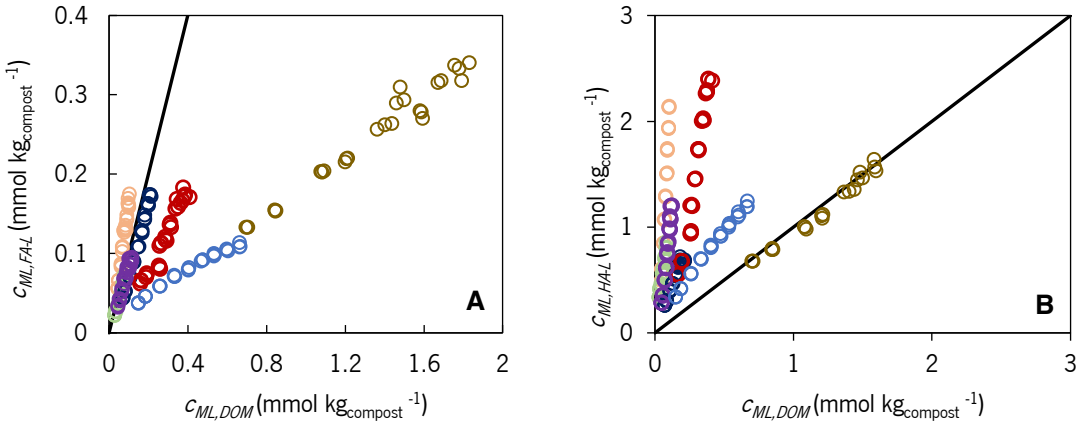

Figure 3.14: Comparison of cadmium binding data at pH 7.0 and 12 mmol L^{-1} ionic strength in $NaNO_3$ and HNO_3 for: (A) FA-L *vs.* DOM and (B) HA-L *vs.* DOM of composts: CDDW (purple), CVDW (red), CVA (green), CA (orange), CUW (blue), CSS (dark blue), CLW (brown). The y=x straight line represents the equivalence between results.

Besides, the values of the $c_{ML,FA-L}/c_{ML,DOM}$ ratio of the samples with lower binding extent is about 0.4 for CVDW and 0.2 for CUW and CLW, that is much higher than the obtained ratio for the corresponding M_T values (about 0.022). From this outcome it can be concluded that the chemical structure of the organic species soluble in the DOM are less reactive with Cd^{2+} as compared to FA-L. A similar conclusion can be drawn from the comparison between HA-L and DOM displayed from data represented in Figure 3.25B. Here all points are located above the y=x line with the exception

of CLW which is over the y=x, despite the HA-L extracts displayed an abundance of acid sites on average about 5 times lower than the DOM and the carbon content of some samples (CVDW, CLW, CSS and CUW) displayed comparable values to the DOM.

1.4. Comparison with an uncomposted organic fertiliser

The extent of reactivity of the compost extracts can be compared to those of a livestock fertiliser using Cd^{2+} binding data. Results from the extent of binding of the three types of extracts, FA-L, HA-L and DOM are depicted in Figure 3.15, where on the vertical axis are represented the values for the compost and on the horizontal axis the values for the fertiliser. The position of the different data series relative to the y=x line that accounts for the equivalence to FLW, provides a simple way to compare the reactivity of all compost samples with that of FLW.

The extent of Cd^{2+} binding by FA-L extract of CLW is the highest and is the only compost whose binding data are located above the line y=x (Figure 3.15A). The FA-L extracts of all the other series that are located below this line display lower binding ability than that of FLW. For the HA-L extracts, CLW, CVDW and CA, whose points are distributed close to the y=x line (Figure 3.15B), have a binding extent comparable to FLW, whereas CSS, CDDW, CVA and CUW, whose points are located below the y=x line have lower binding ability than FLW. Similarly, for the DOM it can be concluded from Figure 3.15C that all points lie well below the equivalence line. CLW is the only sample that can be distinguished from the remaining compost samples whose results are very much alike.

Considering the relative abundance of the different types of extract, the absolute values of c_{ML} and the difference between the c_{ML} values of the different composts, it seems that results from HA-L are the most adequate to compare composts of different origin. Using this parameter, a ranking can be established based on an operative scale defined after the comparison of the reactivity of the HA-L extracts from composts with respect to HA-L extract from the organic fertiliser. The score of each sample can be obtained directly from the slope of each straight line in Figure 3.15B. These slopes represent the mass of fertiliser required to bind an amount of Cd(II) identical to that complexed by the HA-L extracts existing in 1 kg of compost.

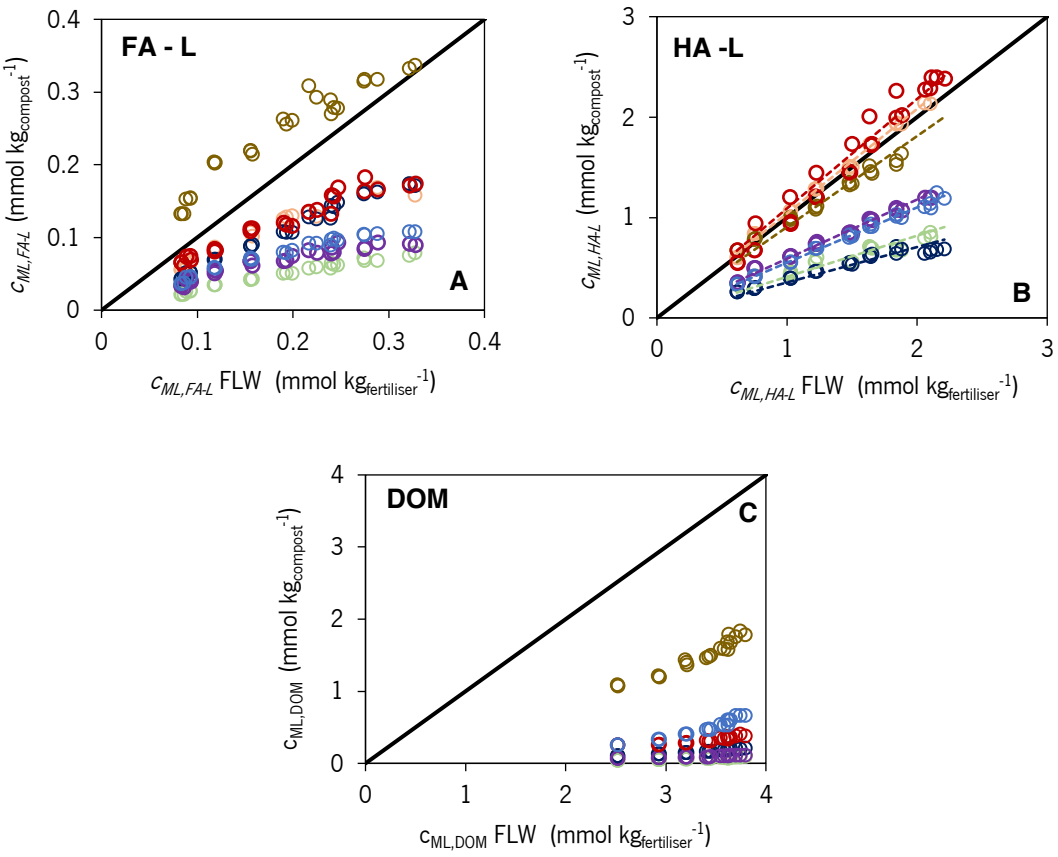

Figure 3.15: Comparison of cadmium binding data of extracts obtained by samples of different origin (CDDW (purple), CVDW (red), CVA (green), CA (orange), CUW (blue), CSS (dark blue), CLW (brown)) at pH 7.0 and ionic strength 12 mmol L^{-1} in $NaNO_3$ and HNO_3: (A) FA-L extracts *vs.* FA-L - FLW, (B) HA-L extracts *vs.* HA-L – FLW and (C) DOM extracts *vs.* DOM – FLW. The y=x straight line represents the equivalence between results. The dotted lines in B correspond to the linear correlations.

This parameter, equivalent mass of fertiliser, m_{EF}, is extensive and can easily be used to obtain other valuable information by compost users or producers, such as the price of the product corresponding to an equivalent effect of FLW. The values of the m_{EF} parameter are displayed in Figure 3.17A. In this ranking the composts CVDW, CA and CLW (with m_{EF}, values of 1.09, 1.04 and 0.906 kg of FLW) are in the top places, followed by CDDW and CUW (with 0.589 and 0.550 kg of FLW) and then CVA and CSS (with 0.409 and 0.353 kg of FLW).

2. Verification of the potential of the HA-L reactivity parameter, $c_{ML,HA-L}$, as a marker of compost bioactivity

A compost reactivity ranking based on the binding extent of the HA-L extracts and expressed as the equivalent mass of FLW has a limited meaning if this reactivity scale is not validated in terms of the relative ability of the extracts in promoting plant growth and crop productivity. For this purpose,

a study involving the characterization of the reactivity and bioactivity of the HA-L extracts of different composts and in different species would be required. In fact, more studies at the field scale to validate lab-derived results concerning HS-L bioactivities are needed [8]. The reactivity parameter $c_{ML,HA\text{-}L}$ from the HA-L extract displayed high compost discrimination capacity, its potential as compost bioactivity marker was investigated. The significance of this reactivity parameter is, in a first attempt, evaluated using results from the previous study (reported in chapter 3.1) ran with lettuce (*Lactuca sativa* L.) in the field, where three samples of compost (CUW, CA, CVA) and the organic fertiliser (FLW) were tested on plant growth by application on the native soil. The effect of the compost origin and dose using the recommended doses provided by the producers, was assessed by measuring the total leaf area (*TLA*) of the lettuce plants 5 weeks after planting.

Results from the equivalent amount of HA-L for a low concentration (0.10 μmol L^{-1}) of added cadmium, $c_{ML,,L}$ (mmol bed^{-1}), were calculated taking into account the applied doses of compost/ fertiliser in each bead. For the sake of comparison, other related quantities, such as the amount of extract deposited, expressed in the mass of carbon, C (g_C bed^{-1}) and the total charge from the deprotonated acid groups at pH 7.0, $Q_{pH\,7}$ (mmol bed^{-1}) were also evaluated. These quantities were also evaluated considering the amount of compost applied *per bed* (kg) and the values of each property expressed *per* gram of compost, *i.e.,* the mass of carbon in each extract (g_C $kg_{compost}^{-1}$) for the amount of compost applied *per bed* (kg) and the yield of the HA-L extraction (g_{HS} $kg_{compost}^{-1}$) and the charge at pH 7.0 (mmol $g_{compost}^{-1}$) for the amount of compost applied *per bed* (kg). These quantities are represented in Figure 3.16, along with the corresponding values for FA-L and DOM, for comparison purposes. From Figure 3.16A it can be seen that the larger amounts of HA-L were estimated for the beds where CA and CVA were deposited, whereas larger amounts of DOM were obtained for the beds where FLW was deposited. The FA-L are the least abundant extracts in each bed. On the other hand, the bed that contains the lowest number of deprotonated acid groups are those of CUW, for which a low effect was noticed on lettuce growth. These results suggest that $Q_{pH\,7}$ may be more closely related to the compost/fertiliser effect on lettuce growth than the amount of the extract, represented in Figure 3.16B, for which comparable values of C (g_C bed^{-1}) are obtained for CA and CVA (despite very different effects on *TLA* were obtained). From Figure 3.16C, where the values of $c_{ML,L}$ are represented, the relative bars height from the different conditions obtained for FA-L and HA-L extracts are similar to those of Figure 3.16B, where CUW displays the lowest and CA the highest values. In opposition, for DOM the highest value is obtained for the higher dose of FLW. Interestingly, CA and CVA, composts obtained from a mixture with algae (Table 2.1), independently from the mode of composting (pile composting vs vermicomposting) were the ones

with the highest $c_{ML,L}$ for HS-L (HA-L and FA-L). Also, knowing that the doses applied of CVA had higher HA-L contents than CA, vermicomposting seems to reduce the potential reactivity of the compost imparted by HA-L extracts; and knowing that FLW had higher FA-L contents, and CA half of HA-L comparing to FLW, the compost matrix seems to maintain better the potential reactivity imparted by HS-L when compared to the non-composted fertiliser.

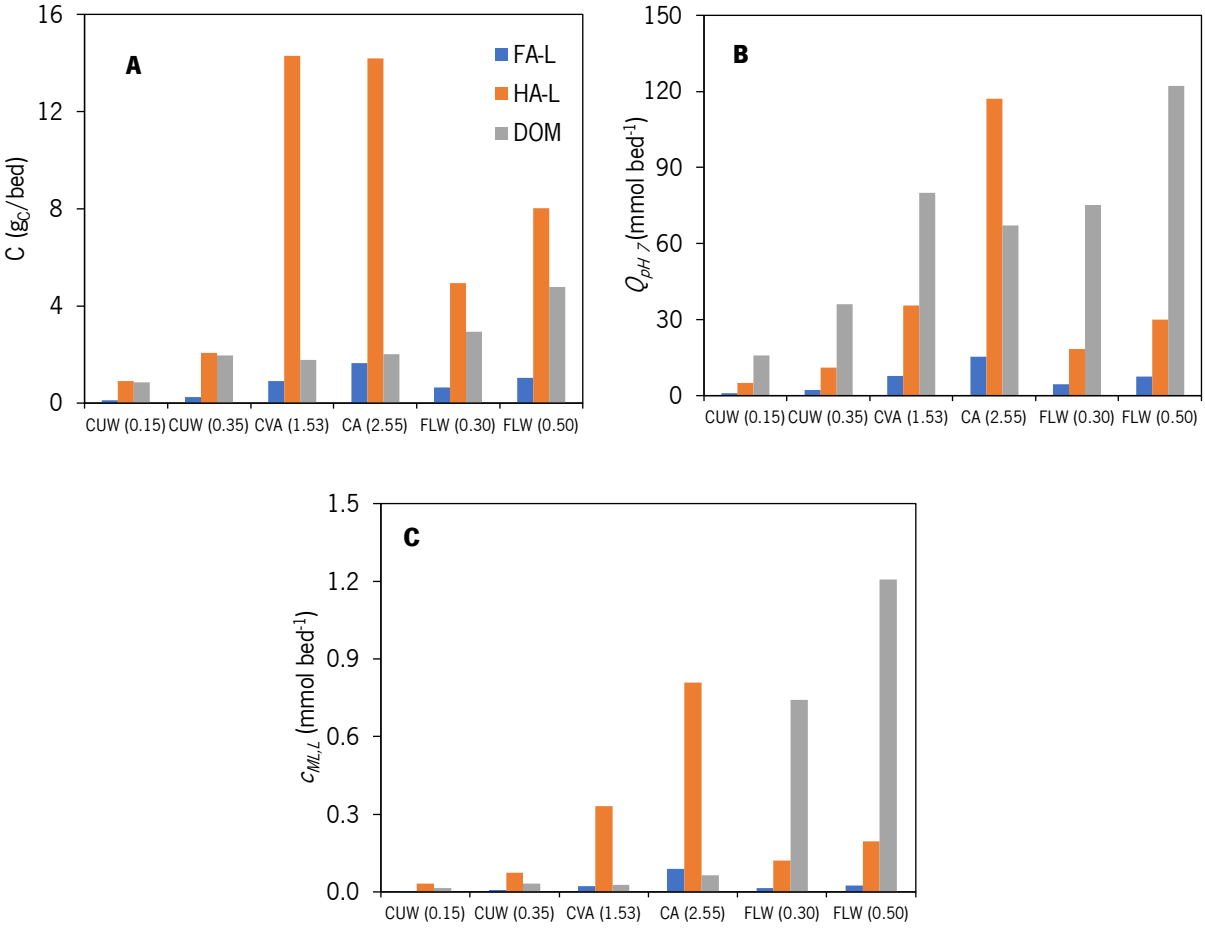

Figure 3.16: Values of different parameters evaluated for the different extracts (FA-L, HA-L and DOM) calculated considering the mass of compost mixed with the soil in the different beds where lettuce was planted and which growing results are displayed in Figure 3.8 of chapter 3.1. (A) carbon content of each extract; (B) quantity of deprotonated acid groups at pH 7.0; and (C) concentration of complexed cadmium at pH 7.0 and an added cadmium concentration of 0.10 µmol L^{-1}. The number in each abbreviation refers to the applied dose in kg m^{-2}.

Notice that CA was also the compost with higher complexation ratios (K) and higher heterogeneity for its HA-L and FA-L extracts (Figure 3.11 and 3.12) as well as higher binding ability, $c_{ML,HA-L}$ and $c_{ML,FA-L}$ (Figure 3.14).

As the reactivity parameter $c_{ML,L}$ of the HA-L extracts (previously used to compare the composts of different origin) were prominent and with high compost discrimination capacity, its potential to be used as a marker for the bioactivity of the compost, in this case of promoting an increase in lettuce

growth (*TLA*), was investigated. The plot of *TLA* against $c_{ML,L}$ is represented in Figure 3.17B depicting the correlation line. The point located on the vertical axis, which corresponds to the control assay (lettuce growth in a bed where no compost/fertiliser was added), was not included in the linear regression. The proximity between the regression line intercept and the *TLA* value of the control assay corroborates to some extent the validity of the correlation found. Results from CVA were not included in the regression analysis as they do not fit the trend defined from the remaining points, that include results from two composts (each one in two doses) and the fertiliser (in two doses). The fit is very tight and CA was the compost that most distanced from the rest with the highest $TLA/c_{ML,L}$ values. This result seems to support the value of this compost obtained from enriched seaweed feedstock by composting. The CVA deviation is difficult to explain, especially because no other vermicomposts with analogous feedstock were tested, but results suggest that this mode of composting not only reduce potential reactivity and binding capacity of the derived extracts and lettuce vegetative growth but also that other growth-promoting compounds that do not contribute to $c_{ML,L}$ were lost or growth-inhibiting components were produced. The robustness of this parameter was tested by calculating the corresponding values for a different concentration of Cd^{2+}. The selected value was 0.30 μmol L^{-1} and the concentration of complexed cadmium is represented by $c_{ML,H}$. At this higher concentration of Cd^{2+} the binding is performed by weaker complexing sites (phenolic groups) in addition to the stronger complexing groups (carboxylic groups) that are essentially accounted for $c_{ML,L}$. The representation of *TLA vs.* $c_{ML,H}$ is displayed in Figure 3.17C, with the corresponding correlation line. The characteristics of this correlation is very similar to that using $c_{ML,L}$ concerning the quality of the fit and the number of points that are fitted.

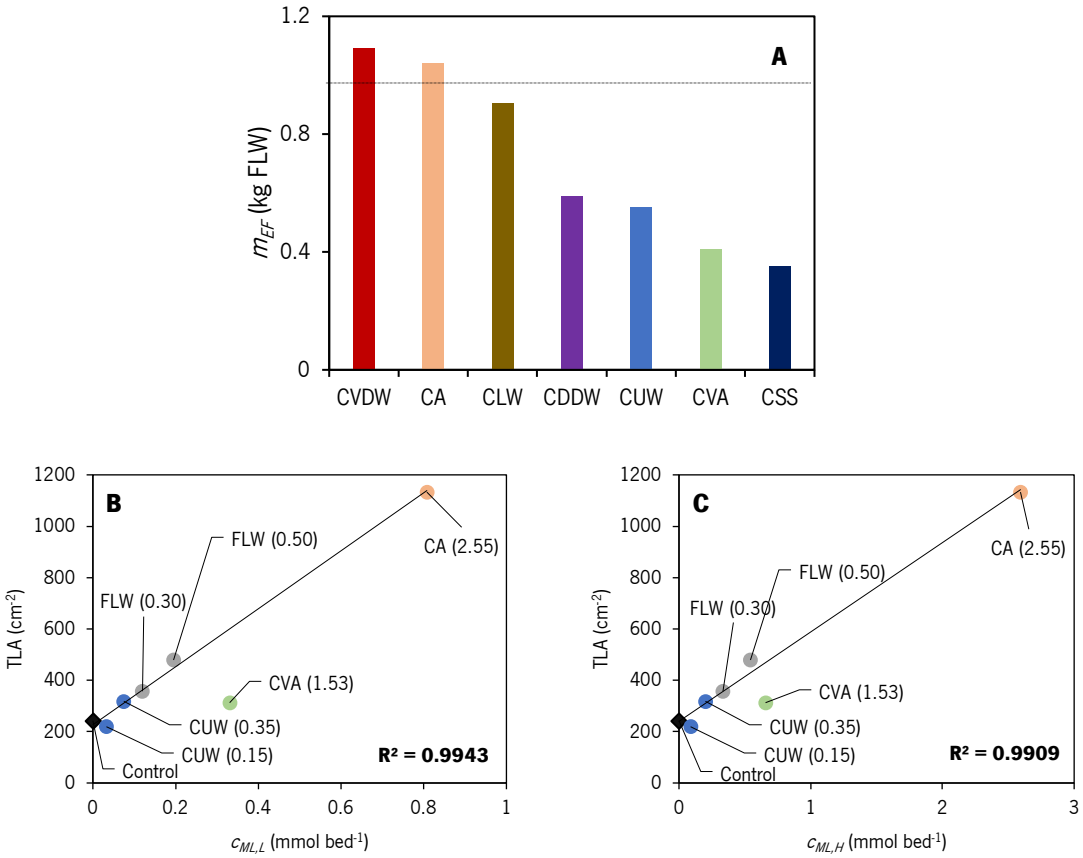

Figure 3.17: (A) Values of the parameter m_{EF} (equivalent mass of FLW) for each compost. The horizontal line is settled for m_{EF}=1 kg FLW and the correlations between the total leaf area (*TLA*) of lettuce from a crop field assay and the parameters (B) $c_{ML,L}$(0.10 µmol L^{-1}), (C) $c_{ML,H}$ (0.30 µmol L^{-1}) obtained from metal titrations of the HA-L extracts.

The regression parameters of these two correlations are displayed in Table 3.7, together with the parameters from the correlations between *TLA* and $c_{ML,L}$ evaluated for the FA-L and DOM extracts. While for FA-L an excellent correlation was also obtained, for DOM the correlation coefficient is almost zero, indicating that this extract is not representative of the bioactivity of the compost or fertiliser.

At a first glance, this result is somewhat puzzling because DOM (water- soluble extract) is the kind of extract expected to obtain in the field by the application of composts, where the composts can be lixiviated into soil solution by irrigation and/or precipitation, and *TLA* is a measure of bioactivity under field natural conditions. However, in the rhizosphere several processes may take place that can facilitate the adsorption of bioactive components. For instance, root exudates, rich in organic acids, can promote the separation of humic aggregates making available bioactive compounds (phytohormones, HA-L, FA-L) capable of inducing plant growth, as well as other physiological, biochemical and metabolic changes [10]. Moreover, organic acids can modify the molecular size of humic substances [11], facilitating the penetration of low molecular weight compounds into the

cells thereby inducing several responses, as auxin polar transport and stimulation of root plasma membrane H^+-ATPase [12], and mediating the direct transport of nutrients [13]. There is an intense soil-root-shoot crosstalk mediated by HS [14].

The fact that the reactivity of both humic-like substances can equally explain the bioactivity of the corresponding compost/fertiliser is significant and corroborates the general knowledge that the denomination of humic and fulvic acids is mainly related an operational classification that is more closely related to the size of the isolated molecules rather than to their intrinsic nature. Together, our results are also in concordance with the accumulated knowledge that the biological activities and plant responses induced by HS depend on many factors such as dosage, origin, molecular size, degree of hydrophobicity and aromaticity [14], and that the mode of production of organic compounds is also relevant for its performance at the field level.

Table 3.7: Regression analysis parameters from the linear correlations between the total leaf area (*TLA*) of lettuce, and $c_{ML,L}$ or $c_{ML,H}$ for the FA-L, HA-L and DOM extracts. *TLA* values were obtained from a crop field assay using the composts and fertilizer whose extracts were characterized by Cd^{2+} titrations. The values for the sample CVA were not included in the correlation analysis.

		HA-L			FA-L			DOM
	TLA of the control assay (cm^2)	**Intercept (cm^2)**	**Slope ($cm^2 mmol^{-1}$ bed)**	***r***	**Intercept (cm^2)**	**Slope ($cm^2 mmol^{-1}$ bed)**	***r***	***r***
$c_{ML,L}$ (mmol bed^{-1})	243	221	1139*	0.997	210	10508*	0.998	0.051
$c_{ML,H}$ (mmol bed^{-1})	243	240	348*	0.995	193	4220*	0.997	0.048

* *r*, coefficient of correlation.

Besides being preliminary these results suggest that the cadmium binding capacity may be a good indicator of the potential of compost in plant growth and crop productivity, at least for lettuce. Further experiments must be carried out to confirm these results on a larger scale and validate the use of $c_{ML,HA-L}$ as marker of compost bioactivity.

3. References

[1]J.C.M. de Wit, W.H. van Riemsdijk, L.K. Koopal, Proton binding to humic substances. 2. Chemical heterogeneity and adsorption models, Environ. Sci. Technol. 27 (1993) 2015–2022. https://doi.org/10.1021/es00047a005.

[2]L. Sciubba, L. Cavani, M. Grigatti, C. Ciavatta, C. Marzadori, Relationships between stability, maturity, water-extractable organic matter of municipal sewage sludge composts and soil functionality, Environmental Science and Pollution Research. 22 (2015) 13393–13403. https://doi.org/10.1007/s11356-015-4611-7.

[3]J.-P. Croué, M.F. Benedetti, D. Violleau, J.A. Leenheer, Characterization and Copper Binding of Humic and Nonhumic Organic Matter Isolated from the South Platte River: Evidence for the Presence of Nitrogenous Binding Site, Environ. Sci. Technol. 37 (2003) 328–336. https://doi.org/10.1021/es020676p.

[4]R.F. Domingos, M.F. Benedetti, J.P. Croué, J.P. Pinheiro, Electrochemical methodology to study labile trace metal/natural organic matter complexation at low concentration levels in natural waters, Analytica Chimica Acta. 521 (2004) 77–86. https://doi.org/10.1016/j.aca.2004.05.027.

[5]R. López, J. Antelo, A.C. Silva, F. Bento, S. Fiol, Factors that affect physicochemical and acid-base properties of compost and vermicompost and its potential use as a soil amendment, Journal of Environmental Management. 300 (2021) 113702. https://doi.org/10.1016/j.jenvman.2021.113702.

[6]E. Tipping, Cation Binding by Humic Substances, 1st ed., Cambridge University Press, 2002. https://doi.org/10.1017/CBO9780511535598.

[7]J. Buffle, R.R. DeVitre, Chemical and Biological Regulation of Aquatic Systems, Lewis Publ, Boca Raton, 1994.

[8]H. Jung, S. Kwon, J.-H. Kim, J.-R. Jeon, Which Traits of Humic Substances Are Investigated to Improve Their Agronomical Value?, Molecules. 26 (2021) 760. https://doi.org/10.3390/molecules26030760.

[9]E. Rotureau, L.S. Rocha, D. Goveia, N.G. Alves, J.P. Pinheiro, Investigating the Binding Heterogeneity of Trace Metal Cations With SiO2 Nanoparticles Using Full Wave Analysis of Stripping Chronopotentiometry at Scanned Deposition Potential, Front. Chem. 8 (2020) 614574. https://doi.org/10.3389/fchem.2020.614574.

[10]D.B. Zandonadi, M.P. Santos, J.G. Busato, L.E.P. Peres, A.R. Façanha, Plant physiology as affected by humified organic matter, Theor. Exp. Plant Physiol. 25 (2013) 13–25. https://doi.org/10.1590/S2197-00252013000100003.

[11]A. Albuzio, G. Ferrari, Modulation of the molecular size of humic substances by organic acids of the root exudates, Plant Soil. 113 (1989) 237–241. https://doi.org/10.1007/BF02280186.

[12]S. Nardi, M. Schiavon, O. Francioso, Chemical Structure and Biological Activity of Humic Substances Define Their Role as Plant Growth Promoters, Molecules. 26 (2021) 2256. https://doi.org/10.3390/molecules26082256.

[13]M. Baltazar, S. Correia, K.J. Guinan, N. Sujeeth, R. Bragança, B. Gonçalves, Recent Advances in the Molecular Effects of Biostimulants in Plants: An Overview, Biomolecules. 11 (2021) 1096. https://doi.org/10.3390/biom11081096.

[14]Z.H. Shah, H.M. Rehman, T. Akhtar, H. Alsamadany, B.T. Hamooh, T. Mujtaba, I. Daur, Y. Al Zahrani, H.A.S. Alzahrani, S. Ali, S.H. Yang, G. Chung, Humic Substances: Determining Potential Molecular Regulatory Processes in Plants, Frontiers in Plant Science. 9 (2018) 1–12. https://doi.org/10.3389/fpls.2018.00263.

Chapter 3.3 - Characterization of DOM and HS-L extracts originated from composts of different origins

Results from the characterization of the humic-like and fulvic-like extracts (HA-L and FA-L) and of the equilibrium solutions, containing the water-soluble organic fraction (dissolved organic matter, DOM) extracted from compost samples of different origins and of organic fertiliser are presented in this chapter. The elemental and structural characterization of the two humic-like substances was performed by EA, UV-vis, ATR-FTIR, TGA, DSC, while the equilibrium solutions were characterised by EA, EC, UV-vis. A correlation study was performed between the characterization results and the reactivity of the extracts (previously presented in chapter 3.2) and with the data of the solid compost (displayed in chapter 3.1).

1. Equilibrium solutions physico-chemical characterization

The values of the parameters used to characterise the equilibrium solutions from composts and fertiliser are shown in Table 3.8. The content of organic matter, evaluated by *DOC,* varies between 111 and 861 mg L^{-1}, where the highest value corresponds to CLW. The salinity of this extract was evaluated by the electrical conductivity (*EC*). The equilibrium solutions from CLW is the only that exceeds the standard limit of 4 S cm^{-1} for agricultural applications [1], the remaining extracts have relatively low values of EC. The *pH* values of the equilibrium solutions vary between 6.3 and 8.5. The highest value is for CLW whereas the lowest values are for the two vermicompost samples (CVA and CVDW). These results suggest that vermicompost tends to have a lower *pH*. The comparison is significant when the compost and vermicompost are obtained from the same raw material, as for CDDW and CVDW for which the lower *pH* is for the vermicompost. A correlation between *pH* and *EC* (r=0.89) is shown in Figure 3.18, that may be related to the pH-dependent occupation of acid sites in the organic matter by cations. The relationship was different in the composted and vermicomposted samples. The *pH* of sample CA was higher than expected from the *EC*, which can be explained by the lower concentration of NH_4^+ in this sample (1.77 mg L^{-1}) relative to the other samples (between 4.6 and 159 mg L^{-1}). The organic fertiliser appears with the composted samples in the same linear correlation.

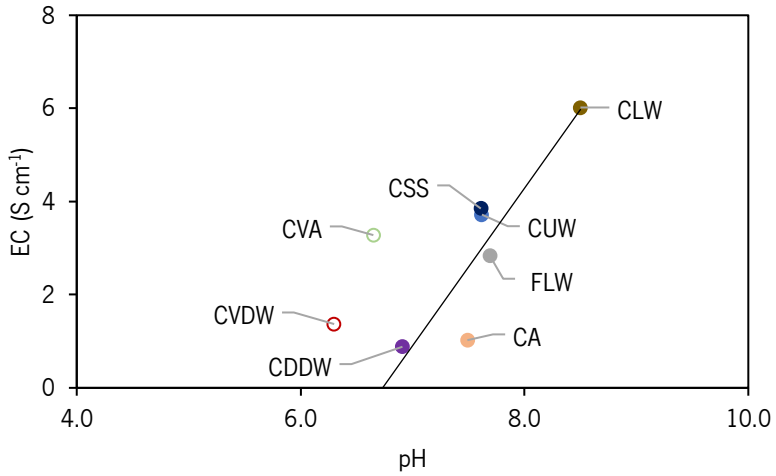

Figure 3.18: Correlation of the electric conductivity (*EC*) as a function of the *pH* of the equilibrium solutions of the compost samples: CDDW (purple), CVDW (red), CVA (green), CA (orange), CUW (blue), CSS (dark blue), CLW (brown) and FLW (grey), where a full line represents the linear fitting (r=0.89). Data from CVA and CVDW (open symbols) were not included in the fitting.

Within the major elements (K, Na, Ca and Mg) Na and K are the most abundant in the equilibrium solutions. This was observed for all samples except for CSS, for which K and Mg (present in identical quantities) were the most abundant (Table 3.8). In none of the samples was found a significatively high concentration of Na, that could limit the potential use of the compost as soil amendment or for other agricultural application, considering its effect in preventing the absorption of Ca and Mg [2]. By comparing results of CDDW and CVDW (compost and vermicompost produced from the same waste material) very similar values are found regarding the major elements released to the solution, suggesting that the feedstock may be the main factor responsible for the availability of the major elements. Results from the non-composted organic fertiliser are in the range of values obtained for the compost samples, suggesting that there are no significant differences between the chemical composition of the two types of materials.

Table 3.8: Characterization results of equilibrium solutions from the compost and organic fertiliser (highlighted).

Parameter	CVA	CVDW	CA	CLW	CUW	CDDW	CSS	FLW
DOC (mg L^{-1})	111	717	75.23	861	548	115	698	921
C_{oxi} (%)	0.81	4.33	2.66	9.69	3.73	1.22	4.53	11.9
Cl (mg L^{-1})	218	63.2	107	977	392	39.2	75.0	183
F^- (mg L^{-1})	0.04	0.03	0.07	0.12	0.18	0.17	0.12	0.11
SO_4^{2-} (mg L^{-1})	41.7	0.03	157	344	105	7.91	362	249
PO_4^{3-} (mg L^{-1})	241	70.3	12	124	29.5	45.2	29.0	189
NO_2^- (mg L^{-1})	1.8	3.9	0.54	6.7	3.9	11.0	2.2	9.17
NO_3^- (mg L^{-1})	609	0.2	40.55	2.6	5.2	203	5.0	0.48
NH_4^+ (mg L^{-1})	14.1	11.1	1.77	21.2	7.8	4.6	159	16.3
NH_4^+/NO_3^-	0.02	69.5	0.04	8.31	1.49	0.02	31.9	34.0
Si (mg L^{-1})	6.2	2.6	1.10	19	1.4	4.1	1.6	8.03
Ca (mg kg^{-1})	80.7	17.8	11.4	22.5	28.0	28.6	95.7	32.4
Mg (mg kg^{-1})	66.1	15.1	17.1	38.9	8.8	12.3	55.8	35.0
Na (mg kg^{-1})	114	26.7	72.1	552	175	17.3	21.1	115
K (mg kg^{-1})	431	333	103.7	1364	349	150	55	724
Fe (mg kg^{-1})	0.01	0.23	0.1	7.00	1.09	0.05	19.3	8.18
Al (mg kg^{-1})	< DL	0.1	< DL	0.2	0.3	< DL	0.3	0.08
As (ug L^{-1})	24	13	24.2	57	54	23	42	18
Cu (mg L^{-1})	0.03	0.09	< DL	1.40	0.11	0.02	0.21	0.34
Mn (mg L^{-1})	0.48	0.02	< DL	0.16	0.03	< DL	0.33	0.46

Note: < DL (lower than the detection limit)

1.1. UV-vis

Combining UV-vis measurements at 280 nm with the TOC values of each extract, the molar absorptivity coefficient at, ε_{280} was calculated for each equilibrium solution (Table 3.9). In turn, these results were used to estimate the relative aromaticity and the average molecular mass of the DOM [3], using semi-empirical relationships (% aromaticity = 0.05 x ε_{280} + 6.74 and molar mass = 3.99 x ε_{280} + 490). For the DOM extract of the compost samples, except for sample CSS, the percentage aromaticity was between 20 and 27 %, which agrees with the presence of hydrophobic moieties, more resistant to degradation, in samples that have already passed through the composting process [4]. It is noteworthy that the highest values of aromaticity and molecular mass were found for the organic non-composted fertiliser.

Table 3.9: Data of UV-vis of DOM (equilibrium solutions), HA-L and FA-L from the compost and organic fertiliser (highlighted).

Parameter		CVA	CVDW	CA	CLW	CUW	CDDW	CSS	FLW
ε_{280} (L molC^{-1} cm^{-1})	HA-L	381	347	408	323	513	145	451	289
	FA-L	381	243	407	247	419	117	351	209
	DOM	306	291	366	267	280	402	146	491
Aromaticity (%)	HA-L	25.8	24.1	27.2	22.9	32.4	29.3	14.0	21.2
	FA-L	25.8	18.9	27.1	19.1	27.7	24.3	12.6	17.2
	DOM	22.1	21.3	25.0	20.1	20.7	26.9	14.0	31.3
Molecular mass (g mol^{-1})	HA-L	2011	1875	2119	1780	2538	2290	1069	1644
	FA-L	2011	1460	2114	1476	2163	1891	958	1324
	DOM	1712	1651	1949	1555	1605	2095	1072	2451

2. HS-L physico-chemical characterization

Results from the extraction yields and elemental characterization of the humic-like substances are presented in Table 3.10. The sum of the extraction yields of CLW were the highest (41.9 g kg^{-1} compost) whereas for CA were the lowest (22.5 g kg^{-1} compost), showing that the content of humic substances can vary substantially. The sum of the yield in the non-composted sample, FLW, 64.5 g kg^{-1} compost, surpasses that of composts. The atomic ratios C/N, O/C and H/C, which are often used to identify the type of HS-L, are plotted in a van Krevelen diagram (Figure 3.19A) and in a bar diagram (Figure 3.19B) [5].

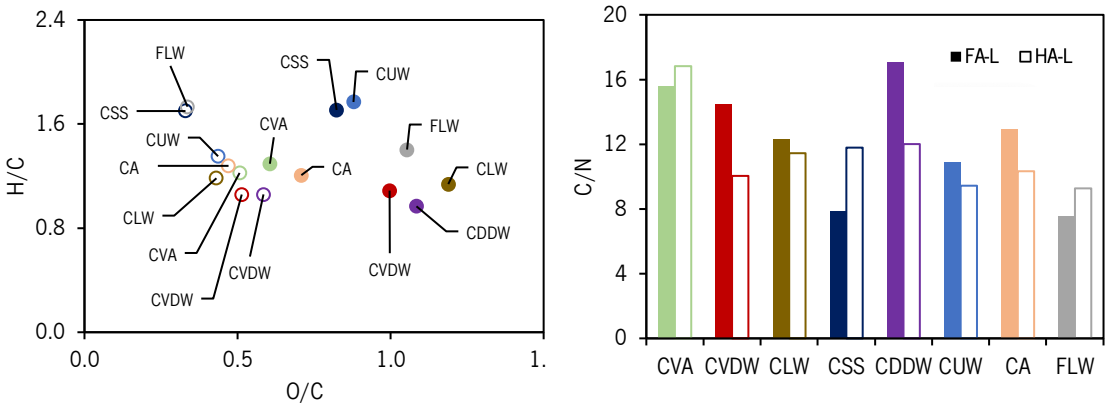

Figure 3.19: Van Krevelen diagram (O/C vs H/C elemental ratios) of (o) HA-L and (●) FA-L extracts of the compost samples: CDDW (purple), CVDW (red), CVA (green), CA (orange), CUW (blue), CSS (dark blue), CLW (brown) and FLW (grey).

For all the samples, the HA-L showed lower values of the *O/C* ratio in comparison with FA-L, in agreement with the expected, as HA-L has a higher carbon content and a lower oxygen content than FA-L. This fact is related to the higher solubility of FA-L fraction in opposition to HA-L whose solubility is limited to basic media (pH>10). The *H/C* ratio has been used as an index that can account for the presence of aliphatic components in the general structure of humic substances. It is, therefore, inversely proportional to the aromaticity or degree of condensation [6]. In general, the *H/C* ratios are similar in both fractions, except in sample CUW, in which the ratio was higher in FA-L displaying the lower aromatic character of the latter in relation to the HA-L. The *C/N* ratio is indicative of the nitrogen enrichment of humic substances [7]. The higher nitrogen content for HA-L, *i.e.* the lower *C/N* ratio, may indicate a larger nitrogen fixation compared to fulvic [8].

Table 3.10: Data related to physico-chemical characterization of HA-L and FA-L from the compost and organic fertiliser (highlighted).

Parameter		CVA	CVDW	CA	CLW	CUW	CDDW	CSS	FLW
C (%)	HA-L	53.5	52.7	53.3	55.2	54.5	50.6	58.5	57.5
	FA-L	49.7	39.8	45.8	35.4	40.8	38.4	40.9	36.9
N (%)	HA-L	3.71	6.12	6.02	5.62	6.74	4.92	5.79	7.24
	FA-L	3.72	3.20	4.13	3.36	4.37	2.62	6.05	5.72
H (%)	HA-L	5.46	4.65	5.68	5.44	6.14	4.47	8.28	8.31
	FA-L	5.36	3.61	4.61	3.36	6.02	3.09	5.83	4.32
S (%)	HA-L	1.14	0.41	1.61	2.07	0.91	0.50	1.88	1.08
	FA-L	1.08	0.46	2.16	1.80	0.96	0.41	2.22	1.11
O (%)	HA-L	36.2	36.1	33.4	31.7	31.7	39.5	25.5	25.8
	FA-L	40.1	52.9	43.3	56.1	47.8	55.5	45.0	51.91
Yield (g kg^{-1})	HA-L	33.4	26.4	19.9	34.9	21.1	23.8	19.0	53.6
	FA-L	2.3	4.7	2.7	7.0	3.3	4.8	4.2	10.9

2.1. Spectroscopic characterization

2.1.1. UV-vis

The molar absorptivity coefficient, ε_{280} was calculated for each FA-L and HA-L (Table 3.9). These results were used to estimate the relative aromaticity and the molecular mass of these extracts [3]. The values of this parameter are higher for HA-L than for FA-L samples, which means a higher percentage of aromaticity for HA-L except in CVA and CA, in which the values are equal. When comparing the values presented for DOM with the humic-like substances it can be indicated that they are lower than the HA-L values, with the exception of CSS and the organic fertiliser. Regarding FA-L, we can divide the samples into two groups. Those with higher values than DOM: CVA, CA, CUW and those with lower values: CVDW, CLW, CDDW, CSS and FLW.

2.1.2. ^{1}H-NMR

The nature and relative abundance of various chemical groups of HA-L and FA-L were characterised by ^{1}H-NMR spectroscopy. The spectra were subdivided into five chemical shift regions, reflecting the signals associated to specific functional groups: δ 0 – 3.0 for C-alkyl and N-alkyl protons, δ 3.0 – 4.5 for O-alkyl including phenolic O-alkyl protons, δ 4.7– 5.0 for H_2O protons, δ 5.0 – 6.0 for the protons of alkenes and CH_2 groups linked to the aromatic ring and δ 6.0 – 9.0 ppm for alkene and aromatic protons.

Table 3.11: Data from ^{1}H-NMR of FA-L and HA-L from the compost and organic fertiliser (highlighted).

Chemical shifts intervals	**δ 0.4 – 4.5 ppm**		**δ 6 - 9 ppm**		**Ratio Aromatic/Aliphatic protons**	
Functional groups	Aliphatic protons		Aromatic protons			
Samples	**FA-L**	**HA-L**	**FA-L**	**HA-L**	**FA-L**	**HA-L**
CVA	7.49	13.7	1.43	3.45	0.191	0.252
CVDW	8.93	17.6	0.95	2.26	0.106	0.129
CLW	9.95	16.0	1.46	2.69	0.147	0.168
CSS	13.6	27.9	0.77	2.04	0.056	0.073
CDDW	8.20	16.2	1.07	2.10	0.130	0.130
CUW	5.09	13.4	0.44	1.80	0.086	0.134
CA	2.23	13.7	0.46	1.91	0.206	0.139
FLW	10.2	19.3	1.5	3.11	0.147	0.161

Considering the aliphatic nature of the protons in the δ 0 – 4.5 ppm region and the aromatic nature of the protons in the δ 6.0 – 9.0 ppm region, a ratio between the abundance of these two types of protons was calculated from the relative areas of those signals. The values of this ratio, summarised in Table 3.11, tend to be higher for HA-L compared to FA-L, except for CDDW, where the same value was obtained and for CA where the situation was reversed, with a higher ratio of aromatic protons for FA-L. The ratio of aromatic/aliphatic protons obtained for HA-L and FA-L from CLW and FLW are remarkably similar, probably reflecting their origin, as both were obtained from similar feedstock (manure), although FLW was not composted.

2.1.3. ATR-FTIR

The ATR-FTIR spectra of the HS-L extracted from compost samples of different origins are shown in Figure 3.20. The spectra displays the typical peaks characteristic of these type of substances, namely: i) a strong and very broad band at 3600-3000 cm^{-1} that can be ascribed to O–H stretching of hydroxyl groups from phenol and alcohol and/or to those from the carboxylic groups and also to amide and amine N–H stretching [9–11]; ii) two other bands appearing at 2925 and 2845 cm^{-1} that can be attributed to asymmetric and symmetric vibrations of C-H aliphatic bonds in CH_3 and CH_2 groups [11–13]; iii) a shoulder at 1700 cm^{-1} that may be ascribed to C=O stretching of COOH and ketones [11,14]; iv) a band centred at around 1640–1630 cm^{-1} that may be attributed to aromatic C=C and C=O stretching of amide groups (amide I band) and quinonic C=O and/or C=O of H-bonded conjugated ketones [11,12]; v) a band centred at around 1530-1520 cm^{-1} that can be associated to stretching vibrations of the aromatic C=C bonds and/or N–H bending vibrations and C=N stretching (amides II) [11,15]; vi) bands between 1450 and 1410 cm^{-1} that can be related to C-H deformations of CH_3 and CH_2 groups [13]; vii) a band at around 1220 cm^{-1} that may be associated to the C–O stretching of aryl ethers and phenols and C–O, O–H bending of carboxylic groups [13,14] and finally, viii) a band at around 1020 cm^{-1} that is ascribed to C-O stretching of polysaccharides [11,15].

The most significant differences between the extracts are in the regions of 3700-2700 cm^{-1} and 1800–1000 cm^{-1}. The relative intensity of the band at 1700 cm^{-1} (C=O bonds of COOH, aldehydes and ketones) with respect to 1630 cm^{-1} varies significantly in the two extracts. In all FA-L samples, the band at 1700 cm^{-1} is of the same intensity or even higher than the band at 1630 cm^{-1} with the exception of the FA-L extracted from the CSS when compared with HA-L.

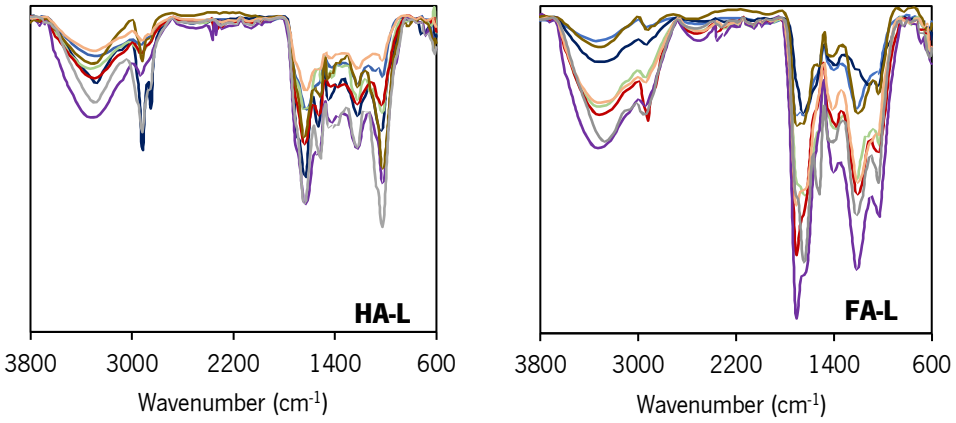

Figure 3.20: ATR-FTIR spectra (3800 – 600 cm^{-1}) of humic-like acid (HA-L) and of fulvic-like acid (FA-L) obtained from compost samples: CDDW (purple), CVDW (red), CVA (green), CA (orange), CUW (blue), CSS (dark blue), CLW (brown) and FLW (grey).

The ratios $I_{1630/2925}$ *and* $I_{1630/2845}$ denominated aromaticity indexes were calculated and are presented in Table 3.12 [10]. According to the values obtained for the two aromaticity indexes, samples can be arranged in three groups. With respect to HA-L, CSS shows the lowest values, CVA, CLW, CUW and CDDW display intermediate values and CA displays the highest values. A different order is found for FA-L, where CVDW has the lowest values, CLW, CA, CVA, CDDW and CSS show intermediate values and CUW has the highest values. The HA-L of CA and FA-L of CUW have a higher degree of aromaticity than the other samples.

Table 3.12: Data of ATR-FTIR of HA-L and FA-L from the compost and organic fertiliser (highlighted).

Parameter		CVA	CVDW	CA	CLW	CUW	CDDW	CSS	FLW
$I_{1630/2845}$	HA-L	2.42	4.45	5.23	3.61	4.31	4.01	2.63	2.42
	FA-L	4.17	2.67	3.47	5.28	9.08	3.52	4.32	n.d.
$I_{1630/2925}$	HA-L	3.46	5.01	8.01	3.46	4.70	4.91	1.76	3.46
	FA-L	4.02	2.61	3.13	3.88	7.56	2.59	3.17	3.43

Note: n.d. (not detected)

2.2. Thermal characterization

2.2.1. DSC

The DSC curves of HS-L of the different samples are displayed in Figure 3.21. Despite the evident differences in shape and height of the thermograms of the different samples, they exhibit important common features, such as a minor endothermic process, at the lower temperature limit (close to 100 °C), usually ascribed to dehydration reactions, and two major broad bands (at 320 °C and

500 °C), corresponding to the overlap of exothermic processes related to the decomposition of recalcitrant and extra-recalcitrant substances, respectively.

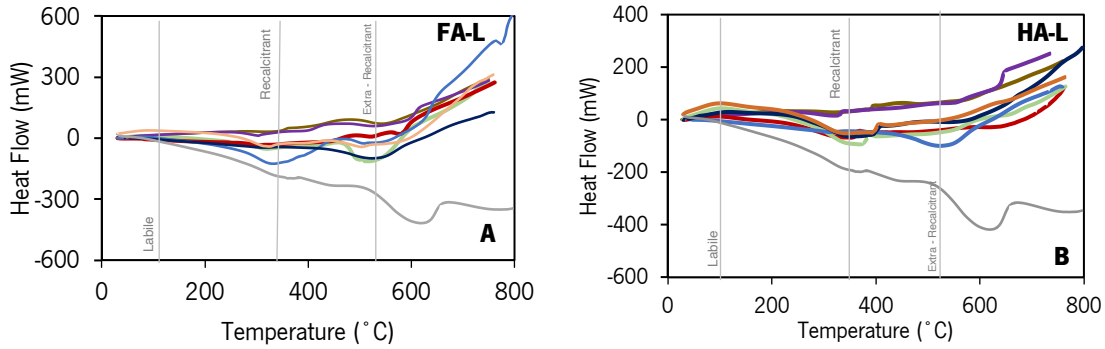

Figure 3.21: DSC curves (A, B) of the fulvic-like acid (FA-L) and humic-like acid (HA-L) extracted from samples with different origin: CDDW (purple), CVDW (red), CVA (green), CA (orange), CUW (blue), CSS (dark blue), CLW (brown) and FLW (grey).

The values obtained by integration of curves at the three temperature ranges 30-177 °C, 177-400 °C, 400-620 °C, designated by H_1, H_2 and H_3 are shown in Table 3.12. The FA-L of all samples share as a common feature that the values of enthalpy of the decomposition of the extra-recalcitrant substances is equal or larger than that of the recalcitrant substances, except for the samples CDDW and CSS. On the contrary, for HA-L the values of enthalpy for the decomposition of the recalcitrant substances are equal or larger than the value for the extra-recalcitrant substances, except for the samples CUW and CSS.

2.2.2. TGA

The TGA and DTG curves of the FA-L and HA-L extracted from composts and fertiliser are depicted in Figure 3.22. In the TGA curves recorded under air atmosphere three main processes were identified namely WL_1 (30 - 177 °C), WL_2 (177 - 400 °C) and WL_3 (400 - 620 °C) where the decomposition processes related to WL_1 can be associated to H_1, WL_2 to H_2 (from recalcitrant substances) and WL_3 to H_3 (from extra-recalcitrant substances).

The total weight loss (*TWL*) shows an important variation among the samples analysed. The FA-L extracts from sample CA exhibited the lowest value of *TWL* (59.8 %), whereas sample CVA show the highest (84.5 %). The HA-L from sample (Figure 3.22) CSS exhibited the lowest value of this parameter (66.9 %), whereas the HA-L extracts from CUW and CDDW show the highest (97.9 % and 93.9 %, respectively). Apparently, there is a direct relation between the *TWL* and the nature of the feedstock, as CDDW and CUW are essentially produced using vegetable sources and display very similar values of this parameter (Figure 3.22C).

Table 3.12: Data from DSC and TGA of HA-L and FA-L extracts from the compost and organic fertiliser (highlighted).

Parameter		CVA	CVDW	CA	CLW	CUW	CDDW	CSS	FLW
H_1 (kJ g^{-1})	HA-L	0.39 ± 0.09	0.14 ± 0.03	0.37 ± 0.09	0.07 ± 0.02	0.27 ± 0.06	0.18 ± 0.04	0.40 ± 0.09	0.07 ± 0.02
	FA-L	0.25 ± 0.06	0.07 ± 0.02	0.20 ± 0.05	0.05 ± 0.01	0.47 ± 0.11	0.23 ± 0.05	0.03 ± 0.01	0.07 ± 0.02
H_2 (kJ g^{-1})	HA-L	-0.82 ± 0.11	-0.67 ± 0.09	-1.10± 0.14	-0.66 ± 0.09	-1.3 ± 0.2	-0.17 ± 0.02	-1.4 ± 0.2	-1.8 ± 0.2
	FA-L	-3.6 ± 0.5	-3.4 ± 0.4	-1.54 ± 0.20	-1.7 ± 0.2	-3.1 ± 0.4	-0.57 ± 0.07	-1.2 ± 0.2	-2.1± 0.3
H_3 (kJ g^{-1})	HA-L	-1.2± 0.06	-1.0± 0.05	-1.09± 0.05	-0.52 ± 0.02	-4.5 ± 0.2	-2.8 ± 0.1	-1.2 ± 0.06	-4.7 ± 0.2
	FA-L	-3.7± 0.2	-2.2 ± 0.1	-1.20 ± 0.06	-1.6 ± 0.08	-2.5 ± 0.1	-2.6 ± 0.1	-2.7± 0.1	-3.2± 0.2
H_2/H_3	HA-L	1.5 ± 0.2	1.5 ± 0.2	0.99 ± 0.1	0.79 ± 0.1	3.6 ± 0.5	-16 ± 2.2	0.8 ± 0.1	2.6 ± 0.4
	FA-L	1.0 ± 0.1	3.6 ± 0.5	0.78 ± 0.1	0.94 ± 0.1	0.82 ± 0.1	4.5 ± 0.6	2.3 ± 0.3	1.5 ± 0.2
WL_1@air (%)	HA-L	3.9 ± 1.0	7.1 ± 1.8	5.0 ± 1.3	7.5 ± 2.0	8.3 ± 2.2	8.6 ± 2.2	2.4 ± 0.6	2.3 ± 0.6
	FA-L	4.5 ± 1.2	3.3 ± 0.9	1.4 ± 0.4	3.4 ± 0.9	6.4 ± 1.7	4.1 ± 1.1	2.4 ± 0.6	4.5 ± 1.2
WL_2@air (%)	HA-L	34.5 ± 2.7	32.9 ± 2.6	32.7 ± 2.6	30.5 ± 2.4	30.9 ± 2.4	30.9 ± 2.4	43.1 ± 3.4	38.7 ± 3.0
	FA-L	42.5 ± 3.3	35.6 ± 2.8	31.2 ± 2.4	20.2 ± 1.6	38.4 ± 3.0	31.1 ± 2.4	29.1 ± 2.3	31.2 ± 2.4
WL_3@air (%)	HA-L	49.3 ± 4.3	46.8 ± 4.1	52.6 ± 4.6	50.4 ± 4.4	58.7 ± 5.2	54.4 ± 4.8	21.4 ± 1.9	54.5 ± 4.8
	FA-L	37.5 ± 3.3	35.6 ± 3.1	27.2 ± 2.4	41.2 ± 3.6	33.5 ± 2.9	34.1 ± 3.0	31.7 ± 2.8	37.4 ± 3.3
Res@air (%)	HA-L	16.6 ± 1.1	12.3 ± 0.8	8.40 ± 0.5	11.8 ± 0.8	2.50 ± 0.2	4.7 ± 0.3	32.1 ± 2.1	4.5± 0.3
	FA-L	12.7 ± 0.8	23.1 ± 1.5	40.2 ± 2.6	33.4 ± 2.2	21.6 ± 1.4	29 ± 1.9	35.7 ± 2.3	26.8 ± 1.7
WL_1@air/WL_2@air	HA-L	1.4 ± 0.2	1.4 ± 0.2	1.6 ± 0.2	1.7 ± 0.2	1.9 ± 0.2	1.8 ± 0.2	0.5 ± 0.06	1.4 ± 0.2
	FA-L	0.9 ± 0.1	1.0 ± 0.1	0.87 ± 0.10	2.0 ± 0.2	0.9 ± 0.1	1.1 ± 0.1	1.1 ± 0.1	1.2 ± 0.1

From the shape of the corresponding DTG curves (Figure 3.22) it can be realised that each of the 3 processes (WL_1, WL_2, and WL_3) may result from the overlay of multiple single processes (as peaks are large and not symmetrical), mainly the 2nd peak that is quite uneven. The shape and position of peaks in the DTG curves are quite varied. Within the FA-L extract the samples that showed the most different profile are CVDW and CA, whereas in the HA-L extract, the samples CSS and CVA showed the most different profiles. The values of weight loss for the 3 regions above identified are presented in Table 3.12. For the first temperature range (30 - 177 °C) all values are between 1.4 ± 0.4 % and 8.6 ± 2.2 %. According to the values of WL_2, from FA-L and HA-L, samples may be divided in two groups; the group with the higher (CVDW, CA and CVA) and with the lower values (CDDW, CUW and CLW) of WL_2. A low value of WL_2 may indicate the presence of a small amount of labile organic structures in the extract. This fact may result from the nature of the feedstock or from the extent of the composting process, that was more efficient in decomposing these structures. CA and CUW are the samples that display higher values of WL_3 for FA-L and HA-L extracts, whereas CVDW and CSS exhibit lower values that may suggest the presence of a larger amount of extra-recalcitrant structures in CA and CUW.

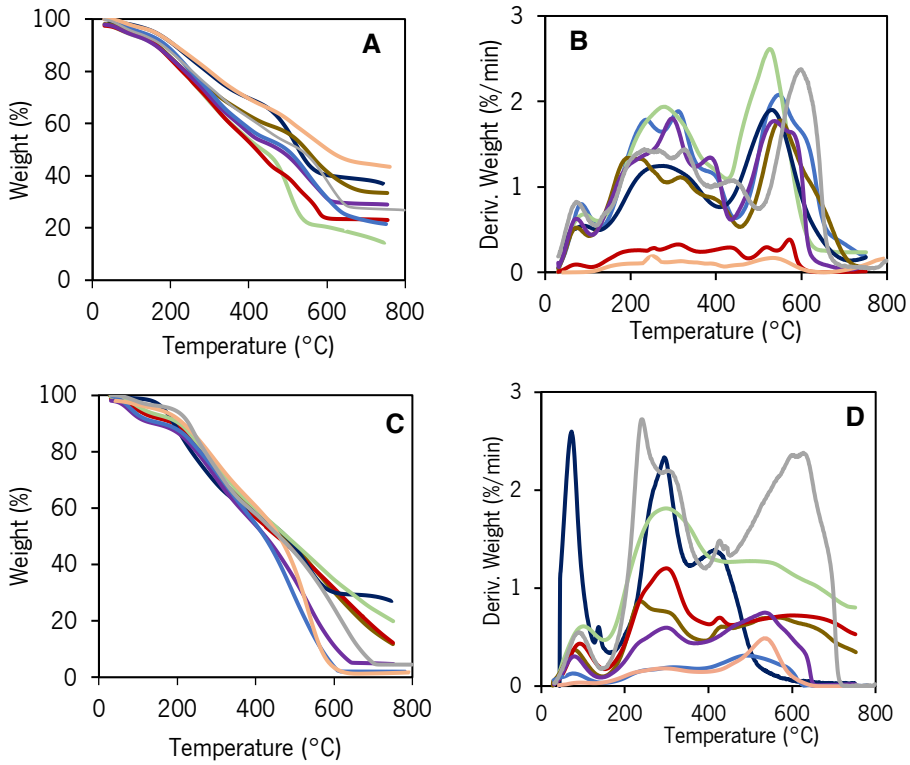

Figure 3.22: TGA (A, C) and DTG (B, D) curves obtained in air atmosphere for the FA-L (A, B) and HA-L (C, D) extracted from compost samples of different origin: CDDW (purple), CVDW (red), CVA (green), CA (orange), CUW (blue), CSS (dark blue), CLW (brown) and FLW (grey).

3. Correlations between physico-chemical and reactivity parameters

Given the high number of parameters that were obtained from the different techniques and the complexity of the samples, the comparison between composts is not simple. The different indexes do not lead to the same ranking of samples. These differences may be due to the complexity of the samples giving rise to overlapped signals which deconvolution is not always simple. The meaning of each parameter can however be tested by comparing results from the different parameters. Significative changes in the composition of the extracts should be detected by simultaneous changes in different techniques. Furthermore, those changes should be noticeable both in the physico-chemical properties and in the reactivity of the chemical entities. Keeping in mind this assumption, parameters from the different physico-chemical and reactivity analysis were compared in a correlation study including the three extracts (FA-L, HA-L and DOM).

In addition, correlations were sought between the physicochemical and reactivity parameters of the extracts and the characterization parameters of the original samples (only compost samples).

3.1. *Correlation between the chemical composition and reactivity of extracts*

Figure 3.23A summarises the number of correlations found for each parameter from the different extracts of the compost samples. The HA-L is the extract with a larger number of correlations (30) among composition and reactivity parameters, while the DOM presents the lowest number of correlations. For this analysis only correlations with $|r|>0.7$ were considered. The correlations between parameters from identical and from different techniques are differentiated in Figure 3.23B. The parameters that were more correlated were ε_{280} of HA-L (5) and DOM (3), followed by $WL_1@air/TWL@air$ (4), $I_{1630/2925}$ (3) and C/N of HA-L (3) and O/C of FA-L (3).

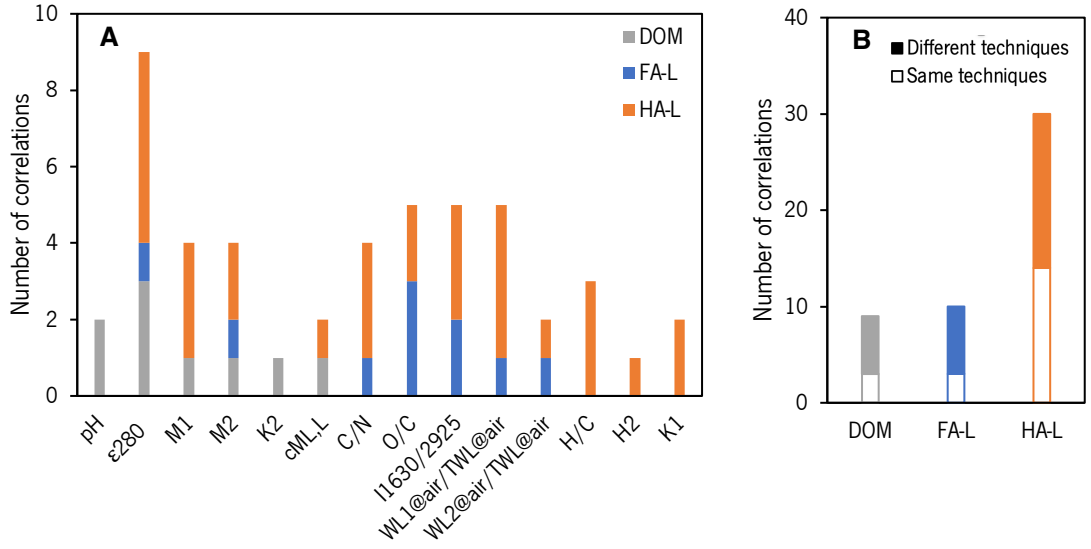

Figure 3.23: (A) Number of correlations found ($|r|>0.7$) for each characterization parameter within data from FA-L, HA-L and DOM and (B) Number of total correlations found for FA-L, HA-L and DOM, where full bars represent the correlations between parameters from different techniques and the empty bars represent correlations between parameters from the same technique.

Results of the correlation analyses from the characterization parameters of FA-L, HA-L and DOM extracts are represented in three heatmaps displayed in Figure 3.24. For FA-L the analysis was performed using a total of eighteen parameters including the physico-chemical and reactivity characterization (Figure 3.24A). Among the ten correlations with $|r|>0.7$, seven are between parameters of different techniques, of each the five positive correlations can be organised in three groups:

i) ε_{280} with H_1; $I_{1630/2925}$ with H_1; $I_{1630/2925}$ with $WL_1@air/TWL@air$;

ii) O/C with K_1;

iii) $c_{ML,H}$ with WL_2@air/TWL@air.

The 2 negative correlations can be arranged in two groups:

iv) O/C with WL_2@air/TWL@air; O/C with M_2;

The positive correlations in the first group suggest a strong association between aromaticity of the FA-L (evaluated either by ε_{280} or by $I_{1630/2925}$) and the ability of these structures to adsorb low molecular weight substances (higher values of H_1 or WL_1@air/TWL@air). The correlations found in the second group suggest an association between the oxygen relative abundance and the median value of the affinity distribution of carboxyl groups. With respect to the third group the correlation suggests that the molecular structures involved in the binding of Cd^{2+} may contribute to the extent of mass loss between 177 and 400 °C, related to the degraded of the easily biodegradable aromatic structures (*e.g.* carbohydrates moieties and aliphatic compounds). With respect to the negative correlations in iv) between WL_2@air/TWL@air with O/C and M_2 with O/C indicate that the higher is the oxygen relative abundance in the molecular structures of FA-L, the lower are the abundance of easily degradable aromatic structures and the abundance of phenolic groups (M_2). This decrease may indicate that the increase in the oxygen contents may result in the conversion of the easily degradable aromatic structures into extra-recalcitrant structures and simultaneously the conversion of phenolic structures into carboxylic groups or even in carbonates or CO_2 (with the mineralization of organic matter).

For HA-L the correlation analysis was also performed using a total of 18 parameters including the physico-chemical and reactivity characterization (Figure 3.24B). Among the 30 correlations with $|r|>0.7$, 16 are between parameters of different techniques, of each the 9 positive correlations can be divided in 5 groups:

i) C/N with H_{ara}/H_{ali};

ii) H/C with WL_2@air/TWL@air;

iii) ε_{280} with WL_1@air/TWL@air, ε_{280} with WL_3@air/ TWL@air; ε_{280} with H_2;

iv) $I_{1630/2925}$ with M_2; ε_{280} with M_2; $I_{1630/2925}$ with $c_{ML,L}$; $I_{1630/2925}$ with $c_{ML,H}$;

v) K_1 with $c_{ML,L}$.

Alongside the 7 negative correlations can be arranged in 3 groups:

vi) H/C with WL_1@air/TWL@air; H/C with WL_3@air/TWL@air,

vii) O/C with WL_2@air/TWL@air;

viii) ε_{280} with WL_2@air/TWL@air;

ix) C/N with K_1 and C/N with K_2;

The positive correlation in the first group indicates a strong association between the C content relative to N and the aromaticity of HA-L (evaluated by ^{1}H-NMR), where higher values of H_{aro} *with* respect to H_{ali} are found for the samples with lower content of N. The correlation found in the second group suggests an association between the degree of condensation of aromatic rings by the HA-L and the abundance of easily degradable aromatic moieties (WL_2*@air/TWL@air*). With respect to the third group the correlations suggest that the aromaticity of the HA-L (evaluated by UV-vis) is related to the ability of the HA-L extracts to adsorb low molecular weight substances. The aromaticity is also associated with both the content of extra-recalcitrant structures and the amounts of heat released in the degradation of easily biodegradable aromatic moieties, suggesting that the decomposition of aromatic structures occurs in all range of temperatures where the exothermic processes take place. The correlations in the fourth group indicate a strong association between aromaticity (evaluated either by ε_{280} or by $I_{1630/2925}$) and abundance of phenolic groups (M_2) and also with the extent of the binding of Cd^{2+} ($c_{ML,L}$, $c_{ML,H}$), that is a consequence of the abundance and reactivity of the acid sites. The correlation found in the fifth group is straightforward as the binding extent of Cd^{2+} is directed related to the reactivity of carboxyl groups towards H.

The negative correlations, in vi), are related to the previously described for iii) which indicates that the extent of the adsorption of low molecular weight substances are directly related to the aromaticity (evaluated from UV-vis) and thus it is inversely related to the relative content of H. With regard to the mass loss extent of extra-recalcitrant structures, the correlations point out an effect that is similar to the previously described, *i.e.* a positive correlation in iii), is found with aromaticity and a negative correlation in vi) with the relative content of H. The correlation in vii) suggests that the abundance of the easily biodegradable aromatic structures is lower for the HA-L with the higher degree of oxidation (*O/C*). This suggests that these structures are converted into extra-recalcitrant structures or even in carbonates or CO_2.

The negative correlation between ε_{280} with WL_2*@air/TWL@air* indicates that samples with the higher aromaticity are those with the lower abundance of recalcitrant structures. This correlation is related

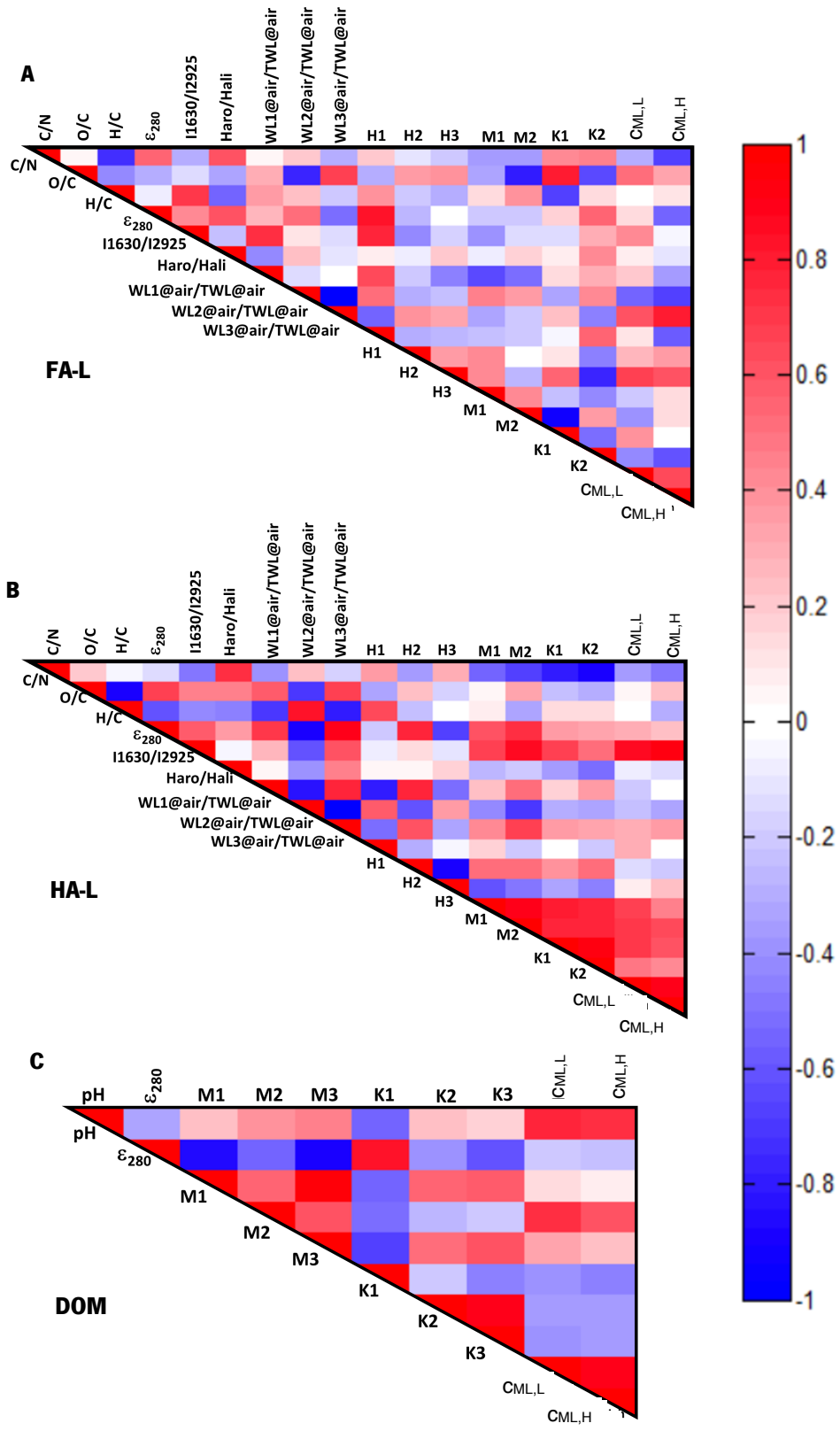

Figure 3.24: Triangular heat map showing the pairwise Pearson correlation coefficients (*r*) of the parameters from (A) FA-L, (B) HA -Land (C) DOM.

to the correlation ii) in the same way that correlations in vi) are related to iii). The correlations between C/N with K_1 and with K_2 indicate that the reactivity of both carboxylic and phenolic structures towards H is positively affected by a lower content of carbon relative to nitrogen. For DOM the correlation analysis was performed using a total of 10 parameters including the physico-chemical and reactivity characterization (Figure 3.24C). Amongst the 9 correlations with $|r|>0.7$, 6 are between parameters of different techniques, of each the 4 positive correlations can be divided in 3 groups:

i) ε_{280} with K_1;

ii) pH with $c_{ML,L}$; pH with $c_{ML,H}$;

iii) M_2 with $c_{ML,L}$;

Simultaneously, the two negative correlations are observed between:

iv) ε_{280} with M_1; ε_{280} with M_3.

The positive correlation in i) indicates that there is an association between the aromaticity (evaluated by UV-vis) and the reactivity of the carboxyl groups towards H. The positive correlations in ii) are associated with the deprotonation of the acid sites that are positively affected by the pH increase. The positive correlation in iii) shows that effectively the strongest groups that contribute to the extent of the binding of Cd^{2+} are those quantified in M_2 that correspond to the carboxylic groups in organics acids.

With respect to the iv) group the correlations suggest that for the DOM that the structures with higher aromaticity (evaluated by UV-vis) are found in the extracts with lower abundance of carboxylic groups in amino acids and phenolic groups.

3.2. Correlation between the composition of the extracts and the compost

In this section, the results of the composition of the three extracts (HA-L, FA-L and equilibrium solutions (containing DOM)) and the compost were used in three correlation analyses.

3.2.1. Equilibrium solutions vs. compost

Figure 3.25A exhibits a correlation analysis performed on the equilibrium solutions versus compost with 10 parameters from equilibrium solutions and 6 from compost (parameters in bold). From this analysis, two correlations were obtained with a Pearson correlation coefficient of $|r|>0.7$. The positive correlations were between ***S*** and SO_4^{2-} and NH_4^+ indicating that there is a strong association

between the S content in the compost and the content of sulphate and ammonium in equilibrium solutions. While the first association can be obvious, the second is more difficult to explain.

Figure 3.25B shows the correlation associated to the mobility of the metals in the compost that can be extracted into the equilibrium solutions. In the diagonal of this figure, four correlations are found with r>0.7, between the content of Na, K, Fe and As in the equilibrium solution and compost. These correlations indicate that the amount of these elements in the equilibrium solutions depends strongly on their content in the compost, due to their low binding extent with the HS-L present in the composts. For the remaining metals the binding extent with HS-L is the prevailing effect and thus correlation coefficients are lower. The correlations found between the content of some metals in the equilibrium solutions and the content of metals of different nature in the compost (*e.g.* Cu or K in the equilibrium solutions with **Na**, **K** and **Mg** in the compost), can be explained by the association between these elements in the compost, related with the nature of the raw materials.

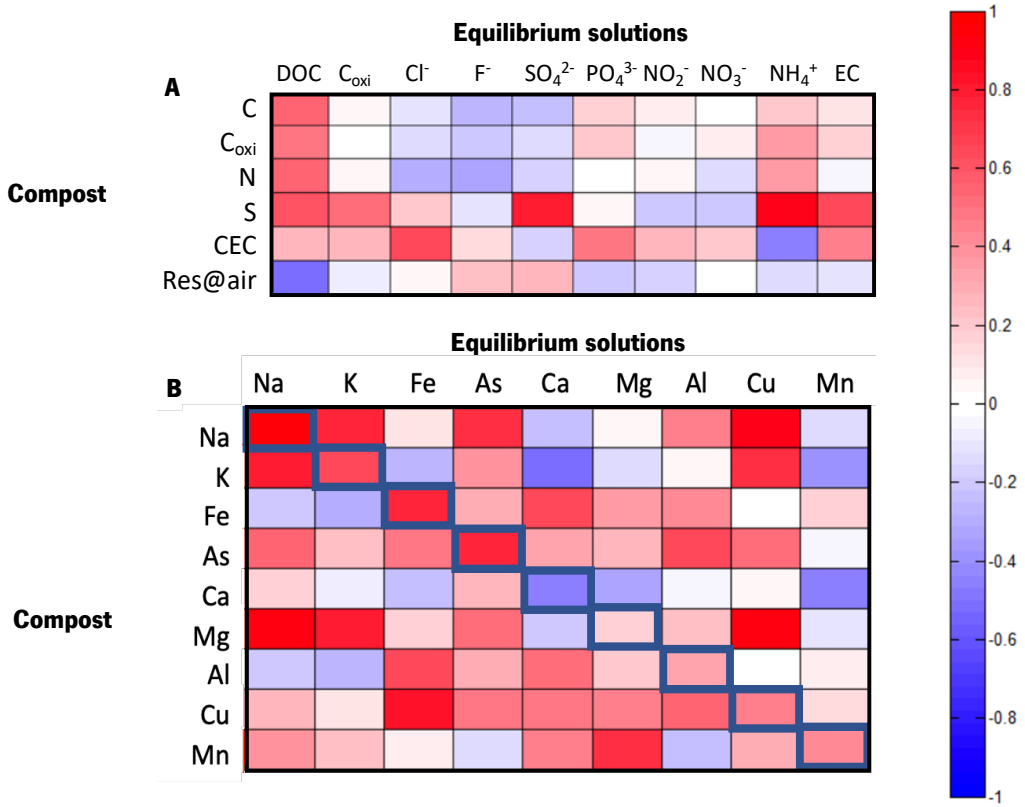

Figure 3.25: (A) Heat map showing the pairwise Pearson correlation coefficients (r) of (A) the characterization parameters of equilibrium solutions *vs.* relatable parameters of compost and of (B) metal content in equilibrium solutions *vs.* metal content of compost. The cells highlighted in diagonal in (B) correspond to the correlations between the same metal in the two samples.

3.2.2. HS-L vs. Compost

Figures 3.26A and 3.26B exhibit a correlation analysis performed with ten parameters of FA or ten parameters of HA with six relatable parameters of compost (in bold). From these two analyses, two correlations were obtained for FA-L and six correlations for HA-L with a Pearson correlation coefficient of $|r|>0.7$. With respect to FA-L, Figure 3.26A, the two positive correlations are: ***CEC*** with *WL_1@air*, and ***CEC*** with *WL_3@air*. These correlations suggest that the FA-L with higher amount of extra-recalcitrant moieties, are associated with the compost ability to exchange cations. The correlation between CEC and WL_1@air suggests that the composts that have higher ability to exchange cations contain the FA-L that have higher ability to adsorb low molecular weight substances.

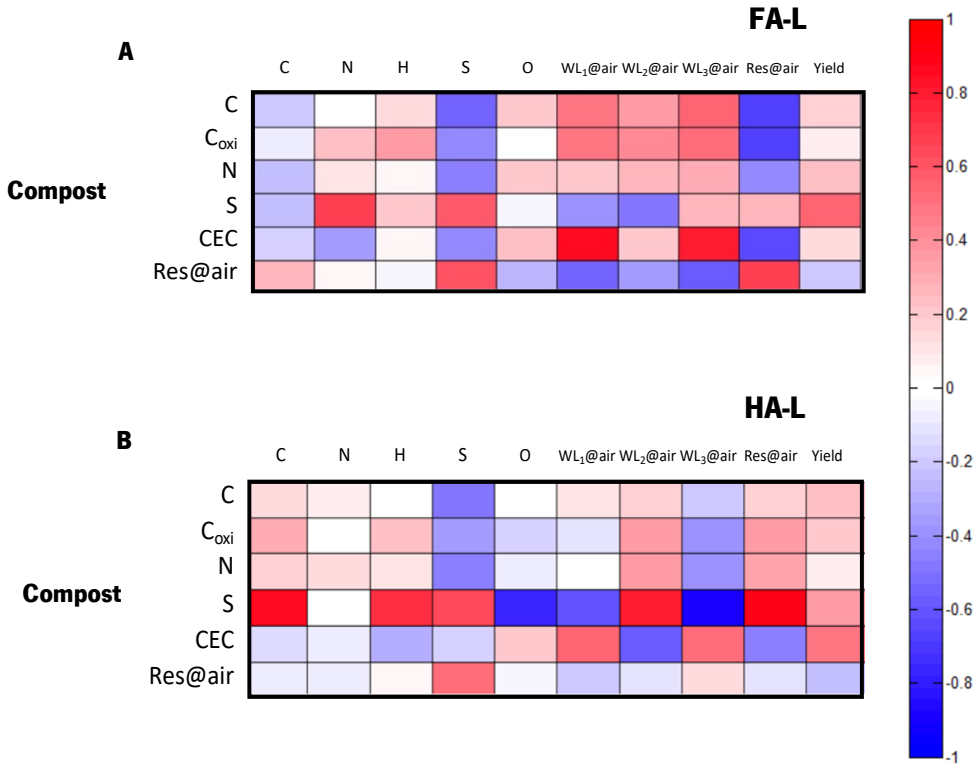

Figure 3.26: Heat map showing the pairwise Pearson correlation coefficients (r) of the parameters from (A) FA-L and (B) HA-L.

Regarding HA-L, Figure 3.26B, the four positive correlations are between ***S*** and *C*, *H*, *WL_2@air* and *Res@air*. These correlations indicate that compost samples with higher sulphur content are those whose HA-L have higher carbon and hydrogen contents and simultaneously have higher content of recalcitrant structures and higher residue in TGA. The negative correlations found are between the content of S of compost and content of O and *WL_3@air* of HA-L. The compost samples with higher

S are those whose HA-L have a lower oxygen content and a lower amount of extra-recalcitrant structures.

3.3. Correlation between the structural and reactivity features of extracts and data related to the molecular structure of the compost

In this last section, the results of the composition of the solid compost were used in three correlation analyses with extracts data related to reactivity. Figure 3.27 summarises the number of correlations found for the compost parameters from the different extracts. The HA-L is the one that presents the highest number of correlations (20) with the compost parameters, whereas the DOM presents the lowest number. From these analyses were considered the relationships with a correlation coefficient of $|r|>0.7$ and the correlations that relate parameters of different techniques. The compost parameters that are correlated with the largest number of extract parameters are: ***WL_3@air/WL_2@air*** (related to 6 parameters from HA-L, 2 from FA-L and 2 from DOM) and ***C_{oxi}/C*** (related to 2 parameters from HA-L, 2 from FA-L and 1 from DOM). Simultaneously, extract parameters that are correlated with the largest number of compost parameters are: M_1 (related to 6 parameters from compost) and ε_{280} (related with 4 parameters from compost).

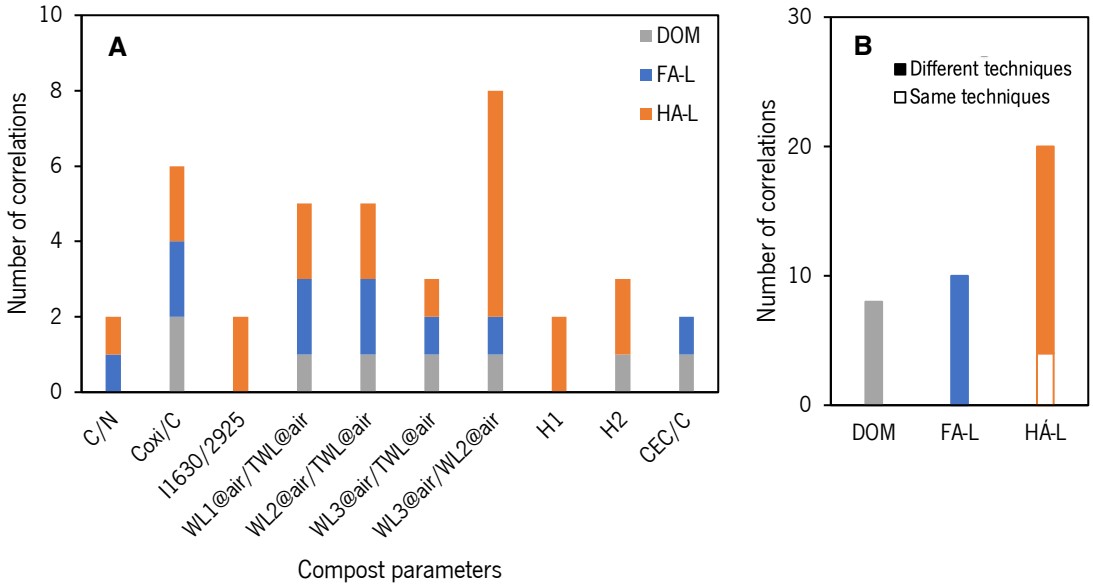

Figure 3.27: (A) Number of correlations between characterization parameter of FA-L, HA-L and DOM with the characterisation parameters of compost and (B) Number of total correlations found for FA-L, HA-L and DOM, where full bars represent the correlations between parameters from different techniques and the empty bars represent correlations between parameters from the same technique.

3.3.1. DOM vs. Compost

Figure 3.28 exhibits a correlation analysis performed with twelve parameters of the compost (in bold) with ten parameters from DOM. Four positive correlations are observed for DOM that can be arranged in two groups:

i) K_2 with ***C_{oxi}/C***; K_3 with ***C_{oxi}/C***;

ii) M_1 with ***WL_1@air/TWL@air***; K_3 with ***WL_2@air/TWL@air***,

Alongside four negative correlations, that can be organised in two groups:

iii) M_1 with ***WL_3@air/TWL@air***; M_1 with ***H_2***; M_1 with ***CEC/C***.

iv) K_3 with ***WL_3@air/WL_2@air***.

The positive correlations between $K_2$and K_3 with ***C_{oxi}/C*** indicate that carboxyl in organic acids and phenolic groups with higher reactivity toward H are of DOM obtained from composts with higher readily oxidizable carbon with respect to the total carbon content. In the group ii) the first correlation indicates that higher abundance of carboxylic in aminoacids groups (M_1) of DOM is observed in composts with higher capacity to adsorb low molecular weight substances. The second correlation suggests that the higher reactivity of phenolic groups toward H are of DOM obtained from composts with higher abundance of recalcitrant structures.

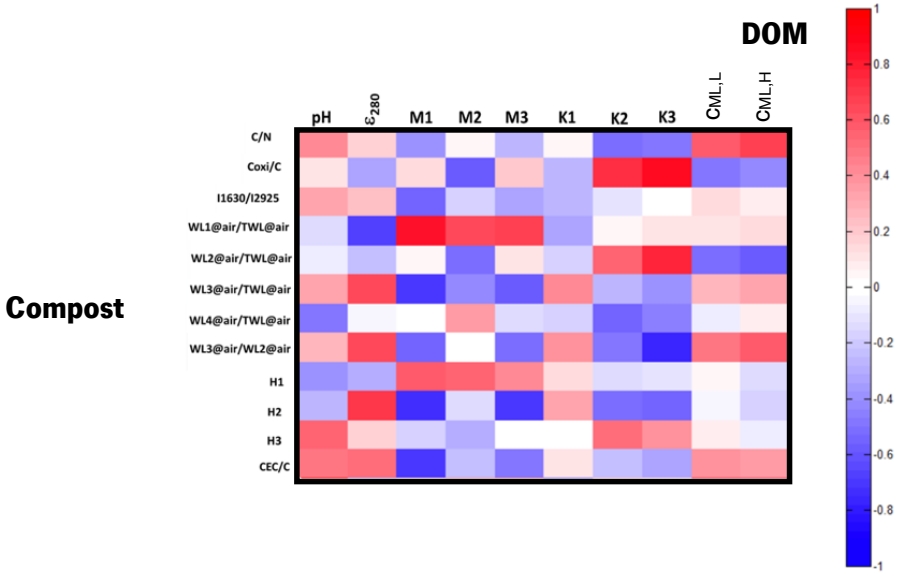

Figure 3.28: Heat map showing the pairwise Pearson correlation coefficients I of the parameters from DOM vs compost.

The negative correlations in group iii) show that the abundance of the carboxylic groups of aminoacids, and therefore of aminoacids, is lower in the composts with higher values of parameters related to the compost maturation (***CEC/C***; ***WL_3@air/TWL@air***; ***H_2***). The negative correlation in

group iv) suggests that the higher reactivity of phenolic groups of DOM toward H are obtained from composts with lower maturation degree.

3.3.2. HS-L vs. compost

Figures 3.29A and 3.29B exhibit the heat maps with the correlation analyses performed using results of the HS-L versus compost with 10 parameters from FA-L and HA-L and 12 from compost (in bold). From these two analyses, 10 correlations were obtained for FA-L and 16 correlations for HA-L with $|r|>0.7$ and that relates parameters of different techniques. The four positive correlations observed for FA-L can be arranged in three groups:

i) M_2 with ***C_{oxi}/C***; M_2 with ***WL_2@air/TWL@air*** ,

ii) ε_{280} with ***WL_3@air/TWL@air***;

iii) H_{aro}/H_{ali} with ***CEC/C***.

Alongside six negative correlations, that can be organised in four groups:

iv) M_1 with ***C/N***;

v) K_1 with ***C_{oxi}/C***; K_1 with ***WL_2@air/TWL@air***;

vi) ε_{280} with ***WL_1@air/TWL@air***; H_{aro}/H_{ali} with ***WL_1@air/TWL@air***;

vii) M_2 with ***WL_3@air/ WL_2@air***.

The positive correlations in group i) indicate that the abundance of phenolic groups toward H of FA-L is higher for composts with higher amount of readily oxidizable carbon that are decomposed in the range 177 and 400 °C. The positive correlation in group ii) shows that the aromaticity of FA-L (evaluated by ε_{280}) is obtained from composts with higher abundance of extra-recalcitrant structures. The aromaticity of FA-L (evaluated by ^{1}H-NMR) is shown to be related to the compost ability to exchange cations *per* carbon content from the correlation iii).

The negative correlation in iv) indicates that abundance of carboxylic groups (M_1) of FA-L is higher in composts with higher content of nitrogen (with respect to carbon). Simultaneously, from v) the carboxyl groups of FA-L with higher reactivity occur in composts with lower content of easily oxidizable structures that are decomposed in the temperature range between 177 and 400 °C.

The correlations in group vi) indicate that the aromaticity in FA-L (evaluated by UV-vis and ^{1}H-NMR) is higher in composts that adsorb lower amounts of low molecular weight structures. The abundance of phenolic groups in FA-L occurs in composts with lower maturation degree (evaluated by ***WL_3@air/ WL_2@air).***

Eleven positive correlations are observed for HA-L among the variables (Figure 3.44B) that can be organised in six groups:

i) H_{aro}/H_{ali} with ***C/N***;

ii) H_1 with $\boldsymbol{C_{oxi}/C}$; H_1 with $\boldsymbol{WL_2@air/TWL@air}$;

iii) ε_{280} with $\boldsymbol{WL_3@air/TWL@air}$; ε_{280} with $\boldsymbol{WL_3@air/WL_2@air}$; $I_{1630/2925}$ with $\boldsymbol{H_2}$

iv) H_2 with $\boldsymbol{WL_3@air/WL_2@air}$; M_2 with $\boldsymbol{WL_3@air/WL_2@air}$;

v) $c_{ML,H}$ with $\boldsymbol{H_2}$; $c_{ML,L}$ with $\boldsymbol{I_{1630/2925}}$; $c_{ML,H}$ with $\boldsymbol{I_{1630/2925}}$;

Simultaneously, the five negative correlations can be organised in 3 groups:

vi) $WL_1@air/TWL@air$ with $\boldsymbol{C_{oxi}/C}$;

vii) $I_{1630/2925}$ with $\boldsymbol{WL_1@air/TWL@air}$;

viii) M_1 with $\boldsymbol{H_1}$ and $c_{ML,L}$ with $\boldsymbol{H_1}$; $c_{ML,L}$ with $\boldsymbol{WL_1@air/TWL@air}$

The positive correlation in the first group shows that the aromaticity of the HA-L (evaluated by ^{1}H-NMR) is higher in composts with lower content of nitrogen (with respect to carbon). The positive correlations in ii) indicate that HA-L ability to adsorb low molecular weight substances is higher for composts with higher amount of readily oxidizable carbon that are decomposed in the range 177 and 400 °C. The correlations in iii) show that the aromaticity of HA-L (evaluated by Uv-vis) is obtained from composts with higher abundance of extra-recalcitrant structures and higher maturation degree. The aromaticity of HA-L (evaluated by ATR-FTIR) is shown to be related to the compost ability to adsorb easily biodegradable aromatic structures. The correlations in iv) indicate that HA-L ability to adsorb easily biodegradable aromatic structure and the HA-L's abundance of phenolic groups toward H are higher from composts with higher maturation degree. Simultaneously, the correlation in v) shows that the strongest and weakest groups that contribute to the higher extent of the binding of Cd^{2+} in HA-L are those present in composts with higher aromaticity (evaluated by ATR-FTIR) and higher capacity to adsorb recalcitrant structures.

The negative correlations in vi) indicate that HA-L is higher for composts with lower amount of readily oxidizable carbon. The correlation in group vii) shows that the aromaticity of HA-L is higher for composts with lower ability to adsorb low molecular weight substances.

The correlations in viii) indicate that the abundance of carboxylic groups (M_1) and the strongest groups that contribute to the extent of the binding of Cd^{2+} in the HA-L ($c_{ML,L}$) are those present in composts with lower ability to adsorb low molecular weight substances (evaluated by $\boldsymbol{H_1}$ and $\boldsymbol{WL_1@air/TWL@air}$).

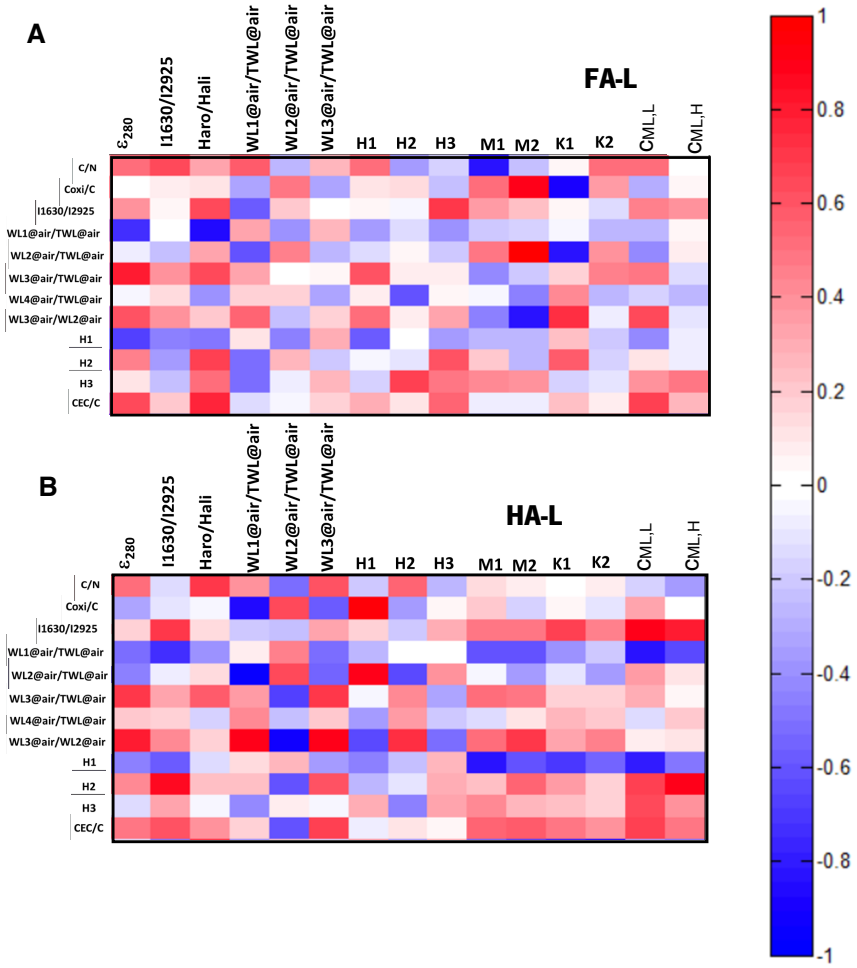

Figure 3.29: Heat map showing the pairwise Pearson correlation coefficients I of the parameters from (A) FA-L and (B) HA-L.

4. References

[1]K. Lasaridi, I. Protopapa, M. Kotsou, G. Pilidis, T. Manios, A. Kyriacou, Quality assessment of composts in the Greek market: The need for standards and quality assurance, Journal of Environmental Management. 80 (2006) 58–65. https://doi.org/10.1016/j.jenvman.2005.08.011.

[2]M. Kucbel, H. Raclavská, J. Růžičková, B. Švédová, V. Sassmanová, J. Drozdová, K. Raclavský, D. Juchelková, Properties of composts from household food waste produced in automatic composters, Journal of Environmental Management. 236 (2019) 657–666. https://doi.org/10.1016/j.jenvman.2019.02.018.

[3]Y.-P. Chin, G. Aiken, E. O'Loughlin, Molecular weight, polydispersity, and spectroscopic properties of aquatic humic substances, Environmental Science & Technology. 28 (1994) 1853–1858. https://doi.org/10.1021/es00060a015.

[4]E. Jamroz, J. Bekier, A. Medynska-Juraszek, A. Kaluza-Haladyn, I. Cwielag-Piasecka, M. Bednik, The contribution of water extractable forms of plant nutrients to evaluate MSW compost maturity: a case study, Sci Rep. 10 (2020) 12842. https://doi.org/10.1038/s41598-020-69860-9.

[5]D.W. Van Krevelen, Graphical-Statistical Method for the Study of Structure and Reaction Processes of Coal, Fuel. 29 (1950) 228–269.

[6]M. Giovanela, J.S. Crespo, M. Antunes, D.S. Adamatti, A.N. Fernandes, A. Barison, C.W.P. da Silva, R. Guégan, M. Motelica-Heino, M.M.D. Sierra, Chemical and spectroscopic characterization of humic acids extracted from the bottom sediments of a Brazilian subtropical microbasin, Journal of Molecular Structure. 981 (2010) 111–119. https://doi.org/10.1016/j.molstruc.2010.07.038.

[7]J.H. See, D.A. Bronk, Changes in C:N ratios and chemical structures of estuarine humic substances during aging, Marine Chemistry. 97 (2005) 334–346. https://doi.org/10.1016/j.marchem.2005.05.006.

[8]M. Fuentes, R. Baigorri, G. González-Gaitano, J.M. García-Mina, The complementary use of 1H NMR, ^{13}C NMR, FTIR and size exclusion chromatography to investigate the principal structural changes associated with composting of organic materials with diverse origin, Organic Geochemistry. 38 (2007) 2012–2023. https://doi.org/10.1016/j.orggeochem.2007.08.007.

[9]J. Pertusatti, A.G.S. Prado, Buffer capacity of humic acid: Thermodynamic approach, Journal of Colloid and Interface Science. 314 (2007) 484–489. https://doi.org/10.1016/j.jcis.2007.06.006.

[10]S. Amir, A. Jouraiphy, A. Meddich, M. El Gharous, P. Winterton, M. Hafidi, Structural study of humic acids during composting of activated sludge-green waste: Elemental analysis, FTIR and 13C NMR, Journal of Hazardous Materials. 177 (2010) 524–529. https://doi.org/10.1016/j.jhazmat.2009.12.064.

[11]G. Ait Baddi, M. Hafidi, J. Cegarra, J.A. Alburquerque, J. Gonzálvez, V. Gilard, J.C. Revel, Characterization of fulvic acids by elemental and spectroscopic (FTIR and ^{13}C-NMR) analyses during composting of olive mill wastes plus straw, Bioresource Technology. 93 (2004) 285–290. https://doi.org/10.1016/j.biortech.2003.10.026.

[12]M.E.F. Silva, L.T.L.T. Lemos, M.M.S.M. Bastos, O.C. Nunes, A.C. Cunha-Queda, Recovery of humic-like susbtances from low quality composts, Bioresource tTchnology. 128 (2013) 624–632. https://doi.org/10.1016/j.biortech.2012.11.013.

[13]A. Hanc, V. Enev, T. Hrebeckova, M. Klucakova, M. Pekar, Characterization of humic acids in a continuous-feeding vermicomposting system with horse manure, Waste Management. 99 (2019) 1–11.

https://doi.org/10.1016/j.wasman.2019.08.032.

[14]M. González Pérez, L. Martin-Neto, S.C. Saab, E.H. Novotny, D.M.B.P. Milori, V.S. Bagnato, L.A. Colnago, W.J. Melo, H. Knicker, Characterization of humic acids from a Brazilian Oxisol under different tillage systems by EPR, ^{13}C-NMR, FTIR and fluorescence spectroscopy, Geoderma. 118 (2004) 181–190. https://doi.org/10.1016/S0016-7061(03)00192-7.

[15]R. Spaccini, A. Piccolo, Molecular characteristics of humic acids extracted from compost at increasing maturity stages, Soil Biology and Biochemistry. 41 (2009) 1164–1172. https://doi.org/10.1016/j.soilbio.2009.02.026.

Chapter 3.4 – Comparison of a variety of physico-chemical techniques in the chronological characterization of a compost from municipal wastes

This chapter was made the characterization of a compost produced from organic urban wastes, at four stages of composting, namely the feedstock material, after one composting cycle, two composting cycles and the final matured compost (Table 2.1). The characterization of the compost samples is presented in two sections. Results obtained from the direct analysis of the compost samples are presented in the 1st section, whereas results from the characterization of the HA-L and FA-L and of the water- soluble extract (obtained from equilibrium solutions), denominated by dissolved organic matter (DOM) are shown in the 2nd section.

The samples were characterized using data from the solid material and three different extracts (HA-L, FA-L and DOM). The compost samples were characterized by EA, CEC, ATR-FTIR, TGA and DSC, on the other hand, the HS-L (HA-L and FA-L) were characterized by EA, UV-vis, ^{1}H-NMR, ATR-FTIR, TGA, DSC and acid-base and metal binding titrations, whereas the DOM was characterized by EA, EC, UV-vis and acid-base and metal binding titrations. The data sets obtained for each sample (including compost, HS-L and DOM), from different techniques, were analysed by the ComDim (Common Dimension) multi-block tool to highlight the ability of each technique to assess the compost evolution.

1. Compost characterization

1.1. Elemental analysis and cation exchange capacity

Elemental characterization of compost, particularly carbon, nitrogen and the carbon to nitrogen ratio (*C/N*) is important for both the feedstock and compost [1]. The monitoring of these parameters at the initial stage of composting is important to control the optimal conditions for microbial growth [2] and to increase the efficiency of composting. As compost is used as a source of nutrients for soil, other parameters, such as sulfur and organic carbon (C_{oxi}, oxidizable carbon) are also commonly characterized [3]. Data from these samples (Figure 3.30A) show a steady decrease for both C and *C/N* values, which is in accordance with the reported results and is related to the CO_2 release during composting. Although a *C/N* value between 20 to 30 is traditionally suggested to ensure that the humification rate proceeds at a high rate [4], the raw material (sample UW_0) has a *C/N* value of 18.6 that is considered low. This value is however higher than 15 which was shown to be acceptable for urban waste mixtures [1].

The cation exchange capacity (*CEC*) is an important parameter for the characterization of organic matter as it is related to the amount of negative charges present at the surface of the solid matrix, that is evaluated from the extent to which cations are exchanged. Although the *CEC* is one of the parameters employed to describe the properties of soils it has also been widely used to monitor the evolution of compost [5]. By comparison of results from CUW_{15} and CUW_{30} with the final matured compost (CUW) (Figure 3.30B), an increase of the *CEC* is observed, as previously described by Harada and Inoko. (1980) [6]. This increase is assigned to the formation of carboxylic and phenolic functional groups that occurs by the humification process [7]. Although this trend is observed in our results for the last 3 samples (CUW_{15}, CUW_{30} and CUW), the uncomposted material (UW_0) exhibited an abnormal high value of *CEC*. The origin of this result may be associated with an initial decrease of the complexing functional groups, due to the occurrence of mineralization reactions that take place at the initial stages of the composting process [8].

1.2. Differential scanning calorimetry and thermogravimetric analysis

The thermal characterization of the samples at the different composting stages was performed by DSC and TGA. The DSC curves (Figure 3.31A) exhibit a minor endothermic process, at the lower temperature limit (close to 100 °C), usually ascribed to dehydration reactions.

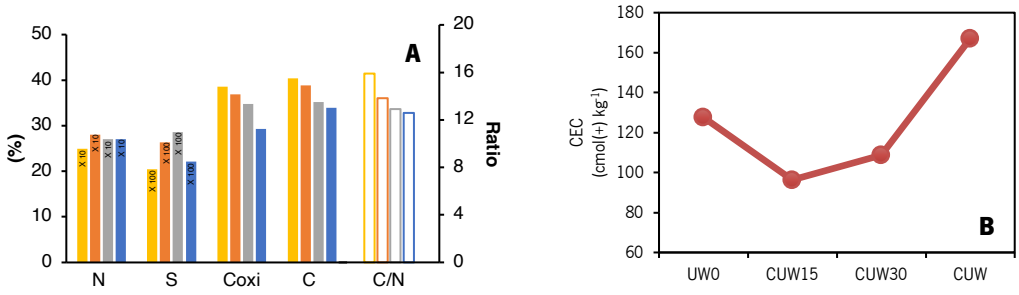

Figure 3.30: (A) Elemental characterization, N, S, C_{oxi}, C and *C/N* and (B) cation exchange capacity, *CEC* of compost samples obtained at different stages of composting: UW_0 (yellow), CUW_{15} (dark orange), CUW_{30} (grey), CUW (blue). For comparison, in Figure A the concentrations of N were multiplied by 10 and for the concentrations of S were multiplied by 100.

Two major regions, corresponding to the overlap of exothermic processes related to the decomposition of recalcitrant and extra-recalcitrant substances, respectively, are also visible. These two exothermic peaks, close to 320 °C and to 500 °C, are characteristic of stabilized organic matter [9]. The DSC curves for the different materials exhibit marked differences in shape and height, nevertheless the values obtained by integration of curves in the three temperature ranges (H_1, H_2, H_3) reveal minor variations (Figure 3.31B). This outcome may be due to the complexity of the materials and of the large number of reactions that take place at close temperatures, making it rather difficult to isolate and quantify the contribution of the separated processes. The value of H_3, the enthalpy of the overlapped processes that take place at the higher temperature range (associated with the decomposition of the extra-recalcitrant structures) is higher than the H_2, corresponding to the processes that take place at temperatures close to 320 °C, associated to the decomposition of the recalcitrant structures, for all the samples. The ratio between these two enthalpy values H_3/H_2 gradually increases (Figure 3.31B) and therefore we propose the use of this ratio as an additional parameter for monitoring the composting progress.

The TGA curves and the corresponding DTG curves from the samples at different stages of composting recorded under an atmosphere of air and N_2 are shown in Figure 3.32A and 3.32B, respectively. Although the air atmosphere is more frequently used for the characterization of compost and soil, we performed the thermal characterization under air and N_2 atmospheres in order to get information on the relative importance of the oxidative reactions in the decomposition process.

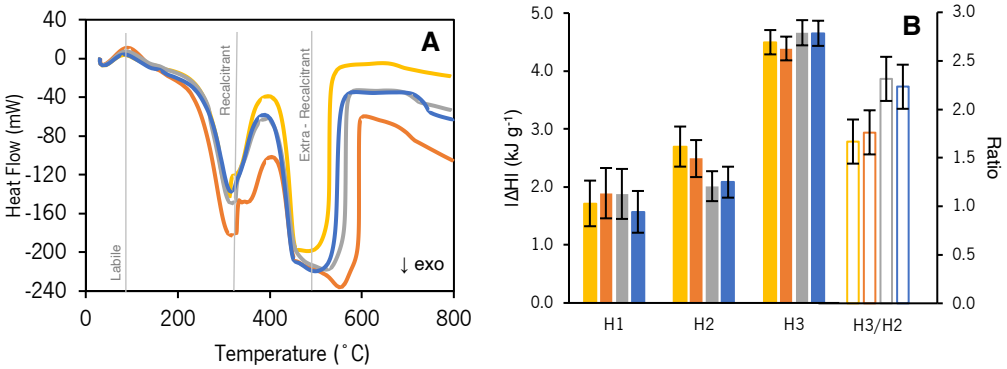

Figure 3.31: (A) DSC curves and (B) Enthalpies values (H_1, H_2, H_3) obtained from 3 temperature ranges and ratio of enthalpies H_3/H_2 for the samples UW_0 (yellow), CUW_{15} (dark orange), CUW_{30} (grey), CUW (blue). The values represented for H_1 were multiplied by 10.

The TGA curves recorded under the air atmosphere contain three main weight loss processes, WL_2 (177 - 400 °C), WL_3 (400 - 620 °C) and WL_4 (620 - 800 °C) and a secondary one at the limit of the lower temperatures, WL_1 (30 - 177 °C). Where the decomposition processes related to WL_2 and WL_3 can be associated to the enthalpy values H_2 and H_3 from the recalcitrant and extra-recalcitrant matter. Regarding the total weight loss, there is a gradual decrease of this quantity throughout composting, which results in an increase in the final residue recovered from the TGA experiments performed in both atmospheres. This trend is expected due to the stabilization of the organic matter that takes place during the composting process. A more detailed analysis of the TGA results can be performed by means of the corresponding DTG curves (Figure 3.32A) that exhibit wide and not symmetrical peaks for each of the four processes, particularly the 3rd peak that is rather bumpy. This outcome indicates that these processes result from the overlap of more than one single process. The values of weight loss from the four regions above identified are displayed in Table 3.13. The values of WL_1 (associated to dehydration and desorption processes) and WL_3 (related to the degradation of complex aromatic structures, such as lignin, complex aromatic structures, and humic substances) [10] do not show a notable variation considering the uncertainty associated with these results. The steadiness of WL_3 may result from the fact that the decrease of the extent of the degradation of the uncomposted matter (such as aromatic structures and lignins) is compensated by an increase of the extent of the thermal decomposition of the composted matter (such as humic-like complex structures). The values of WL_2 and WL_4 show a steady variation. The decrease of WL_2 is related with a progressive decrease of the easily biodegradable aromatic structures (carbohydrates moieties and aliphatic compounds) [10], while the increase of WL_4 is due to the formation of inorganic species, such as carbonates [10,11]. The ratio WL_3/WL_2, that can be taken as a measure of the relative amount of the thermally more stable fraction of organic matter compared to the least stable [12] was

calculated and is depicted in Table 3.13. This ratio shows a continuous increase during composting that is mainly associated with the decrease of *WL_2*.

The profile of the TGA curves under N_2 atmosphere appear to be less complex than those obtained under air atmosphere (Figure 3.32B). Nevertheless, the corresponding DTG curves (Figure 3.32B) display the same number of regions observed for the TGA in air, with a significant overlap between the 2nd and the 3rd processes. Furthermore, the shape of the derivate curve of the 3rd process is narrower, indicating that the number of processes occurring at this temperature range may be fewer. The nature of the atmosphere used to record the TGA significantly affected the relative height of the 2nd and 3rd peaks and the position of the 4th process (that occurs at lower temperatures for the N_2 atmosphere). The evaluation of *WL_3* from the TGA obtained under N_2 atmosphere is difficult, particularly for the UW_0 and CUW_{15}, as the peaks corresponding to the 2nd and 3rd regions are quite overlapped. The values of *WL_4* under N_2 atmosphere seem to be rather constant (Table 3.13).

Table 3.13: Weight losses values (% of dry sample) from the main processes during the thermal degradation of the samples (UW_0, CUW_{15}, CUW_{30} and CUW) in air and N_2 atmospheres and values of the ratios *WL_3@air/WL_2@air, WL_3@N_2/WL_2@N_2, WL_3@N_2/WL_3@air*.

Parameter	UW_0	CUW_{15}	CUW_{30}	CUW
WL_1@air (%)	7.8 ± 2.0	8.8 ± 2.3	9.3 ± 2.4	9.4 ± 2.4
WL_2@air (%)	43 ± 3.4	40 ± 3.1	32 ± 2.5	28 ± 2.2
WL_3@air (%)	28 ± 2.5	29 ± 2.5	29 ± 2.6	27 ± 2.4
WL_4@air (%)	2.1 ± 0.6	2.2 ± 0.7	3.4 ± 1.0	7.4 ± 2.2
Res@air (%)	18 ± 1.2	20 ± 1.3	25 ± 1.7	28 ± 1.8
WL_3@air/WL_2@air	0.64 ± 0.08	0.72 ± 0.08	0.91 ± 0.11	0.96 ± 0.11
WL_1@N_2 (%)	6.8 ± 1.8	1.7 ± 0.4	2.4 ± 0.6	4.9 ± 1.3
WL_2@N_2 (%)	38 ± 2.9	50 ± 3.9	36 ± 2.8	20 ± 1.5
WL_3@N_2 (%)	13 ± 1.2	7.0 ± 0.6	7.0 ± 0.6	27 ± 2.3
WL_4@N_2 (%)	5.9 ± 1.8	5.8 ± 1.8	4.6 ± 1.4	10 ± 3.1
Res@N_2 (%)	36 ± 2.4	37 ± 2.4	50 ± 3.2	38 ± 2.5
WL_3@N_2/WL_2@N_2	0.35 ± 0.04	0.13 ± 0.02	0.20 ± 0.02	1.34 ± 0.16
WL_3@N_2/WL_3@air	0.47 ± 0.06	0.23 ± 0.03	0.24 ± 0.03	0.99 ± 0.12

The value of *WL_3/WL_2* obtained from TGA data under N_2 atmosphere displays a larger increase from CUW_{15} to CUW. The abnormally high value obtained for UW_0 may result from the difficulties associated with the

measurement of WL_3 and WL_2, due to the large overlap of these two processes for the samples at the early stages of composting (UW_0 and CUW_{15}).

The comparison of results obtained under both atmospheres (N_2 and air) is highlighted in Figure 3.32C.

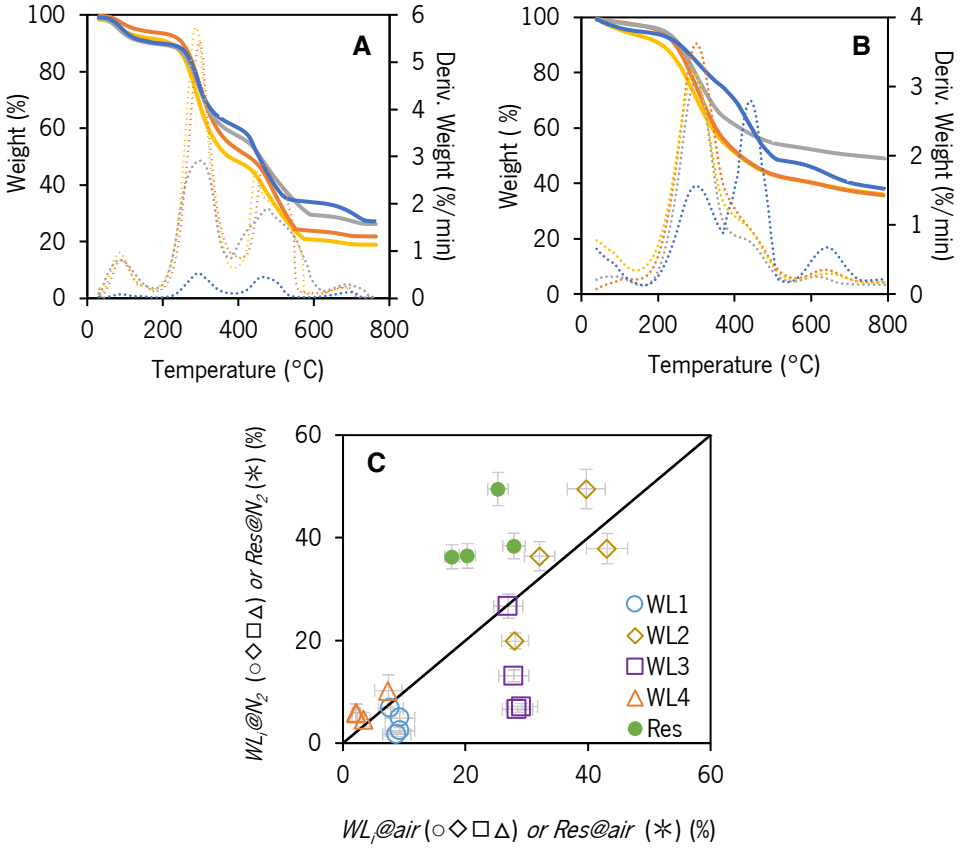

Figure 3.32: TGA and DTG curves obtained in (A) air and (B) N_2 atmospheres for solid compost. (C) Comparison of TGA data obtained under the atmospheres of N_2 and air with error bars. Results of samples from different stages of composting: UW_0 (yellow), CUW_{15} (dark orange), CUW_{30} (grey), CUW (blue).

As most of the data points of the weight loss values (open symbols) are found below the y=x line, indicating that the decomposition extent tends to be larger in the presence of oxygen, the values of the residue (full symbols) of all samples are larger for the N_2 atmosphere. Besides, the value of the residue of CUW in air displays the lower distance to the y=x line. The presence of higher amounts of oxygen structures in this sample may justify that the extent of its thermal decomposition by pyrolysis is like that from combustion. As the values of WL_1 are larger under the air atmosphere, this process should result from the overlay of processes such as the endothermic processes of dehydration and desorption (as previously discussed) via oxidative pathways. With respect to WL_3, that corresponds to the thermal decomposition of the most stabilized organic matter, significantly higher values were obtained for all samples in the presence of oxygen, except for CUW, whose point is located over this line. This result indicates that the thermal

decomposition of CUW, that has undergone extensive oxidation reactions, may take place by pyrolysis. The value of WL_3, that results from the decomposition of uncomposted and composted matter, depends significantly on the nature of the TGA atmosphere. While WL_3 in N_2 varies significantly, in air it is almost constant. Under the N_2 atmosphere, WL_3 should mainly be due to the decomposition of the composted matter by pyrolysis, that increases throughout composting, in opposition to air, where the weight loss may include the contribution of the combustion of uncomposted and composted matter. The values of WL_2 and WL_4 obtained under the two atmospheres are rather similar, indicating that the thermal decomposition of the easily biodegradable aromatic structures and of inorganic carbonates occurs to a similar extent. Following this reasoning, we proposed a ratio between the values of WL_3 obtained in the two atmospheres (Table 3.13). The ratio for CUW is the highest, close to 1, while samples CUW_{15}, CUW_{30} display values that are much lower, both close to 0.2. Although the expected ratio for the starting material (UW_0) was lower than 0.2, a value of 0.5 was obtained. This result can be due to the difficulty of measuring WL_3 from the TGA obtained under N_2 atmosphere due to the overlap of the processes 2 and 3, particularly for UW_0.

1.3. ATR-FTIR spectroscopy

The ATR-FTIR spectroscopy is recurrently used to characterize compost samples, as the corresponding spectra exhibit features that are related to the presence of functional groups that are directly involved in the humification process. Using absorption intensity ratios at characteristic wavenumbers, three empiric parameters, designated by aromaticity indexes, were defined to account for the increase of the amount of aromatic moieties and the simultaneous decrease of aliphatic structures in the humified organic matter [13]. The ATR-FTIR spectra of the samples obtained at different stages of composting are shown in Figure 3.33. The spectra of the samples obtained at different stages of composting shows important features that are present in all samples, namely: a band at 3320 cm^{-1} that can be ascribed to C-H bonds and to O-H of alcohols, phenols or O-H carboxyl and also to N-H vibrations in amide functions [14]; two characteristic bands at 2925 and 2845 cm^{-1} that may be attributed to asymmetric and symmetric vibrations of C-H stretching of CH_3 and CH_2 groups [15]; a band centred at around 1640–1630 cm^{-1} that may be attributed to aromatic C=C and C=O stretching of amide groups and quinonic C=O and/or C=O of H-bonded conjugated ketones [14]; a band at 1540 cm^{-1} that may be ascribed to secondary amides [14]; two bands between 1440 and 1420 cm^{-1} that can be associated to the O-H deformation and C-O stretching of carboxylic group, C-H deformations of CH_3 and CH_2 groups and/or asymmetric stretching of

COO^- groups [16]; and a band at around 1020 cm^{-1} that may be due to the combination of C-O stretching of polysaccharides, in addition to Si-O-Si bonds of silica and to the group Si-O-C [14].

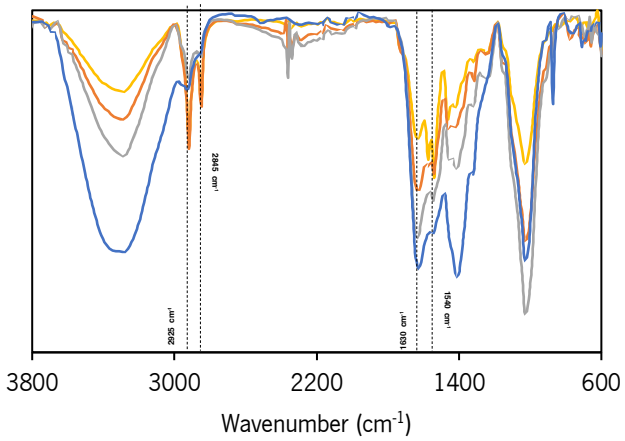

Figure 3.33: ATR-FTIR spectra of the compost samples collected at different times of the composting process: UW_0 (yellow), CUW_{15} (dark orange), CUW_{30} (grey), CUW (blue).

Using the absorption intensity values of the most significant bands of the ATR-FTIR spectra (2915, 2845, 1630 and 1540 cm^{-1}) associated to aliphatic and aromatic moieties, three ratios were calculated to define the aromaticity indexes [13]: $I_{1630/2925}$, $I_{1630/2845}$ and $I_{1540/2925}$. The values of these ratios increase throughout the composting process (Table 3.14), associated to a net increase of the aromaticity degree of the chemical structures related to the formation of HS-L, such as HA-L and FA-L, and the decomposition/transformation of aliphatic components such as polysaccharides and alcohols. These ratios are regarded as indicators of maturity and stability of the organic matter in transformation [17].

Table 3.14: Aromaticity indexes of the samples, UW_0, CUW_{15}, CUW_{30} and CUW, calculated from FTIR characteristic peak wavenumbers.

Parameter	UW_0	CUW_{15}	CUW_{30}	CUW
$I_{1630/I2925}$	0.91	1.44	3.69	3.40
$I_{1630/I2845}$	1.30	2.03	6.32	19.8
$I_{1540/2925}$	0.71	1.16	1.67	2.34

2. Characterization of the extracts of HS-L and DOM

2.1. Equilibrium solutions physico-chemical characterization

Values of the dissolved organic carbon (*DOC*), electrical conductivity (*EC*) and pH, are reported in Table 3.15. The values of *DOC* show a marked decrease when the feedstock material (UW_0) is compared with the matured compost (CUW). This effect is identical to the previously reported by Wang et al. (2014) [18] and is attributed to the degradation of easily biodegradable organic matter, especially carbohydrates, organic acids and hemicellulose. The *EC* of the DOM extract also tends to decrease, with the most pronounced variation occurring during the first cycle of composting. The *pH* values show an increasing trend throughout the composting process, of about 0.4 units after the first cycle of the composting process, followed by an increase of approximately one unit, in the second cycle. The maturation process does not seem to significantly affect this parameter.

Table 3.15: Physico-chemical parameters of the equilibrium solutions from the samples UW_0, CUW_{15}, CUW_{30} and CUW.

Parameter	UW_0	CUW_{15}	CUW_{30}	CUW
DOC (mg L^{-1})	1187	429	430	548
C_{ox} (%)	6.2	2.3	2.5	3.7
Cl^- (mg L^{-1})	415	352	579	392
F^- (mg L^{-1})	0.12	0.08	0.08	0.18
SO_4^{2-} (mg L^{-1})	43.1	30.0	22.8	105
PO_4^{3-} (mg L^{-1})	110	80.4	60.3	29.5
NO_2^- (mg L^{-1})	1.71	2.72	4.18	3.94
NO_3^- (mg L^{-1})	2.56	1.05	1.28	5.21
NH_4^+ (mg L^{-1})	10.8	13.2	10.1	7.78
NH_4^+/NO_3^-	4.22	12.56	7.85	1.49
pH	6.41	6.81	7.93	7.69
EC (µs cm^{-1})	3870	3030	3300	2840

2.2. HS-L physico-chemical characterization

Considering that the organic matter humification occurs throughout composting, the amount of FA-L and HA-L extracted should increase from UW_0 to CUW. Furthermore, a negligible amount of these substances should be isolated from the feedstock material (UW_0). This idea arises from the results previously described from the compost samples characterization that clearly showed an increase in both, the

stabilization of organic matter and the chemical functions that are typical of HS-L throughout composting. However, a significant amount of FA-L and HA-L was found in UW_0 as compared to the matured compost, CUW. The yield increases from 2.2 g kg^{-1} (UW_0) to 3.3 g kg^{-1} (CUW) for FA-L and exhibits an unexpected decrease from 33.1 g kg^{-1} (UW_0) to 21.1 g kg^{-1} (CUW) for HA-L (Table 3.16). This atypical variation of HA-L and FA-L yields seems to indicate that the extraction/purification process (that was originally developed and optimized for soils) does not provide sufficient selectivity for isolating the HA-L and FA-L from fresh or not completely degraded biowastes. The carbon content of HA-L and FA-L shows a decrease throughout composting, with values between 52.2 % and 40.8 % for FA-L and 59.8 % and 54.5 % for HA-L (Table 3.16).

Table 3.16: Elemental characterization of the HA-L and FA-L extracted from the samples UW_0, CUW_{15}, CUW_{30} and CUW.

Parameter		**UW_0**	**CUW_{15}**	**CUW_{30}**	**CUW**
C (%)	HA-L	59.8	54.4	54.6	54.5
	FA-L	52.2	52.3	50.3	40.8
N (%)	HA-L	5.45	5.44	5.64	6.74
	FA-L	6.16	5.17	4.25	4.37
H (%)	HA-L	7.97	6.9	5.75	6.14
	FA-L	6.17	6.1	5.65	6.02
S (%)	HA-L	0.69	0.9	0.91	0.91
	FA-L	0.97	0.77	1.05	0.96
O (%)	HA-L	26.1	32.4	33.1	31.7
	FA-L	34.6	35.7	38.8	47.8
C/N	HA-L	13	12	11	9.4
	FA-L	9.9	11.8	13.8	10.9
O/C	HA-L	0.33	0.45	0.45	0.44
	FA-L	0.5	0.5	0.6	0.9
H/C	HA-L	1.6	1.5	1.3	1.4
	FA-L	1.4	1.4	1.3	1.8
Yield (g kg^{-1})	HA-L	33.1	19.8	21.9	21.1
	FA-L	2.2	2.7	2.4	3.3

The atomic ratios of *C/N*, *O/C* and *H/C* from the FA-L and HA-L extracted from the compost samples at different stages of composting are presented in Table 3.16. The observed variations are similar to those reported in previous studies [19]. The increase of *O/C* ratio, that is more pronounced for FA-L extracts, can be related to the increase of the oxygen containing moieties such as carboxylic and phenolic compounds [20]. The *H/C* ratio remains almost constant and does not seem to provide any information regarding the reactions that are taking place. The *C/N* ratio does not show a systematic decrease for the extracted FA-L and HA-L as for the corresponding compost samples (Table 3.16), particularly for the FA-L extracts where there is a tendency for an increase between UW_0 and CUW_{30}. This result can relate to

the lack of selectivity of the extractions, considering that other organic substances may have been extracted besides HS-L, especially in the samples where HA-L or FA-L exists in small amounts.

2.3. Differential scanning calorimetry and thermogravimetric analysis of HS-L

DSC thermal characterization of FA-L and HA-L extracts from compost samples at different composting stages are presented in the supplementary material. The qualitative behaviour of the HS-L is similar to that of the compost. The DSC curves (Figures 3.34A and 3.34B) from the different materials exhibit marked differences in shape and height, leading to major variations in the values obtained by integration of the curves in the three temperature ranges (Figures 3.34C and 3.34D). This result may be due to the complexity of the extracted material and the large number of reactions that take place at close temperatures, making it rather difficult to isolate and quantify the contribution of each process.

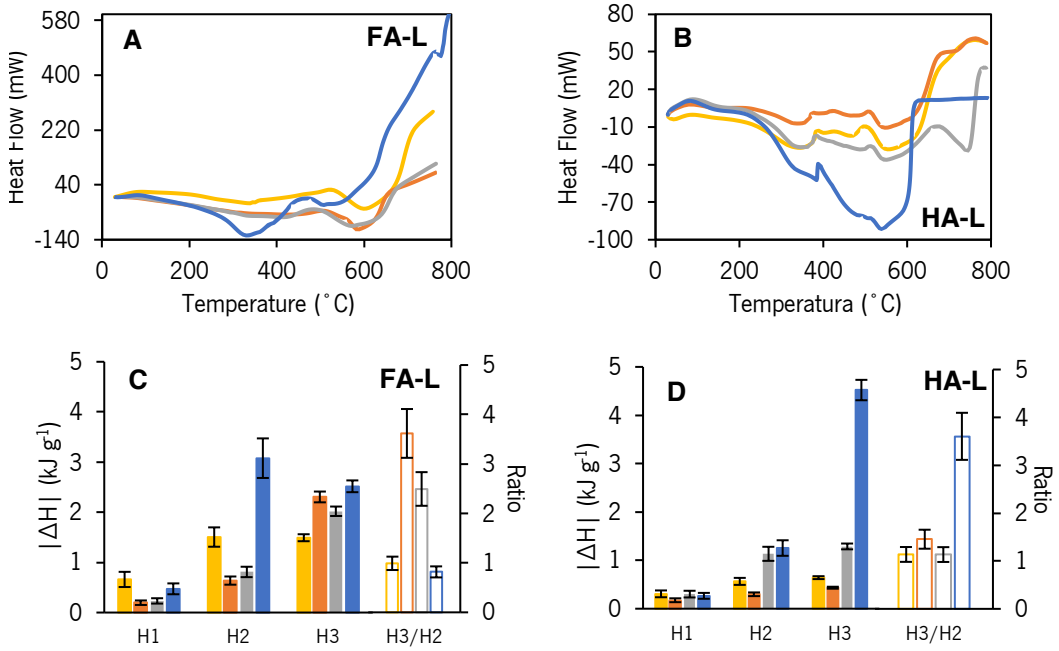

Figure 3.34: (A, B) DSC curves and (C, D) Enthalpies values (H_1, H_2, H_3) obtained from 3 temperature ranges and ratio of enthalpies H_3/H_2; of the (A, C) fulvic-like acid and (B, D) humic-like acid extracted from compost samples: UW_0 (yellow), CUW_{15} (dark orange), CUW_{30} (grey), CUW (blue).

For FA-L samples the enthalpy associated with the decomposition of the recalcitrant substances (H_2) was higher than in case of HA-L (Figures 3.34C and 3.34D). This indicates that FA-L has a higher number of polar and oxygen-containing functional groups compared to HA-L. The enthalpy associated with the decomposition of the extra-recalcitrant substances (H_3) was higher for FA-L samples than for HA-L

samples, apart from CUW. This fact may seem to be unexpected, due to the higher amount of nitrogen and aromatic structures in HA-L samples [21].

The TGA and the corresponding DTG curves of both FA-L and HA-L (Figures 3.35A and 3.35B) display two major processes and a secondary one at the lower temperatures. For the first temperature range (30 - 177 °C) the increase of WL_1 with the composting time is not meaningful considering the uncertainty associated with these results. The values of WL_2 (177 - 400 °C) tend to decrease with the composting time, indicating a progressive decomposition of simple and labile organic structures such as functional groups (carboxylic, methylene, alcohol, aldehydes, amides, amines and phenol groups), C-O of polysaccharides and simple aromatic bonds (biodegradable components) [21]. Simultaneously, the values of WL_3 (400 - 620 °C) tend to increase with the composting time, due to the increase of the amount of nitrogen-containing structures, long chain of hydrocarbons, refractory structures, aromatic, polyaromatic and polyheterocyclic structures, as well as C-C bond cleavage [21].

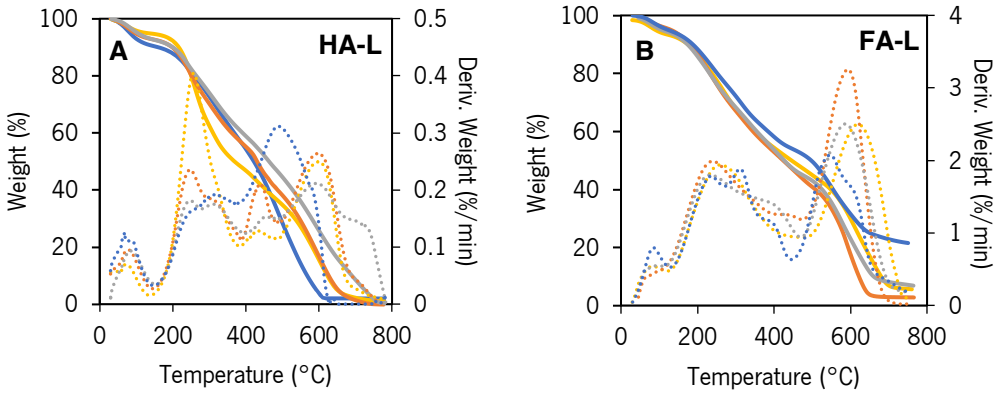

Figure 3.35: TGA and DTG curves obtained in air atmosphere for: (A) HA-L and (B) FA-L. Results of samples from different stages of composting: UW_0 (yellow), CUW_{15} (dark orange), CUW_{30} (grey), CUW (blue).

Regarding the results from FA-L (Table 3.17), it is difficult to define a trend for the variation throughout composting (for each temperature range). In opposition, the results of the weight loss, WL_2, of HA-L show a decrease throughout composting, that is followed by the increase of WL_3. The increase of the residue is also a significant result indicating that it may be a consistent indicator of the increase of chemical stability of the HA-L and FA-L produced by composting.

Table 3.17: Weight losses values (% of dry sample) from the main processes during the thermal degradation of the HA-L and FA-L extracts of the samples (UW_0, CUW_{15}, CUW_{30} and CUW) in air atmosphere and value of the ratio *WL_3@air/WL_2@air*.

Parameter		UW_0	CUW_{15}	CUW_{30}	CUW
WL_1@air (%)	HA-L	4.1 ± 1.1	5.5 ± 1.4	5.2 ± 1.4	10 ± 2.6
	FA-L	2.5 ± 0.65	3.7 ± 1.0	2.7 ± 0.7	6.4 ± 1.7
WL_2@air (%)	HA-L	48 ± 3.7	28 ± 2.1	31 ± 2.4	31 ± 2.4
	FA-L	44 ± 3.4	47 ± 3.7	49 ± 3.8	38 ± 3.0
WL_3@air (%)	HA-L	46 ± 4.0	61 ± 5.4	56 ± 4.9	57 ± 5.0
	FA-L	48 ± 4.3	45 ± 4.0	42 ± 3.7	36 ± 2.9
Res@air (%)	HA-L	1.2 ± 0.08	5.5 ± 0.36	6.4 ± 0.42	2.0 ± 0.13
	FA-L	4.1 ± 0.3	2.6 ± 0.2	6.1 ± 0.4	22 ± 1.4
WL_3@air/WL_2@air	HA-L	1.0 ± 0.1	2.2 ± 0.23	1.8 ± 0.17	1.8 ± 0.22
	FA-L	1.1 ± 0.13	1 ± 0.1	0.9 ± 0.1	0.9 ± 0.1

2.4. UV-vis, ^{1}H-NMR and ATR-FTIR spectroscopy

The molar absorptivity coefficient at 280 nm, ε_{280} obtained for FA-L, HA-L and DOM was calculated from absorptivity data. The increase of this parameter throughout the composting process (Table 3.18) is related to the increase of the aromaticity of the extracts obtained throughout composting [22].

Table 3.18: The absorptivity coefficient ε_{280} obtained for FA-L, HA-L and DOM of the samples UW_0, CUW_{15}, CUW_{30} and CUW.

Parameter		UW_0	CUW_{15}	CUW_{30}	CUW
ε_{280} (L molC^{-1} cm^{-1})	HA-L	212	293	366	513
	FA-L	186	233	358	419
	DOM	75.5	166	237	280

^{1}H-NMR spectroscopy is a tool that can be used successfully to characterize the content and relative abundance of various chemical groups of HA-L and FA-L. Based on qualitative analysis, the ^{1}H-NMR spectra of HA-L and FA-L were subdivided into five chemical shift regions, reflecting the signals associated to specific functional groups: δ 0 – 3.0 for C-alkyl and N-alkyl protons, δ 3.0 – 4.5 for O-alkyl including phenolic O-alkyl protons, δ 4.7– 5.0 for H_2O protons, δ 5.0 – 6.0 for the protons of alkenes and CH_2 groups linked to the aromatic ring and δ 6.0 – 9.0 ppm for alkene and aromatic protons. The relative areas of those signals, directly correlated to the number of protons that are present in that particular environment of the chemical entity are summarized in Table 3.19. The ^{1}H-NMR spectra were obtained from D_2O/NaOD solutions and the intense water peak that is always observed, reflects not only the water molecules retained by each sample but also those generated by D_2O exchange with the labile protons from carboxylic acids, phenols, and amines present in the molecular assemblies. For FA-L, the mole ratio of aliphatic versus aromatic protons (Table 3.19) increases slightly at the beginning of the composting

process, and this can be due to a slight increase in the size of the alkyl chains, associated with a small decrease in the aromatic protons. This decrease may result from oxidation processes in the aromatic chains, more evident during maturation. The comparative analysis of the number of moles of protons in aliphatic carbon chains and in carbons adjacent to the oxygen atom shows a minor reduction in the beginning of the composting process (after 15 days). It remains practically unchanged, recovering the initial values at the end of the maturation process. For HA-L, the molar ratio of aliphatic versus aromatic protons (Table 3.19) steadily decreases during the composting process, which can result from the fragmentation of long carbon chains to generate progressively shorter units, with the subsequent loss of soluble small fragments. This trend seems to proceed during maturation to generate the final compost. This reduction in the length of the alkyl chains in HA-L is also supported by the reduction in the ratio of the number of hydrogen atoms in these alkyl chains, when compared to the number of hydrogen atoms in carbons adjacent to oxygen, responsible for signals between 3 and 4.5 ppm in the ^{1}H-NMR spectrum. The molecular ratio of water molecules (Table 3.19), when compared with the total number of aliphatic and aromatic protons, shows a marked increase for HA-L after 15 days of maturation, with minor alterations after this initial process.

Table 3.19: Ratio of aliphatic versus aromatic protons in fulvic-like acids (FA-L) and humic-like acids (HA-L), along the maturation process, based on ^{1}H-NMR data. Ratio of water protons versus aliphatic and aromatic protons in FA-L and HA-L, according to the ^{1}H-NMR data, reflecting their capacity to retain water molecules.

Chemical shifts intervals	**δ 0 – 4.5 ppm**		**δ 4.7 - 5 ppm**		**δ 5 - 9 ppm**		**Ratio Aliphatic/Aromatic protons**		**Ratio H_2O/ Aliphatic + Aromatic protons**	
Functional groups	Aliphatic protons		H_2O		Aromatic protons					
Samples	**FA-L**	**HA-L**	**FA-L**	**HA-L**	**FA-L**	**HA-L**	**FA-L**	**HA-L**	**FA-L**	**HA-L**
UW_0	7.8	33	91	64	1.3	3.8	6.0	8.7	10	1.7
CUW_{15}	9.6	11	89	87	1.5	1.5	6.4	7.3	8.0	7.0
CUW_{30}	7.0	16	92	81	1.1	2.4	6.4	6.7	11	4.4
CUW	5.0	13	94	85	0.90	2.7	5.6	4.8	16	5.4

In contrast, FA-L shows a decrease in the ratio of water molecules versus aliphatic and aromatic protons after 15 days of maturation, followed by a significant increase during the final maturation period and the composting process. This demonstrates the high capacity of FA-L to retain water molecules in the compost material.

The ATR-FTIR spectra of the HA-L and FA-L extracts are shown in Figures 3.36A and 3.36B. The information contained in these spectra is relevant regarding the monitoring of composting. The spectra display absorption bands typical of the FA-L and HA-L extracts. Those adsorption bands were identified considering previous studies [23–25].

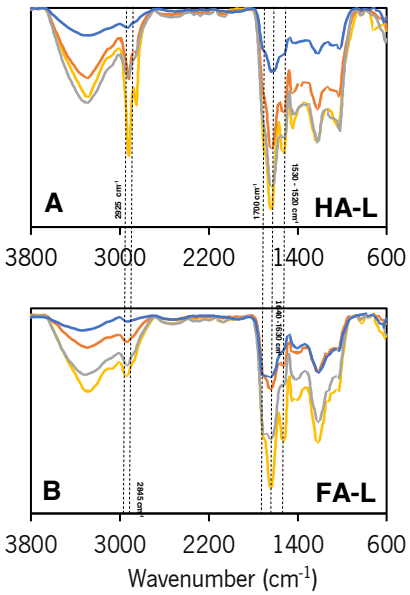

Figure 3.36: ATR-FTIR spectra of the (A) HA-L and (B) FA-L extracts collected at different times of the composting process: UW_0 (yellow), CUW_{15} (dark orange), CUW_{30} (grey), CUW (blue).

Same intensity ratios as indicated for compost, $I_{1630/2925}$, $I_{1630/2845}$ and $I_{1530/2925}$ were used for HS-L (Table 3.20). The values of the three ratios obtained for the HA-L extracts increase throughout composting, suggesting that the extracted substances exhibit an increase of aromatic moieties and/or a decrease of aliphatic moieties. The values of these ratios for the FA-L extracts did not follow a regular trend. The values from the samples at the initial stages of composting even display a decrease. A significant increase of the ratios $I_{1630/2845}$ and $I_{1630/2925}$ was only observed for the last stage of composting, associated with the maturation stage. In opposition, the ratio $I_{1530/2925}$ did not change significantly along the entire process. This rather irregular variation throughout composting has already been reported by Amir et al. (2010) [19] and shows that these indexes may exhibit some limitations for the monitoring of the composting process.

Table 3.20: Aromaticity indexes of the HA-L and FA-L extracts of the samples UW_0 and CUW_{15}, CUW_{30} and CUW.

Parameter		UW_0	CUW_{15}	CUW_{30}	CUW
$I_{1630/12925}$	HA-L	1.6	2	2.5	4.7
	FA-L	2.7	2	2.1	7.6
$I_{1630/12845}$	HA-L	2.7	3	3.8	4.3
	FA-L	3.5	4.8	3.1	9.1
$I_{1540/2925}$	HA-L	1	0.75	1.4	2
	FA-L	1.8	1.3	1.3	1.3

2.5. Acid-base titrations

The acid-base properties of HA-L, FA-L and DOM extracts were performed by potentiometric titrations and discussed in detail by López et al. (2021) [26]. This method enables to estimate relevant physico-chemical parameters, such as the protonation constant, K_i, and the abundance, M_i, of functional groups. The values of these parameters for the FA-L and HA-L extracts and DOM throughout composting (Table 3.21) were calculated by fitting the Equations 3.7 and 3.8 to the experimental data [26].

$$Q = Q_0 + \frac{M_1}{1 + (K_1[H^+])^{m_1}} + \frac{M_2}{1 + (K_2[H^+])^{m_2}} \quad \text{(Equation 3.7)}$$

$$Q = Q_0 + \frac{M_1}{1 + (K_1[H^+])} + \frac{M_2}{1 + (K_2[H^+])} + \frac{M_3}{1 + (K_3[H^+])} \quad \text{(Equation 3.8)}$$

where K_i is the protonation constant of the different groups, M_i is the abundance of each type of acid site, and Q_0 is the charge due to occupation of the acid sites by cations that must be displaced by protonation. The acid-base properties of HA-L, FA-L and DOM extracts were performed by potentiometric titrations and discussed in detail by López et al. (2021) [26]. This method enables to estimate relevant physico-chemical parameters, such as the protonation constant, K_i, and the abundance, M_i, of functional groups.

Table 3.21: Acid-base parameters of the HA-L, FA-L and DOM from samples obtained by fitting Equations 3.1 and 3.2 to experimental data at 0.1 mol L^{-1} in KNO_3.

Parameter		UW_0	CUW_{15}	CUW_{30}	CUW
M_1(mmol/g_{HS-L})	HA-L	2.2 ± 0.05	2.3 ± 0.05	2.7 ± 0.07	2.9 ± 0.18
	FA-L	2.4 ± 0.09	3.4 ± 0.03	3.6 ± 0.02	3.7 ± 0.05
M_1(mmol/$g_{compost}$)	DOM	0.42 ± 0.01	0.05 ± 0.01	0.03 ± 0.01	0.06 ± 0.01
M_2(mmol/g_{HS-L})	HA-L	1.1 ± 0.3	1.2 ± 0.2	1.2 ± 0.3	1.8 ± 0.5
	FA-L	2.2 ± 0.2	1.6 ± 0.1	1.5 ± 0.07	1.5 ± 0.2
M_2(mmol/$g_{compost}$)	DOM	0.16 ± 0.01	0.24 ± 0.01	0.25 ± 0.01	0.18 ± 0.01
M_3(mmol/$g_{compost}$)	DOM	0.27 ± 0.01	0.22 ± 0.01	0.21 ± 0.01	0.19 ± 0.01
log K_1	HA-L	6.1 ± 0.04	5.3 ± 0.03	5.2 ± 0.04	4.7 ± 0.06
	FA-L	4.2 ± 0.01	4.3 ± 0.01	4.1 ± 0.01	4 ± 0.02
	DOM	4.5 ± 0.01	3.99 ± 0.05	3.57 ± 0.07	3.69 ± 0.03
log K_2	HA-L	10.2 ± 0.32	9.9 ± 0.2	9.9 ± 0.4	9.7 ± 0.2
	FA-L	8.4 ± 0.05	9.1 ± 0.08	9.5± 0.07	9.4 ± 0.2
	DOM	6.05 ± 0.01	6.54 ± 0.01	6.65 ± 0.01	6.51 ± 0.01
log K_3	DOM	9.73 ± 0.01	10.06 ± 0.01	10.08 ± 0.01	10.11 ± 0.01

Two types of acid sites, carboxylic-type, K_1 and phenolic-type, K_2 were identified for HA-L and FA-L extracts (Figures 3.37A and 3.37B). The abundance of the carboxylic groups, M_1, showed a significant increase for both extracts, whereas the abundance of phenolic groups, M_2, increased for HA-L and decreased for FA-L. The decrease of M_2 for FA-L, can be a consequence of a more effective oxidation of the phenolic groups to the corresponding carboxylic acids comparatively to the rate of formation of new phenolic groups. The decrease of the pK_1 values (from 6.09 to 4.43 for HA-L and from 4.24 to 3.99 for FA-L) may be directly related to the rise of the number of aromatic structures. With respect to pK_2 this effect is also found for the HA-L extracts, decreasing from 10.17 to 9.81. For the FA-L extracts an increase was observed for pK_2 values from 8.38 to 9.38. The three types of sites were identified for DOM corresponding to: i) carboxylic groups in amino acids, ii) carboxylic groups in organic acids and iii) phenolic hydroxyl groups, hydroxyl in carbohydrate units and amino groups from amino acids (Figure 3.37C). The variation trend of the acidity constants and abundance of the acidic groups is not constant throughout composting. The large value of M_1 obtained in UW_0 can be attributed to the presence of amino acids that are largely consumed in the first stage of composting. The value of M_2 tends to increase, despite the small decrease observed for CUW. For M_3 a continuous decrease is observed, similar to that observed for M_2 of FA-L, which confirms the presence of FA-L, in the equilibrium solutions. This statement is supported by the similarity of the values of pK_2 of FA-L and pK_3 of DOM.

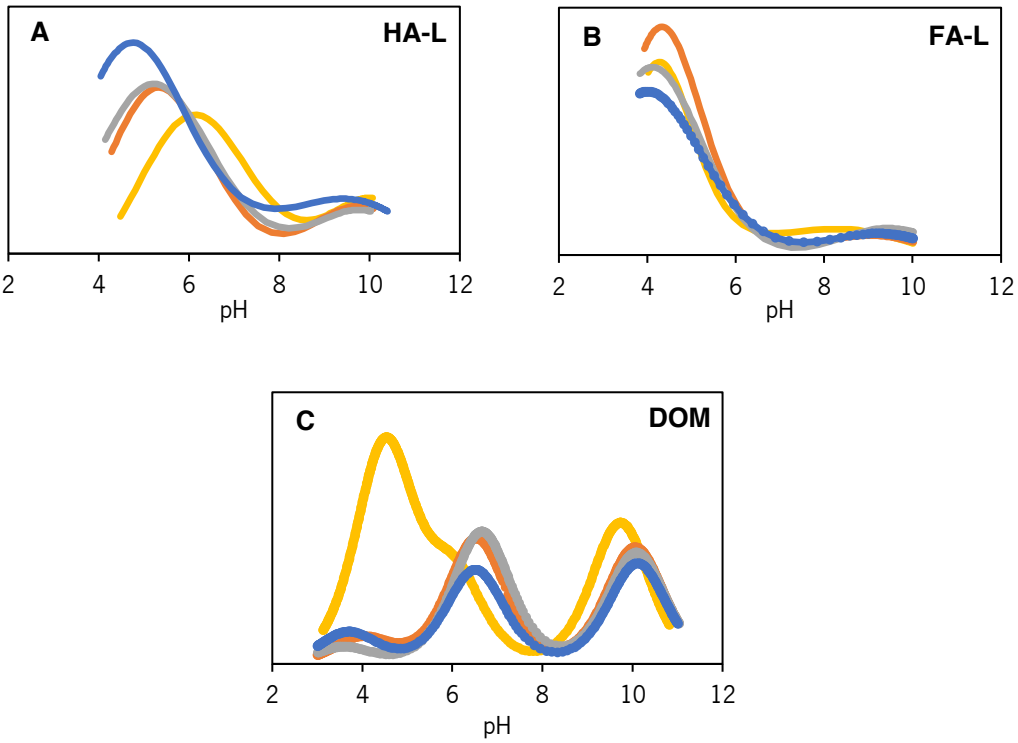

Figure 3.37: Proton affinity distributions obtained for the (A) HA-L, (B) FA-L and (C) DOM from the compost samples: UW_0 (yellow), CUW_{15} (dark orange), CUW_{30} (grey), CUW (blue).

2.6. *Metal binding extent*

The evaluation of the binding of metal ions by the HS-L extracts may be used for the characterization of these substances, as the extent of this process is strongly associated with the nature of the functional groups present and with the structure of molecular aggregates formed by HS-L. Besides the chemical characterization purposes, the complexing ability of the DOM is also relevant to understand the fate of environmental pollutants [27]. The organic substances present in DOM are the most mobile and therefore the most accessible to participate in several equilibria in environment.

Results obtained for the binding of cadmium by HA-L, FA-L and DOM are shown in Figures 3.38A to 3.38C. The plots represent the average complexation constant K' as a function of the total cadmium concentration, c_{MT}, (in mol L^{-1}), where K' values were calculated as the ratio c_{ML}/c_M, where c_{ML} is the metal complex concentration and c_M is the free metal concentration. This ratio is related to the stability constant of metal complexes. From plots in Figures 3.38A to 3.38C it is observed that all curves follow the same order, from UW_0 (at the bottom) to CUW (at the top). The shape of these curves (decreasing K' with increasing c_{MT}) is typical of heterogeneous materials, where the binding by the strongest groups occurs for the first additions of Cd^{2+}. The decrease of the average value of K' occurs progressively with the increasing involvement of the weaker binding groups due to the occupation of the stronger sites.

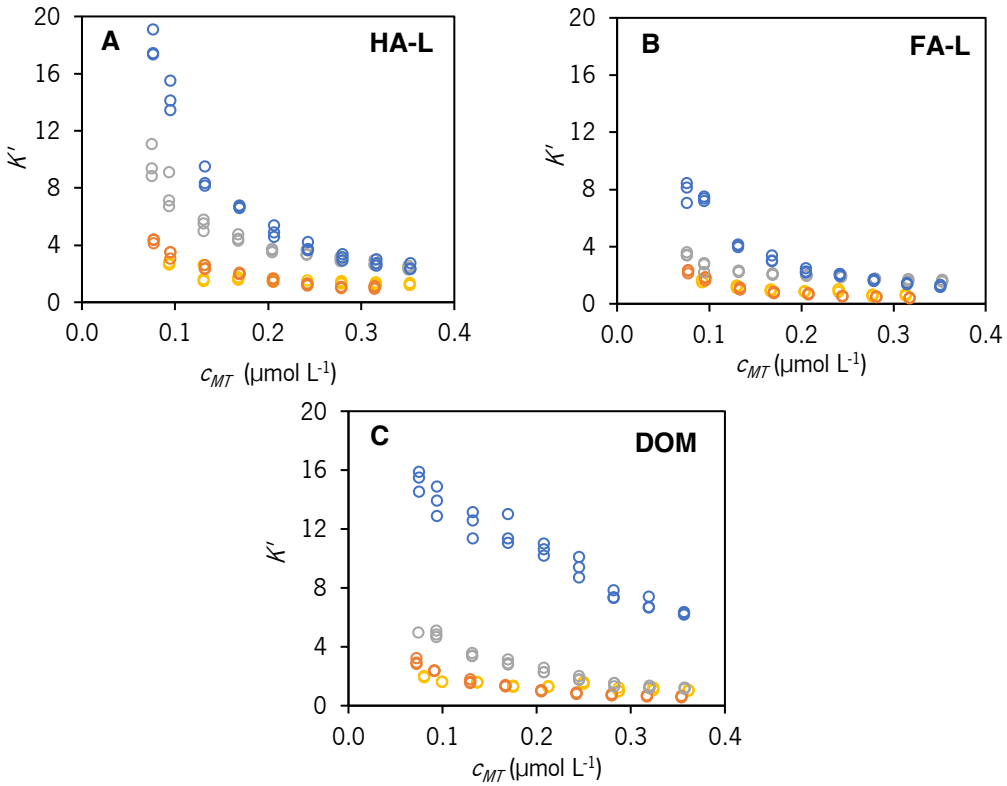

Figure 3.38: Experimental data for cadmium binding obtained for the (A) HA-L, (B) FA-L and (C) DOM from the compost samples: UW_0 (yellow), CUW_{15} (dark orange), CUW_{30} (grey), CUW (blue).

To facilitate the comparison between the extracts at different composting stages the values of $C_{ML,L}$ and $C_{ML,H}$ were calculated (Table 3.22). These quantities correspond to K'/c_L, where c_L represents the concentration of organic matter for a low (0.10 μmol L^{-1}) and a high (0.30 μmol L^{-1}) concentration of total metal in solution. The values of $C_{ML,L}$ and $C_{ML,H}$ are a measure of the average binding ability of the strongest groups and of the overall groups, respectively. Both parameters displayed a gradual increase throughout composting in all extract (with only one exception, $C_{ML,H}$ of the FA-L extract of CUW_{15}, which is lower than UW_0). However, the differences between the values $C_{ML,H}$ are more relevant, indicating that the molecular changes associated with composting impose pronounced modifications on the strong complexing groups. These results confirm what was previously discussed, that during the maturation period there is an increase of the number of strong binding sites of the extracts, while the number of weak binding sites does not seem to vary.

Table 3.22: Metal binding parameters ($C_{ML,L}$ and $C_{ML,H}$) of the HA-L, FA-L and DOM extracts of the samples, UW_0 and CUW_{15}, CUW_{30} and CUW.

Parameter		UW_0	CUW_{15}	CUW_{30}	CUW
$c_{ML,HS-L,L}$ (L μg C^{-1})	HA-L	0.75	1	2.4	5.9
	FA-L	0.52	0.57	0.86	3
$c_{ML,DOM,L}$ (L μg DOC^{-1})	DOM	0.14	0.59	1.18	2.67
$c_{ML,HS-L,H}$ (L μg C^{-1})	HA-L	0.36	0.36	0.87	1.2
	FA-L	0.2	0.14	0.57	0.59
$c_{ML,DOM,H}$ (L μg DOC^{-1})	DOM	0.11	0.17	0.32	1.36

The ability of the different extracts for binding Cd^{2+} is compared in Figure 3.39. The values of c_{ML} corresponding to the concentration of the metal bound to each extract, for an identical added [Cd^{2+}], are represented in each plot together with the y=x straight-line. For all plots, points of the different series are dispersed along the straight-line and tend to be located over the line, indicating that the binding extent of HA-L extracts is higher than that of the FA-L extracts (Figure 3.39A) and of the species in the DOM (Figure 3.39B), and the binding extent of FA-L extracts is higher than that of the species in the DOM (Figure 3.39C).

In Figure 3.39A the larger deviations from the straight-line are observed for the points obtained for the higher concentrations of Cd^{2+} cation, for which the Cd^{2+} is bound by the weakest binding sites. This result suggests that the ability of the strong binding sites of HA-L and FA-L do not differ significantly, but the weakest binding sites of HA-L are more efficient for binding Cd^{2+} than from those of FA-L. The representations of the binding extent by FA-L and HA-L regarding the species present in DOM, in Figure

3.39B and Figure 3.39C, show larger differences. The dispersion of the experimental data points follows a similar trend in the two plots, as data from all series are located above the y=x straight-line and the results form UW_0 and CUW are those that exhibit larger deviations. This result indicated that the extent of the binding of Cd^{2+} by HS-L in the two extracts, HA-L or FA-L, is larger than that accomplished by organic substances present in the DOM. This result could be due to the different nature of the species, and also to from differences in the pH and ionic strength of the solutions, that are higher for the DOM in comparison to the FA-L and HA-L, as salts were not removed from these extracts by dialysis (performed in extraction/purification assays).

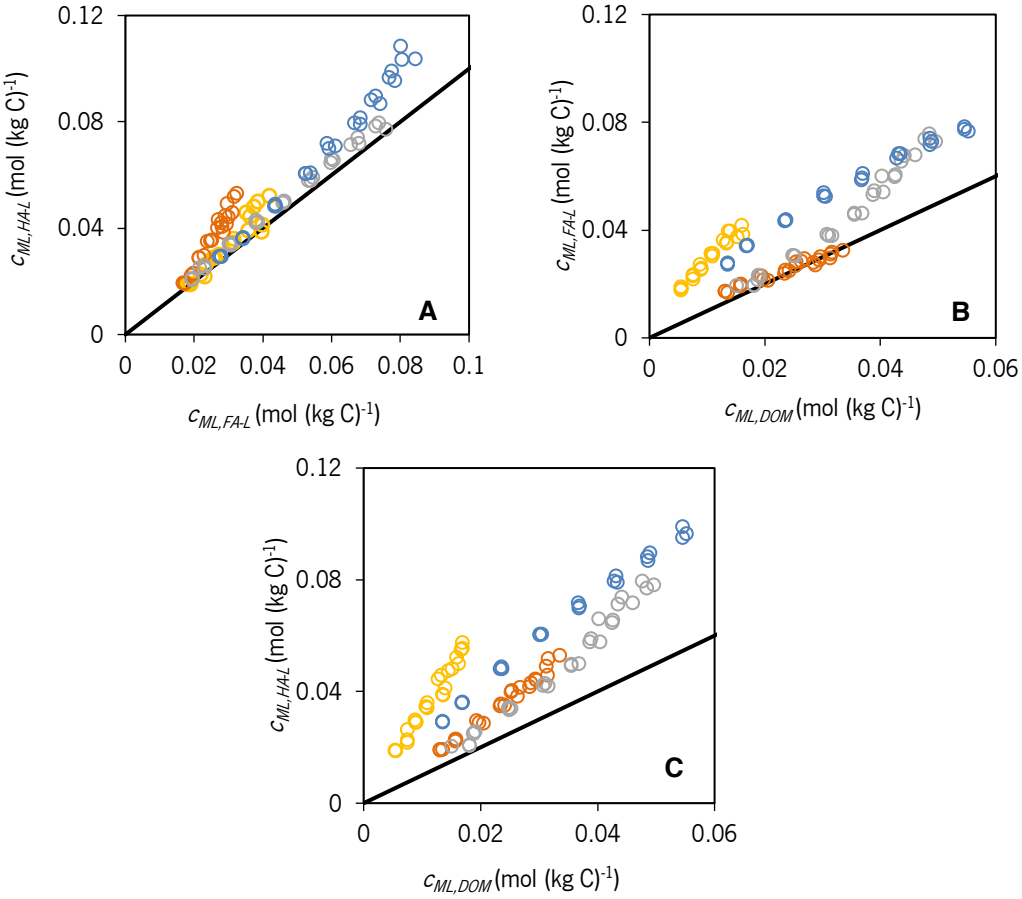

Figure 3.39: Comparison of cadmium binding data obtained by AGNES: (A) HA-L *vs.* FA-L, (B) FA-L *vs.* DOM and (C) HA-L *vs.* DOM. The y=x straight line represents the equivalence between results. Compost samples from different times of the composting process: UW_0 (yellow), CUW_{15} (dark orange), CUW_{30} (grey), CUW (blue).

2.7. Multi – block data analysis

The main premise of this work is to determine which are the most suitable techniques and parameters to characterize the evolution of compost throughout the composting process. This is a complex task due to the diversity of methodologies used for this purpose that requires the use of an adequate statistical tool like the multi-blocks analysis. The ComDim evaluation was applied to explore the multiple data blocks

defined using results from the chronological characterization of a compost (CUW) and of its extracts (HA-L, FA-L and equilibrium solutions (containing DOM). The analysis was performed separating the results from each sample (compost, HA-L, FA-L and equilibrium solutions) in two groups: the first (blocks 1, 3, 5, and 7) with data related to the elemental composition of each sample (comprising data from elemental analysis and content of ionic species) and the second (blocks 2, 4, 6, and 8) with data related to the molecular structure of species in each sample (comprising data from yield of HA-L and FA-L extractions, pH, CEC, EC, UV-vis, ATR-FTIR, ^{1}H-NMR, TGA, DSC, acid-base and metal binding titrations). Results of the solid compost at different composting stages are in blocks 1 and 2, of equilibrium solutions are in blocks 3 and 4, of HA-L are in blocks 5 and 6, and of FA-L are in blocks 7 and 8. Data included in each block is presented in Tables 3.23 and 3.24. Results obtained from ComDim analysis, with the informative graphics of the saliences, scores, and loadings are shown in Figures 3.40A to 3.40C, respectively. Eight common components, CCs, were computed on this ComDim evaluation and considered sufficient to take into account all sources of variation in the eight data blocks (Figure 3.40A). No significant information was observed in saliences from CCs 4 to 8, and compared to the CC1, an inferior variability was observed in the CCs 2 and 3. On CC1 it is possible to suggest that an inter-block relationship was achieved, although blocks 4, 6 (corresponding to the results related to molecular structure of DOM and HA-L) and block 5 (corresponding to the elemental composition of HA-L), presented higher saliences. This outcome indicates that results from analytical parameters related either to the elemental composition or to molecular structure of the solid compost, DOM, HA-L or FA-L are able to distinguish samples obtained at the different stages of composting. The ComDim scores on CC1 (Figure 3.40B) show the chronological development of the solid compost and of its extracts. The samples (compost and extracts) from the feedstock (UW_0), with more negative scores, were differentiated from those of the matured compost (CUW), with more positive scores. The samples from CUW_{15} and CUW_{30} present intermediate scores. The relative importance of the different analytical techniques for monitoring composting can be recognized from the loadings plot in Figure 3.40C. The variables that display higher loadings correspond to the analytical parameters that are more successful to distinguish CUW and the lower loadings correspond to the analytical parameters that are more successful to distinguish UW_0 from the remaining samples. For the identification of the techniques and parameters that were more successful, the variables were divided in 3 ranges according to the absolute values of the loadings, $|L|>0.8$, $0.4<|L|<0.8$ and $|L|<0.4$. Besides, the variation trend of the analytical parameters was examined. The selected analytical parameters, that display at least for one sample $|L|>0.4$ and vary in a single way along the process, are listed in Table 3.25.

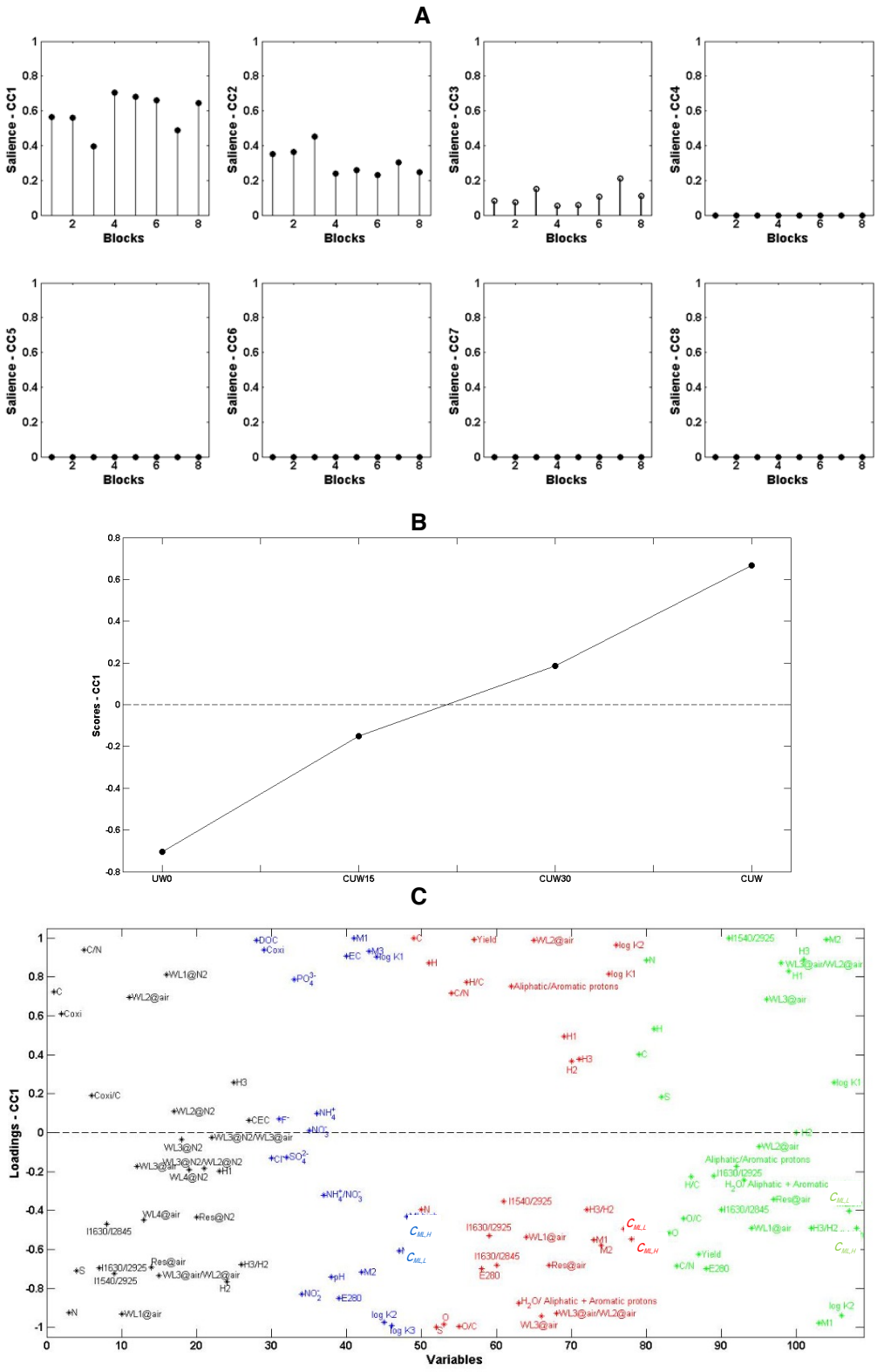

Figure 3.40: ComDim results. (A) Saliences from CC1 to CC8: blocks 1, 3, 5, and 7 obtained from data of elemental composition and blocks 2, 4, 6, and 8 obtained from data related to molecular structure, where block 1, 2 are from solid compost; 3, 4 are from equilibrium solutions; 5, 6 are from HA-L and 7, 8 are from FA-L; (B) Scores of CC1; (C) Loadings of the CC1, are displayed in different colours according to the sample nature: solid compost (black), water-soluble extract (light blue), HA-L (red) and FA-L (green).

With respect to the elemental characterization of the solid compost and its extracts the most relevant parameters were: C, C_{oxi} and C/N for compost; C_{oxi}, DOC, PO_4^{3-} and NO_2^- for equilibrium solutions and C, N, H, C/N and O/C for HS-L extracts (HA-L and FA). Concerning the parameters related to molecular structure, ε_{280} was relevant for DOM and HS-L extracts. The pH and EC were also relevant for DOM characterization. The ratios $I_{1630/2845}$, $I_{1630/2925}$ and $I_{1540/2925}$ (from the ATR-FTIR analysis) were meaningful for compost, whereas for HS-L extracts only $I_{1630/2845}$ was adequate.

Table 3.23: Data of elemental composition (from EA) and related to molecular structure (from CEC, UV-vis, ATR-FTIR, ^{1}H-NMR, TGA and DSC) of solid compost (blocks 1, 2).

Block	Technique	Parameter	UW_0	CUW_{15}	CUW_{30}	CUW
1	EA	C (%)	40.4	38.9	35.2	34.0
		C_{ox} (%)	38.6	36.9	34.8	29.3
		N (%)	2.54	2.81	2.73	2.71
		S (%)	0.204	0.264	0.286	0.222
		C/N	18.6	16.1	15.0	14.7
		C_{ox}/C	95.4	95.0	98.9	86.1
2	ATR-FTIR	$I_{1630/2925}$	0.91	1.44	3.69	3.40
		$I_{1630/2845}$	1.30	2.03	6.32	19.8
		$I_{1540/2925}$	0.71	1.16	1.67	2.34
	TGA	WL_1@air (%)	7.8	8.8	9.3	9.4
		WL_2@air (%)	43	40	32	28
		WL_3@air (%)	28	29	29	27
		WL_4@air (%)	2.1	2.2	3.4	7.4
		Res@air (%)	18	20	25	28
		WL_3@air/WL_2@air	0.64	0.72	0.91	0.96
		$WL_1@N_2$ (%)	6.8	1.7	2.4	4.9
		$WL_2@N_2$ (%)	38	50	36	20
		$WL_3@N_2$ (%)	13	7	7	27
		$WL_4@N_2$ (%)	5.9	5.8	4.6	10
		$Res@N_2$ (%)	36	37	50	38
		$WL_3@N_2/WL_2@N_2$	0.35	0.13	0.20	1.34
		$WL_3@N_2/WL_3$@air	0.47	0.23	0.24	0.99
	DSC	H_1 (kJ g^{-1})	1.72	1.89	1.88	1.57
		H_2 (kJ g^{-1})	-2.70	-2.49	-2.01	-2.08
		H_3 (kJ g^{-1})	-4.50	-4.39	-4.66	-4.65
		H_4/H_2	1.7	1.8	2.3	2.2
	Cation exchange capacity	CEC ($cmol_{(+)}$ kg^{-1})	128	96.3	109	167

Table 3.24: Data of elemental composition (from EA, wet chemistry analysis, ion chromatography, pH and EC) and related to molecular structure (from UV-vis, ATR-FTIR, ^{1}H-NMR, TGA, DSC, acid-base and metal binding titrations) of HA-L, FA-L and equilibrium solutions (containing DOM) (blocks 3 to 8).

Block	Technique	Parameter		UW_0	CUW_{15}	CUW_{30}	CUW
5, 7	EA	C (%)	HA-L	59.8	54.4	54.6	54.5
			FA-L	52.2	52.3	50.3	40.8
		N (%)	HA-L	5.45	5.44	5.64	6.74
			FA-L	6.16	5.17	4.25	4.37
		H (%)	HA-L	7.97	6.9	5.75	6.14
			FA-L	6.17	6.1	5.65	6.02
		S (%)	HA-L	0.69	0.9	0.91	0.91
			FA-L	0.97	0.77	1.05	0.96
		O (%)	HA-L	26.1	32.4	33.1	31.7
			FA-L	34.6	35.7	38.8	47.8
		C/N	HA-L	13	12	11	9.4
			FA-L	9.9	11.8	13.8	10.9
		O/C	HA-L	0.33	0.45	0.45	0.44
			FA-L	0.5	0.5	0.6	0.9
		H/C	HA-L	1.6	1.5	1.3	1.4
			FA-L	1.4	1.4	1.3	1.8
3	Wet chemistry analysis	DOC (mg L^{-1})	DOM	1187	429	430	548
		C_{ox} (%)		6.2	2.3	2.5	3.7
	Ion chromatography	Cl (mg L^{-1})		415	352	579	392
		F^- (mg L^{-1})		0.12	0.08	0.08	0.18
		SO_4^{2-} (mg L^{-1})		43.1	30.0	22.8	105
		PO_4^{3-} (mg L^{-1})		110	80.4	60.3	29.5
		NO_2^- (mg L^{-1})		1.71	2.72	4.18	3.94
		NO_3^- (mg L^{-1})		2.56	1.05	1.28	5.21
		NH_4^+ (mg L^{-1})		10.8	13.2	10.1	7.78
		NH_4^+/NO_3^-		4.22	12.56	7.85	1.49
	Potentiometry	pH		6.41	6.81	7.93	7.69
	Conductivity	*EC* (µs cm^{-1})		3870	3030	3300	2840
6, 8	Extraction yield	*Yield* (g kg^{-1})	HA-L	33.1	19.8	21.9	21.1
			FA-L	2.2	2.7	2.4	3.3
4, 6, 8	Uv-vis	ε_{280} (L $molC^{-1}$ cm^{-1})	HA-L	212	293	366	513
			FA-L	186	233	358	419
			DOM	75.5	166	237	280
6, 8	^{1}H-NMR	Aliphatic/Aromatic protons	HA-L	8.7	7.3	6.7	4.8
			FA-L	6	6.4	6.4	5.6
		H_2O/ Aliphatic + Aromatic protons	HA-L	1.7	7	4.4	5.4
			FA-L	10	8	11	16
6, 8	ATR-FTIR	$I_{1630/1925}$	HA-L	1.6	2	2.5	4.7
			FA-L	2.7	2	2.1	7.6
		$I_{1630/2845}$	HA-L	2.7	3	3.8	4.3
			FA-L	3.5	4.8	3.1	9.1
		$I_{1540/2925}$	HA-L	1	0.75	1.4	2
			FA-L	1.8	1.3	1.3	1.3
6, 8	TGA	WL_1@air (%)	HA-L	4.1	5.5	5.2	10
			FA-L	2.5	3.7	2.7	6.4
		WL_2@air (%)	HA-L	48	28	31	31
			FA-L	44	47	49	38
		WL_3@air (%)	HA-L	46	61	56	57
			FA-L	48	45	42	36
		Res@air (%)	HA-L	1.2	5.5	6.4	2
			FA-L	4.1	2.6	6.1	22
		WL_2@air/WL_3@air	HA-L	1	2.2	1.8	1.8
			FA-L	1.1	1	0.9	0.9
6, 8	DSC	H_1 (kJ g^{-1})	HA-L	0.31	0.17	0.3	0.27
			FA-L	0.66	0.2	0.23	0.47
		H_2 (kJ g^{-1})	HA-L	-0.56	-0.3	-1.13	-1.25
			FA-L	-1.51	-0.64	-0.81	-3.08
		H_3 (kJ g^{-1})	HA-L	-0.64	-0.43	-1.29	-4.52
			FA-L	-1.49	-2.3	-2.02	-2.52
		H_3/H_T	HA-L	1.14	1.45	1.13	3.62
			FA-L	0.99	3.62	2.49	0.82
4, 6, 8	Acid-base properties	M_1(mmol/g_{HS-L})	HA-L	2.2	2.3	2.7	2.9
			FA-L	2.4	3.4	3.6	3.7
		M_1(mmol/$g_{compost}$)	DOM	0.42	0.05	0.03	0.06
		M_2(mmol/g_{HS-L})	HA-L	1.1	1.2	1.2	1.8
			FA-L	2.2	1.6	1.5	1.5
		M_2(mmol/$g_{compost}$)	DOM	0.16	0.24	0.25	0.18
		M_3(mmol/$g_{compost}$)	DOM	0.27	0.22	0.21	0.19
		log K_1	HA-L	6.1	5.3	5.2	4.7
			FA-L	4.2	4.3	4.1	4
			DOM	4.5	3.99	3.57	3.69
		log K_2	HA-L	10.2	9.9	9.9	9.7
			FA-L	8.4	9.1	9.5	9.4
			DOM	6.05	6.54	6.65	6.51
		log K_3	DOM	9.73	10.06	10.08	10.11
4, 6, 8	Metal binding properties	$C_{ML,HS-L1}$ (L µg C^{-1})	HA-L	0.75	1	2.4	5.9
			FA-L	0.52	0.57	0.86	3
		$C_{ML,DOM,1}$ (L µg DOC^{-1})	DOM	0.14	0.59	1.18	2.67
		$C_{ML,HS-L2}$ (L µg C^{-1})	HA-L	0.36	0.36	0.87	1.2
			FA-L	0.2	0.14	0.57	0.59
		$C_{ML,DOM,2}$ (L µg DOC^{-1})	DOM	0.11	0.17	0.32	1.36

The variables H_2 and H_3/H_2 (from DSC) were relevant for compost whereas for the HS-L extracts H_1 and H_3/H_2 were significant. The variables $WL_1@air$, $WL_2@air$, $WL_4@air$, $Res@air$, $WL_3@air/WL_2@air$, $WL_1@N_2$ and $Res@N_2$ (from TGA analysis) were relevant for compost, while for HS-L extracts just $WL_1@air$ and $WL_3@air$ were meaningful. The acid-base parameters M_1, M_2, M_3 and log K_1 of DOM and M_1, M_2 and log K_2 of HS-L extracts were relevant. Regarding the metal binding parameters both $C_{ML,DOM,L}$ and $C_{ML,DOM,H}$ were relevant for DOM, whereas for the HS-L extracts only the $C_{ML,HS\text{-}L,H}$ were meaningful.

Table 3.25: Identification of the variables that display |L|>0.4 and exhibit a continuous variation for at least one sample. The highlighted cells assign that the variation of the parameter was not continuous.

Technique	Parameter	Compost	DOM	HA-L	FA-L
Elemental composition	C	< 0.8; > 0.4	-	> 0.8	< 0.8; > 0.4
	C_{oxi}	< 0.8; > 0.4	> 0.8	-	-
	N	> 0.8	-	< 0.8; > 0.4	>0.8
	S	< 0.8; > 0.4		>0.8	< 0.4
	H	-	-	> 0.8	< 0.8; > 0.4
	O	-	-	> 0.8	< 0.8; > 0.4
	C/N	> 0.8	-	< 0.8; > 0.4	< 0.8; > 0.4
	O/C	-	-	> 0.8	< 0.8; > 0.4
	H/C	-	-	> 0.8	< 0.4
	DOC	-	> 0.8	-	-
	PO_4^{3-}	-	> 0.8	-	-
	NO_2^-	-	> 0.8	-	-
	pH	-	< 0.8; > 0.4	-	-
UV-vis	ε_{280}	-	> 0.8	< 0.8; > 0.4	< 0.8; > 0.4
	EC	-	> 0.8	-	-
HS-L extraction	*Yield*	-	-	> 0.8	< 0.8; > 0.4
^{1}H-NMR	Aliphatic /Aromatic protons			< 0.8; > 0.4	< 0.4
	H_20/aliphatic + aromatic protons			> 0.8	< 0.4
ATR-FTIR	$I_{1630/I2925}$	< 0.8; > 0.4	-	< 0.8; > 0.4	< 0.4
	$I_{1630/I2845}$	< 0.8; > 0.4	-	< 0.8; > 0.4	< 0.8; > 0.4
	$I_{1540/2925}$	< 0.8; > 0.4	-	< 0.4	> 0.8
TGA	$WL_1@air$	> 0.8	-	< 0.8; > 0.4	< 0.8; > 0.4
	$WL_2@air$	< 0.8; > 0.4	-	> 0.8	< 0.4
	$WL_3@air$	< 0.4	-	> 0.8	< 0.8; > 0.4
	$WL_4@air$	< 0.8; > 0.4	-	-	-
	$Res@air$	< 0.8; > 0.4	-	< 0.8; > 0.4	<0.4
	$WL_3@air/WL_2@air$	< 0.8; > 0.4	-	> 0.8	>0.8
	$WL_1@N_2$	> 0.8	-	-	-
	$Res@N_2$	< 0.8; > 0.4	-	-	-
DSC	H_1	< 0.4	-	< 0.8; > 0.4	< 0.8; > 0.4
	H_2	< 0.8; > 0.4	-	< 0.4	< 0.4
	H_3	< 0.4	-	< 0.4	< 0.8; > 0.4
	H_3/H_2	< 0.8; > 0.4	-	< 0.8; > 0.4	< 0.8; > 0.4
Acid-base	M_1	-	> 0.8	< 0.8; > 0.4	> 0.8
	M_2	-	< 0.8; > 0.4	< 0.8; > 0.4	> 0.8
	M_3	-	> 0.8	-	-
	log K_1	-	> 0.8	> 0.8	< 0.4
	log K_2	-	> 0.8	> 0.8	> 0.8
	log K_3	-	> 0.8	-	-
Metal binding	$C_{ML,L}$	-	< 0.8; > 0.4	< 0.8; > 0.4	< 0.4
	$C_{ML,H}$	-	< 0.8; > 0.4	< 0.8; > 0.4	< 0.8; > 0.4

3. References

[1]G.F. Huang, J.W.C. Wong, Q.T. Wu, B.B. Nagar, Effect of C/N on composting of pig manure with sawdust, Waste Management. 24 (2004) 805–813. https://doi.org/10.1016/j.wasman.2004.03.011.

[2]X. Guo, H. Liu, S. Wu, Humic substances developed during organic waste composting: Formation mechanisms, structural properties, and agronomic functions, Science of the Total Environment. 662 (2019) 501–510. https://doi.org/10.1016/j.scitotenv.2019.01.137.

[3]S.K. Awasthi, S. Sarsaiya, M.K. Awasthi, T. Liu, J. Zhao, S. Kumar, Z. Zhang, Changes in global trends in food waste composting: Research challenges and opportunities, Bioresource Technology. 299 (2020) 122555. https://doi.org/10.1016/j.biortech.2019.122555.

[4]L.F. Diaz, C.G. Golueke, G.M. Savage, L.L. Eggerth, Composting and recycling municipal solid waste, 2020.

[5]M.H. Saharinen, Evaluation of changes in CEC during composting, Compost Science and Utilization. 6 (1998) 29–37. https://doi.org/10.1080/1065657X.1998.10701938.

[6]Y. Harada, A. Inoko, Relationship between cation-exchange capacity and degree of maturity of city refuse composts, Soil Science and Plant Nutrition. 26 (1980) 353–362. https://doi.org/10.1080/00380768.1980.10431220.

[7]K. Azim, B. Soudi, S. Boukhari, C. Perissol, S. Roussos, I. Thami Alami, Composting parameters and compost quality: a literature review, Organic Agriculture. 8 (2018) 141–158. https://doi.org/10.1007/s13165-017-0180-z.

[8]J. Wu, Y. Zhao, W. Zhao, T. Yang, X. Zhang, X. Xie, H. Cui, Z. Wei, Effect of precursors combined with bacteria communities on the formation of humic substances during different materials composting, Bioresource Technology. 226 (2017) 191–199. https://doi.org/10.1016/j.biortech.2016.12.031.

[9]J.M. Fernández, C. Plaza, A. Polo, A.F. Plante, Use of thermal analysis techniques (TG-DSC) for the characterization of diverse organic municipal waste streams to predict biological stability prior to land application, Waste Management. 32 (2012) 158–164. https://doi.org/10.1016/j.wasman.2011.08.011.

[10]M.P. Som, L. Lemée, A. Amblès, Stability and maturity of a green waste and biowaste compost assessed on the basis of a molecular study using spectroscopy, thermal analysis, thermodesorption and thermochemolysis, Bioresource Technology. 100 (2009) 4404–4416. https://doi.org/10.1016/j.biortech.2009.04.019.

[11]P. Melis, P. Castaldi, Thermal analysis for the evaluation of the organic matter evolution during municipal solid waste aerobic composting process, Thermochimica Acta. 413 (2004) 209–214. https://doi.org/10.1016/j.tca.2003.09.026.

[12]M.T. Dell'Abate, S. Canali, A. Trinchera, A. Benedetti, P. Sequi, Thermal analysis in the evaluation of compost stability: A comparison with humification parameters, Nutrient Cycling in Agroecosystems. 51 (1998) 217–224. https://doi.org/10.1023/A:1009734816502.

[13]Y. Inbar, Y. Chen, Y. Hadar, Solid-state carbon-13 nuclear magnetic resonance and infrared spectroscopy of composted organic matter, Soil Science Society of America Journal. 53 (1989) 1695–1701. https://doi.org/10.2136/sssaj1989.03615995005300060014x.

[14]A. Ouatmane, M.R. Provenzano, M. Hafidi, N. Senesi, Compost maturity assessment using

calorimetry, spectroscopy and chemical analysis, Compost Science & Utilization. 8 (2000) 124–134. https://doi.org/10.1080/1065657X.2000.10701758.

[15]M. Kaiser, R.H. Ellerbrock, Functional characterization of soil organic matter fractions different in solubility originating from a long-term field experiment, Geoderma. 127 (2005) 196–206. https://doi.org/10.1016/j.geoderma.2004.12.002.

[16]M. Fuentes, R. Baigorri, G. González-Gaitano, J.M. García-Mina, The complementary use of ^{1}H NMR, ^{13}C NMR, FTIR and size exclusion chromatography to investigate the principal structural changes associated with composting of organic materials with diverse origin, Organic Geochemistry. 38 (2007) 2012–2023. https://doi.org/10.1016/j.orggeochem.2007.08.007.

[17]J.H. Hsu, S.L. Lo, Chemical and spectroscopic analysis of organic matter transformations during composting of pig manure, Environmental Pollution. 104 (1999) 189–196. https://doi.org/10.1016/S0269-7491(98)00193-6.

[18]K. Wang, X. Li, C. He, C.L. Chen, J. Bai, N. Ren, J.Y. Wang, Transformation of dissolved organic matters in swine, cow and chicken manures during composting, Bioresource Technology. 168 (2014) 222–228. https://doi.org/10.1016/j.biortech.2014.03.129.

[19]S. Amir, A. Jouraiphy, A. Meddich, M. El Gharous, P. Winterton, M. Hafidi, Structural study of humic acids during composting of activated sludge-green waste: Elemental analysis, FTIR and ^{13}C NMR, Journal of Hazardous Materials. 177 (2010) 524–529. https://doi.org/10.1016/j.jhazmat.2009.12.064.

[20]A. Hanc, V. Enev, T. Hrebeckova, M. Klucakova, M. Pekar, Characterization of humic acids in a continuous-feeding vermicomposting system with horse manure, Waste Management. 99 (2019) 1–11. https://doi.org/10.1016/j.wasman.2019.08.032.

[21]P. Boguta, Z. Sokołowska, K. Skic, Use of thermal analysis coupled with differential scanning calorimetry, quadrupole mass spectrometry and infrared spectroscopy (TG-DSC-QMS-FTIR) to monitor chemical properties and thermal stability of fulvic and humic acids, PLoS ONE. 12 (2017) 1–18. https://doi.org/10.1371/journal.pone.0189653.

[22]Y.-P. Chin, G. Aiken, E. O'Loughlin, Molecular weight, polydispersity, and spectroscopic properties of aquatic humic substances, Environmental Science & Technology. 28 (1994) 1853–1858. https://doi.org/10.1021/es00060a015.

[23]G.A. Baddi, M. Hafidi, J. Cegarra, J.A. Alburquerque, J. Gonzálvez, V. Gilard, J.C. Revel, Characterization of fulvic acids by elemental and spectroscopic (FTIR and ^{13}C-NMR) analyses during composting of olive mill wastes plus straw, Bioresource Technology. 93 (2004) 285–290. https://doi.org/10.1016/j.biortech.2003.10.026.

[24]M. González Pérez, L. Martin-Neto, S.C. Saab, E.H. Novotny, D.M.B.P. Milori, V.S. Bagnato, L.A. Colnago, W.J. Melo, H. Knicker, Characterization of humic acids from a Brazilian Oxisol under different tillage systems by EPR, ^{13}C NMR, FTIR and fluorescence spectroscopy, Geoderma. 118 (2004) 181–190. https://doi.org/10.1016/S0016-7061(03)00192-7.

[25]R. Spaccini, A. Piccolo, Molecular characteristics of humic acids extracted from compost at increasing maturity stages, Soil Biology and Biochemistry. 41 (2009) 1164–1172. https://doi.org/10.1016/j.soilbio.2009.02.026.

[26]R. López, J. Antelo, A.C. Silva, F. Bento, S. Fiol, Factors that affect physicochemical and acid-base properties of compost and vermicompost and its potential use as a soil amendment, Journal of Environmental Management. 300 (2021) 113702. https://doi.org/10.1016/j.jenvman.2021.113702

[27]J. Buffle, R.R. DeVitre, Chemical and Biological Regulation of Aquatic Systems, Lewis Pub., Boca

Raton, 1994.

Chapter 3.5 - Characterizing the HS-L originated from urban waste compost through the NICA-Donnan model

The NICA-Donnan model is commonly applied for the characterization of HS from natural samples, such as peat, soil and leonardite, considering data both from proton and metal binding titrations. The extracted parameters provide relevant information regarding site density and proton affinity and also intrinsic heterogeneity when data from metal binding titrations are also available [1,2]. These parameters are extremely relevant concerning the assessment of reactivity of the HS that play a major role on their properties in the environment [3].

Although it is well known that compost is an important source of humic-like substances that are being increasingly applied as fertilisers and soil amendments [4], there are few papers that report the fitting of proton binding titrations in compost extracts using NICA-Donnan model [2,5–7] and was not found any data for the HS-L modelling from compost using proton and metal binding titrations.

In this chapter are presented the data (acid-base titrations and titrations with metallic cations at different ionic strengths and different pH values) and results of the fitting parameters from the NICA-Donnan model for the two extracts humic-like acid (HA-L) and fulvic-like acid (FA-L) of one of the composts characterized in the previous chapters, CUW, that is produced from a selective collection of urban wastes. The modelling was carried out using the PEST-ORCHESTRA tool.

1. Proton binding

Proton binding titrations were carried out at two values of ionic strengths, 0.1 and 0.01 mol L^{-1}, in order to characterize the reactivity of the extracts through the model parameters (see Chapter 2): *b,* that accounts for the Donnan volume, and the NICA proton binding parameters namely the abundance of carboxylic group and phenolic OH group, M_1 and M_2, respectively; the median value of affinity distribution of carboxyl and phenolic groups, K_1 and K_2; and width of proton-affinity distribution of carboxyl and phenolic OH groups, $m_{H,1}$ and $m_{H,2}$ [8]. The experimental data of proton binding from HA-L and FA-L (symbols) and modelling results (lines) are shown in Figure 3.41, while the best estimated parameters are shown in Table 3.26. The HA-L modelling exhibits a good fit at all pH values, as the value of the determination coefficient (R^2) is high, and the value of the root mean square error (*RMSE*) is low. The modelling results for FA-L are not as good as for HA-L as it can be seen by the values of R^2 and *RMSE*. This result is a consequence of the worst quality of the fitting for pH values higher than 9.0.

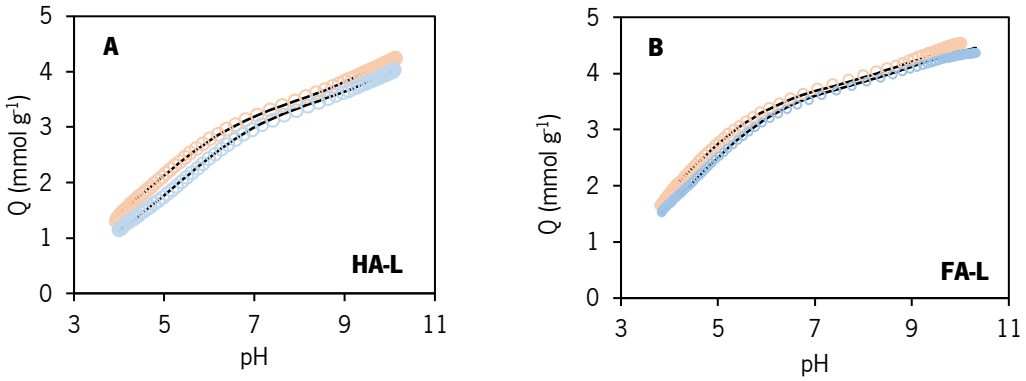

Figure 3.41: Charge behaviour of (A) HA-L - CUW and (B) FA-L - CUW as a function of pH values and ionic strength ((○) 0.01 mol L^{-1} and (○) 0.1 mol L^{-1} in KNO_3). Open markers represent the experimental data obtained from acid-base titrations and the continuous lines represent the fitting with the NICA-Donnan model.

Table 3.21 shows the comparison of the optimised NICA-Donnan parameters for the FA-L and HA-L of CUW with the generic values of the fulvic and humic acid parameters obtained by Milne et al. (2001) [8] and with the parameters obtained for other humic-like substances extracted from different composts.

The *b* values obtained from FA-L - CUW and HA-L - CUW are similar to those of composted mixture of olive oil mill wastewater sludge and tree cutting (C118 [5]). Regarding the comparison to the

generic parameters, the result for FA-L - CUW is slightly above while the value of HA -L- CUW is slightly below the generic values.

Table 3.26: Comparison of NICA-Donnan parameters for proton binding by humic-like (HA-L) and fulvic-like (FA-L) acids extracted from urban waste compost (CUW) with other compost samples presented in the bibliography (MSW and MSWC - compost of municipal solid waste, C118 - compost of olive oil mill wastewater sludge and tree cutting and CS - compost of sewage sludge) and with the generic values for humic substances from different natural sources[a].

	b	log K_1	M_1 (mmol/g_{ash})	$m_{H,1}$	log K_2	M_2 (mmol/g_{ash})	$m_{H,2}$	R^2	RMSE	M_T (mmol/g_{ash})	*Reference*
						Fulvic Acid					
FA-L – CUW	**0.64**	**2.87**	**3.77**	**0.49**	**7.44**	**0.86**	**0.55**	**0.9989**	**0.051**	**4.63**	
generic	*0.57*	*2.34*	*5.88*	*0.38*	*8.6*	*1.86*	*0.53*	*0.9920*	*0.123*	*7.74*	[8]
FA – MSW	0.75	2.74	6.02	0.50	7.00	0.71	0.92	0.9999	0.010	6.73	[6]
FA – C118	0.62	2.55	4.68	0.56	6.96	2.52	0.20	0.9984	0.0476	7.20	[5]
FA – CS	0.69	3.29	4.97	0.62	8.51	1.86	0.61	0.9999	0.0169	6.83	[2]
						Humic Acid					
HA-L – CUW	**0.43**	**2.99**	**3.55**	**0.40**	**7.78**	**1.10**	**0.58**	**0.9998**	**0.020**	**4.65**	
generic	*0.49*	*2.93*	*3.15*	*0.5*	*8*	*2.55*	*0.26*	*0.9890*	*0.127*	*5.70*	[8]
HA – MSW	0.75	4.29	2.43	0.53	7.38	0.93	0.79	0.9999	0.004	3.36	[6]
HA – C118	0.46	2.80	3.63	0.43	7.15	1.87	0.20	0.9989	0.0345	5.50	[5]
HA – CS	0.61	3.43	2.67	0.66	8.05	1.66	0.43	0.9999	0.0090	4.33	[2]
HA – MSWC	0.50	3.41	2.59	0.64	7.46	1.66	0.40	0.9985	0.0463	4.25	[9]
HA – MSWC*	0.60	3.33	2.57	0.65	8.50	2.08	0.48	0.995	0.0068	4.65	[10]

[a] R^2, coefficient of determination; *RMSE*, root-mean-square error after optimization; *b*, empirical parameter describing how the Donnan volume varies with ionic strength; M_1, carboxyl group content (mmol g^{-1} on moisture- and ash-free basis); K_1, median value of affinity distribution for proton binding by carboxyl groups; $m_{H,1}$, width of proton-affinity distribution of carboxyl groups; M_2, phenolic OH group content (mmol g^{-1} on moisture- and ash-free basis); K_2, median value of affinity distribution for proton binding by phenolic OH groups; $m_{H,2}$, width of proton-affinity distribution of phenolic OH groups.

The values of the proton affinity constants of carboxylic and phenolic groups (log K_1, log K_2) for FA-L- CUW are lower than those for HA-L - CUW, indicating that FA are more acidic. The carboxylic groups of FA-L - CUW also display a higher proton affinity constant (log K_1) than the generic value for the natural occurring materials, while HA-L - CUW is very similar to the generic value. The phenolic groups (log K_2) of FA-L - CUW and HA-L - CUW are lower than the corresponding values of the natural occurring materials, suggesting that the extracts from the analysed compost are more acidic.

The relative abundance of the carboxylic and phenolic groups are higher in FA-L - CUW and in HA-L - CUW, respectively. The relative abundance of carboxylic groups (M_1) of FA-L - CUW and phenolic groups (M_2) of FA-L - CUW and in HA-L - CUW are lower than the generic values, while the carboxylic groups (M_1) of HA-L - CUW is higher than the corresponding generic values.

2. Cadmium binding

The NICA equation that is used for the humic and fulvic-like acids characterization is a multi-component equation that implicitly considers competition between different cations (including hydrogen).

The modelling of the reactivity of the humic-like substances isolated from CUW was carried out conjugating the previously obtained data with results from metal titrations at different pH values. From a physicochemical point of view when the transition from one-component to a multi-component system is performed, an important approximation is made as it is considered that the active binding positions for hydrogen are the same as those that can complex other cations. Therefore, the fitting of potentiometric proton titration data of proton should simultaneously contain, and whenever possible data from metal reactivity [7].

Figure 3.30 shows the experimental data of cadmium binding to HA-L-CUW and FA-L-CUW. The cadmium binding titration was carried out at three pH 6.0, 7.0 and 8.0 to characterise the metal binding extent in competitions with different concentrations of the proton. The best results were obtained for the fitting of the metal binding data of HA-L - CUW (RMSE =0.025) as compared with the FA-L -CUW (RMSE =0.52) (Figures 3.42A and 3.42B), as previously reported for the proton binding fitting.

The metal ion binding decreases at more acidic conditions as the proton-metal ion competition for binding sites increases. Results in Figure 3.42C show that the extent of Cd binding to HA-L is larger than to FA-L at pH 7.0. Identical results are found for the two other pH values.

The fitting parameters for cadmium binding to FA-L–CUW and HA-L–CUW and the generic parameters derived for natural organic matter from soils and surface waters provided by Milne el al. (2003) [11] are displayed in Table 3.27. The values for cadmium binding by carboxylic-type groups, log $K_{M,1}$, of FA-L – CUW and HA-L – CUW are lower than those of natural organic matter, indicating that the humic-like substances from CUW have a lower binding capacity. An opposite result is observed for phenolic-type groups log $K_{M,2}$ of FA-L – CUW and HA-L – CUW. The values for CUW are significantly higher than those of the humic material from natural sources, indicating that the extracts from CUW have a stronger cadmium binding capacity.

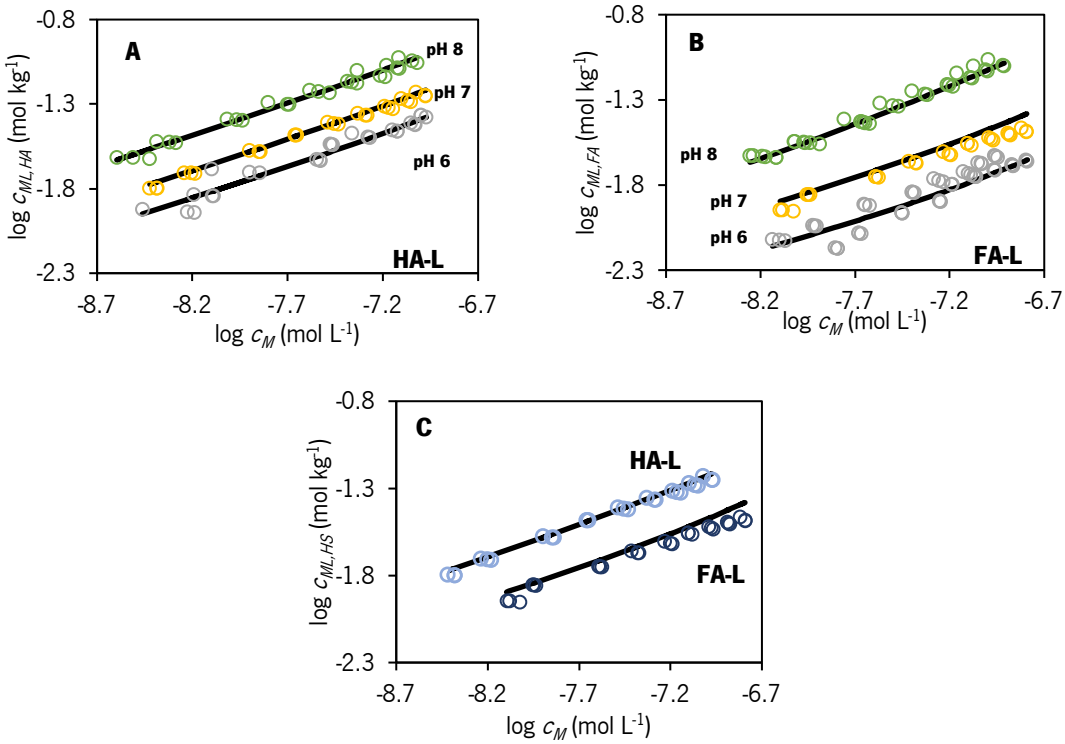

Figure 3.42: Metal binding data obtained for (A) HA-L - CUW and (B) FA-L - CUW (symbols) and the NICA–Donnan model fitting (lines): Cd binding at 12 mmol L^{-1} (KNO_3 and $NaNO_3$) at pH 6.0 (grey dots), 7.0 (yellow dots) and pH 8.0 (green dots) and (C) comparison between HA-L - CUW (○) and FA-L - CUW (o) at pH 7.0.

Regarding the ion-specific parameters, $n_{M,1}$, identical values are obtained for FA-L - CUW binding and natural organic matter, while HA-L - CUW has a lower value than the generic one. For $n_{M,2}$ from both FA-L - CUW and HA-L - CUW are lower than the generic values. Relatively to the intrinsic heterogeneity of the macromolecule, p, lower values were obtained for the intrinsic heterogeneity of carboxyl group, p_1, of FA-L - CUW, whereas the intrinsic heterogeneity of phenolic OH group, p_2, of HA-L - CUW and FA-L - CUW are lower than the generic values.

Table 3.27: Optimised NICA–Donnan parameters for cadmium binding to FA-L – CUW and HA-L - CUW and values of the generic metal binding parameters[a].

	p_1	log $K_{M,1}$	$n_{M,1}$	p_2	log $K_{M,2}$	$n_{M,2}$	R^2	RMSE
				Cd-FA				
CUW	**0.30**	**-2.53**	**0.68**	**0.25**	**0.82**	**0.30**	**0.99765**	**0.074**
generic [11]	*0.59*	*-0.97*	*0.68*	*0.70*	*0.50*	*0.50*	*0.93*	*0.16*
				Cd-HA				
CUW	**1.00**	**-2.33**	**0.35**	**0.34**	**6.08**	**0.40**	**0.99942**	**0.045**
generic [11]	*0.62*	*-0.20*	*0.73*	*0.41*	*2.37*	*0.54*	*0.97*	*0.14*

[a] R^2, coefficient of determination; RMSE, root-mean-square error after optimization; p_1, intrinsic heterogeneity by carboxyl groups; $K_{M,1}$, median value of affinity distribution for metal binding by carboxyl groups; $n_{M,1}$, non-ideality factor of carboxyl groups; p_2, intrinsic heterogeneity by phenolic OH group; $K_{M,2}$, median value of affinity distribution for metal binding by phenolic OH groups; $n_{M,2}$, non-ideality factor of phenolic OH groups.

3. Lead binding

The lead titrations were carried out at pH 5.0, 5.5, 6.0 and 7.0, to allow different competition extent with the proton. The experimental data of lead binding to HA-L - CUW and FA-L - CUW are represented in Figure 3.43. Similar to cadmium titrations, the quality of the fitting of the lead binding titrations of HA-L is better than those of FA-L and may be related to the original quality of the fitting of the proton binding. For HA-L these fits are acceptable as the slope of the curves follows the experimental data, while for FA-L the fits show a different slope than the experimental data.

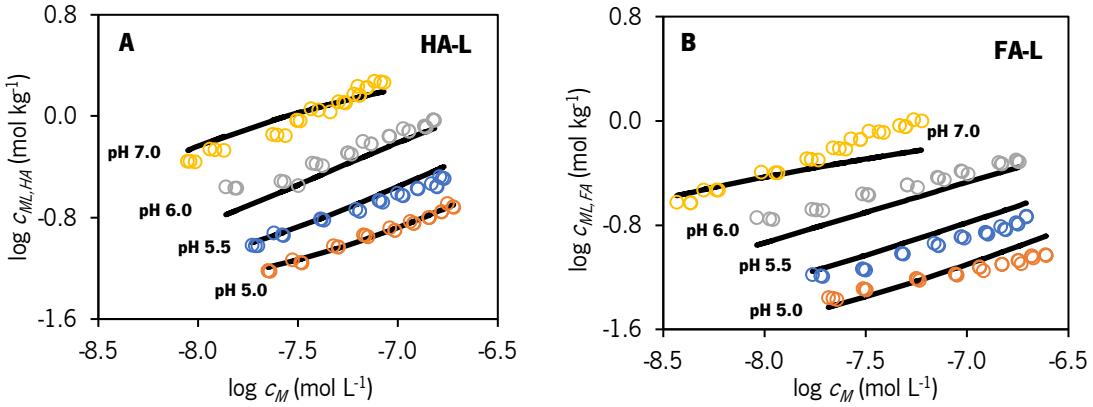

Figure 3.43: Metal binding data obtained for (A) HA-L - CUW and (B) FA -L- CUW (symbols) and the NICA–Donnan fitting (lines): Pb binding at 12 mmol L^{-1} (KNO_3 and $NaNO_3$) at pH 5.0 (orange dots), pH 5.5 (blue dots), pH 6.0 (grey dots) and 7.0 (yellow dots).

Results from the fitting of lead binding to FA-L - CUW and HA-L - CUW and the generic parameters of natural organic matter are presented in Table 3.28. The log $K_{M,1}$ and log $K_{M,2}$ from both extracts are significantly different from the generic values. The values log $K_{M,1}$ of the carboxylic-type and of log $K_{M,2}$ of the phenolic-type groups for HA-L - CUW and FA-L - CUW exhibit an opposite trend. Whereas the binding capacity of the carboxylic-type groups from HA-L - CUW is lower than the generic values, the phenolic-type groups for FA-L - CUW is higher. Considering the ion-specific parameters there is a close similarity between $n_{M,1}$ for FA-L - CUW and the generic value, while $n_{M,1}$ for HA-L - CUW is significantly lower than the corresponding generic value. For the parameter $n_{M,2}$ a lower value was obtained for FA-L - CUW compared to the generic value.

Results of the proton reactivity of the HA-L - CUW and FA-L - CUW extracted from compost were adequately fitted to the NICA-Donnan model, except for FA-L - CUW at pH 9.0 (Figure 3.41B). The fitted parameters differ from the generic parameters of HS from natural organic matter.

Table 3.28: Optimised NICA–Donnan parameters for lead binding to FA-L - CUW and HA-L - CUW and values of the generic metal binding parameters[a].

	p_1	log $K_{M,1}$	$n_{M,1}$	p_2	log $K_{M,2}$	$n_{M,2}$	R^2	RMSE
					Pb - FA			
CUW	**0.30**	**1.05**	**0.57**	**0.25**	**3.02**	**0.10**	**0.99765**	**0.074**
generic [11]	*0.59*	*-1.16*	*0.60*	*0.70*	*6.92*	*0.69*	*0.87*	*0.28*
					Pb - HA			
CUW	**1.00**	**-4.64**	**0.12**	**0.34**	**6.85**	**0.98**	**0.99942**	**0.045**
generic [11]	*0.62*	*1.25*	*0.60*	*0.41*	*4.84*	*0.69*	*0.94*	*0.24*

[a] R^2, coefficient of determination; RMSE, root-mean-square error after optimization; p_1, intrinsic heterogeneity by carboxyl groups; $K_{M,1}$, median value of affinity distribution for metal binding by carboxyl groups; $n_{M,1}$, non-ideality factor of carboxyl groups; p_2, intrinsic heterogeneity by phenolic OH group; $K_{M,2}$, median value of affinity distribution for metal binding by phenolic OH groups; $n_{M,2}$, non-ideality factor of phenolic OH groups.

The lower values were obtained for the abundance of carboxylic sites, M_1 and the proton affinity distribution of phenolic sites, log K_2 for FA-L - CUW and for the abundance of phenolic sites, M_2 of the FA-L - CUW and HA-L - CUW. Nevertheless, the fitted results are comparable to literature values from humic-like substances extracted from other composts (Table 3.26).

Regarding the reactivity towards both cadmium and lead (Figure 3.44), results exhibit some differences in relation to the generic parameters, particularly the median values of the affinity distributions for the metal binding by carboxyl (log $K_{M,1}$) and by phenolic groups (log $K_{M,2}$). While the values of log $K_{M,1}$ are lower, the log $K_{M,2}$ values are higher than the corresponding generic values. This behaviour indicates that in comparison to the humic substances from soils and surface waters, the carboxylic-type groups of the CUW extracts have lower binding capacity and the phenolic-type groups higher binding capacity. The deviation from this behaviour by FA-L - CUW with respect to lead may be due to the fitting quality which was less good than the rest.

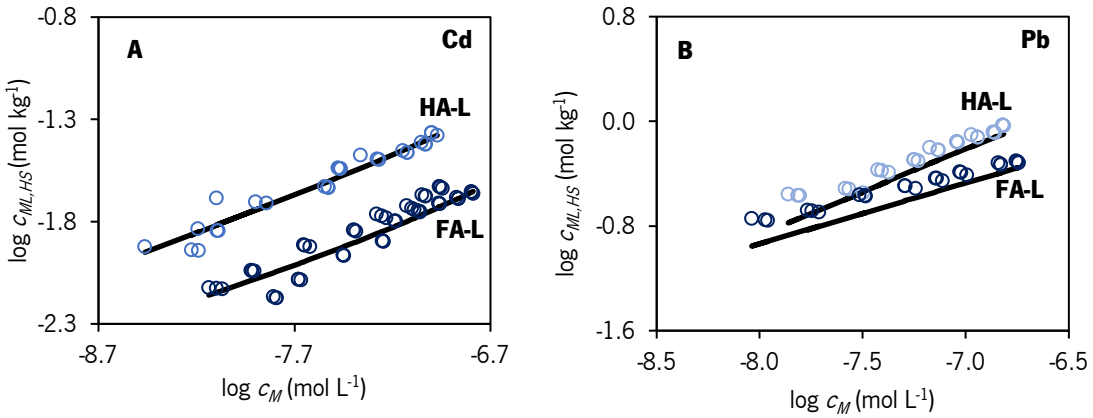

Figure 3.44: Comparison between HA-L – CUW (○) and FA-L – CUW (o) for (A) Cd and (B) Pb binding (symbols) and the NICA–Donnan model fitting (lines) at 12 mmol L^{-1} (KNO_3 and $NaNO_3$) at pH 6.0.

The values of the difference between log $K_{M,2}$ - log $K_{M,1}$ evaluate the differences between the binding ability of carboxylic and phenolic sites (Table 3.27 and Table 3.28). The obtained values for HA-L - CUW are 8.4 (for Cd) and 11.5 (for Pb), while the corresponding differences for the generic values are much lower, 2.6 and 3.6, respectively. For FA-L - CUW the values of this difference are 3.4 (for Cd) and 1.5 (for Pb). The value of the difference between log $K_{M,2}$ - log $K_{M,1}$ obtained for Cd is higher than the difference from the generic values (1.5 = 0.50 – (- 0.97)) in opposition to the value from Pb that is the only one that is lower than calculated for the generic values (8.1 = 6.92 – (-1.16)). This result indicates that the binding capacity of carboxylic sites from the compost extracts tends to be much different from that of phenolic sites as compared to the natural organic matter. Regarding the most abundant HS-L extract, humic-like acid, the lower capacity of the compost extract for binding metals by carboxylic sites is balanced with a higher abundance of this type of groups (M_1 is 11 % higher = (3.55-3.15)/3.55). Similarly, the lower abundance of phenolic sites (M_2 is 57 % lower = (2.55-1.10)/2.55) is balanced by a higher capacity of the compost extract for binding metals. These differences suggest that the production of humic material in shorter maturation times lead to effective differences in their chemical structures.

4. References

[1]D.G. Kinniburgh, C.J. Milne, M.F. Benedetti, J.P. Pinheiro, J. Filius, L.K. Koopal, W.H. Van Riemsdijk, Metal Ion Binding by Humic Acid: Application of the NICA-Donnan Model, Environ. Sci. Technol. 30 (1996) 1687–1698. https://doi.org/10.1021/es950695h.

[2]J.M. Fernández, C. Plaza, N. Senesi, A. Polo, Acid-base properties of humic substances from composted and thermally-dried sewage sludges and amended soils as determined by potentiometric titration and the NICA-Donnan model, Chemosphere. 69 (2007) 630–635. https://doi.org/10.1016/j.chemosphere.2007.02.063.

[3]J. Weber, Y. Chen, E. Jamroz, T. Miano, Preface: humic substances in the environment, J Soils Sediments. 18 (2018) 2665–2667. https://doi.org/10.1007/s11368-018-2052-x.

[4]Y. Zhao, M.A. Naeth, Soil amendment with a humic substance and arbuscular mycorrhizal Fungi enhance coal mine reclamation, Science of The Total Environment. 823 (2022) 153696. https://doi.org/10.1016/j.scitotenv.2022.153696.

[5]C. Plaza, N. Senesi, A. Polo, G. Brunetti, Acid-base properties of humic and fulvic acids formed during composting, Environmental Science & Technology. 39 (2005) 7141–7146. https://doi.org/10.1021/es050613h.

[6]A. van Zomeren, A. Costa, J.P. Pinheiro, R.N.J. Comans, Proton Binding Properties of Humic Substances Originating from Natural and Contaminated Materials, Environ. Sci. Technol. 43 (2009) 1393–1399. https://doi.org/10.1021/es801924x.

[7]A.H. Rosa, J.P. Pinheiro, A.S.C. Monteiro, N. Janot, B.J. Groenenberg, Especiação termodinâmica de metais traço com substâncias húmicas: o modelo Nica-Donnan, Química Nova. 40 (2017) 1191–1203. https://doi.org/10.21577/0100-4042.20170107.

[8]C.J. Milne, D.G. Kinniburgh, E. Tipping, Generic NICA-Donnan model parameters for proton binding by humic substances, Environmental Science and Technology. 35 (2001) 2049–2059. https://doi.org/10.1021/es000123j.

[9]C. Plaza, G. Brunetti, N. Senesi, A. Polo, Proton Binding to Humic Acids from Organic Amendments and Amended Soils by the NICA-Donnan Model, Environ. Sci. Technol. 39 (2005) 6692–6697. https://doi.org/10.1021/es0503377.

[10]F. Pedra, C. Plaza, J.C. García-Gil, A. Polo, Effects of municipal waste compost and sewage sludge on proton binding behavior of humic acids from Portuguese sandy and clay loam soils, Bioresource Technology. 99 (2008) 2141–2147. https://doi.org/10.1016/j.biortech.2007.05.043.

[11]C.J. Milne, D.G. Kinniburgh, W.H. van Riemsdijk, E. Tipping, Generic NICA–Donnan Model Parameters for Metal-Ion Binding by Humic Substances, Environ. Sci. Technol. 37 (2003) 958–971. https://doi.org/10.1021/es0258879

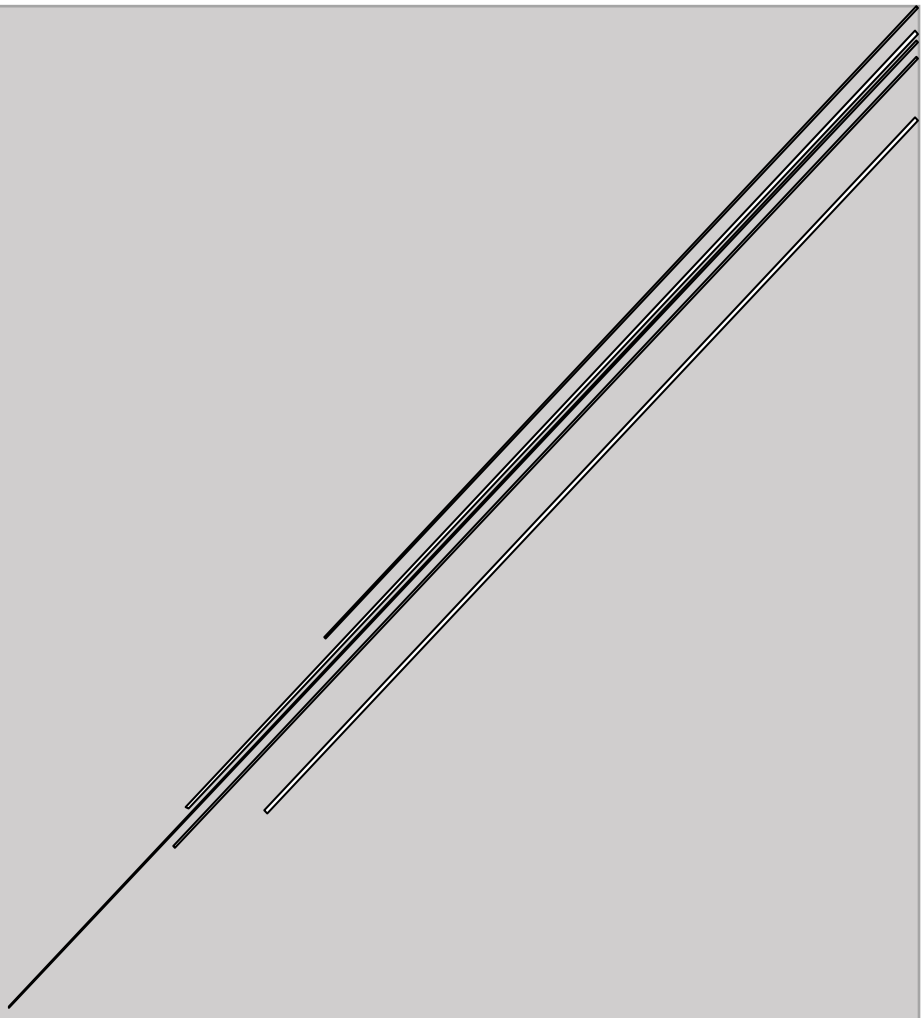

CHAPTER 4 - CONCLUSIONS

The elemental and structural characterization of compost is of great importance for the valorisation of this type of material. However, the interpretation of analytical data is not straightforward as the organic matter present in compost is of great complexity, not only due to the diversity of structures but also to the heterogeneity of the material.

The work performed in this thesis included the characterization of 7 compost samples and a non-composted organic fertiliser and of their extracts, and the analysis of these results. Through the comparison of the results of the analysis of a compost (from selective collection of urban wastes) at different composting stages it was investigated how the chemical modifications of the residues impacted the different characterization parameters and the analytical parameters that were more sensitive to monitor the composting process were identified. From an inter-block analysis, it was concluded that results from the analytical parameters related either to the elemental composition or to the molecular structure of solid compost, water soluble extract (containing DOM), humic-like acid (HA-L) extract or fulvic like acid (FA-L) extract are able to distinguish between samples obtained at the different stages of composting. For monitoring the composting process, the most significant parameters for the solid compost were: the C/N molar ratio and the weight loss between 30 and 100 °C. For the water-soluble extract, the most relevant parameters were: the dissolved organic carbon, the oxidizable carbon, the electric conductivity, the concentrations of PO_4^{3-} and NO_2^-, the absorptivity coefficient at 280 nm, the abundance of acid sites and the medium value of the proton affinity distribution of the carboxylic groups and the abundance of acid sites of phenolic groups. For HA-L extracts the most relevant parameters were: the contents of C, S, H, the ratios O/C, H/C, the weight losses at the temperature ranges 177-400 °C and 400-620 °C, the ratio between these two weight losses and medium values of the proton affinity distribution of the carboxylic and phenolic groups. For the FA-L the most significative parameters were the content of N, the abundance of acid sites of the carboxylic groups, the abundance of acid sites and the medium value of the proton affinity distribution of the phenolic groups.

The comparison of characterization results of the composts of different origin showed that there are significant differences between the content of constituents such as C and N and between the amount of recalcitrant and extra-recalcitrant substances. The nature of the compost residues in TGA was also diverse, while the residues of some composts (CVDW and CUW) were predominantly metal oxides, the residues of other (CA and CVA) contain high amounts of other inert materials, mainly silicates. From two principal components analysis (PCA) it was possible to conclude that the samples distribution pattern in the representation plots followed a trend that is more closely

associated with the nature of the raw materials than with the composting methodology. Several correlations were found between analytical parameters, mostly reported for the first time, suggesting that the chemical structure of the constituents of the composts produced from different feedstock and composting methodologies possess important similarities. Furthermore, the existence of these correlations enables reducing the number of analyses to be performed for the compost characterization. From a crop field experiment, it was observed that the algae compost (CA) led to the largest effect in terms of the increase of the leaf area on lettuce, as compared with the algae vermicompost (CVA), the compost of urban residues (CUW) and the organic non-composted fertiliser (FLW). This result was not directly related to the content of macronutrients, N, P or K or with another parameter that was distinctive of CA.

The extracts of different composts were characterised and were differentiated by means of the reactivity of the DOM, FA-L and HA-L extracts. Specifically, the HA-L extracts exhibited marked differences between the reactivity of the different samples. In particular, the HS-L extracts from CUW were characterised considering the fitting to the experimental data from proton and metal binding titrations to obtain parameters such as the site density and proton affinity and also intrinsic heterogeneity. Due to the absence of similar data in the bibliography, the results obtained were compared with the generic parameters of organic matter of natural sources. It was found that the carboxylic sites in HA-L have lower capacity for binding metals being balanced with a higher abundance of this type of groups. In relation to the phenolic sites in HA-L, these have a higher capacity for binding metals, which is balanced with lower abundance of these sites.

From the comparison of the characterization results of the extracts of the composts of different origins a systematic correlation analysis was carried out to identify the parameters that are more sensitive to the differences between the chemical composition, structure and reactivity of the different composts. The higher number of correlations found within the extracts of the same nature were for the HA-L extracts (a total of 30 correlations), where 5 correlations were found with the absorptivity coefficient at 280 nm (ε_{280}) and 4 correlations were found with the relative value of weight loss from 30 to 100 °C (WL_1@air/TWL@air) that were the two parameters with the larger number of correlations. The HA-L extract was also the extract that exhibited a larger number of correlations with the compost characterization parameters (a total of 20 correlations), where 3 parameters of HA-L extract were related to the maturation degree (WL_2@air/ WL_3@air) of compost.

The extent of the interaction between the extracts of the different composts with Cd^{2+} was also compared with the extracts of a non-composted fertiliser (FLW). From these results a scale of

compost quality, expressed in units of equivalent mass of fertiliser was proposed for the first time. Using the experimental values of the metal complex concentration ($c_{ML,HA\text{-}L}$) this scale takes into account both the abundance (estimated from the yield of the extraction) and reactivity of the HA-L extracts. Using the proposed quality scale, the composts characterised in this work were ranked as follows: CVDW > CA > CLW > CDDW > CUW > CVA > CSS. The validity of this scale was verified by comparing the reactivity parameter ($c_{ML,HA\text{-}L}$) with growth results from a lettuce crop, expressed as the total leaf area (*TLA*). The high correlation (r=0.997) obtained between *TLA* and $c_{ML,HA\text{-}L}$ demonstrates that the reactivity parameter used for the definition of the compost quality scale has a high potential to assess the bioactivity of the compost, and therefore could serve as a marker of the bioactivity of composts.

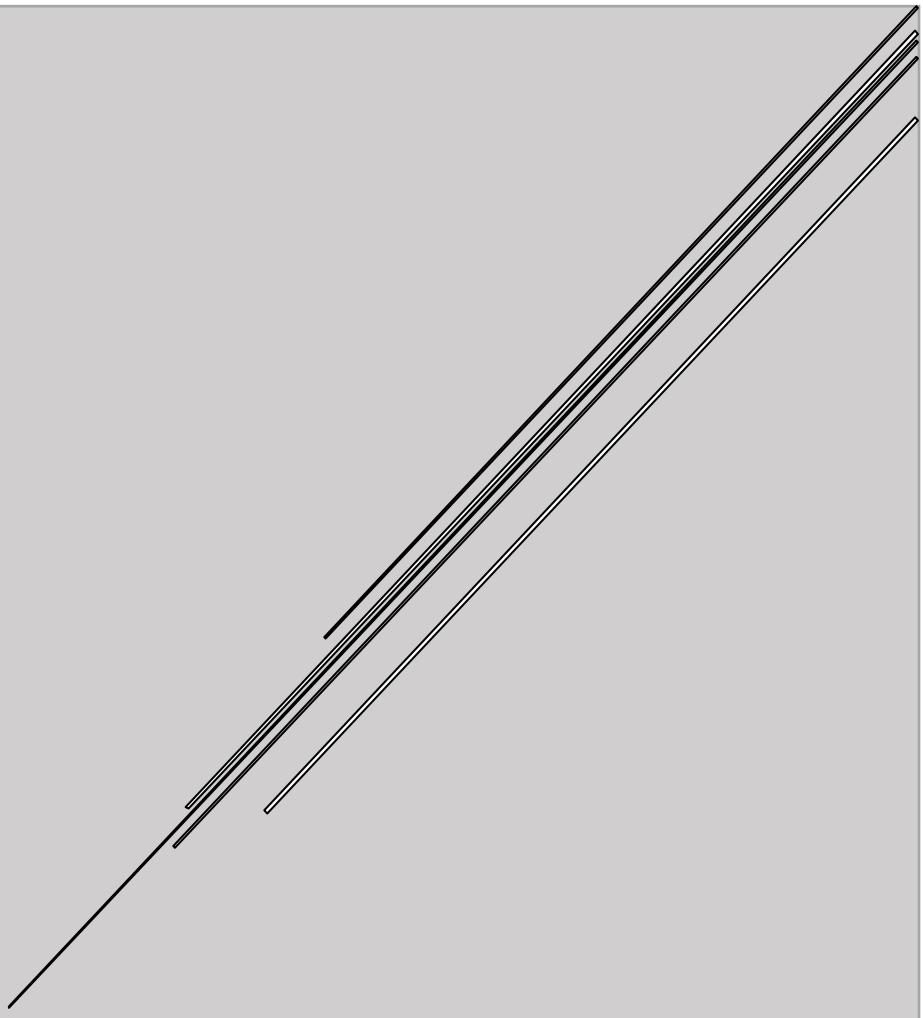

ANNEXES

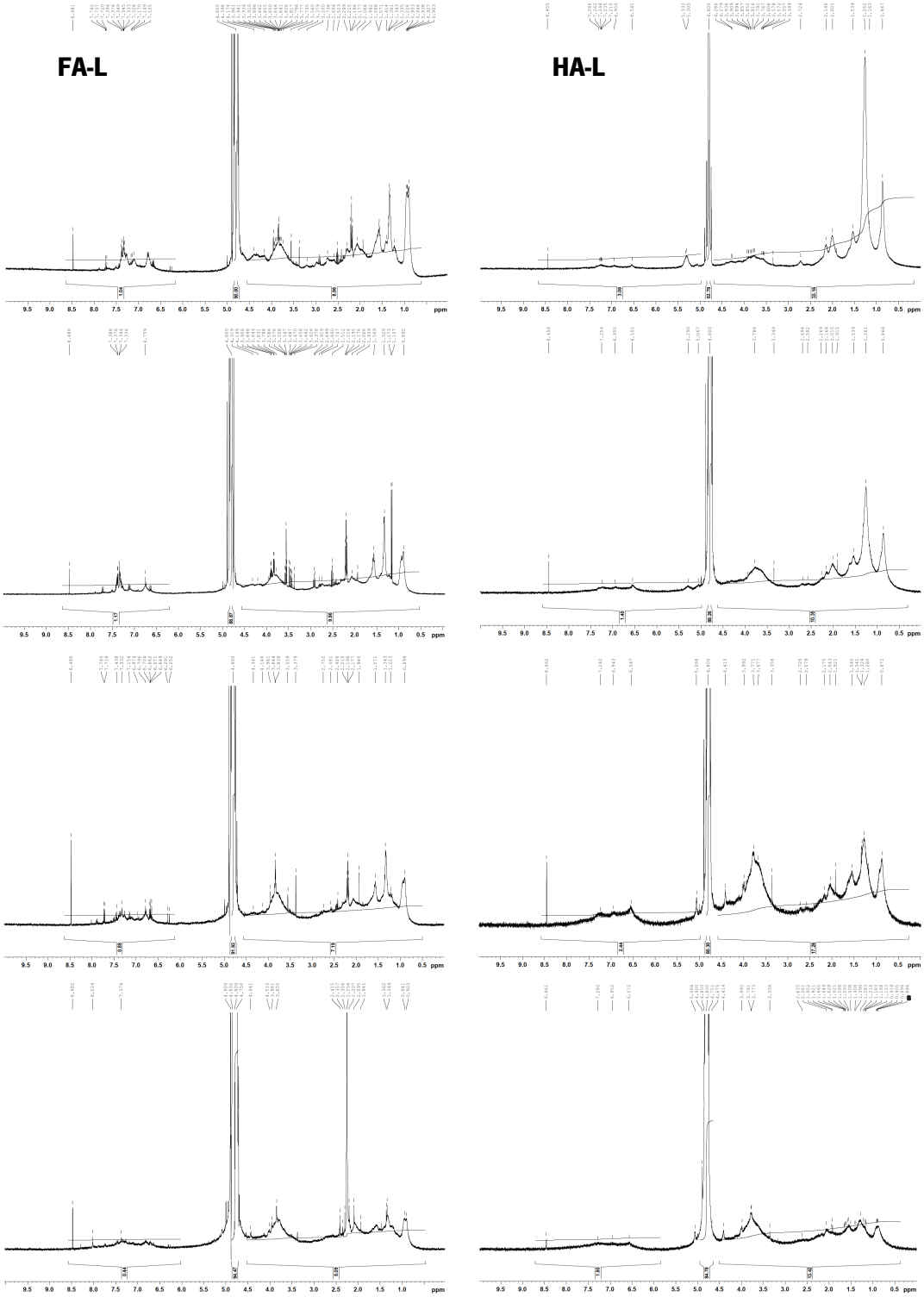

Figure A1: Proton NMR spectra of FA-L and HA-L from the samples UW_0, CUW_{15}, CUW_{30} and CUW, respectively.

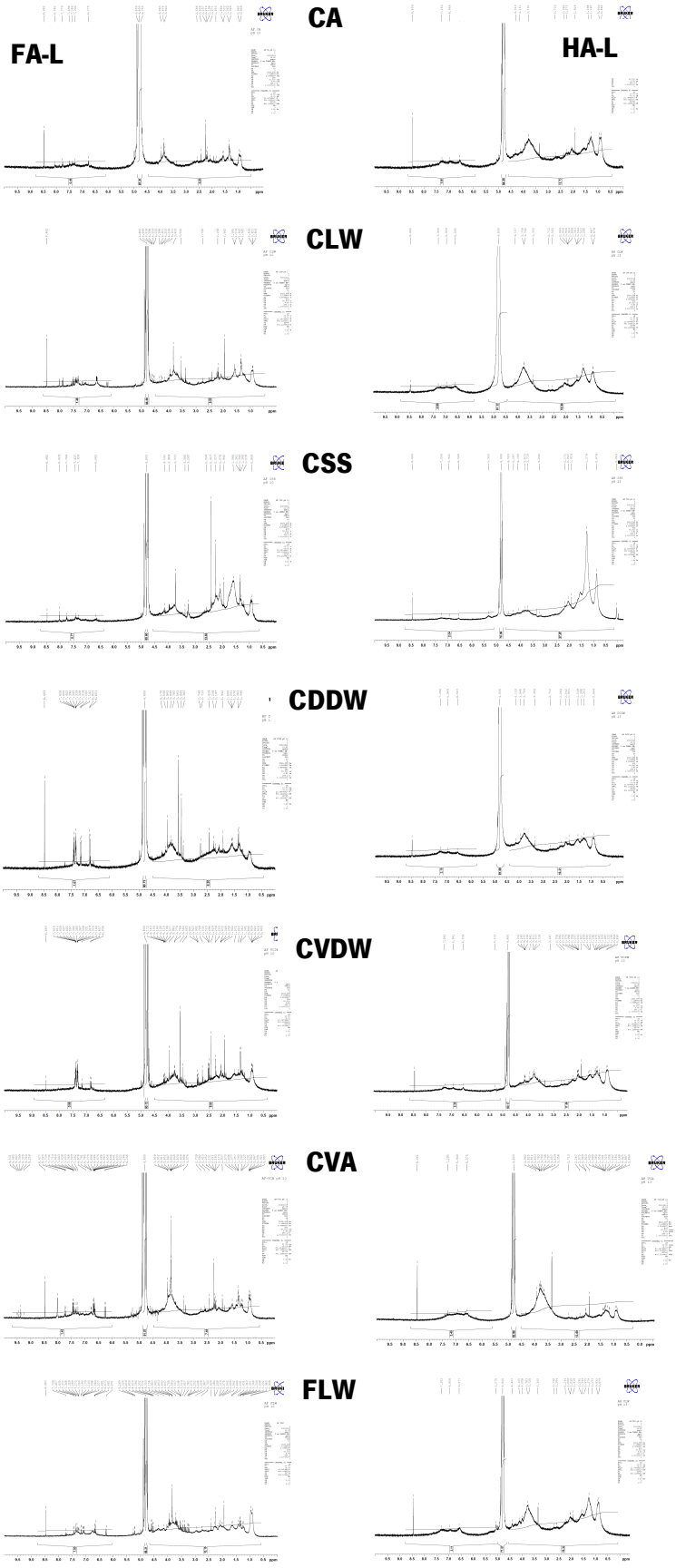

Figure A2: Proton NMR spectra of FA-L and HA-L from the samples CA, CLW, CSS, CDDW, CVDW, CVA and FLW respectively

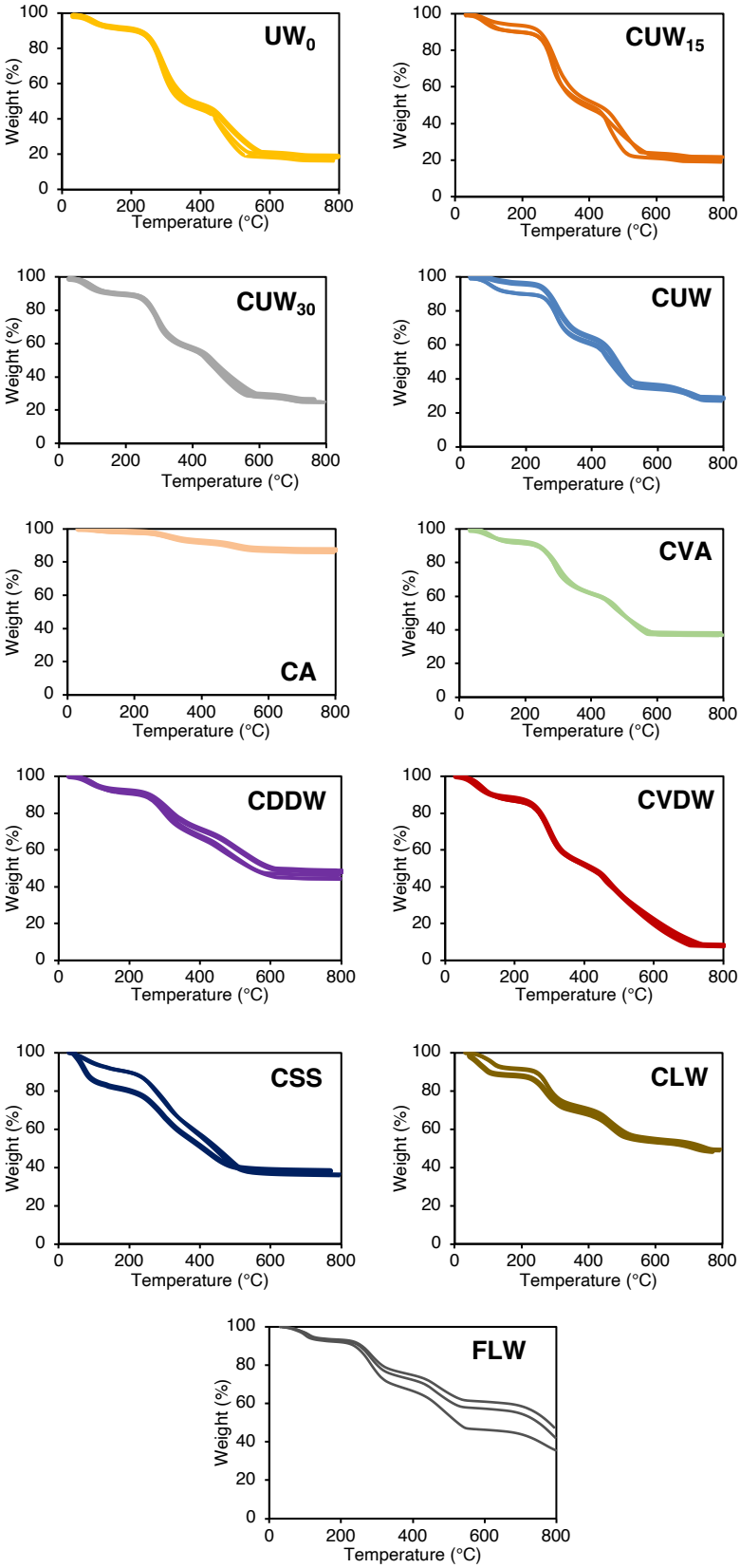

Figure A3: TGA curves of the three replicates of each of the compost samples: UW_0 (yellow), CUW_{15} (dark orange), CUW_{30} (grey), CUW (blue), CDDW (purple), CVDW (red), CVA (green), CA (orange), CSS (dark blue), CLW (brown) and the organic fertiliser FLW (dark grey).

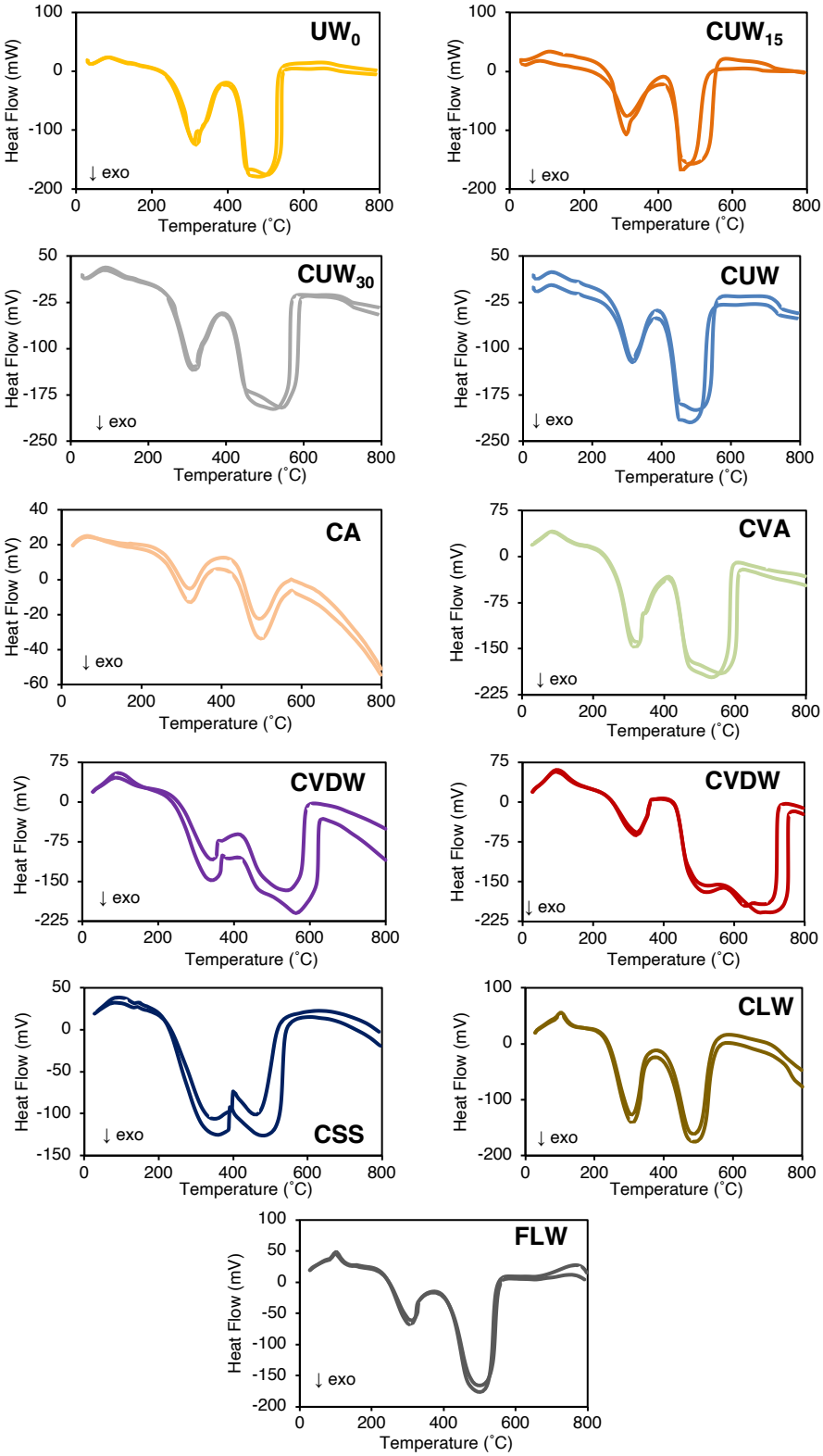

Figure A4: DSC curves of the two replicates of each of the compost samples: UW_0 (yellow), CUW_{15} (dark orange), CUW_{30} (grey), CUW (blue), CDDW (purple), CVDW (red), CVA (green), CA (orange), CSS (dark blue), CLW (brown) and the organic fertiliser FLW (dark grey).